GEOLOGICAL AND INTEGRATED GEOPHYSICAL INVESTIGATION OF ASSOCIATED SULPHIDE MINERALISATION AROUND BABAN-TSAUNI AREA, NORTH CENTRAL NIGERIA

BY

OLUFEMI DAPO OLASEHINDE

MATRIC NUMBER: 183555

A THESIS

SUBMITTED TO THE SCHOOL OF POSTGRADUATE STUDIES IN PARTIAL FULFILMENT FOR THE AWARD OF DOCTOR OF PHILOSOPHY (PHD) DEGREE IN APPLIED GEOPHYSICS

DEPARTMENT OF GEOLOGY

UNIVERSITY OF IBADAN, IBADAN, NIGERIA

AUGUST, 2021

CERTIFICATION

This is to certify that this work was carried out by Olasehinde, Olufemi Dapo in the Department of Geology, University of Ibadan, Ibadan, Nigeria.

Supervisor	**Co-Supervisor**
Prof. A.I. Olayinka	***Dr. M. A. Oladunjoye***
Department of Geology,	Department of Geology
University of Ibadan	University of Ibadan

DEDICATION

Dedicated to the glory of the Lord, for His mercy endures forever and to the loving memories of my mentor and father Professor Peter Ibikunle Olasehinde and my beloved brother Arch. Engr. Gideon Opeyemi Olasehinde.

ACKNOWLEDGMENTS

The author is indebted to Prof. A.I. Olayinka for his supervisory roles and unrelenting encouragement that have resulted in the completion of this study. My special appreciation goes to my co-supervisor Dr. M.A. Oladunjoye for taking out time to read through and align me on the right path. I am sincerely grateful.

My special thanks goes to the HOD of Geology Department Prof. O.A. Okunlola, for his fatherly roles and the Coordinator of Postgraduate studies in the department Dr. I.A. Oyediran, for his passionate and dedicated role in coordination and guidance. I must not fail to appreciate the following lecturers: Prof. G.O. Adeyemi, , Prof. M.N. Tijani, Prof. O.A. Ehinola, Prof. M. E. Nton, Dr. O.A. Boboye, Dr. A.T. Bolarinwa, Dr. A.S. Olatunji, Dr. O.O. Omitogun, Dr. O.C. Adeigbe, Dr. O.O. Osinowo, Dr. A.M. Adeleye, Mr. A. Jayeoba, Mr. J. A. Aladejana and Mrs F. A. Ajayi for their willingness to serve during my presentations and for their priceless comments and suggestions that have contributed to the successful completion of this study.

I cannot fail to acknowledge the support, encouragement and motivation from my family. My lovely wife Kikelomo, Omolara and my children Bryan (Inioluwa), Bree (Anjolaoluwa) and Brayden (Araoluwa). I love you guys and am so blessed to have you. My sincere appreciation goes to my late father, mentor and inspiration in the field of geosciences (Prof. Olasehinde), my loving and caring mother Dr (Mrs) M.O. Olasehinde and my siblings, the Abioduns, The Joshuas, The Atolanis, Dr. Toyin and family, Engr. Ibukun and family and Engr. David and family.

To my friends and colleagues who have at one time or the other contributed to this research; the Odunlami's family, Dorothy Iseghohi, Bukky Adejuwon, Wale Afolabi Dele Olaniyan, and Bunmi Adeniyi thank you so much.

To others that I cannot list, God bless you all

Olasehinde, Olufemi Dapo

ABSTRACT

The associated sulphide mineralisation provinces comprising lead-zinc ore in Nigeria have always been associated with the sedimentary Benue trough. However, there had been reports of associated sulphide mineralisation within the basement complex, which are not fully understood in terms of the controlling structures and geometry. Thus, this study focused on the evaluation of structural setting, lithological association and ore body geometry of the sulphide ores around Baban-Tsauni, Northcentral Nigeria.

Aeromagnetic and airborne radiometric datasets were obtained from Nigerian Geological Survey Agency acquired at 500m inter-profile spacing and 80m terrain clearance. The data were processed using Fast Fourier Transform filters and grid rationing, respectively for enhanced interpretation of structural settings and lithological delineations. Geological ground truthing and petrographic study were carried out over prospective areas delineated from the interpreted airborne data. Ground magnetic survey was conducted over the delineated areas with 50 profiles, each measuring 5 km at 100 m inter-profile spacing. Interpreted structures were then characterised using electrical resistivity and induced polarisation responses in time domain, acquired with a 5000-Watt transmitter and 8-channel receiver. Profile running across an open mineralised pit was used as control profile. Electrode configuration was dipole-dipole, with 50m dipole spacing and 25m station interval. Three-dimensional model was generated from the stack plot of the resistivity and chargeability pseudo-sections, to configure the associated sulphide ore body geometry and volume estimation, using voxel mathematical algorithm.

Primary NE-SW structural setting and secondary NNE-SSW, NW-SE and WNW-ESE geological structures were delineated. Granitic intrusives suspected to be co-genetic but occurred at different depths as reflected in the variations of their signature intensities. Sulphide mineralisations were related to regions of high thorium concentration with quartzo-feldspathic and quartz veins lithology. The area is underlain by basement rock comprising gneisses, quartzite, granitic intrusions and pegmatite. Ground magnetic data isolated more of the NW-SE and NNE-SSW trending secondary structures indicating that the mineralisations were structurally controlled and epigenetic. Induced polarisation and resistivity structures delineated regions of relatively high chargeability with corresponding high resistivity signatures, which correlated with the mapped structures from the ground magnetic interpretation confirming disseminated mineralisations. The estimated depths to the interpreted ore bodies were between 5 m to 30 m from the surface. The signature extended in a disseminated pattern down to depth of approximately 167 m, which was the maximum depth for the survey. Resistivity and chargeability anomalies with values higher than 1000 Ωm and 30 mV/V, respectively were set as threshold as obtained from the control profile and a 3-dimensional model of the ore body geometry gave a volumetric value of 23,328,000 m^3 with a mean chargeability value of 54.98 mV/V.

The NW-SE and NNE-SSW structures controlled the emplacement of the associated sulphide mineralisation in Baban-Tsauni area corresponding to regions of high thorium enrichment. A 3-dimensional model was successfully configured for the ore body geometry.

Keywords: Aeromagnetic survey, Radiometric prospecting, Resistivity survey, Induced polarisation

Word Count: 474

TABLE OF CONTENTS

LIST OF FIGURES

LIST OF TABLES

CHAPTER ONE

INTRODUCTION

1.1 General Statement

The process of looking for indications of mineralisation in rocks is known as mineral exploration. The principle operates by obtaining bits of geological data from many locations and, in some cases, combining techniques to construct a geological framework. Thus, mineral exploration involves collecting and gathering geoscientific data. These data when integrated together gives a better insight into the geology, structural setting and mineralisation style, with surface and subsurface geometry of the ore body. There are various geophysical methods, each based on a particular physical property of the earth. These properties include electrical conductivity, magnetic susceptibility, density, radioactivity, reflectance and refraction, etc. These geophysical techniques are either used singly or combined with others to provide answers to geological questions which include structural setting and ore body geometry.

In geophysical exploration, the different techniques may be either airborne or ground based. Airborne geophysical survey is a very fast way to quickly investigate large areas of the earth compared to ground geophysics. Since the early days of balloon photography broad coverage of the earth provided by the airborne method has been well recognized. (Dobrin, 1976). Thus, with geophysical application, subsurface geological in-homogeneities are shown as observed surface geophysical anomaly, where these in-homogeneities are themselves accompanied with distinct and detectable changes in the concerned physical properties.

In magnetic surveys, magnetic susceptibility is the primary factor responsible for a given anomaly. Other factors that affect magnetic field over a given source body are; the thickness and type of the overburden, geometry and dimension of the source. In radiometric survey, decay in radioactive elements account for detectable changes in elemental composition of the associated lithology. With electrical resistivity, electrical

conductivity of the material account for the changes detected and helps identify anomaly of interest. Over the last couple of decades, electrical resistivity method of geophysical prospecting has found its application in solving vast geological problems and its development had been rapid over the years. This stems from advancement in data acquisition and inversion techniques, together with easy access to automated processing software with high configuration computer systems thereby increasing its application. This geophysical method is widely used in various fields of geosciences, ranging from environment, engineering, hydrological surveys and mineral explorations because of its ability in providing more accurate depth information. The Induced Polarization (IP) technique is similar to the electrical resistivity and in most cases the data can be acquired simultaneously. The induced polarization measures the degree of chargeability when charges are been sent into the ground and the source is cut off. The stored charges for materials that are chargeable are released in form of decay and the technique determines the variation in the degree of their chargeability. Each geophysical technique explores a distinctive physical property of the crustal Earth that tends to resolve a particular geoscientific question in the subsurface of the Earth, whereas in some cases; a mixture of two or more of these techniques might be required for better result (Keary *et al*., 2002).

The associated sulphide mineralisation around Baban-Tsauni, North central Nigeria which includes lead/zinc mineralisation within the basement complex among others is of excellent scholarly concern as compared to common belief in Nigerian that lead/zinc mineralisations are restricted to the Benue trough. The Nigerian Pre-Cambrian Basement lies between the West African Craton to the West and the Congo Craton to the Southeast within the Pan-African mobile belt. McConnell (1949) conducted a regional geological reconnaissance survey identifying the Izom lead / zinc mineralisation within the crystalline rocks. According to him, this is Nigeria's only known significant lead/zinc deposit outside the region covered by Cretaceous rocks and the lodes appear to be moving in the same direction. He identified two types of veins, one of hard glassy quartz with small quantities of pyrite, galena and magnetite, and the other of shattered limonitic quartz with irregular lenses and galena bodies found in Nigeria's Cretaceous rocks. The first type is considered to be associated with the initial Pre-Cambrian mineralisation, while the

second type is of the second generation and has many features in common with the lead deposits discovered in Nigeria's Cretaceous rocks. Burke *et al.* (1972) recognized the rock formation in the area (migmatite-gneisses) as having a comparable trend and could be as a result of a single tectonic episode of various stages marked by the Pan-African Orogenic event. He also found the structural pattern showing a general trending foliation of N-S and NE-SW. Oluyide *et al*. (2004) also documented areas underlined by migmatitic and low-grade schist.

Gravity studies by Cratchely and Jones (1965) showed that the Benue trough is characterized by a central area of positive Bouguer anomalies flanked by most anomalies. The Benue trough's positive anomalies were attributed to a zonation in which the oldest Cretan rocks (about 105 million years of Albian era) are close to the surface and contain magmatic material of intermediate to basic composition associated with the Lead-Zinc mineralisation belt and positive bouguer anomalous area. The existence of ancient and recent mining pits in the region also suggests mineralisation.

The Geological Survey Department contracted Hunting Geology and Geophysics Limited, England in 1975 to carry out airborne magnetic survey over the entire country. Russ (1957) and Truswell and Cope (1963) conducted a national geological survey of the Paiko Sheet 185 under the auspices of the Geological Survey Department also. In 1984, Woakes and Bafor equally researched into mineralisation elements of gold and associated sulphide in the region. Nigeria's Geological Survey (2006) also conducted series of work covering the study area. These include Fugro Airborne Survey's recent airborne magnetic and radiometric data acquisition across the country between 2006 to 2007. The geological mapping of the entire sheet 185 (Paiko) was conducted equally and published on a scale of 1:100,000 as a geological map.

1.2 Problem Statement

The associated sulphide mineralisation provinces comprising lead-zinc ore in Nigeria have always been associated with the sedimentary Benue trough. However, there has been reports of associated sulphide mineralisation within the basement complex (Okunlola *et al.*, 2007), which are not fully understood in terms of the controlling

structures and geometry. Thus, this study focuses on the evaluation of structural setting, lithological association and ore body geometry of the sulphide ores around Baban-Tsauni, Northcentral Nigeria.

The assessment and evaluation of mineralisation have over the years been evaluated, using various techniques such as geophysics and geochemistry. To some extent, the industry had recorded success from the application of these various techniques.

The challenge had always been a geometric representation of the subsurface in line with the structural setting for estimating geometrical volume to a very close approximation, before drilling operation. Consequently, this research work evaluates the structural setting associated with the epigenetic disseminated structurally controlled mineralisation within the basement complex section of central Nigeria (Paiko 185), its mode of occurrence and ore body geometry. This was done using an integrated geophysical approach of airborne magnetic studies for regional structural delineations which could host mineralisation, airborne radiometric method for lithologic boundary delineation, and geological ground truthing. The ore body geometry was configured using electrical resistivity tomography coupled with chargeability responses of the induced polarization over the higher resolution structural setting evaluation from the ground magnetic survey.

1.3 Aim and Objectives of the Research

This research work is aimed at evaluating the structural setting and ore body geometry of the suspected disseminated sulphide mineralisation using geological and integrated geophysical methods.

This research is focused on the following objectives:

i. To assess and evaluate the structural setting
ii. Update the geological map, to produce a geological and structural maps of the study area
iii. Identify target area that could play host to the associated sulphide mineralisation
iv. Ground truth the delineated structure for disseminated sulphide
v. Determine the resistivity and chargeability values over the delineated structures
vi. Develop a subsurface geometry for the ore body

1.4 The Study Area: Location and Physiography

The research area lies within the north-central part of Nigeria with Baban-Tsauni being a prominent settlement. The area lies at the boundary of the Capital Territory Abuja and Niger State, West Africa (Figs. 1.1). It lies between Longitudes 6° 45′ to 7° 00′ and Latitudes 9° 00′ to 9° 15′ which is the southeastern quadrant of the Nigerian standard 1:100,000 topographic sheet 185 Paiko. Niger state and FCT are notably rich in minerals resources.

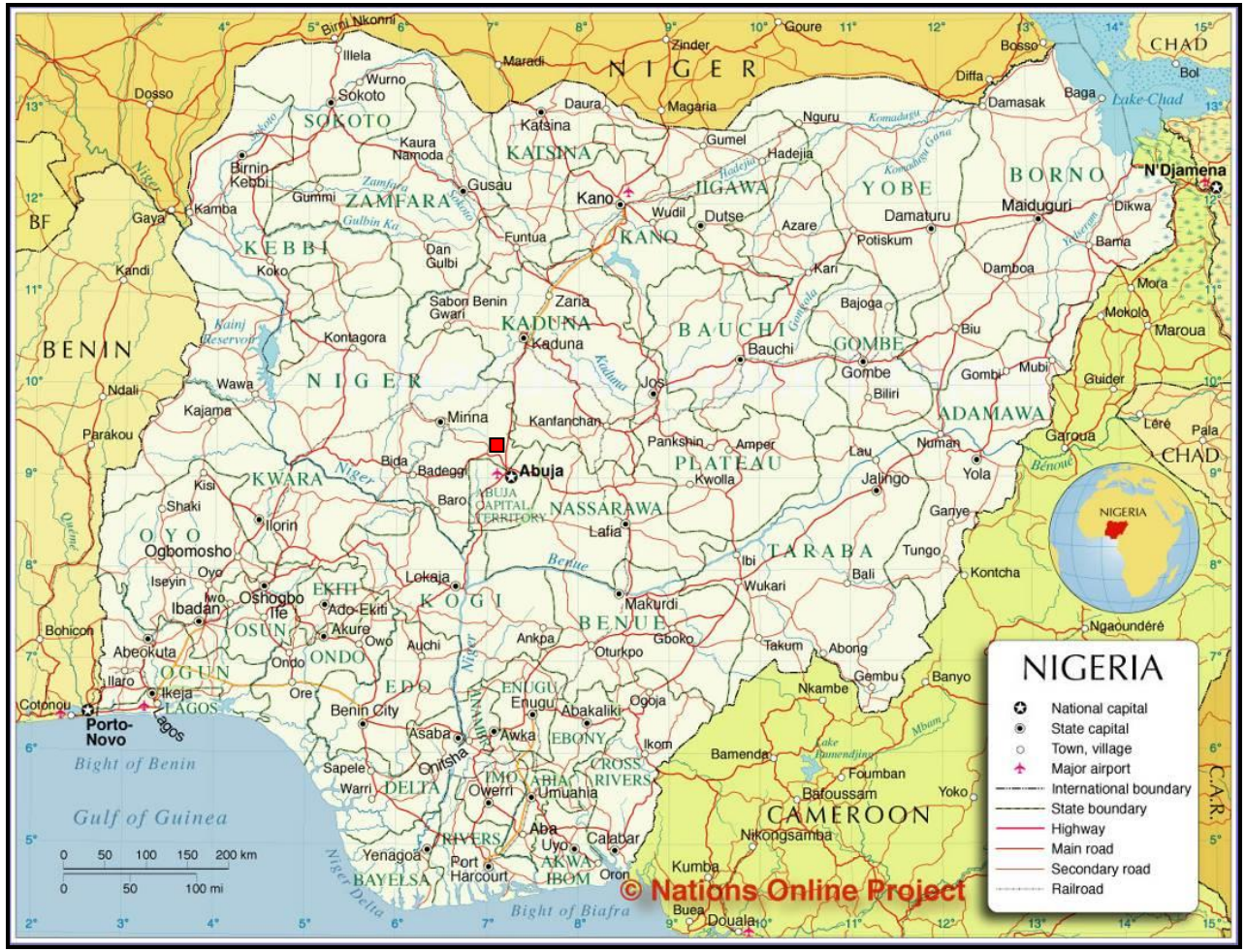

Figure 1.1: Administrative Map of Nigeria showing the project area in red box (Nations Online project, 2021)

The study area falls within the Guinea Savannah belt of Nigeria. This belt is marked by rainy and dry season that overlap each other. The rains starts from around April and ends at about October. The dry season which gradually sets in, starts around October at the stop of the rains and runs till March of the following year. The average annual rainfall from studies is between 1,000 and 1,500 mm (Ayoade, 1974; Adefolalu, 1988). The temperature within this region ranges from 26.5°C to 27.8°C. From March to June typifies the maximum temperature, while the minimum temperatures are always recorded between December to January (Odekunle, 2006).

The study area has an undulating topography characterized by chains of uplifts and ridges especially at the central parts of the project area towards the north-eastern part. The elevation of the area rises from about 150 m to about 470 m at the peak of the highest point, and regionally decreases from the northeast to the southwest (Figs. 1.2).

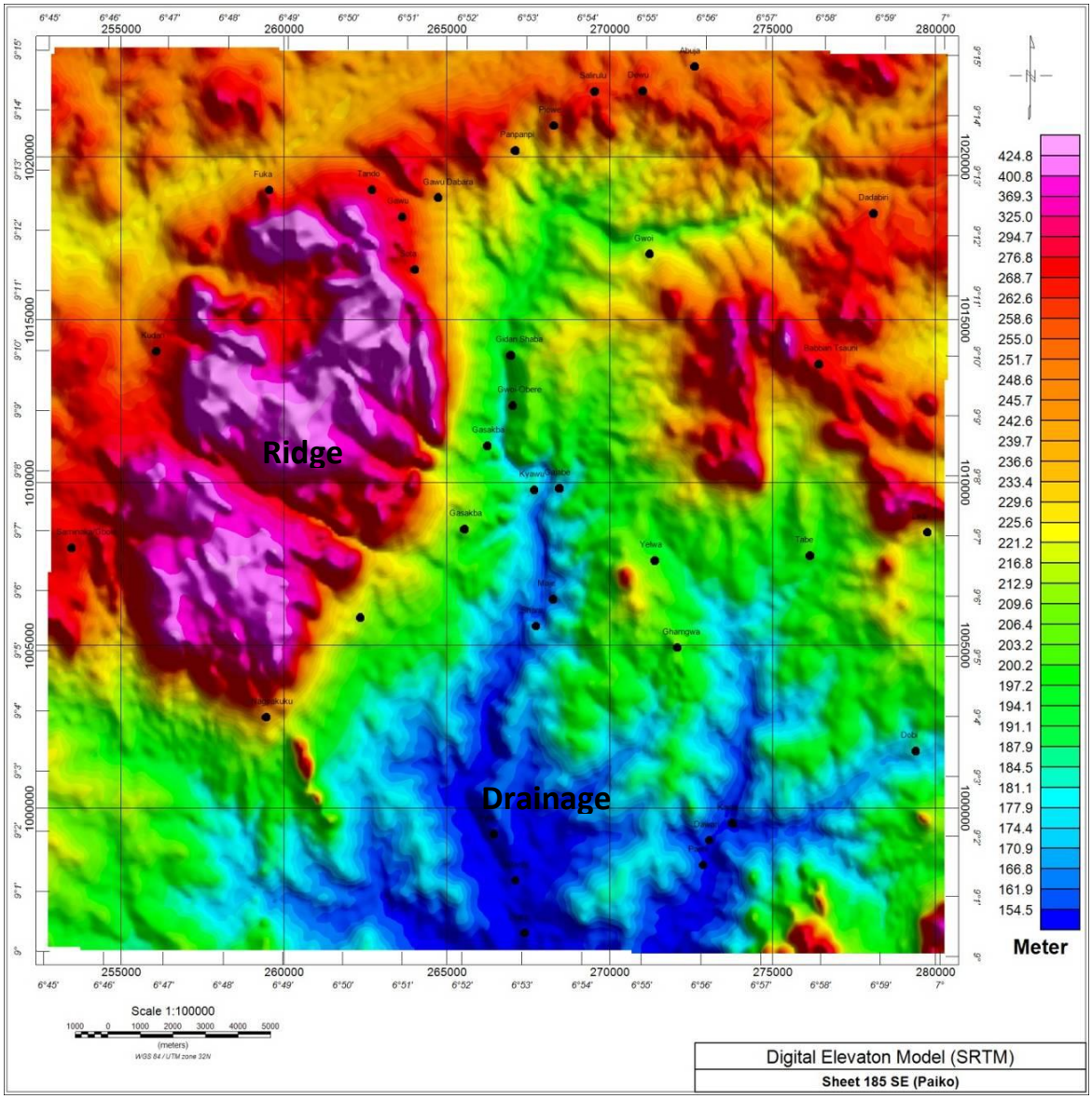

Figure 1.2: Digital Elevation Model from SRTM data covering the Sheet 185 (Paiko SE)

The general relief of the project areas comprises plains made up of metasedimentary rocks such as schist and amphibolites that are surrounded by Older Granites, Migmatites, Gneisses and Quartzite intrusion that formed isolated hills. In some areas, granites and gneisses outcrop as conspicuous inselbergs. The drainage pattern is dendritic. The area is well drained by dendritic-patterned streams which source water from the uplands. Most of the streams empty into the River Gurrara that flows in a northeast to southwest direction cutting through the study area.

CHAPTER TWO

LITERATURE REVIEW AND THEORETICAL FRAMEWORK

2.1 Regional Geology

The area of study is located in the north central part of Nigeria in west Africa. It lies within the Precambrian basement complex of Nigeria. Nigeria is underlain by the reactivated late Proterozoic to Early Paleozoic (Pan African) terrain. The Precambrian rocks are found in the Dahomeyan Terrane's Benin-Nigeria Shield, which separates the Achaean to Meso Proterozoic West African and Congo Cratons to the west and east of Nigeria, respectively (Grant,1967,1969; Odeyemi,1981; Ajibade *et al*.,1987; Ajibade and Wright, 1989); Key and Pitfield, 2009). The latest reactivation i.e. the Pan African (600±150Ma) which affected the whole region imposed N-S structural trend on the rocks with emplacement of granitoids (Turner 1983; Fitches *et al*., 1985 and Wright, 1985). These rocks were overlain by Cretaceous to Recent sediments. The Neo-Proterozoic-Ordovician Pan-African orogenic belts on the African network includes the Dahomeyan Terrane. This is a sub-fold belt (mobile belt) of the larger Trans-Sahara fold belt which extends from Hoggar (Algeria) to the Dahomiyides (Ghana, Togo, Benin, Nigeria and Cameroon).

The Dahomeyan fold belt represents the southern portion of the Trans-Sahara mobile belt. Nigeria lies in the heart of the Dahomeyan zone. It represents a collection of Neo-Proterozoic and older Precambrian rocks (believed to be part of the initial continental interpreted as originally forming parts of continental remains, island arcs and intervening basins) formed when the different lithosphere plates collided, with the West African and Congo Cratons been part of it (Fig. 2.1). The Eastern and Western Nigerian terranes are divisions of the Trans-Saharan Belt (Ferré *et al*., 1996).

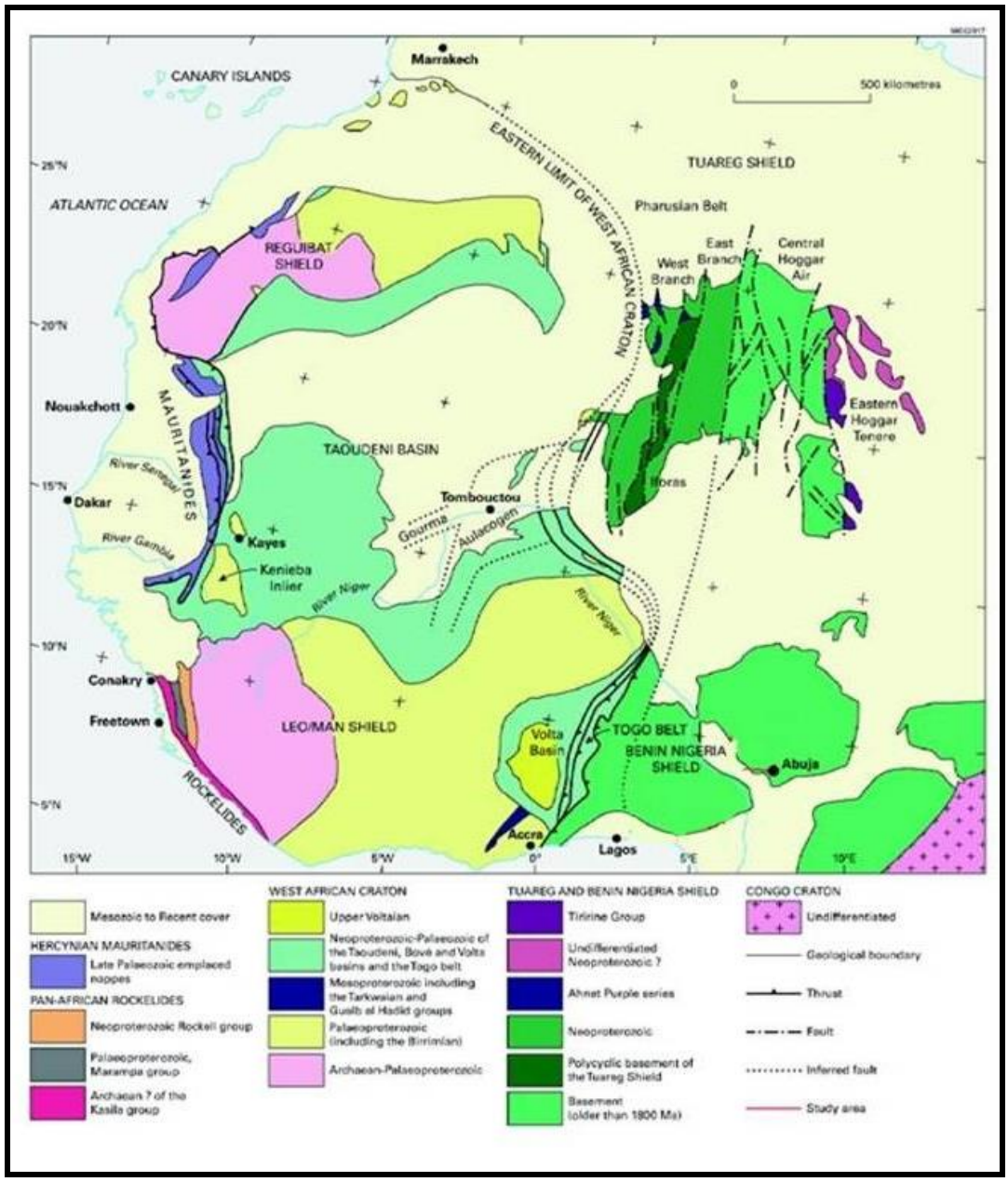

Figure 2.1: The Benin-Nigeria Shield in the context of the geology of West Africa (Ajibade and Wright, 1989).

The absolute ages of the protoliths of the Precambrian metamorphic rocks are poorly constrained but it is likely that Paleo-Proterozoic and Archaean rocks are present within the metamorphic terranes (Grant, 1970; Grant *et al*., 1972; Oversby, 1975; Ogezi, 1977, 1988; Bruguier *et al*., 1994; Dada, 1998, 2006; Dada *et al*., 1993). The basement rocks within Nigeria outcrop largely in the south-western and north central parts of Nigeria and minimally in the North-eastern and South eastern parts of the country (Fig. 2.2).

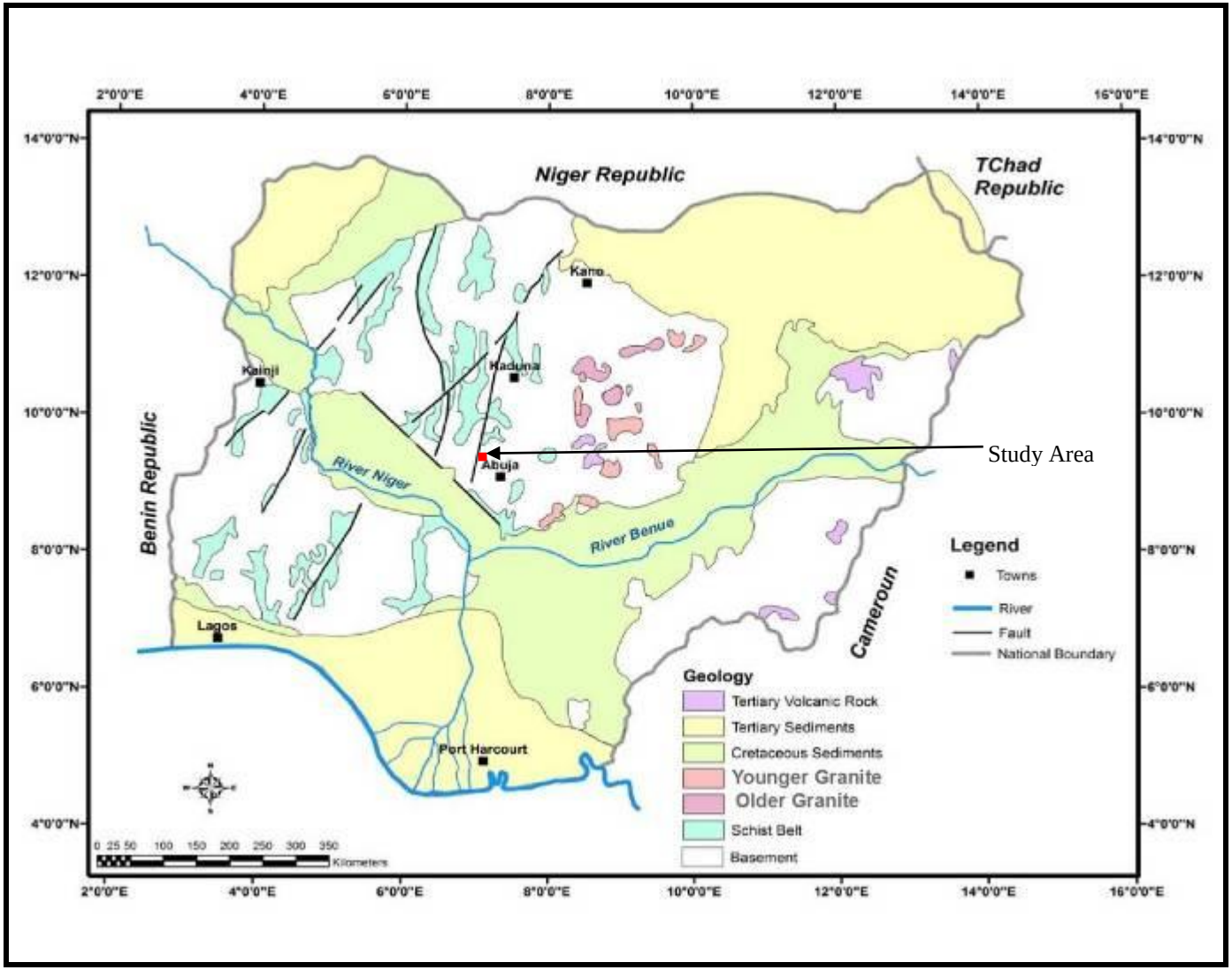

Figure 2.2: Generalized geological map of Nigeria (Modified after Nigerian Geological Survey Agency, 2014)

Rahaman (1988) classified the rocks into the following groups:

Migmatite–Gneiss–Quartzite Complexes: A heterogeneous group that comprises migmatitic and granitic gneisses, as well as small quantities of basic rocks (basic schist and amphibolites) and relict meta-sediments (Calc-gneisses and quartzite).

Pelitic and semi-pelitic schists: Quartzites, polymitic meta-conglomerates, calc-gneisses, marble, and meta-igneous rocks make up the lithology (amphibolites and talc-bearing actinonite-chlorite-chlorite schist).

Charnockitic, gabbroic and dioritic rocks: They are igneous rocks ranging in composition from norites to pyroxene diorites, enderbites, true charnockites, monzonites to pyroxene-syenites.

Members of the older Granites suite. These rocks are widely distributed throughout the Nigeria basement complex and they are in distinct plutons often of batholitic proportions. Compositionally they range from diorite to Tonalite to syenite and in texture from aplite to coarse porphyritic granite.

Metamorphosed to un-metamorphosed calc-alkaline volcanics and hypabassal rocks: Restricted to the Anka Schist belt of northeastern Nigeria. These comprise tuffs, rhyolites, rhyodacites, and dacites.

Unmetamorphosed dolerite and syenite dykes: These are a group of minor rock types found as dykes emplaced in older rocks.

2.2 Regional Geological Setting of the Study Area

The ‘Older Granites' which are suites of Pan-African (600–150 Ma) orogenic granitoids were intruded into the migmatite and schist within basement complex part of the study area (Figs 2.3a and b, Table 2.1). Ages ranging from Liberian (2,700 Ma), Eburnean (2,000–2,700 Ma; Grant, 1978; Ogezi, 1977), and Kibaran (1,100 Ma; Holt *et al*., 1978; Ogezi, 1977) down to Pan-African period (Russ, 1957) have been recorded for the migmatites, gneisses, and schists. The 'gniess-schist complex,' are the oldest rocks, after which the meta-sediments made up of pelitic and semi-pelitic schistose rock were deposited (Adekoya, 1993).

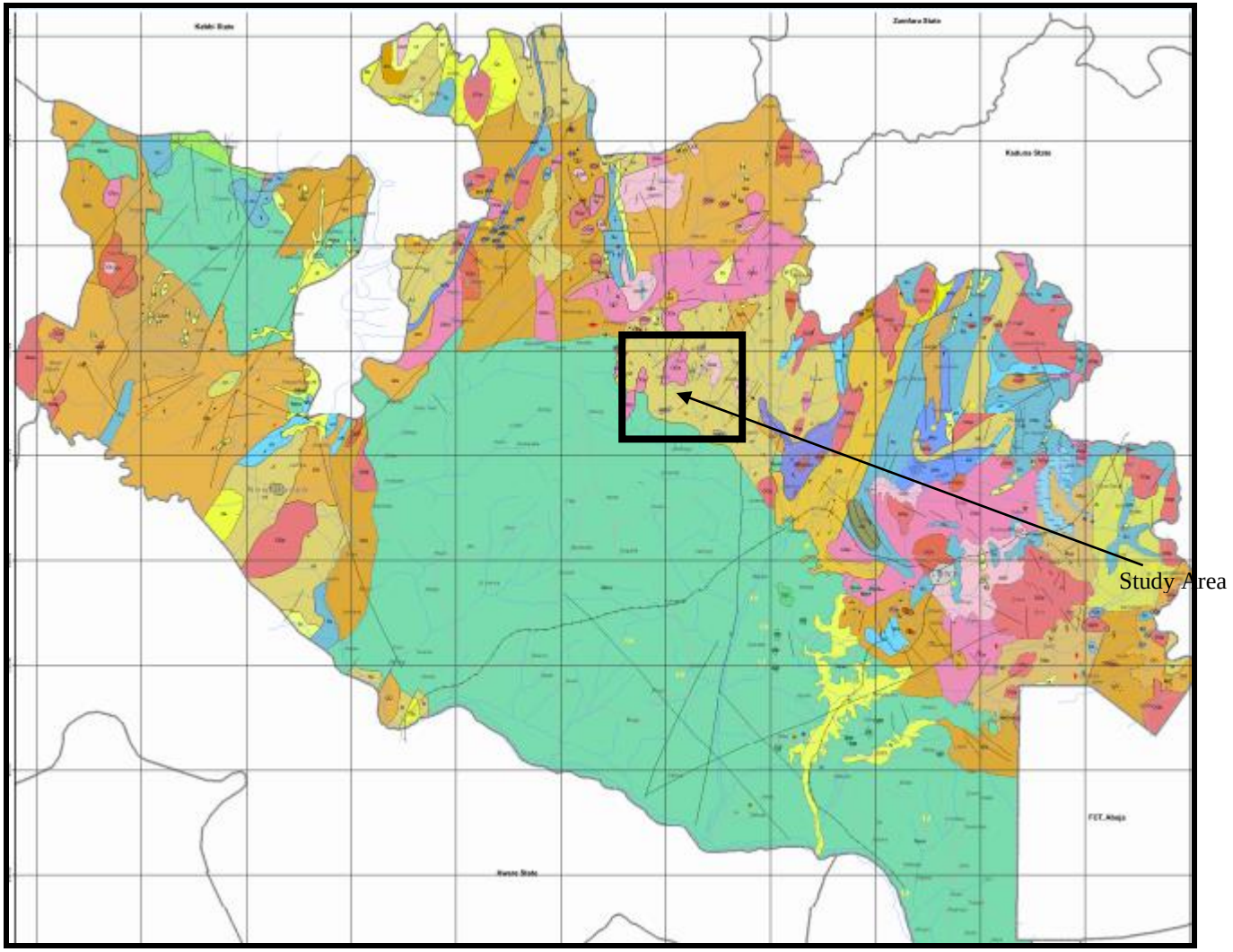

Figure 2.3a: Geological map of North-central Nigeria showing the study area. (Source: Nigerian Geological Survey Agency, 2006)

Table 2.1: Explanation to Geological map of North-central Nigeria showing the study area (Source: Nigerian Geological Survey Agency, 2006)

Explanation

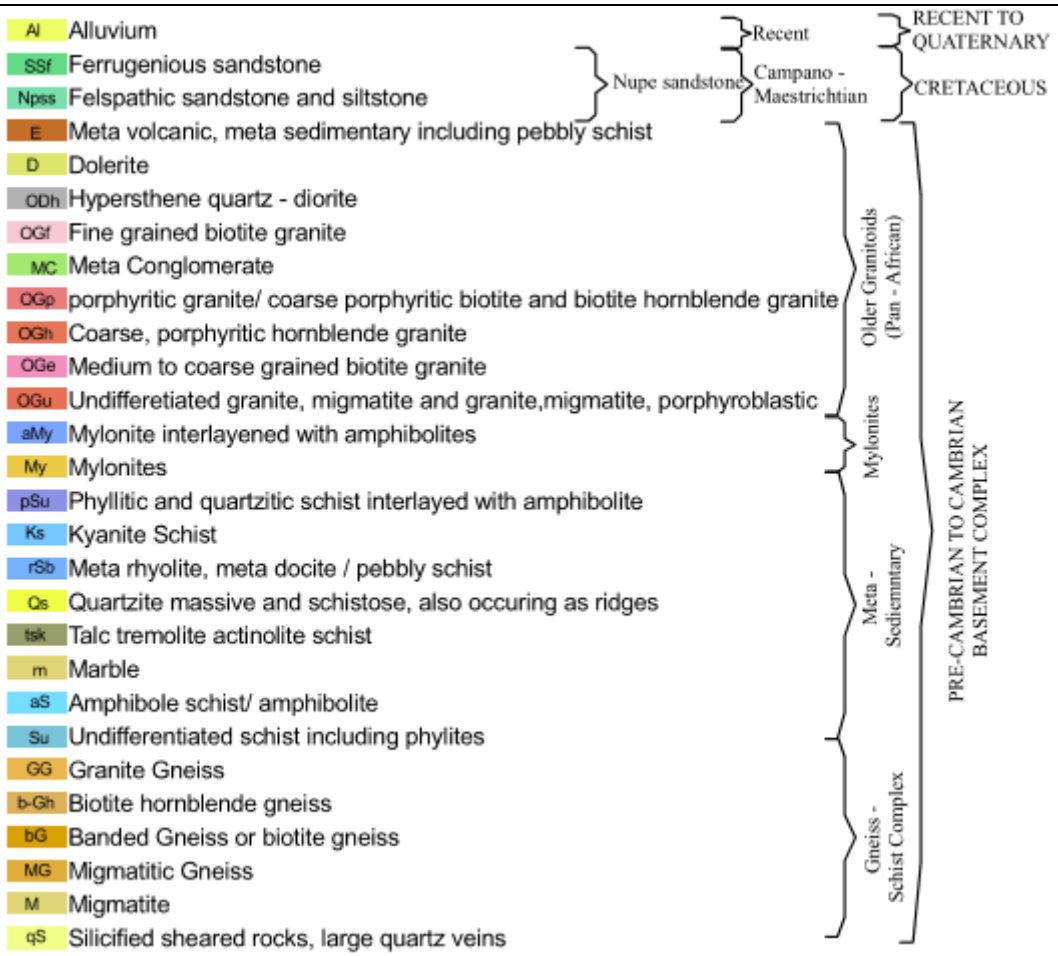

The Paiko Sheet 185 covers an area that is underlain by the western Nigerian Terrane and comprises migmatitic gneisses with infolds of low- to medium-grade supracrustal belts (schist belts), dominated by clastic meta-sediments, as well as variably deformed Neo-Proterozoic (Pan-African Older Granites) granitic intrusions, and smaller and less common meta-basic and meta-ultrabasic intrusions (Ogezi, 1977). The study area is underlain by basement rocks, mainly migmatite and meta-sedimentary rocks. Migmatite, banded – gneiss, quartzite, highly fractured granites with few intrusion of pegmatite and aplite are dominant. The main structural features in the area include the general N-S and NE-SW trending foliation (Fig. 2.3b).

The rocks (migmatites and gneisses) are of similar structural trend. This might probably suggest that they were deformed by a similar tectonic episode of different phase during the Pan Africa orogenic event. The migmatite-gneiss complex is considered to be the basement sensu stricto, and isotopic ages varying from Liberian to Pan-African ages have been obtained from the rocks. The Pan-African ages have been interpreted as due to isotopic re-homogenization in pre-existing rocks during the Pan-African orogeny (Oluyide *et al*., 2004*).*

The widely spread 'grey gneiss' of most metamorphic terranes which are Precambrian analogous to the magmatitic gneiss. The 'grey gneiss' are made up of variably migmatitic, quartzo-feldspathic gneisses which are equally erratically deformed, creating a wide array of tectonic and metamorphic fabrics. Though they are badly dated, values above 3.0 Ga are reported (Kröner *et al*., 2001), together with a range of about 1160 Ma for Meso-proterozoic (Grant *et al*., 1972; Ogezi, 1977). In general, the Precambrian rocks of Nigeria can be classified into three classes. The migmatite–gneiss complex, schist belts, and the Pan African Older Granite Series (Okunlola and Jimba, 2006).

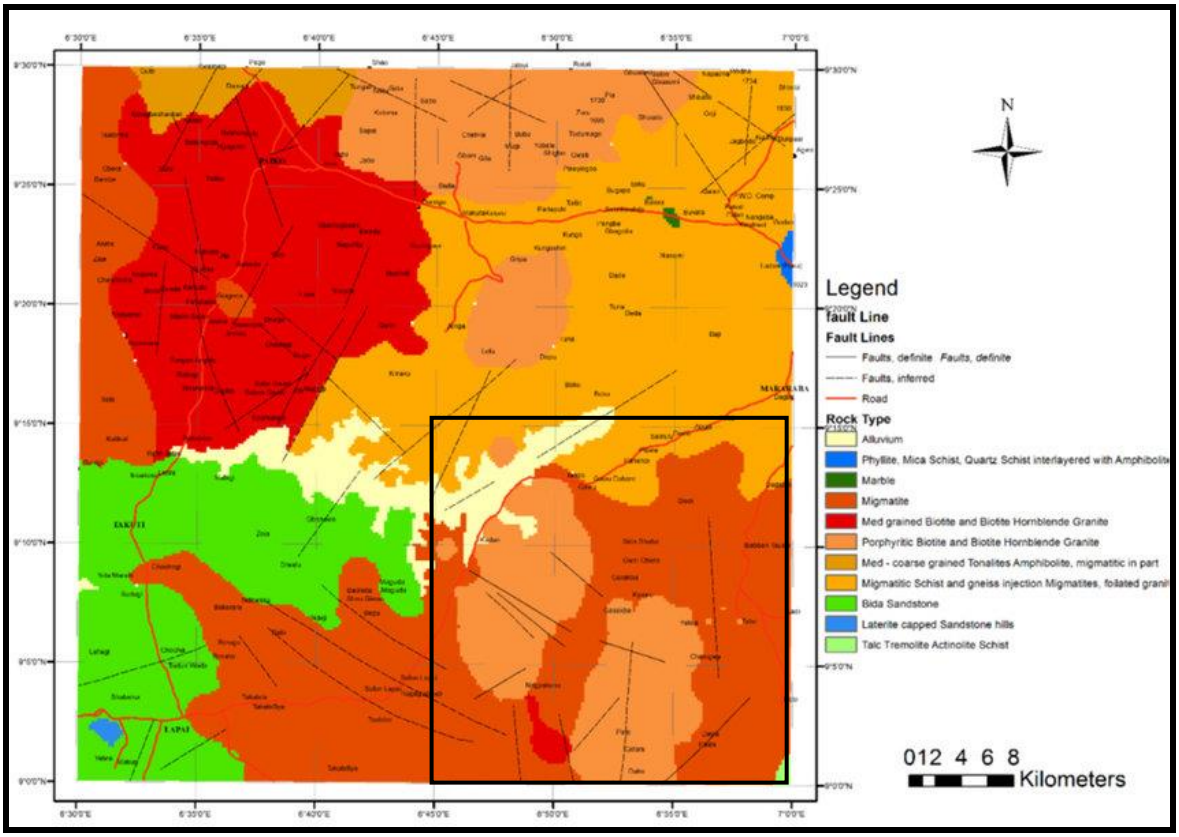

Figure 2.3b: Geological Map of Sheet 185 Paiko with the southeastern study area in black box (Source: Geological Survey of Nigeria, 2000)

The Baban Tsauni area according to Okunlola *et al*. (2007) is sitting on migmatite gneiss basement complex rock comprising of banded gneiss, granite gneiss, pegmatised migmatite, migmatised amphibolite, pegmatites, dolerite dyke and quartz veins. From their work (Okunlola *et al*., 2007), the pegmatised migmatite constitutes by far the most widely occurring rock type in the area. Their results indicate that the host rock, migmatite, is pervasively intruded by many bodies of medium to coarse grained complex pegmatites and quartz veins, resulting in its lithological classification as a pegmatised migmatitic rock in the region. The pegmatites are coarse-grained and somehow inherit the gneissic texture of the host rock. According to field observations, the pegmatites have fills fractures and shear zones that mainly trend northwest-southeast, with a few oriented north-south and northeast-southeast.

2.2.1 Structures

The main structural trends within the study area are the prominent N-S structures, NE-SW and NW-SE. These are structures related to the Pan-African orogeny (Burke and Dewey, 1972). According to Okunlola *et al.* (2007), the Pan African thermotectonic events (550 ± 100ma)is attributed as the most recent deformation episode within the study area which is researched to have being through a minimum of three deformation episodes (Fig. 2.4).

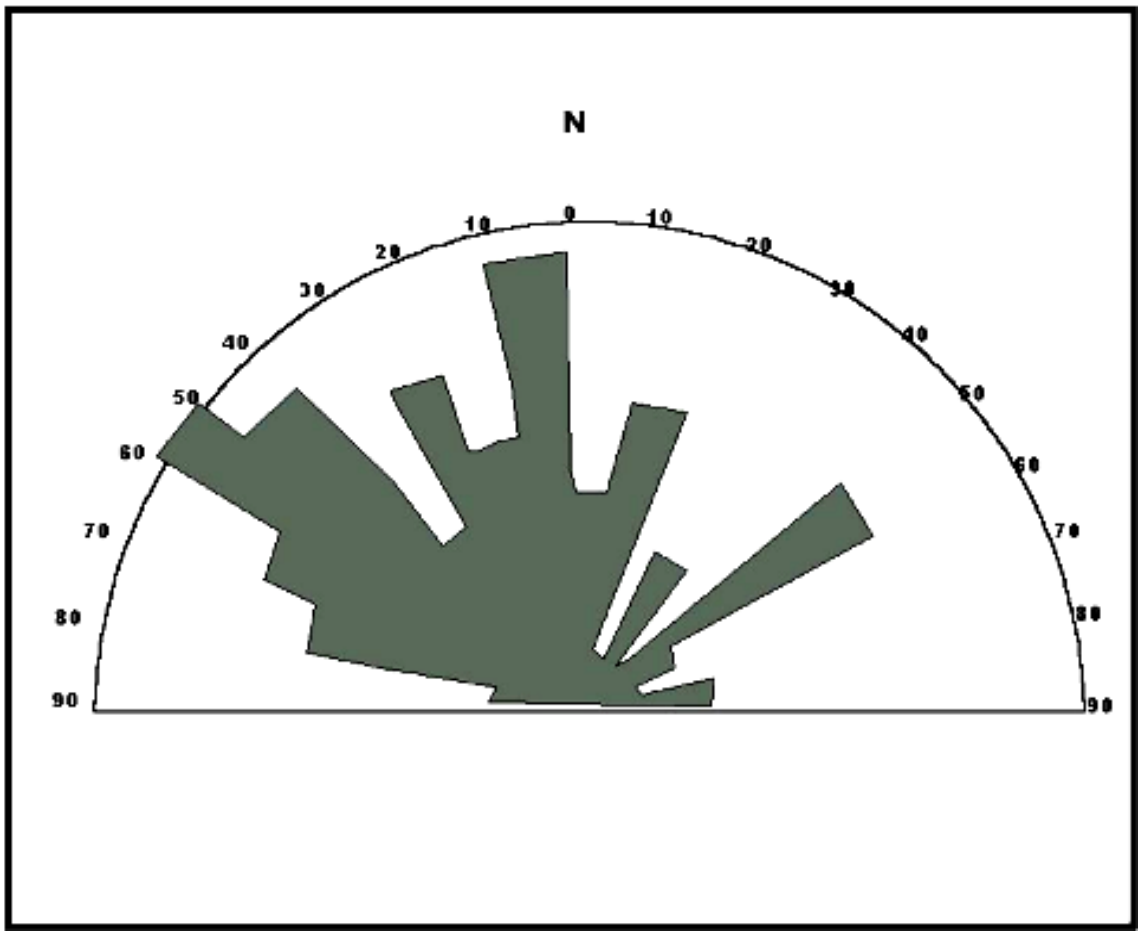

Figure 2.4: Frequency distribution diagram of strike within the study area (Source: Okunlola *et al*., 2007)

These deformation episodes resulted into observable fabrics of lineations, foliations, folds, faults and fractures. The foliation fabrics on the gneiss and migmatites are defined by prefeered alignment of the mineral associated with segregation into alternates band of felsic and mafic units. These banding of melanocratic and leucrocraatic segregations are often times truncated by augens boudins, remains of pre-existing rocks and quartzo-feldspathic veins, typifying various foliation trends of relatively different ages. It also confirms that the basement rock have undergo multiple foldings as observed from the exposures on the field. The folding patterns changes from tight intre folds on the migmatites to open folds on the banded gneiss. The plunge of the axial trace of the well rounded open folds is measured to be NNW/SSE (Okunlola *et al*., 2007). The quartz veins that play host to the sulphide mineralisation follow these NNW/SSE structural trends.

2.2.2 Mineralisation

The pegmatised migmatite gneiss is interpreted as the most inclined to mineralizing fluids. There have been a lot of artisanal mining activities in the area which is evident from the fresh and old mining pits in the area. Distinct sulphide mineralisation of the Pb ores varieties were observed as disseminated bodies within the pegmatite and quartz veins

These are more in locations where there are mapable shearing and fracture zones (Okunlola *et al*., 2007). Gold and associated sulphide mineralisation has been reported to be found in auriferous quartz veins, stringers, lenses, and oxidized regions in several sulphide mineralisation fields, (Garba, 2000; Woakes and Bafor, 1984; Russ, 1957). Primary gold mineralisation associated with quartz veins was documented by Truswell and Cope (1963).

2.3 Theories of Methods Used

In mineral prospecting, physical properties of the target mineral determine the method or combination of methods to be used. The associated sulphide mineralisations within the study area are epigenetic structurally controlled and disseminated within the host lithology. Consequently, the magnetic method would be used for structural setting and delineating intrusives, the radiometric method would be used for lithological boundary

delineation, while the electrical method would be used for characterization of the delineated structures and lithologies in terms of their resistivity and chargeability composition.

2.3.1 Magnetic Prospecting Theories

Over the years, magnetic prospecting has helped to locate faults, shear zones and fractures. These structures are targets for epigenetic structurally controlled mineralisation that host a broad range of mineral deposits and indirectly guide exploration for associated mineralisation. Igneous and metamorphic rocks are much more magnetic than sedimentary rocks (Dobrin, 1976). During magnetic survey, variations in magnetic susceptibility and remanent magnetization are used to interpret magnetic anomalies. Magnetic surveying is a natural source technique of geophysical exploration as it makes use of the earth's potential fields to assess and interpret geological problems. An aeromagnetic survey is a field acquisition method of geophysical survey conducted using an aircraft towed magnetometer for wider coverage with respect to time and field operations. The principle behind its operations is comparable to a ground magnetic survey performed with a handheld magnetometer, but it is possible to rapidly cover bigger regions of the earth's surface. As the aircraft flies over the target area, records of ambient magnetic intensity spatial variation which are as a result of variation in the earth’s magnetic field and temporal variations in solar wind are measured by the magnetometer. This variation arises from both regional effects and local effects from the distribution of magnetic minerals within the underlying rocks. A subtraction of the regional effect from the composite result gives the residual effect. The residual effects are due to spatial distribution and relative abundance of magnetic mineral. This is presented in the form of aeromagnetic maps.

For locations where regolith, water and weathered materials covers the rock outcrops and exposures, the spatial variation in the magnetic mineral content of the underlying rocks can be measured and presented inform of magnetic maps, to understand the geological structures within the upper crust (Burger *et al.,* 2006). Magnetic survey has been found to be very useful in geological mapping for lithology characterization and also in mineral prospecting. Some mineral deposits are associated with high magnetic

susceptibility as in the case of iron ore, while structural delineation has also been very useful in locating epigenetic structurally controlled mineralisation (Burger *et al.*, 2006).

2.3.1.1 Geomagnetic Field of the Earth

The geomagnetic field differs over time, and this variation is a very good measure to understudy the dynamics taking place within the core. The external field accounts for the Earth's magnetic field together with the internal field. The internal field, also known as the primary field, originates deep within the Earth (Herndon, 1996). Seismic studies showed the inner core to be in solid state and liquid for the outer core. The temperature of the core which is greater than the Curie temperature has a zero effect on the magnetic field of the earth. Studies indicate that the earth's magnetic field is as a result of flow of material in the outer core which generates electricity related to the flow of electrical current. An enormous electromagnet is efficiently created by the flow of these electric currents (Clark and Emerson, 1991).

According to Telford *et al.* (1990), the Earth's geomagnetic field is made up of three major parts which together makes up the priority in magnetic prospecting. The primary field, which deviate relatively with a little magnitude, is of internal origin. The second being a smaller field, when compared to the primary field and this field varies much quickly and originates outside the Earth. The third major part is made up of the spatial variations of the main field, which are usually smaller and are almost constant in place and time, and are as a result of shorter wavelength magnetic anomalies of the earth. He postulated that when an un-magnetized needle is allowed to orient itself freely when hinged at its focal point of gravity without any interference, it would naturally point in the direction that does not coincide with the earth's geographic limit called the earth's total magnetic field. This direction is the direction of the earth's magnetic field. This direction can be described using its declination (D) and the angle between the horizontal and direction of the total field with the true north. To define the major component of the magnetic field can thus be described in term of the magnitude of the Magnetic field (F_e), the dip angle from the horizontal (I) and its angle of declination (D) with the true north (Kono and Schubert, 2007). The seven magnetic elements are therefore the total magnetic

intensity ($F_{e)}$, inclination (I), declination (D), vertical field intensity (Z_e), horizontal field intensity ($H_{e)}$, component in x-axis ($X_{e)}$ and the its component on the Y-axis (Y_e) (Fig. 2.5).

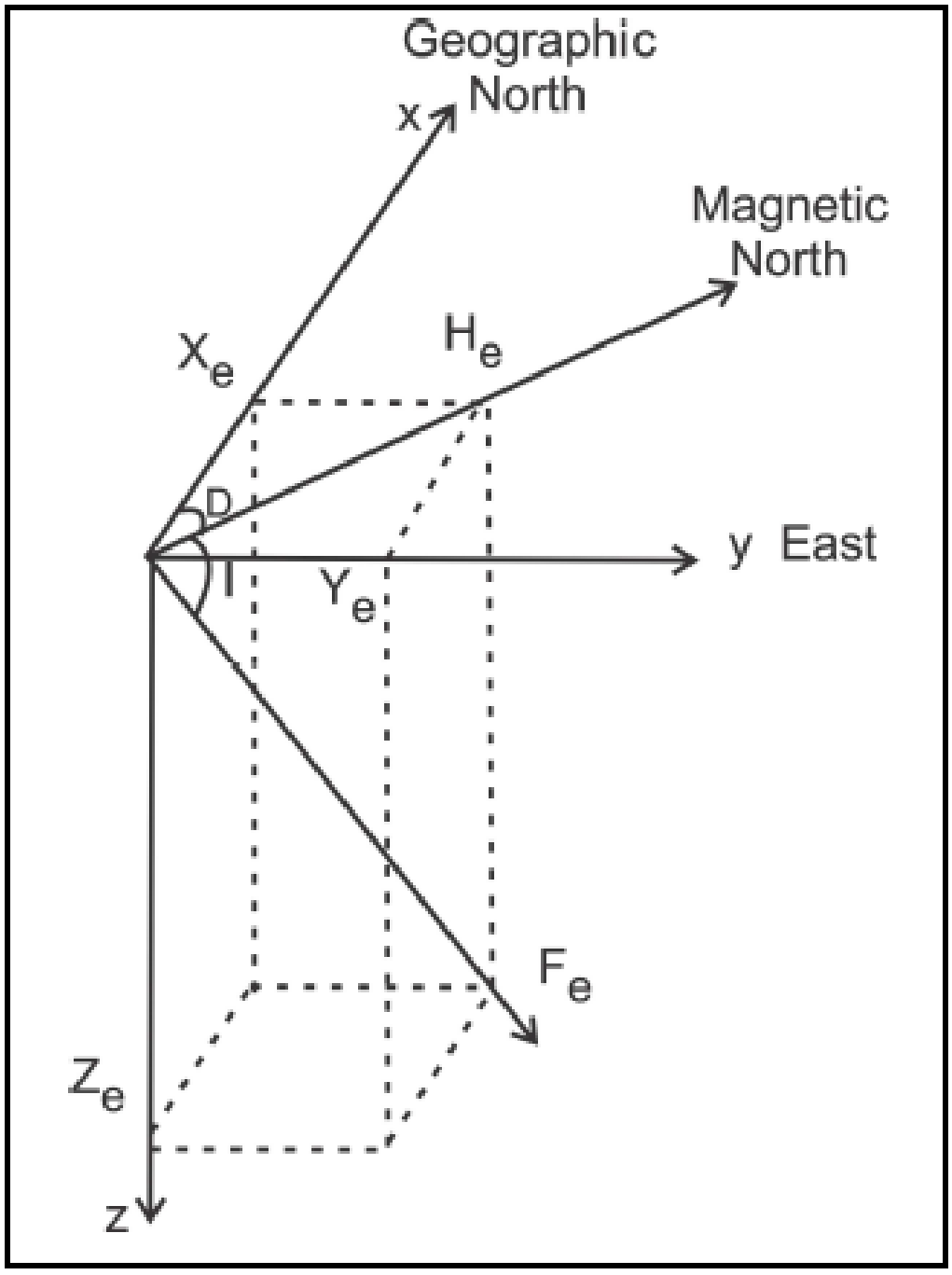

Figure 2.5: Earth's Magnetic Field Elements (Whitham, 1960)

Iron-bearing minerals in rock formed from cooling of molten magma behave like magnets and the minerals are oriented in the magnetic field. This phenomenon is equally obtainable in the sedimentary basin where the iron-bearing minerals within the sediments align in the direction of the magnetic field (Reeves, 1989; Petersen, 1990). Iron-bearing magnetic minerals (e.g. pyrrhotite and magnetite) create magnetic anomalies in (Rajagopalan, 2003).

2.3.1.2 Magnetic Susceptibility

This is the measure of propensity or natural tendency of a material to get attracted to a magnet or get magnetized when placed in a magnetic field. This is a function of the relative abundance of its composition in terms of iron-bearing magnetic materials and its geometry (shape and size) (Wemegah *et al.,* 2009). Despite the fact that there is remarkable variation in the susceptibility according to Telford *et al*. (1990) for a specific rock and an overlap between different rock types, the intrusive rocks igneous of basic composition has the highest while the sedimentary rocks has the lowest magnetic susceptibility.

Mathematically, the inducing field when expressed per unit volume can be related with the induced magnetization as shown: Volume susceptibility (κ): = J/H = M/H. Unit of volume susceptibility is related to the measurement system used. Hence, it is dimensionless. Where J is the magnetization magnitude (Induced strength or volume of magnetization in a susceptible material with magnetic susceptibility κ) and H is a function of an external filed applied (Clark, 1997).

2.3.1.3 Remanent Magnetization

As magnetic material is put in a magnetic field, it becomes magnetized by the external field, and the material becomes energized and magnetized by the magnetic field. Though some materials can retain the magnetization which is called permanent or remanent magnetization with its direction in the same direction as the inducing external field, naturally the induced magnetization effect is removed once the external field is removed. Rocks with variety of composition of mineral with varying susceptibility can

exhibit any of these two types of magnetization (Clark and Emerson, 1991). Remanent magnetization would still be active when the external field is removed, but the induced magnetization is only active when the inducing field is present. The phenomenon of paleo-magnetism is based on these principles and it is actually a preserved magnetic direction at the time the rock is formed, which helps in the study of rock movement over time (Strangway, 1970).

2.3.1.4 Geomagnetism at Low Magnetic Latitudes

The ambient magnetic field around the magnetic equator of the earth, which is about 10° of the geographic equator, is in a direction nearly horizontal and an almost N-S trend (Beard and Goitom, 2000). Within this low latitude region, the range of magnetic field intensity is between 25,00nT and 40,000 nT which is about half of the magnetic field intensity at the poles. Due to the reduction in the magnetic field intensity of the regions at the magnetic equator (low latitudes), local magnetic anomalies of same or similar sources with those at high latitudes are relatively lower at lower latitudes and higher at higher latitudes towards the poles.

With the orientation of the inducing magnetic field in a horizontal direction, extending magnetic anomalies trending N-S may show no significant anomaly except for locations close to the poles of the structures. Magnetic readings near and around a path that passes through a magnetic object in the direction of the Earth's Field are high, while values everywhere else are low. The amplitude correction for N-S trending features at very low latitudes, amplifies more noise which causes distortions of the anomalies due to effects of magnetized bodies in other direction from the inducing field. Magnetic anomalies observed anywhere rather than magnetic poles are asymmetric due to the dipolar nature of the geomagnetic field, despite the fact that causative bodies' distribution could be symmetric. The result of this is the complications encountered in magnetic data interpretation (Rajagopalan, 2003).

2.3.2 Radiometric Prospecting Theories

The physical properties of source rocks or material that are radioactive in nature and the ability to detect these sources through the use of remotely sensed data formed the basic principle of operation in radiometric prospecting (Boadi *et al*., 2013). In radiometric prospecting, the spatial distributions of radioactive decays are measured in rock units a function of gamma radiation. The energy (frequency) which shows the isotope that produces the radioactive decay. It serves as a guide in geology mapping, as pathfinders or indicators in mineral exploration and as a detector radioactive mineral exploration. It detects and maps out radioactivity in rocks and soils. In geology mapping, depth of penetration is a constraining factor as the depth of penetration is very shallow. The technique gives spatial concentration of estimated apparent values for the most naturally occurring radioactive elements, potassium (K), equivalent uranium (eU), and equivalent thorium (eTh). The use in mapping is on the assumption that the spatial distribution of relative or absolute concentration of radioactive elements vary significantly with lithology.

Like some other airborne approaches in geophysical surveys, gamma-ray data can equally be collected as airborne, making acquisition over a large area very rapid. Radiometric signature of the major naturally occurring radio-elements depicts the unweathered rock type making the geology of the study area (Gunn *et al*., 1997). During mineral exploration programmes, various datasets are collected, ranging from geochemical to various geophysical methods, hence radiometric data compliments the other data for better interpretation of the geological setting and mineralisation style (Shives *et al*., 1997). Radiometric survey is quite fast for geochemical studies of the major naturally occurring radio-elements and it's cost-effective.

2.3.2.1 Fundamentals of Radioactivity

Nuclear decay or disintegration is a state when two different atoms of an element are having different neutron number (mass number) but equal atomic number; they are referred to as isotopes of each other. In a situation where one of the isotopes becomes unstable, it emits energetic ionization radiation thereby changes to a more stable nuclei. Such isotopes are referred to as radioactive isotopes, while the nuclei are referred to as

radio-nuclei. (Nicolet and Erdi-Krausz, 2003). The time taken for half of particular radio-nuclei to decay or disintegrate is the half-life of the radio-nuclei. In essence, after an half-life, half of the original radio-isotope is left, and after another half-life, one quarter of the initial radio-isotope is left (Minty, 1996). Thus, determining the magnitude of the daughter radio-nuclei can be use to estimate the initial concentration of the individual element in the decay series.

The specific parameter measured on the field is the gamma-ray intensity. The geophysical equipment used to obtain this target parameter is called Gamma-ray spectrometer. Its potentials lies in the fact that it employs sensitive, automated calibrated detector systems that provide a good estimate of ground concentrations of the three most common, naturally occurring radioactive elements. Due to the usually elevated contrasts in the radioactive components of granitic and gneissic rocks, the method is ideally suited for mapping levels of radioactive components within these terrains. Sedimentary terrains typically have low K, U, and Th abundance. Killeen (1979) showed that surface ground studies and radioactivity logs for borehole geophysics, frequently differentiate separate lithologies by differences in thorium or potassium-bearing mineral abundances. Therefore, given sufficient sensitivities and ground controls, even minor radioactive elements variations can be delineated.

2.3.2.2 Disequilibrium in Radioactive Series

The removal or partial addition of one or more decay products to the system in a decay series results in Disequilibrium in the series (Minty, 1996). Disequilibrium is not associated with potassium as it has no disequilibrium problem. Thorium on the other hand rarely have problem of disequilibrium, but disequilibrium is common with uranium decay series, which shows up at various positions along the Uranium decay sequence: Uranium isotope ^{238}U can decay to give ^{234}U, while ^{234}U can also be leached selectively to ^{238}U. It is therefore possible to discard Thorium (^{230Th}) and Radium (^{226}Ra) in the decay series. Due to the mobility of Radon (^{222}Rn) gas, it readily gets leached to the atmosphere from rocks and soils (Nicolet and Erdi-Krausz, 2003).

Based on the assumption of equilibrium and disequilibrium conditions, uranium concentration is estimated as 'equivalent' uranium (eU), likewise thorium as 'equivalent' Thorium (eTh). Though thorium concentration is nearly at equilibrium (Milsom, 2003). 'Equivalent' refers to the assumed equilibrium between the daughter nuclei and its original isotope. With Uranium, gamma rays emitted by ^{214}Bi at 1.76 MeV are estimated and for Thorium, the gamma radiations emitted by ^{208}Ti at 2.41 MeV are estimated also. i.e. eU is equivalent uranium concentration by weight unit is ppm, eTh is equivalent thorium concentration by weight unit is ppm. K is Potassium concentration K^{40} and the unit is %. The methods depends upon the fact that absolute and relative concentration of the radio elements K, U and Th vary measurably and significantly with lithology.

2.3.2.3 Geometry of the Source Detector

Gregory and Horwood (1961) showed that, scattering of the source is experienced due to the increasing Compton continuum, when the source thickness increases. Therefore, the photo-peaks are decreased in comparison to the background of Compton. This impact is more pronounced at lower energy level, due to the fact that there is spontaneous attenuation with photons of high-energy than the photons for low-energy.

Thus, thickness has a significant effect on the shape of observed spectra. Material between the source and the detector Terrestrial increases the source radiation. The attenuating material in between the detector and the source determines the shape of the observed spectrum. In relation to the energy continuum the photo-peaks are reduced as in the case of increasing attenuation. The detector height above the ground, thickness of overburden that are not radioactive, the detector response function and more importantly the source geometry are all factors that determines the concentration of the measured spectra (Nicolet and Erdi-Krausz, 2003).

2.3.2.4 Geochemistry of Radioelements

Potassium (K): The chemistry of potassium is monovalent under neutral state. With a percentage composition of about 2.35%, it forms one of the major constituent elements of the earth crust. It exhibits a volatile lithopile property being an alkali element. (Nicolet

and Erdi-Krausz, 2003). Orthoclase and microcline feldspars with about 13% abundance mark the major host of potassium in rock forming minerals. This is relatively followed by Biotite and Muscovites that makes up the micas with about 8% potassium composition. Potassium on the other hand is practically zero in mafic minerals (Dickson and Scott, 1997). Thus, potassium concentrations are relatively high in felsic rocks but absent or low in mafic rocks (Fertl, 1983). Potassium is released during weathering,. These are taken up to form potassium bearing minerals or small amount absorbed by under suitable conditions. In metamorphic rocks and intrusives, the continuous series as shown on the Bowen reaction series containing the plagioclase feldspar series, the nepheline and leucite feldspathoids, biotite and muscovite contains the greater percentage of the potassium contents (Dickson and Scott, 1997).

Thorium: Thorium as a cation exhibits a valency of Th^{4+} in solution and forms insoluble precipitates with the anions fluoride, oxalate, iodate and phosphate. In solid state, Th shows valency lower than Th4+ (Krishnaswami, 1999).Thorium is soluble in acid solutions, with increasing solubility in the presence of humic acid (Chopin, 1988). Major Thorium bearing minerals (such as monazite and zircon) may accumulate as heavy mineral sand deposits as they are not easily broken down during weathering activities. Thorium occurring with Fe or Ti-oxides-hydroxides and with clay is as a result of breakdown of minerals during weathering. Thorium occurs in trace amount in some rock forming minerals and is a major constituent of the accessory minerals zircon, apatite and sphenes at levels greater than 1000ppm (Dickson and Scott, 1997).

Uranium: Uranium is highly mobile and reactive, having a mean concentration of about 3 ppm in the crust (Langmuir and Hermans, 1980). It occurs in trace amount the rocks such as granites, but the percentage can be larger in mineralized granites and also pegmatites. Other occurrences of uranium can be found in sedimentary formations and hydrothermal veins. As in the case of potassium, uranium is equally released during weathering. When such happens, they are found in authigenic iron oxides and clays. They could also

precipitate, forming huge deposits under a favourable reducing condition (Dickson and Scott, 1997).

2.3.2.5 Applications of Radiometric Method

Explorations for Uranium and Thorium deposits about 3-4decades ago mark the most direct application of radiometric surveying using the gamma ray spectrometer (Dickson and Scott, 1997). In its application, anomalies of uranium and thorium enrichment can be delineated on profile plots and gridded map presentations, where subtle radiometric anomalies are attenuated using ratios of the measured radioactive elements coupled with statistical analysis of image processing. The mineral phase that makes up the radioelement in a radiometric survey would be better understand using the standard geochemical analysis and microscopic studies of samples from the host rock or sediments (Charbonneau, 1991).

- The changes in concentration of the three radio-elements accompany most major changes in lithology; hence the method can be used as a geologic mapping tool.
- Uranium deposit can be directly detected with radiometric surveys.
- Primary geologic processes can be indicative of variations in radioelement concentrations such as the action of metamorphic processes.
- Intrusives and mineralisation related to them can be detected with their variation and concentration.
- Secondary geological processes like supergene alteration and leaching are equally characterized by these variations.

Gamma rays are limited in term of depth penetration when passing through soil and rocks. Thus, the exploration of radioactive elements such as uranium largely depends on factors such as the location at which the measurement is taken, the relative concentration of uranium in the source been mapped and its size and geometry (Nicolet and Erdi-Krausz, 2003). The percentage composition of radioelement in a source varies with hydrothermal processes. This occurs often with potassium, where the potassium concentration becomes elevated when the source rock is undergoing alteration processes. The alteration signature intensity invariable gets masked off with weathering activities. Thorium and Uranium are

less affected, with thorium been more susceptible than uranium (Dickson and Scott, 1997).

To understand alteration process and effectively delineate alteration zones, the ratio of potassium to thorium (K/Th) concentration gives a better resolution and classification than just the potassium concentration alone. With the potassium alteration process, thorium could get mobilized owing to mineralisation processes and becomes depleted with respect to areas of k-alteration and intense silicification. On the other hand, the thorium mobilization effect is observed on thorium rich materials such as laterite where the concentration is elevated. Establishing the responses due to the effect of alteration, weathering, silicification and different rock type would positively guide exploration, where their signature and effect can be evaluated for mineralisation potential as related to radio-elements.

2.3.2.6 Radioelement Distribution in Rocks and Soils

According to Dickson and Scott (1997), various rock types and formations can be classified based on the relative abundance of radioactive elements. Findings from research work conducted by Killeen (1979) for Geological Survey of Canada on igneous rocks shows that a rock having composition of the three (3) major relatively abundance radio-elements of potassium, thorium and uranium in the ratios 2.5%, 3 ppm and 15 ppm respectively might likely be an intrusive or extrusive (granitic) rock or shale, while a ratio of less than 1%, less than 1 ppm and less than 5 ppm respectively could be anything except shale or felsic magmatic rocks, During magmatic crystallization, potassium is highly incompatible.

The radioelement composition of a rock is not altered during metamorphism as shown in the case of granite metamorphosing to gneissic rock and ordinarily, sedimentary rocks shows characteristic radio-element composition of the parent rocks where the sediments comes from. Significant variation does exist with mature and immature sediments. While immature sediments shows prominently the radio-element composition of the source rock, more mature sediments could possible show characteristic change in radio-element composition. A typical example is granitic source rock showing relatively

high radio-element as compared to mature sediments composed majorly of quartzitic materials and showing relatively low radio-element content (Dickson and Scott, 1997).

Mineralogical composition in granitic rocks varies, thus granite exhibit wide variation in weathering patterns and this could also be due to physiographic conditions and the weathering regime. During the process of soil formation (pedogenesis), granitoids for example lose close to 20% of the radio-element content. Other significant changes could be due to contamination through sediment transportation (Darnley, 1996)

According to Wilford *et al*. (1997), processes such as transportation by air, eluviations, colluvial materials and soil movement apart from in-situ weathering could show significant variation in radio-elements content especially within the top horizon of the soil profile.

2.3.3 Theories of Electrical Prospecting

In investigating near surface anomaly that has a distinctive physical property related directed or inversely to conductivity, the use of electrical method of geophysical prospecting is readily deployed to characterize the anomaly for subsequent interpretation. This method of geophysical prospecting dates back to 1912 and 1915 with the debut work of Conrad Schlumberger and Frank Wenner respectively (Kunetz, 1966). Subsequently, various authors and researchers have solved lots of applied geology problems using the electrical method. This method had metamorphosed and improved greatly especially with resistivity and induced polarization as used in hydrological studies, mineral exploration, engineering geology and environmental studies (Dahlin and Loke, 1998; Olayinka and Yaramanci, 2000). Over the years, there had been great improvements from the traditional horizontal layering techniques of interpretation which are fast been replaced with 2-dimensional and 3-dimensional models for effective interpretation. Data acquisition systems have also undergone lot of technological advancement from the point measurement to use of multi-electrode configuration automated systems.

With electrical method, the resistivity at the subsurface are measured alongside the metallic mineral distribution in form of degree of chargeability. These measurements give apparent resistivity and degree of chargeability of the source body. These measurements

are related to various geological parameters like fluid and mineral composition, porosity and permeability of the source been measured. Advancement in the data acquisition system has given rise to better results with higher resolution and more credibility. Now, powerful transmitters and multi-channel receivers are been deployed to simultaneously carry out data acquisition of various electrical parameters including apparent resistivity and chargeability (Stummer and Maurer, 2001; Auken *et al*., 2006). With the induced polarization method, though similar to the resistivity method other than it requires higher current than the resistivity sent into the ground as charges. This method is growing significantly with mineral exploration to detect disseminated or low concentration conductive or chargeable mineral deposit.

While determining the resistivity of rocks, Schlumberger Conrad also discovered the polarization effect from chargeable subsurface materials (ores). Thus, induce polarization as a geophysical prospecting technique is use to identify the electrical chargeability of subsurface materials. The measurement can either be made in the Time Domain or in Frequency Domain. In Time domain, when the injected current is cut off, the voltage decays is measured as a function of time, while for frequency domain alternating current is injected with varying frequencies. In response to this, voltage phase-shift is measured to evaluate the spectrum of the impedance with the varying frequencies of current injections.

2.3.3.1 Fundamental Theory of Geo-electrical Resistivity Survey

Electrical Resistivity technique of geophysical prospecting is based on the physics principles of Ohm's law. This governs the flow of current into the ground and the determination of its potential difference. Thus, resistivity contrast (inverse of conductivity) within the subsurface defines a particular anomaly been investigated or interpreted. The geo-electrical resistivity technique is based on the Maxwell's equation of electromagnetic (Grant and West, 1965; Ward and Hohmann, 1987).

Ohm's law: $R = V/I$

Where R is the electrical resistance, V is the potential difference and I is the injected current. The resistance, *R is* related to the geometry or dimension; cross-sectional area, *A* and length, *l* through the resistivity (ρ) or its inverse, conductivity (σ) by: $\rho = 1/\sigma = RA/l$.

Given a wire (cylinder) of length (l) and cross sectional area (A) carrying current (I) (Fig. 2.6).

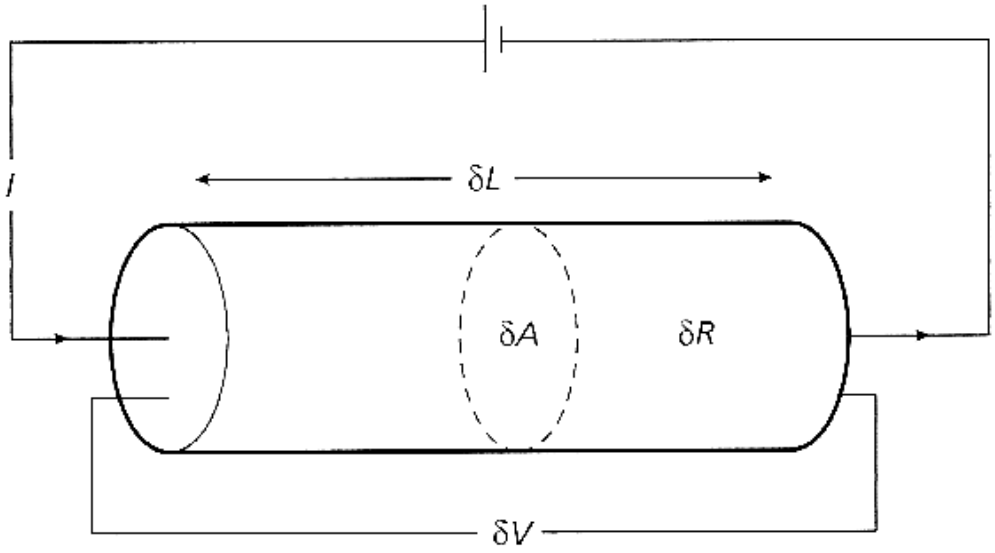

Figure 2.6: Illustration of Electrical Resistivity based on Ohm's Law

The resistance (R) of the wire to the flow of current is related directly to the length (L) and cross sectional area (A) as expressed in equation below:

$$R \propto \frac{L}{A} \tag{2.1}$$

$$R = \rho \frac{L}{A} \tag{2.2}$$

Where the constant of proportionality (ρ) is the electrical resistivity (in Ωm).
According to the Ohm's Law

$$R = \frac{\Delta V}{I} \tag{2.3}$$

Where ΔV is the potential difference across the wire and I is the electric current through it. Combining equations 1.2 and 1.3 and re-arrange,

$$\rho = \frac{A\Delta V}{LI} \tag{2.4}$$

Thus, from equation 1.4, the resistivity of a simple geometry can be calculated for any homogeneous and isotropic medium. However, for a semi infinite medium, the resistivity at every point must be defined. If parameters A and L of an element within the semi-infinite medium are shrunk to infinitesimal size then:

$$\rho = \frac{\lim_{t \Rightarrow 0} \frac{\Delta V}{L}}{\lim_{A \Rightarrow 0} \frac{I}{A}} = \frac{E}{J} \tag{2.5}$$

Where J is the current density and E is the electric field. Therefore:

$$J = \frac{E}{\rho} = \sigma E \tag{2.6a}$$

Where σ is the conductivity.

The ground apparent resistivity equation can be developed by considering a current source located at the surface of a semi – infinite earth (Fig. 2.7). The current flows radially from point C through a hemisphere of radius r and surface area $2\pi r^2$. The current density (J) at distance r is defined as:

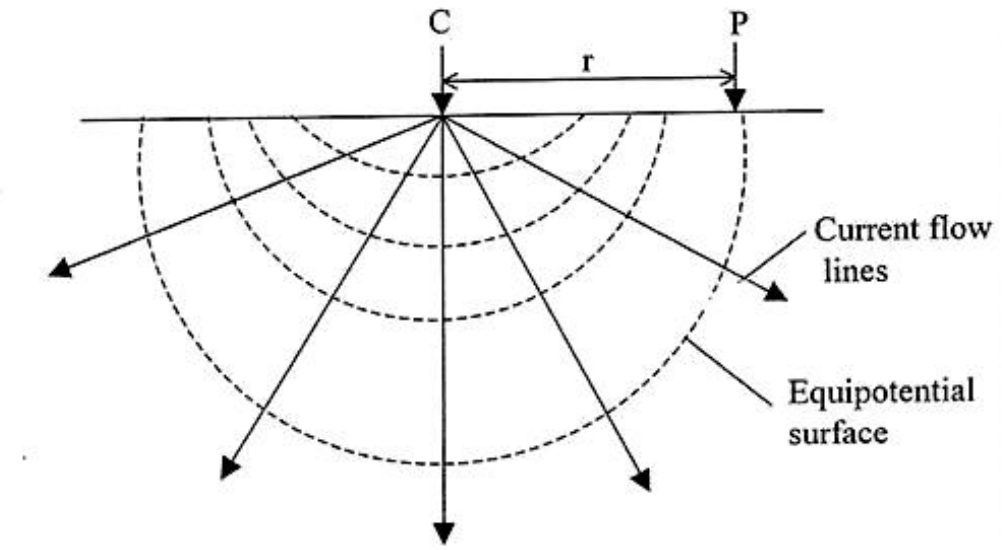

Figure 2.7: Point Current Source at the Surface of a Hemispherical Earth(C- Current source electrode, P – Potential measuring point electrode)

$$J = \frac{I}{A} \quad (2.6b)$$

Where A is the surface area ($2\pi r^2$) of the hemisphere.

$$J = \frac{I}{2\pi r^2} \quad (2.7)$$

But

$$J = \sigma E = -\sigma \nabla V \quad (2.8)$$

Where σ is conductivity (or inverse resistivity), E is electric field and V is potential. Therefore:

$$J = \frac{I}{2\pi r^2} = -\sigma \nabla V = -\sigma \frac{dV}{dr} \quad (2.9)$$

Equation 1.4 can rearranged thus:

$$dV = -\frac{I}{2\sigma\pi r^2} dr = -\frac{I\rho}{2\pi r^2} dr \quad (2.10)$$

Integrate both sides of equation (1.5)

$$\int dV = -\frac{I\rho}{2\pi} \int \frac{1}{r^2} dr \quad (2.11)$$

$$V = \frac{I\rho}{2\pi r} \quad (2.12)$$

Equation 1.12 defines the potential at point P due to current at point C. That is, equation 1.12 defines the potential equation of a 2 – electrode array system (one current and one potential). But four electrodes (2 current and 2 potential) (Fig. 2.8) are used in electrical resistivity survey.

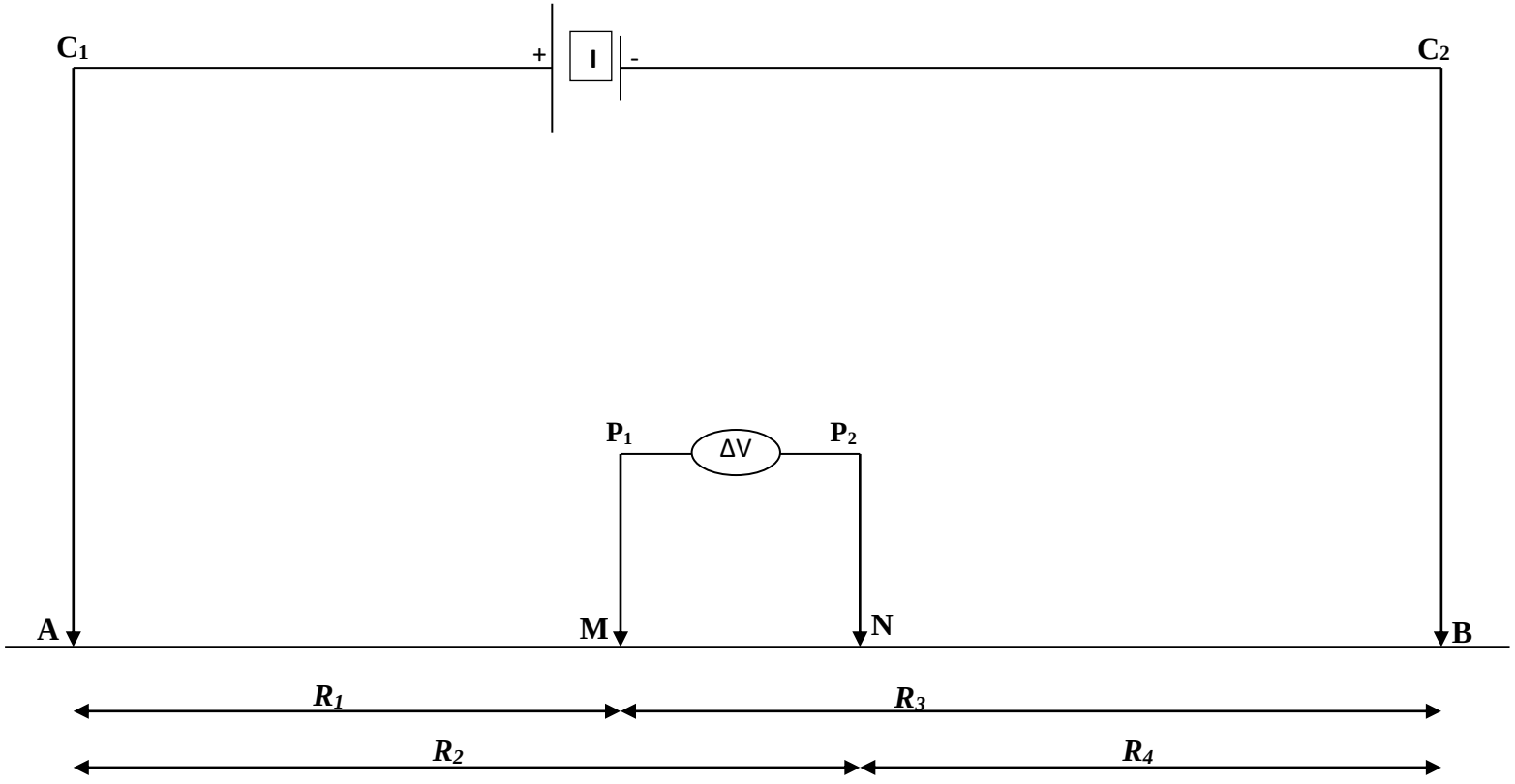

Figure 2.8: Typical four electrode array system used in resistivity

The potential (V) at M due to current at (A) is defined by the equation

$$V_M^A = \frac{I\rho}{2\pi r_1} \tag{2.13}$$

The potential at M due to current at B is expressed as:

$$V_M^B = -\frac{I\rho}{2\pi r_2} \tag{2.14}$$

Potential at M due to current at A and B can be expressed as

$$V_M^{A,B} = \frac{I\rho}{2\pi}\left(\frac{1}{r_1} - \frac{1}{r_2}\right) \tag{2.15}$$

Potential at N due to current at A is defined as

$$V_N^A = \frac{I\rho}{2\pi r_3} \tag{2.16}$$

Potential at N due to current at B is defined as

$$V_N^B = -\frac{I\rho}{2\pi r_4} \tag{2.17}$$

Potential at N due to current at A and B can be expressed as:

$$V_N^{A,B} = \frac{I\rho}{2\pi}\left(\frac{1}{r_3} - \frac{1}{r_4}\right) \tag{2.18}$$

What is measured in resistivity survey is the potential difference between M and N which is defined as:

$$V_M^{A,B} - V_N^{A,B} = \Delta V = \frac{I\rho}{2\pi}\left(\frac{1}{r_1} - \frac{1}{r_2} - \frac{1}{r_3} + \frac{1}{r_4}\right) = \tag{2.19}$$

If equation (1.19) is re – arranged:

$$\rho = 2\pi \frac{\Delta V}{I}\left(\frac{1}{\frac{1}{r_1}-\frac{1}{r_2}-\frac{1}{r_3}+\frac{1}{r_4}}\right) \quad (2.20)$$

But $\frac{\Delta V}{I}$ = R (Resistance)

Hence;

$$\rho = 2\pi R\left(\frac{1}{\frac{1}{r_1}-\frac{1}{r_2}-\frac{1}{r_3}+\frac{1}{r_4}}\right) \quad (2.21)$$

Equation 1.21 is the true resistivity equation for a homogeneous and isotropic earth. The earth is however not homogeneous so what is measured is an apparent resistivity (ρ_a) defined as:

$$\rho_a = 2\pi R\left(\frac{1}{\frac{1}{r_1}-\frac{1}{r_2}-\frac{1}{r_3}+\frac{1}{r_4}}\right) \quad (2.22)$$

Equation 1.17 can be simply expressed as: $\rho_a = RG$ (2.23)

Where G = $2\pi\left(\frac{1}{\frac{1}{r_1}-\frac{1}{r_2}-\frac{1}{r_3}+\frac{1}{r_4}}\right)$ (2.24)

G is the geometric factor of the electrode array.

2.3.3.1.1 Electrical properties of earth materials

There are two ways in which electric current flows within the earth's subsurface at near-surface depth. These are electrolytic and electronic conduction. In electrolytic conduction, the current flows through ions in the underground water while current flows through electrons that are free e.g. metals for electronic conduction. Current flows through underground water i.e. electrolytic conduction are common mechanism in engineering, environment and hydrological studies. Electronic conduction is more particular with mineral prospecting where conductive minerals are present, such as sulphides and graphites.

The resistivity values of Igneous and Metamorphic rocks are relatively higher than that of sedimentary rock, but the resistivity value actually depends of their intensity of fracturing if fractured, and the degree or percentage of the fractures filled by underground water. With this, the range of resistivity value of a particular rock type can varies over a wide range e.g. between 1000 – 10,000,000 Ωm depending on the level of fluid filling the fractures. This property is very useful in hydrological groundwater survey and solving engineering geology problems (Table 2.2).

Table 2.2: Rocks and Minerals physical properties (Modified after Parasnis, 1971)

Type	Saturated Density	Magnetic Susceptibility K X 10^6 (Si)	Electrical Resistivity (Ohm-Metre)
Arsenopyrite (FeAsS)	5.9-6.2	2.103	10^{-4} – 10
Cassiterite ($Sn0_2$)	6.8-7.0	-	$5x10^{-4}$ - $1o^{+4}$
Chalcocite (Cu_2S)	5.5-5.8	-	10^{-4} - $4x10^{-2}$
Chalcopyrite ($CuFeS_2$)	4.3	$4x10^2$ – $2x10^3$	$3x10^{-5}$ - $5x10^{-2}$
Copper (Cu)	9.0	-10	$2x10^8$
Galena (PbS)	7.6	-33	$3x10^{-5}$ - $6x10^{-1}$
Graphite (C)	2.3	-224 - -608//c -6 - -79 ⊥c	$4x10^{-7}$ - 10^{-6} //c $3x10^5$ - 10^2 ⊥c
Haematite (Fe_20_3)	5.1	$4.2x10^2$ - 10^4	10^{-3} - 10^4
Ilmenite ($FeOTi0_2$)	4.4-5.0	-	10^{-3} – 4
Lead (Pb)	11.3	-17.1	21x10-^{8}
Magnetite (Fe_3O_4)	5.2	$15x10^6$	$5x10^{-5}$ – 10^{-3}
Molybdenite (MoS_2)	4.9	-	7 - 10^4
Pyrite (FeS_2)	5.1	35 – 60	10^{-5} – 10^{-2}
Pyrrhotite ($Fe_{1-x}S_x$)	4.6	10^4 – $25x10^4$	$2x10^{-6}$ – $1x6x10^{-4}$
Quartz (SiO_2)	2.65		$2x10^{14}$ ⊥c 10^{12} // c
Spalerite (ZnS)	3.5 – 4.2	-13100	$2x10^{-2}$ – $4x10^4$
Wolframite (Fe,Mn)WO	7.2		10^3 -10^7
ROCKS			
Clay	1.5 – 2.5	50 – $6x10^2$	10 - 10^2
Gneiss	2.6 – 2.9	0 – $3x10^3$	10^3 – $7x10^4$
Granite	2.65	10 – $5x10^4$	10^3 – $2x10^4$

Due to the increase level of porosity and subsequent permeability for sedimentary rocks, they exhibit relatively lower resistivity values compared to other rock types. The resistivity value depends to a great extent the salinity of the water and porosity-permeability of the rock. For loose unconsolidated sediments, the resistivity values are much lower. This is a typical lowering due to high porosity of the unconsolidated sediments and also the clay content determines resistivity to a large extent. Clayey soils have reduced resistivity values than sandy soil. In all, there are overlaps in resistivity values and this are due to factors such as porosity-permeability, water saturation, salinity content, clay content and degree of fracture.

The level of fluid saturation for a porous rock and its resistivity are related by the Archie's law. This law is favourable for rock units and sediments with low clay-content. The conductivity is associated with the fluids filling the pores or fractures of the rock.

Archie's Law = $\rho = a\rho_w\varphi^{-m}$ (2.25)

(ρ is rock resistivity, ρ*w* is resistivity of the fluid, fraction of the rock filled with the fluid is given by φ, while *a* and *m* are two empirical parameters (Keller and Frischknecht, 1966). For most rocks, '*a'* is about 1 while *m* is about 2.

Metallic sulphides have low resistivity values of <1Ωm. The resistivity value of a particular ore body can vary from that of individual crystals. Other factors responsible include nature of the ore body (massive or disseminated). Graphitic slate has a low resistivity value, similar to the metallic sulfides, which can give rise to problems in mineral surveys. Oxides have significantly high resistivity value, with exemption to magnetite.

2.3.3.2 Fundamental Theory of Induced Polarization Method

Observation of polarization effect with low frequency from earth material was first reported in 1927 by Conrad Schlumberger when electric current was injected. The subsequent measurement of the varying degree of polarization called induced polarization and its interpretation to geology in line with earth's material properties at the subsurface makes up the technique of Induced Polarization (IP) method. This method was greatly advanced during the World War II, for identification of buried landmines. The work of

Bleil (1953) revealed that the polarization effect of disseminated metallic minerals can be detected and measured in terms of their subsurface properties. This in turn stirs up a great awareness and continuous research into the application of the method for mineral exploration. This new technique became widely spread between 1960's to 1970's, due to improved technological advancements and interpretation method accompanied by understanding of the polarization effect sources (Pelton *et al*., 1978). At the moment, the application of the method has gone beyond mineral exploration, and found very useful in environmental and engineering works (Ward *et al*., 1995).

As with the pioneer work of Conrad Schlumberger, researcher later discovered that the polarization effect observed then was not actually caused by metallic materials. This was investigated with the absence of significant metal concentrations. Subsequently, laboratory and field investigation deduced the relationship between the induced polarization magnitude and clay content for the responses measured. (Marshall and Madden, 1959; Ogilvy and Kuzmina, 1972). With the new discovery, models using electrochemical approach to show the relationship between clay and induce polarization was designed and designated as "membrane polarization" effect (Marshall and Madden, 1959). There had been several limitations to the induced polarization method accounted for by instrumentation and computer-aided interpretation software. Over the years, these limitations have been overcome with the technological advancement in data acquisition system and algorithms for modeling. Also, better knowledge of induced polarization responses enhanced the effective use of the method.

The principle of induced polarization response effect in essence determines the degree at which electrical charges can be stored by chargeable materials at the subsurface (Summer, 1976). The measured polarization which is as a result of ion re-distribution at interface could be either 'membrane polarization'; i.e. between non-metallic materials (e.g. clay minerals) and fluid or 'electrode polarization; which occurs between the interface of a metal and fluid (Fig. 2.9). The membrane polarization effect produces a lesser response when compared to the electrode polarization responses. The ions re-distributed relax back to state of equilibrium when the current is removed. The diffusion-controlled relaxation is the source of the subsurface induces polarization responses.

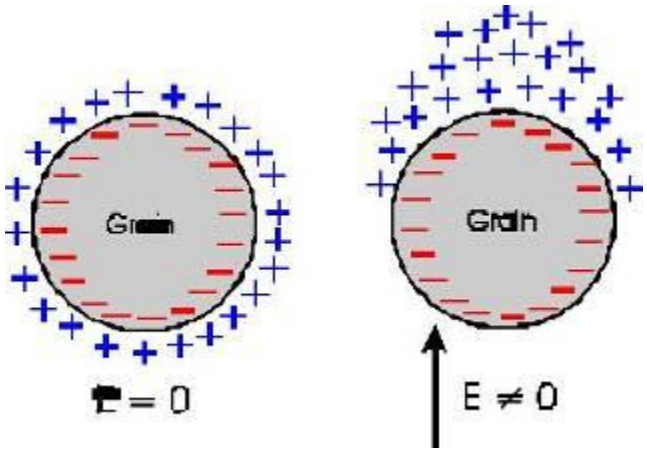

Figure 2.9: [a] Equilibrium (E) ion distribution [b] polarization following application of an electric field. Residual current flow occurs as ions relax to equilibrium following removal of electric field (Source: Slater and Lesmes, 2002)

The degrees of chargeability in induce polarization measurements could either be in time domain or frequency domain. In time domain induce polarization technique; a decay rate which is exponential with respect to time of a secondary voltage (Vs) is measured when the charging current is cut-off. The time of decay can be I order of seconds or minutes. For frequency domain induce polarization technique, measurements of variation in ground resistivity with frequency of charging current is use to determine the induce polarization effect responses. Where the resistivity measured at two different frequencies is different for a particular medium. With increase in frequency of the charging current, the ground resistivity decreases.

2.3.3.2.1 Types of Induced Polarization

Two types of IP effect can be observed on rocks. These include:

(i). Membrane Polarization.

(ii). Electrode Polarization.

Membrane Polarization

The membrane polarization or electrolytic polarization or background or the normal effect is observed on all clay bearing rocks with or without metallic ores provided the clay minerals occur in disseminated form. The IP effect arises from differential mobility of ions contained in fluid saturating a given clay bearing rock (Fig. 2.10a). This IP effect is measured in groundwater, engineering and environmental investigations.

Electrode Potential

The electrode polarization or the overvoltage effect is observed on ore bearing rocks provided the ore occurs in disseminated form. The phenomenon arises as a result of a change in the mode of electric conduction between an electrolyte and a metal or between a metal and the adjoining electrolyte. Electric conduction changes from ionic or electrolytic to electronic or vice versa (Fig. 2.10b). The amplitude of electrode polarization is larger than that of membrane polarization as shown in Table 2.3. Electrode polarization is measured in mineral exploration.

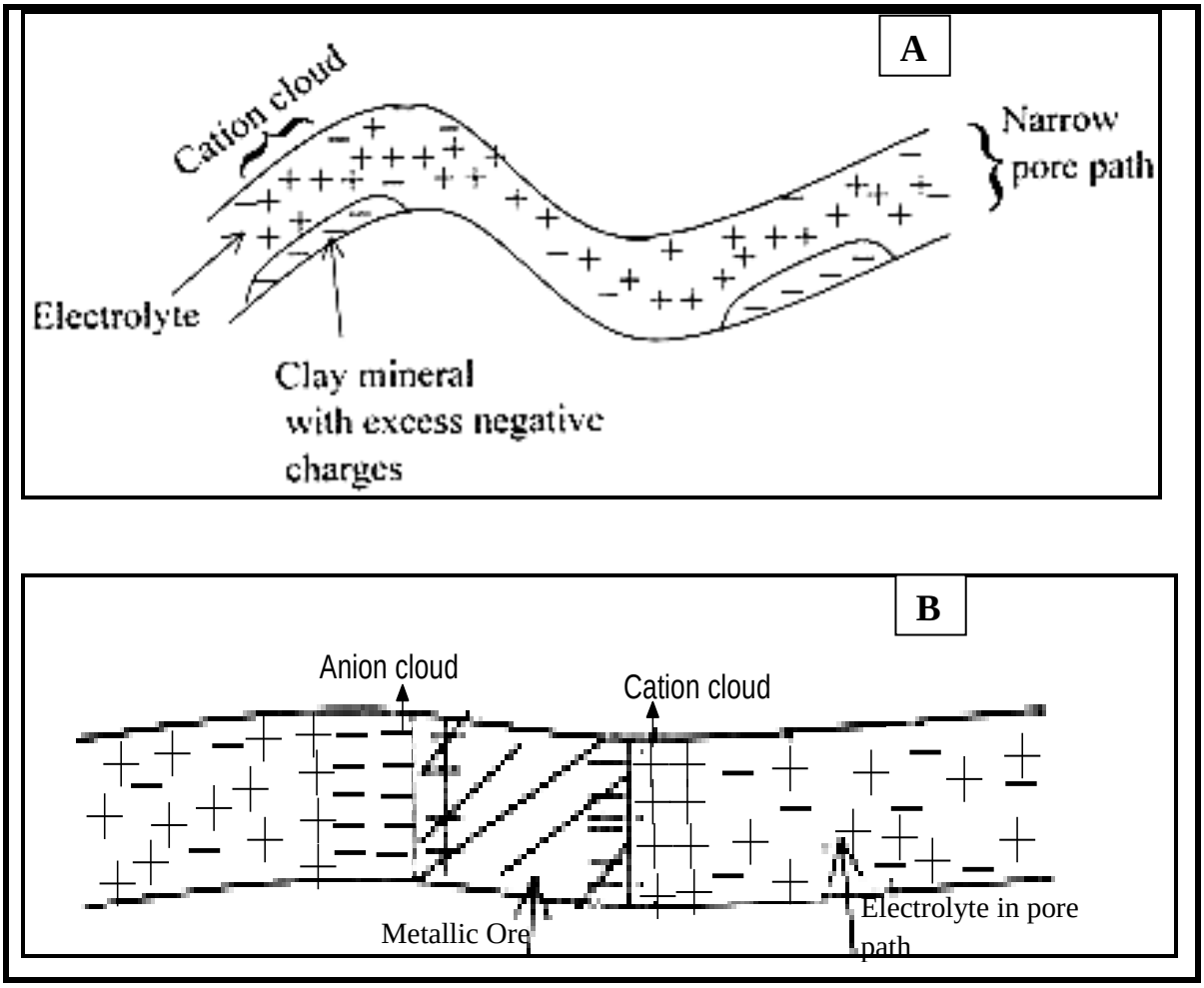

Figure 2.10: a) Membrane polarization phenomenon in clay bearing rock. b) Typical Electrode polarization phenomenon in ore bearing rock (Adapted from Olorunfemi, 2006)

Table 2.3 Chargeability of various minerals and rocks

S / N	Material	Chargeability (ms)
1	20% Sulphides	2000 – 3000
2	8 - 20% Sulphides	1000 – 2000
3	2 - 8% Sulphides	500 – 1000
4	Volcanic tuffs	300 – 800
5	Sandstone, Siltstone	100 – 500
6	Dense volcanic rocks	100 – 500
7	Shale	50 – 100
8	Granite, granodiorite	10 – 50
9	Limestone, dolomite	10 – 20

Nos. 1-3, (Electrode Polarization); 4 – 9, (Membrane Polarization) (Telford *et al.*, 1990)

2.3.3.2.2 Parameters That Are Measured in Induced Polarization

As mentioned earlier, the IP phenomenon can manifest in either Time or Frequency Domain, hence the phenomenon can be measured in either Domain.

Time Domain Measurement

Consider the input and output signals of Time Domain IP as shown in Figure 2.11. In the Time Domain, induced polarization measurement is expressed as chargeability (M) defined as:

$$M = \frac{V_s(o)}{V_p} \quad \text{x } 100\ \% \qquad (2.26)$$

Where $V_s(o)$ is the secondary voltage at time t = 0, V_p is the steady state (primary) voltage at time $t \Rightarrow \infty$

But $V_s(o)$ is usually difficult to measure accurately due to electromagnetic coupling, hence, the secondary voltage is often measured at a particular time t after interruption of the current.

The IP measurement now becomes apparent chargeability which is defined as:

$$Ma = \frac{V_s(t)}{V_p} \text{x}100\% \text{ (in millivolt/volt)} \qquad (2.27)$$

Alternatively, the area under the decaying (Vs) curve can be determined within two time limits t_1 and t_2 in which case:

$$Ma = \frac{1}{V_p}\int_{t_1}^{t_2} V_s(t)dt \text{ (in millisecs)} \qquad (2.28)$$

The advantage of this measurement mode is that the amplitude of Ma is higher since V_s is higher in amplitude than V_p.

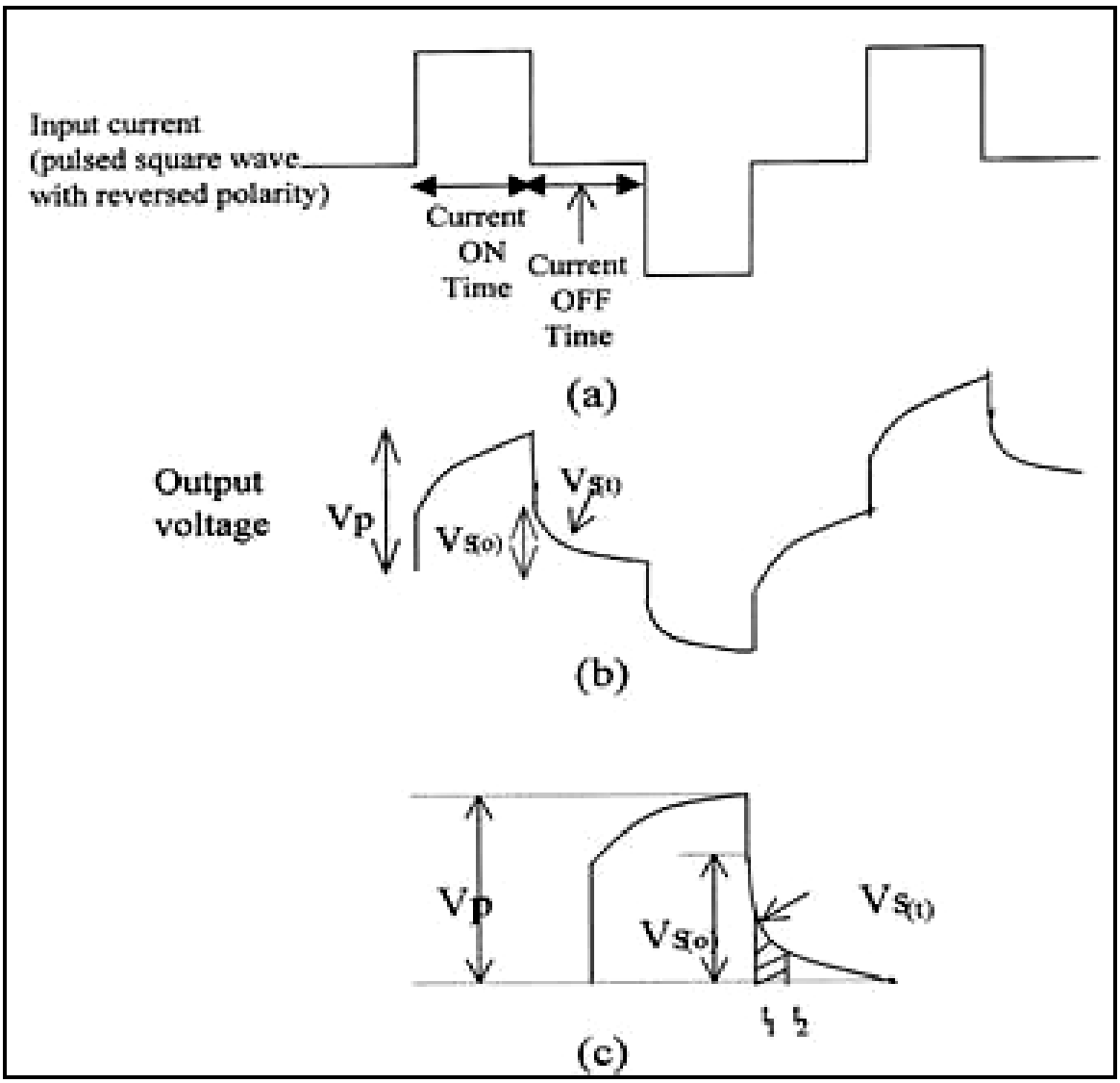

Figure 2.11: (a) Input current signal (b) Output voltage signal (c) Typical voltage build up and decay (Olorunfemi, 2006)

Frequency Domain Measurement

In the frequency domain, the ground impedance or resistivity is measured at two frequencies often a decade apart and usually not greater than 10 Hz (e.g., 0.5 and 5 Hz; 0.7 and 7 Hz, etc.). The various IP measurements in Frequency Domain are:

i. Frequency Effect (FE) defined as: $FE = \frac{\rho_{dc} - \rho_{ac}}{\rho_{ac}} = \frac{\rho_{dc}}{\rho_{ac}} - 1$ (2.29)

Where ρ_{dc} is the resistivity measurement at low frequency; ρ_{ac} is the resistivity measurement at high frequency.

ii. Percentage Frequency Effect (PFE) is defined as $PFE = \frac{\rho_{dc} - \rho_{ac}}{\rho_{ac}}$ x 100 % (2.30)

iii. Metal Conduction Factor (MCF) can be defined as:

$$MCF = \frac{\rho_{dc} - \rho_{ac}}{\rho_{ac}\rho_{dc}} \times 2\pi \times 10^5 \text{ mhos / m (or Siemens/m)} \quad (2.31)$$

Or $$MCF = \frac{PFE}{\rho_{dc}} \times 2\pi \times 10^3 \text{ mhos / m} \quad (2.32)$$

Or $$MCF = \underset{ac.\ dc}{(\sigma_{dc} - \sigma_{ac})} \times 2\pi \times 10^5 \text{ mhos / m} \quad (2.33)$$

Where σ_{dc} is the conductivity measurement at low frequency and σ_{ac} is the conductivity measurement at high frequency.

Frequency Domain measurement can be made in terms of the phase difference (shift) between the input and output signals if both are assumed to sinusoidal. The phase angle is usually less than 1^0.

CHAPTER THREE
MATERIALS AND METHODS

3.1 Materials Used

The materials used for this research work can be broadly categorized based on the geophysical methods and operations. The field acquisition ranges from geological ground truthing, ground magnetic survey, electrical resistivity and induced polarization survey. The materials used for these purpose are as listed below:

Geologic Mapping: Hammer, Compass Clinometer, Magnifying glass, Sample bags, GPS, Measuring tape, Field Map and Observation/Field Booklet, thin sections and petrological microscopes.

Surveying: Ranging Poles, Compass, Station-tags/wooden pegs and GPS.

Ground Magnetic: GEM Overhauser Magnetometer, GPS, 12Volt Battery for Base Station Magnetometer unit

Electrical Method: 5000W GDD Time Domain Induced Polarization Transmitter and Receiver, Anhydrous Copper Sulphate (CuSO4), Porous Pot for CuSO4, Wire rolls for both transmitter and receiver, Jerry cans for water, table salt for transmitter electrode station to enhance conductivity and electrical current transmission into the ground, umbrella, communication two-ways radios (walkie talkie), 6KVA Generating set, GPS and digger/hoe.

For the airborne magnetic and airborne radiometric survey which are secondary data, the acquisition was done by Fugro Airborne Survey for Nigerian Geological Survey Agency with the magnetometer and spectrometer onboard an aircraft. Other materials used includes petrological microscope for photo-micrographs, high configuration computer system for data compilation and processing with geophysical and geographic Information System softwares (Oasis Montaj and ArcGIS)

3.2 Data Acquisition for Aeromagnetic and Airborne Radiometric Survey

Federal Government of Nigeria in 2006 commissioned the acquisition of aeromagnetic survey of the entire country. In line with this, the dataset has since been available with the Nigerian Geological Survey Agency. The Radiometric data was acquired simultaneously with the magnetic data. Below are the survey and equipment specification used for the data acquisition:

Specifications for the Airborne Data Acquisition

Magnetic Data Recording Interval	0.1 seconds
Radiometric Data Recording Interval	1 second
Sensor Mean Terrain Clearance	80 meters
Flight Line Spacing	500 meters
Tie Line Spacing	2000 meters
Flight Line Trend	125 degrees

Equipment Specifications

Magnetometers	3 x Scintrex CS3 Cesium Vapour
Data Acquisition System	FASDAS
Magnetic Counter	FASDAS
Radar Altimeter	KING KR405/KING KR405B
Barometric Altimeter	ENVIRO BARO/DIGIQUARTZ
Radiometric Crystal Volume-Down	32litres
Radiometric Crystal Volume-Up	8litres
Radiometric Crystals	GPX 1024/256
Radiometric Data Acquisition	GR-820-3
Aircraft Supplied By	Fugro Airborne Surveys
Aircraft	Cessna Caravan 208B ZS-FSA
Aircraft	Cessna Caravan 208 ZS-MSJ
Aircraft	Cessna 406 ZS-SSC
Survey Date	07/12/06 - 31/05/07
Data Acquisition by	Fugro Airborne Surveys
Data Processing by	Fugro Airborne Surveys.

3.3 Data Processing and Enhancement Techniques for Airborne Magnetic Data

The initial step was removing the geomagnetic gradient from the data in an x,y,z format using the International Geomagnetic Reference Field, where x and y represent the spatial location (coordinate of the point data) and z values represent the total magnetic intensity at the points recorded. The data was transformed from the database format into a gridded format using the minimum curvature gridding algorithm extension in Oasis Montaj software. The gridded data was then filtered and enhanced to attenuate various magnetic structures for qualitative analysis.

Extracting valuable structural information from magnetic data is a key factor using the various enhancements for effective interpretation. The enhancement techniques among others help to attenuate:

i. The nature of discrete anomalous bodies including intrusions, faults and lineaments.
ii. disruptive cross cutting features like strike slip faults
iii. effect of mutual interference
iv. relative ages of intersecting faults
v. structural styles
vi. Unifying tectonic features or events that integrate seemingly interpreted features.

Thus, the aeromagnetic data was compiled and processed using algorithm for the various enhancement in Oasis Montaj geophysical software. After processing and generating various derivative grids, the grids where exported in geotiff file format, which was brought into ArcGIS where interpreted structures and anomalies where digitized into shapefiles in the ESRI ArcGIS 9.3.

3.3.1 Image Enhancement and Filtering

The gridded Total Magnetic Intensity (TMI) map was subjected to various filtering and enhancement techniques to attenuate subtle magnetic structures.

Fast Fourier Transform (FFT) filter was used to compute the vertical and horizontal derivative grids of the various degrees of polynomials, thereby enhancing more of the near

surface structures that could have been masked off by the regional effect. It was also used to transform total-field data to its vertical component or to adjust the effective field inclination (reduction-to-pole).

The Fast Fourier Transform (FFT), which combines the reassign functions of the short wavelength enhancing filters (low pass) and first vertical derivative, was used to compute the first vertical derivative values directly from the results of the magnetic intensity residual gridded data of the magnetic field. The first vertical derivative enhancement attenuates anomalies over the source body, thereby reducing the complexity of the anomalies and provides a better imaging of the causative structures. The filter is a little bit noisy since it amplifies shorter wavelengths.

The second vertical derivative is a plane polynomial fitting of degree 2. This enhancement is similar to 'residual' filtering in gravity data. The second vertical derivative was capered with the first vertical derivative since it attenuates more of the shorter wavelengths, removing the effect of longer wavelengths or regional signatures. This enhancement major use is the null values for the potential field data (magnetic and gravity) closely follows sub-vertical edges of intra-basement blocks, or the edges of supra-basement disturbances or faults. Like other derivatives, its usefulness is of importance in the data processing stage to constraint noise or mis-levelling.

While more discontinuous than a normal horizontal gradient, the analytic signal produces a peak directly over distinct bodies and their boundaries. As long as the signal from a single contact can be resolve, the width of the peak, or ridge, is a measure of contact depth. The analytic signal was computed using the square root of the sum of the squares of the derivatives in the x, y, and z directions:

$$\text{ANSIG} = \sqrt{(dx^2 + dy^2 + dz^2)}$$

This transformation is often useful at low magnetic latitudes because of the inherent problems with RTP (reduction-to-pole) at such low latitudes. It helps to centre the peaks on causative bodiy.

The computation was carried out using a combination of the horizontal and vertical gradients of the magnetic anomaly within the Magmap extension of the Oasis Montaj software.

The Total Horizontal Derivative and the tilt derivative are both useful in mapping out shallow near surface structures. These enhancements are also designed to look at fault and contact features. They are complementary to the filtered and first vertical derivative enhancements above. They usually produce a more exact location for faults than the first vertical derivative.

A magnetic body is spatially more closely aligned with the corresponding magnetic response after the reduction-to-pole correction. The anomaly slope's highest horizontal gradient (or, more accurately, the maxima of the overall horizontal gradient) is then situated above the body side. That is, in map form, the horizontal gradient operator creates maximal ridges along the contact of magnetic basement columns, faults, and other magnetic sources. Furthermore, linear characteristics of the horizontal gradient are illustrated in the data collections that are connected to contacts (Milligan and Gunn, 1997). Due to artificial effect of mainly the NNPC Pipeline that passes through the study area, upward and downward continuation operation would be performed on the dataset to masked off the effect of the local disturbances. Generally the source body is responsible for a magnetic anomaly that lies below the plane of observation of the magnetic field. As the plane of observation increases (decreases) in distance from the causative source, the anomaly decreases (increases) in amplitude proportional to $1/r$ n, where r is the distance between the plane of observation and the causative body, and n is determined by source geometry. The result of this process known as upward or downward continuation, is to produce a map where the anomaly being investigated becomes more clearly defined by the removal of lower or higher frequency “clutter” of near-surface sources, and is of higher amplitude as the upper surface of the causative body is approached.

In comparison to low-frequency anomalies, upward continuation smoothes out high-frequency anomalies. By taking disturbances closer to the plane of measurement (enhance high frequencies), while downward continuation sharpens their impact (simulates the survey being flown lower to the field) (Milligan and Gunn, 1997). As a consequence, there would be less spatial variation for the anomalies and easier to discern from one another. This procedure not only decreases the overlap of neighboring irregularities, but also increases their amplitude (Gunn, 1975).

3.4 Methodology for Processing Airborne Radiometric Data

This is one of the most cost-effective and rapid techniques for geochemical mapping of the three major radioactive elements: potassium, uranium and thorium. The goal is to recognize and understand radiometric signatures associated with the host rocks important to mineralisation. The airborne radiometric data like the aeromagnetic data was equally processed in oasis Montaj software before exporting as a geotiff file format into ESRI ArcGIS software.

3.4.1 Total Count (TC), Potassium (K), Thorium (Th) and Uranium (U) Channels

Total count image was created after micro-levelling the entire dataset to remove any apparent residual errors. These images were generated by employing mini-curvature gridding since the data were collected in grid window. The grids were then compared to the geological units' pattern and trend. The theory is that mafic and ultramafic rock units, for example, have a low radiometric responses, according to the literature.

To assist in the detection of regions with greater concentrations of each radio-element, the data sets were gridded using the minimum curvature gridding algorithm in the Oasis Montaj software. The potassium was gridded as a measure of percentages while thorium and uranium values in ppm (part per million) were gridded in their respective units. Purple colouration was assigned to the highest values while blue colour was to the lowest value.

3.4.2 Ratio Maps Composite and Images

A RGB (Red, Green and Blue) color model was used to depict the concentration in terms of intensity for each of the three radio-elements. The colors red, green and blue were assigned to potassium, thorium and uranium, respectively, since the blue helps to minimize the uranium channel's worst signal-to-noise ratio. The resulting images contain colors created by the relative intensities of the three components and display slight differences in the proportions of the three components. The ratio maps were also produced for the purpose of eliminating lithological variations and data effects caused by soil moisture variations, non-planar source geometry, and errors associated with altitude

correction. Lithological variations tend to be reduced as radioelement concentrations often vary when lithology varies (Silva *et al*. 2003). For example, U/Th and U/K ratios have been established for the determination of areas where uranium relative concentrations are high.

3.5 Geological Mapping and Ground Truthing

Geological mapping and ground truthing entails the art of assessing and observing rocks in the field that show surface expression as outcrops, ridges or hills, and recording observable physical geological information on the rock surface. These information ranges from geological boundaries and contacts, faults and fractures including lineaments, strike and dip angles, and also tectonism and deformation activities represented on the rock fabrics. This is important because understanding of the geological setting forms the foundation on which all geoscientific data are superimposed on.

The geological ground truthing which was done over the delineated target area carved out after the processing and interpretation of the airborne dataset (magnetic and radiometric) was traverse using footpaths and track roads (Fig. 3.1).

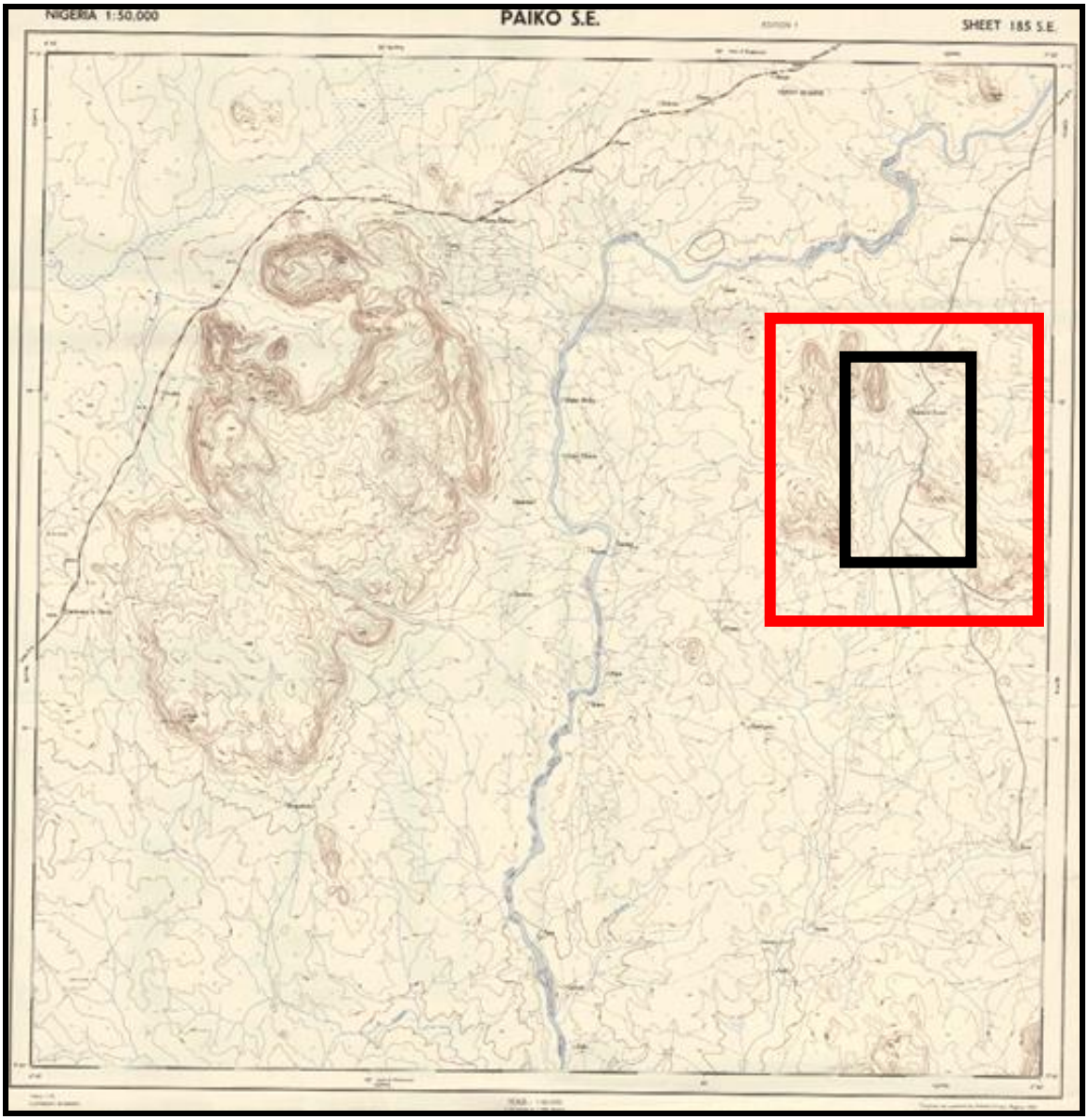

Figure 3.1: Topographical map showing the delineated area (in red box) for detail mapping after reconnaissance ground truthing.

Accessibility was fair over the area as a major road connecting Izom in Niger State to Gwagwalada in Federal Capital Territory passes through the target site in an almost NNW-SSE direction, with Baban Tsauni village as the target site area. The ground truthing entails assessment and inspection of rock types encountered, measurement of structural information, and oral discussions with farmers about the mineral potential around the area. All these information were input into a database system that had been prepared. An example is as shown in Table 3.1.

Table 3.1: Sample database for the geological mapping and ground truthing

Loc	Long	Lat	Rock Type	Rock Name	Colour	Structure	Texture	Strike	DIP
IZ01	6.98408	9.21367	Metamorphic/Igneous	Biotite Gneiss/Coarse grain Granite	dark grey/ light		Medium grain (banded)/ Coarse	75	25N
IZ02	6.98158	9.21392	Metamorphic	Biotite Gneiss	dark grey		Medium grain (banded)		
IZ03	6.98111	9.21494	Metamorphic/Igneous	Biotite Gneiss/Coarse grain Granite					
IZ04	6.98022	9.21447	Igneous	Granite	light gray		Coarse		
IZ05	6.97964	9.21489	Metamorphic	Biotite Gneiss	Grayish		Medium-Fine	88	75S
IZ06	6.97864	9.21508	Igneous	Granite	Brownish		fine	91	
IZ07	6.97711	9.21461	Metamorphic/Igneous	Biotite Gneiss/Coarse grain Granite	Pinkish/grayish		Pegmatitic	71	25N
IZ08	6.97561	9.21403	Metamorphic	Biotite Gneiss	Grayish		medium, Banded	61	22NW
IZ09	6.97344	9.21431	Igneous	Pegmatite	Pinkish		Pegmatitic	115	
IZ10	6.97158	9.21497	Igneous	Granite	pinkish		Fine	10	
IZ12	6.96944	9.21417	Igneous	Granite	Pinkish		fine	110	
IZ13	6.96869	9.21464	Igneous		Dark gray		fine, Porphyritic	48	
IZ14	6.96769	9.21258	Igneous	Quartz vein	milky white		massive, granoblast	79	
IZ15	6.96567	9.21303	Igneous	Granite	Brownish		Fine-medium	165	
IZ16	6.96511	9.21344	Metamorphic	Gneiss	Dark gray		Banded	40	56W
IZ17	6.96892	9.21233	Igneous	Granite	Brownish		Medium	165	
IZ18	6.97492	9.20964	Igneous	Quartz vein	milky white			47	
IZ19	6.96119	9.12008	Igneous	Granite	Pinkish		Medium	145	
IZ20	6.95731	9.12036	Metamorphic	Biotite Gneiss	grayish		Medium	135	
IZ21	6.95672	9.12039	Igneous	Quartz vein				146	
IZ22	6.95597	9.12000	Metamorphic	Sheared zone	fold, shearing		130 (Aplite), 61 (gneiss) 30SE		
IZ23	6.95569	9.12236	Metamorphic	Biotite Gneiss	grayish		Medium	10, 15	41W, 36W
IZ24	6.95519	9.12839	Metamorphic	greenish gray	highly weathered	179	57		

Structural information as observed from outcrops were also measured and recorded. Rock samples were inspected for mineral composition, alterations, metamorphism among others. Data collected from the field are daily populated into the database system, and this form the main ancillary data for the digital map production. Apart from the lithology and structures taken note of in the field, other information such as alteration zones and artisanal workings were also examined and documented.

The hand specimen grabbed sampled were taken to the laboratory for preparation of thin sections for petrographic studies. Each sample was cut in two different faces and prepared on two different slides which were studied under the petrological microscope at the Nigerian Geological Survey Agency, Kaduna where photo micrographs were taken, identifying various constituent minerals and modal analysis evaluated from the assessment.

3.6 Ground Magnetic Acquisition

Based on the information from aeromagnetic data, airborne radiometric data and local geology of the area, the survey was designed and the traverses were established in an east-west direction which is mostly perpendicular or almost orthogonal to the strike direction of aeromagnetic anomalies and structural trends observed in the field during the geological mapping. The profiles which run from east-west were in some cases truncated due to land owners/farmers not in agreement. These were basically in two areas, one to the southeast where the profile lines was to pass through a farm and the other towards the northeast over a ridge where cultural activities were been performed (Fig. 3.2).

The magnetic sensor measures the variation of magnetic field. Different rocks have varying magnetic properties due to the presence or absence of magnetic minerals such as magnetite, ilmenite and pyrrhotite in them. The magnetic sensor hence measures the magnetic susceptibility of the rocks, which is the measure of the quantity of the magnetic minerals present in the rock. Hence, the continuity or discontinuities of these magnetic minerals in the rock were used to understand and map the rock geological contacts, as well as the sub-subsurface structural trends.

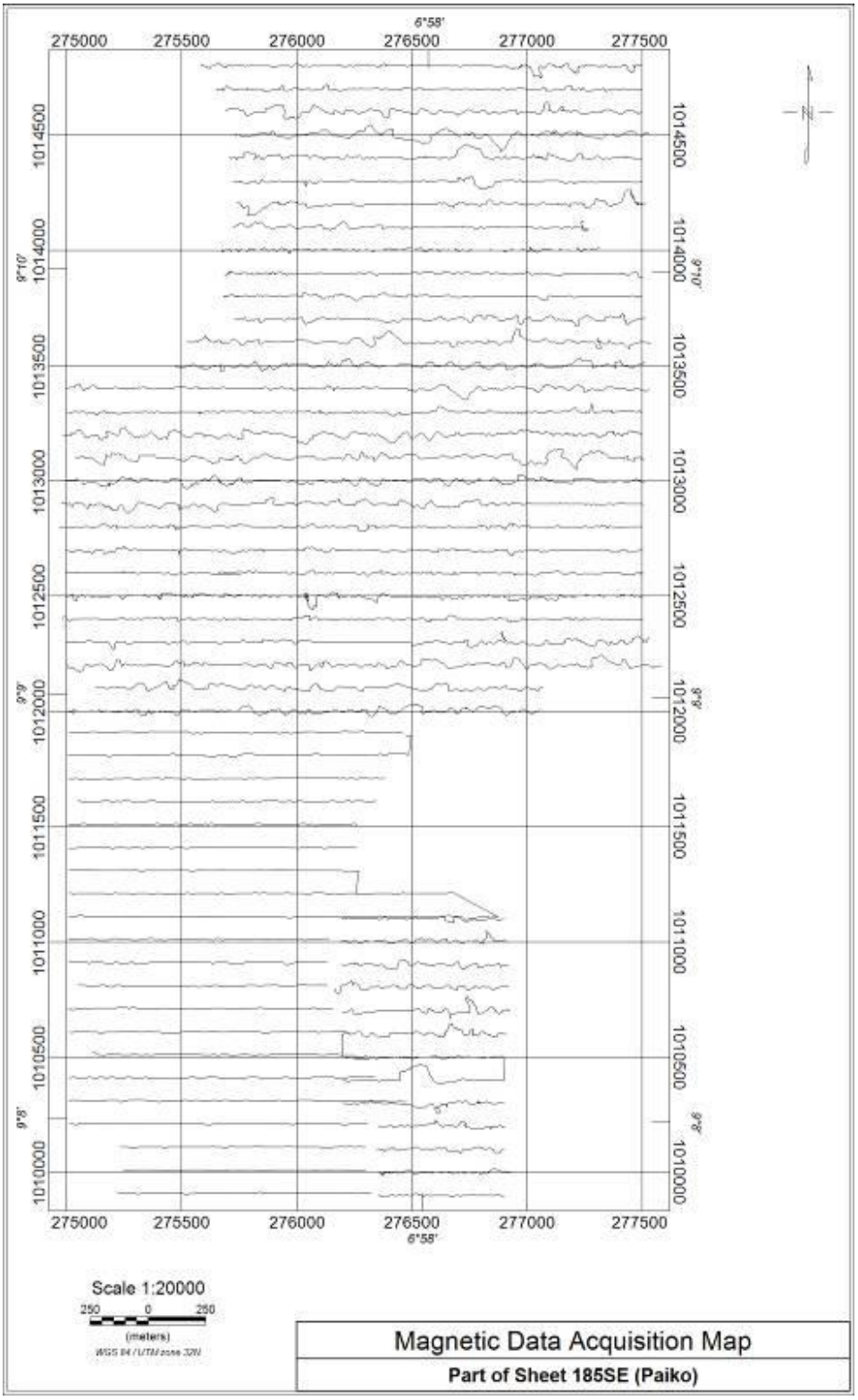

Figure 3.2: Magnetic Survey Data Acquisition Map

Most structural discontinuities in rock or in-between rocks will exhibit low magnetic intensity due to destruction or absence of the magnetic minerals or infill of more or less magnetic materials. Understanding the structural trend is important in mineral exploration, as pre-existing fault zones and shear zones will mostly control the emplacement of the later mineralisation. Similarly, post emplacement structural deformation is paramount to understand the geometry, as well as likely displacement of ore bodies at the subsurface.

For the purpose of these research work, ground magnetic survey have been carried out to investigate near surface structures and magnetic bodies that might have controlled the lead-zinc mineralisation emplacement within this prospect area.

The GEM 19 Overhauser Magnetometer Rover and the base units with in-built GPS were used to collect ground magnetic data along 50 nos of east-west profiles at a profile interval of 100 m in continuous mode (walk-mag mode). The survey parameter is as listed below:

Profile length – 2.6 km
Inter-profile spacing – 100 m
Number of Profiles – 51
Equipment – GEM 19 Overhauser Magnetometer (walk-mag mode)

3.6.1 Ground Magnetic Data Processing Methodology

Acquired total magnetic data was diurnal corrected and downloaded into the survey database for quality control and checks. Profile data plotting and preliminary gridding using minimum curvature method at cell size of 25 m was done to assess noise in the data. Dropouts and spikes were filtered from the data on a daily basis using the non-linear filters in Oasis montaj. At the completion of the approximately 130-km line survey, the compiled raw magnetic data was micro-leveled using the Minty approach to remove directional noises along and across the survey line (Minty, 1991). The leveled data was gridded using the minimum curvature method at 25 m cell size, which is a quarter of the profile line spacing.

The leveled total magnetic intensity (TMI) was further processed to enhance the near surface related features as done with the airborne magnetic data, with computation of derivatives from the filtered total magnetic intensity data.

3.7 Electrical Resistivity and Induced Polarization

An electrical current is passed through the ground and potential electrodes (porous pots of copper rod in copper sulphate solution) are used to record the resultant potential difference between them. For this research work, dipole-dipole electrode configuration was adopted along structures delineated by integration of the airborne data, ground magnetic and geological mapping.

Time Domain Induced Polarization (TDIP) coupled with electrical resistivity tomography (ERTM) survey was conducted across the suspected mineralised structures and a control profile over an open artisanal pit. The acquired IP data was corrected, post-processed and plotted to generate 2D pseudo-section showing the variation of the IP chargeability and resistivity. 3-dimension geometry model was also computed to isolate anomalous zones with high chargeability and resistivity values in order to define high probability area likely related to the lead and associated sulphide mineralisation.

Time domain IP data were collected along the 14 nos of approximately 1.5 km long east-west profiles using GDD 5000-watt transmitter and 16-channel receiver over delineated anomaly from the ground magnetic and geological mapping. The setup utilized dipole-dipole array, conductor cables, two steel current electrodes and nine non-polarizable copper sulphate electrode pots spaced at 50 m dipole spacing. The data were collected at every 25 m along the 1.5 km profile (Fig. 3.3). The acquired data was post processed in the GDD post processing software (trial version) obtained from the manufacturer in response to mail for the sole purpose of this research work.

The current was injected to the subsurface with a 2 seconds on and 2 seconds off duty cycle via a 5000-watt transmitter (Tx), while the receiver measures the decay of the primary voltage. 30 readings were stacked to improve the signal to noise ratio and this was repeated thrice for each station.

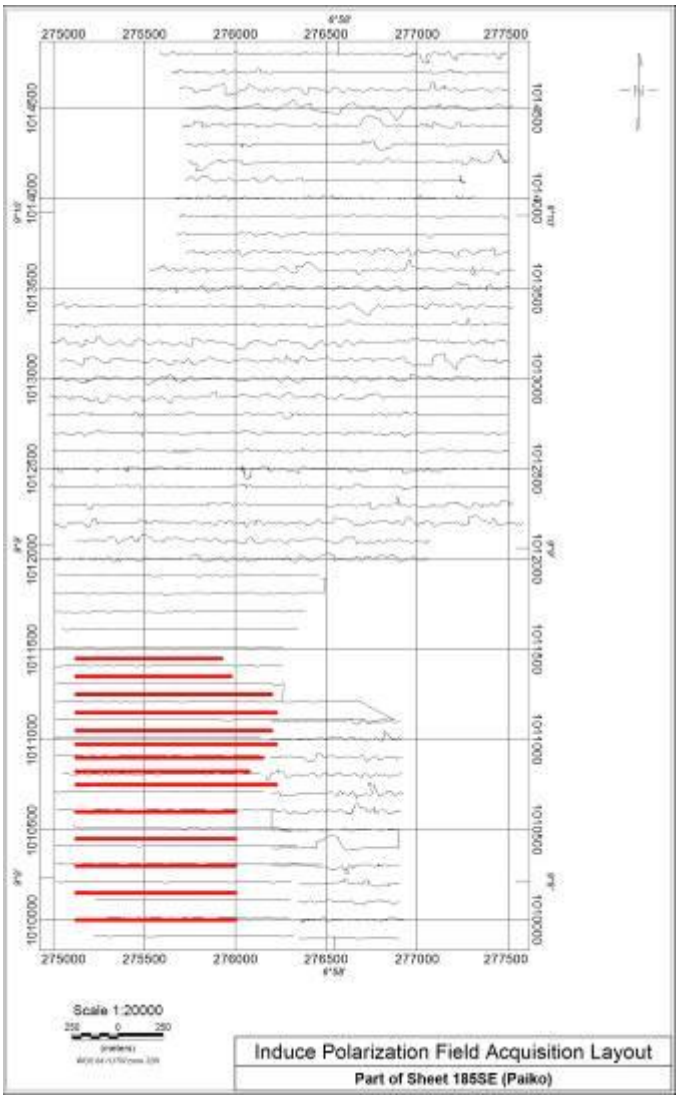

Figure 3.3: The IP data were acquired across the suspected mineralised structures trending in the NW-SE and NNE-SSW directions along the survey profile, at a spacing of 25 m. Profile spacing is 100 m interval with in-fillings of 50m in some locations for ambiguity elimination

The IP reading for each surveying day were downloaded to a computer and saved into a database on a daily basis. Quality control of the acquired data was done using the Geosoft Oasis Montaj IP module, where the decay curve and the noise level of each channel are reviewed and noisy channels were eliminated.

3.7.1 Induced Polarization and Apparent Resistivity Data Presentation

The dipole-dipole IP data were presented as pseudo-sections and the same was used to concurrently presents the apparent resistivity data for enhanced comparison and interpretation ease. The IP data were plotted at the point of intersection of 45^0 inclined lines from the mid – points of the current and the potential dipoles. The IP data were thereafter contoured. This helps to:

(i) Gives at a glance, the variations of IP effect in 2 – Dimensions (laterally and vertically).

(ii) It is possible to estimate though approximately, the width extent of the target, its dip direction and depth extent, when the dipole-dipole data were inverted.

(iii) The dipole – dipole array has significant depth of investigation hence its section can be indicative of sources at relatively deep depth.

The IP chargeability and resistivity data pseudo-section were plotted using the IP module of Oasis Montaj software. The software contours the IP chargeability values acquired at different depths and locations, and also assign a color scale as defined by the user. On the pseudo-section, the high IP chargeability portions are in color pink, while the low IP areas are in green-blue color. In the resistivity section, the low resistivity areas are in blues, while the pink areas are the highly resistive area.

A 3-dimension geometry was also generated by stacking the parallel profile and visualizing the stack plot in 3-dimension. The model was constraints to regions with relatively high chargeability and relatively high resistivity.

CHAPTER FOUR

RESULTS AND DISCUSSIONS

4.0 General Statement

In this chapter the results of the study are presented and discussed in the sequence of the applied geophysical methods. Starting with the airborne magnetic data processing and interpretation to delineate the structural setting over the study area and map out intrusive bodies. This was followed by the data processing and interpretation of the radio-elements from the airborne radiometric data. The interpretation from the airborne radiometric was use for lithological boundaries delineation, in order to effectively place the geologic boundaries of each lithology. Subsequently, the integration of the magnetic and radiometric data were used to update the existing geological map and carve out target area with high susceptibility for associated sulphide mineralisation, using structural interaction and host geology.

The carved out area was followed-up by ground magnetic studies for a higher resolution structural delineation and more accurate spatial location information on the suspected host structures. The ore body geometry configuration which is at the later part, was surveyed with the integration of Electrical Resistivity Tomography (ERT) and chargeability responses from Induced Polarization (IP) profiling. This sequence of presentation of the results and discussions was adopted, so as to effectively tie the results and discussion with the set objectives of this research work with the aim of evaluating the structural setting and ore body geometry configuration.

4.1. Structural Setting Delineation from Airborne Magnetic

The aeromagnetic data collected from the Nigerian Geological Survey Agency, was acquired following the topographic sheet division of the Nigerian standard 1:100,000 topographic sheet divisions. This was done by windowing out the rectangle of interest which covers the sheet 185 (paiko). The data was thus gridded using minimum curvature

method of gridding and displayed (Fig. 4.1a and b) using contour lines and colour composite. This was done in order to narrow down the symbology classification to a localized scale to enhance anomaly differentiation for interpretational ease. For the purpose of this research work, random gridding otherwise known as minimum curvature was used to interpolate the corrected airborne magnetic data set, fitting a minimum curvature surface to the data sets. This gridding method gives a smooth surface to the interpolated datasets and it is relatively fast. The advantage of this method for geological data is that just like the geological data and specifically magnetic data; it has its mathematical basis in Laplace's equation.

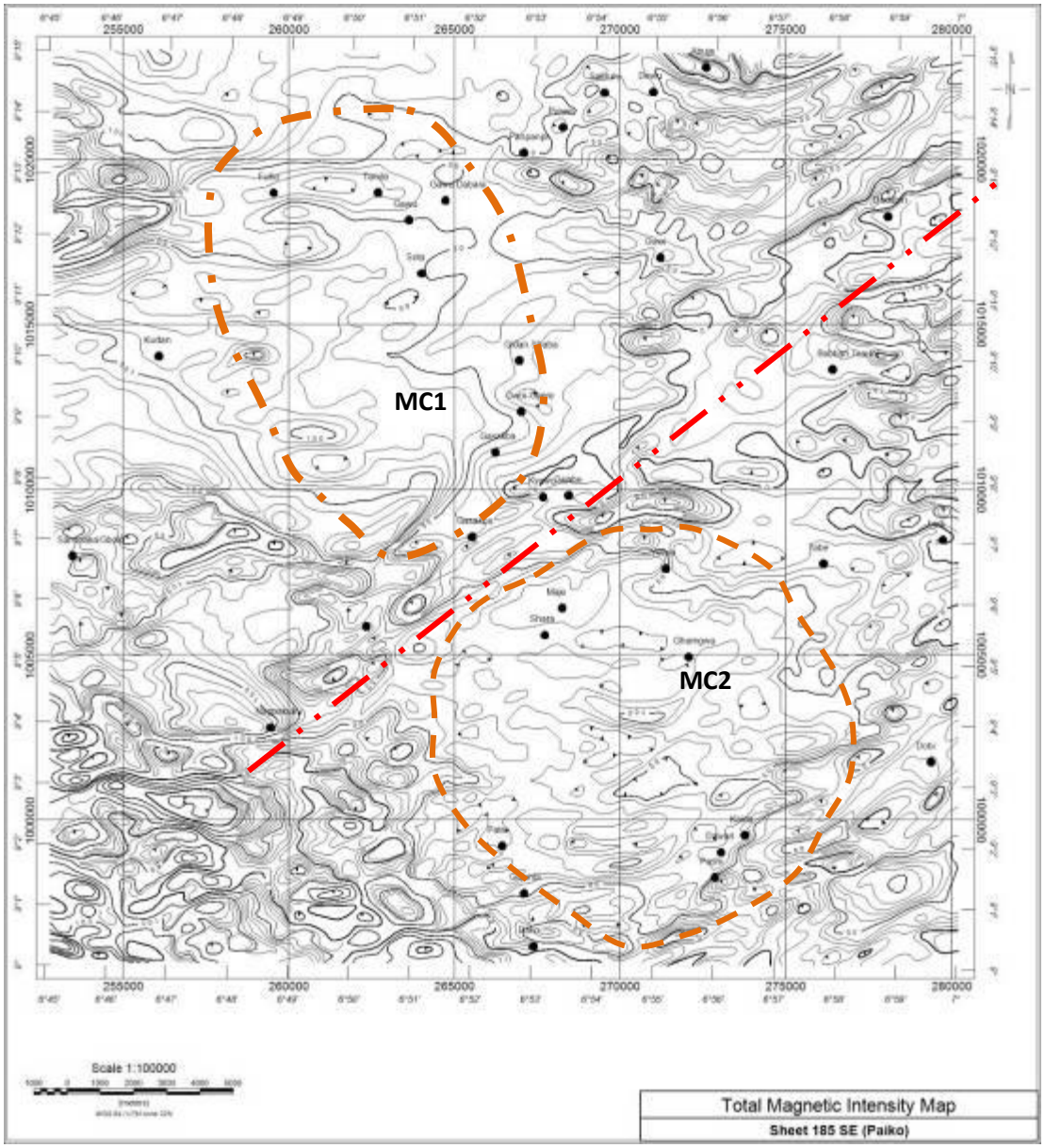

Figure 4.1a: Contoured Map of the Total Magnetic Intensity (TMI) covering Sheet 185 (Paiko SE)

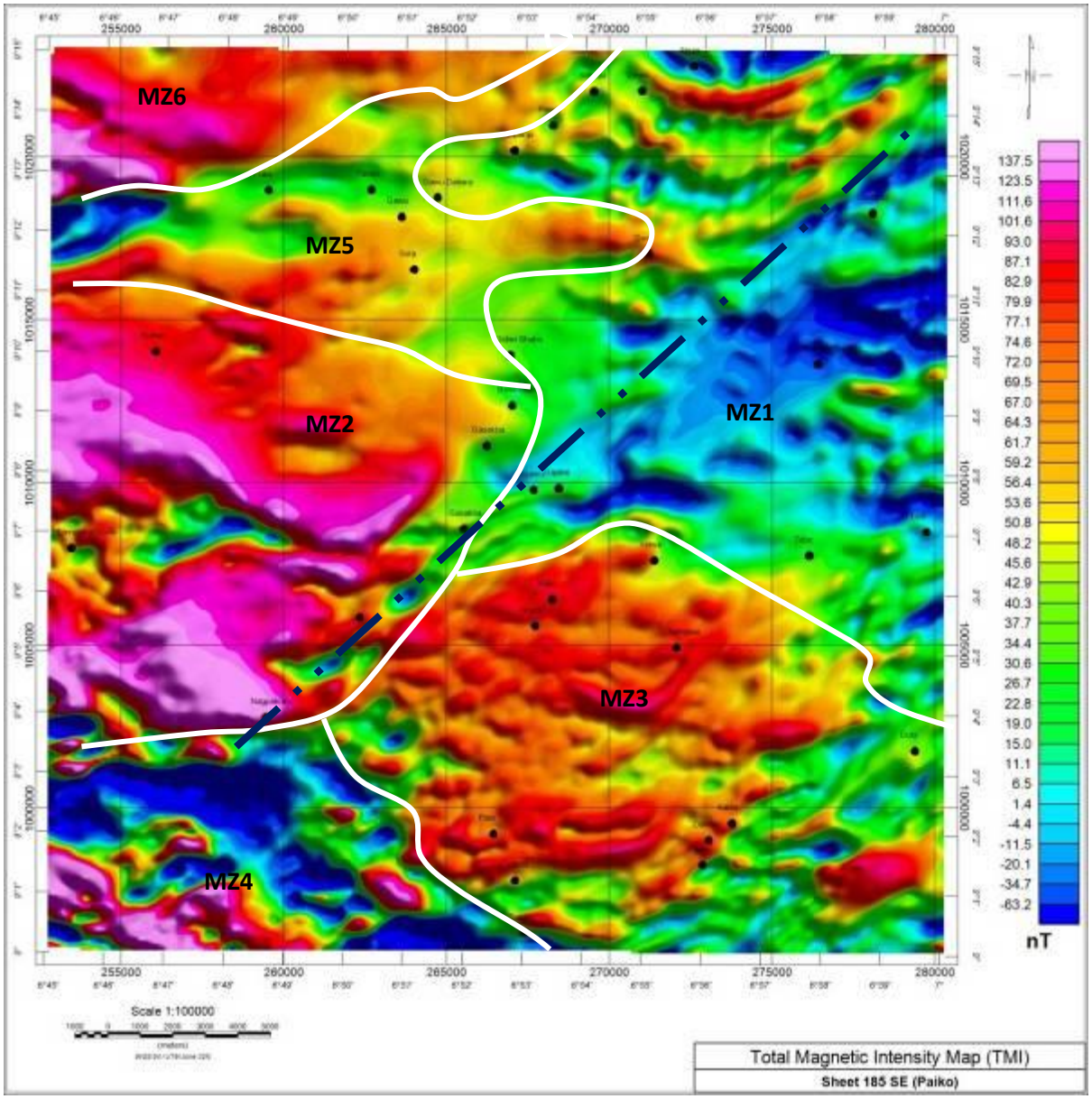

Figure 4.1b: Total Magnetic Intensity Map covering Sheet 185 (Paiko SE)

The Total Magnetic Intensity map is at low latitude and requires to be reduced to the pole (RTP) to removed errors associated with low latitudes. Reducing a dataset or grid to the pole gives a transformation that simulates the data acquisition at the pole (magnetic north) with a vertical magnetization and regional field, instead of acquisition at low latitude. The non-vertical magnetization experienced at low latitudes makes a symmetric body to give an asymmetric anomaly, whereas at the pole it would give a resultant symmetric anomaly removing or eliminating the error associated with asymmetric anomaly and resulting in interpretational ease. This technique is commonly used and actually the best method to eliminate anomaly distortion. The derived map would then give a direct relationship for magnetic high and low causative bodies. For lower latitude less than 10° north or south as with the study area, a false north-south anomaly is enforced on the data. Thus, the data set was reduced finally to the equator and inverted to give a pole reduced data.

It was observed that the RTP algorithm enforced a pseudo North-South structure on the map and thus the data was reduced to the magnetic equator and inverted (Fig. 4.2). The inversion thus made the areas with high intensity values to become low while the lower intensity regions became high. Thus errors associated with data acquired at low latitude (less than 10°) were removed or reduced making it look as if the data were acquired at the pole and relocate anomalies over their sources. The Fast Fourier Transform (FFT) filtering removes the dipolar nature of the magnetic field.

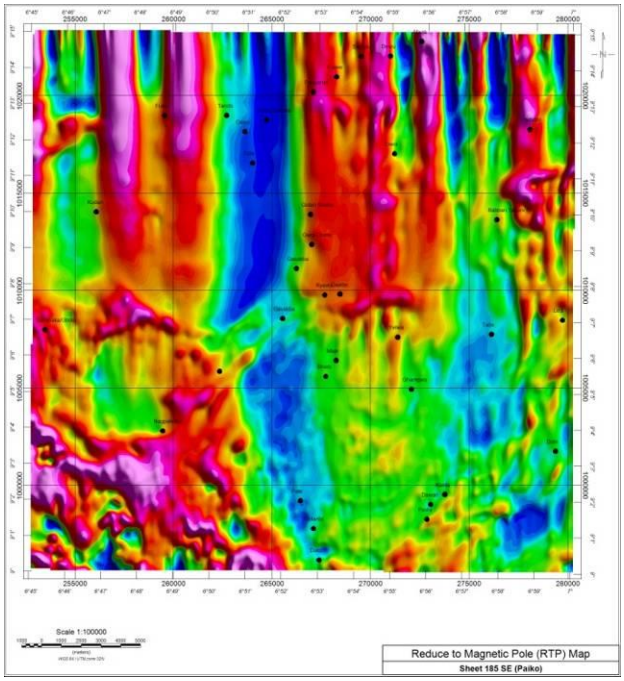

RTP

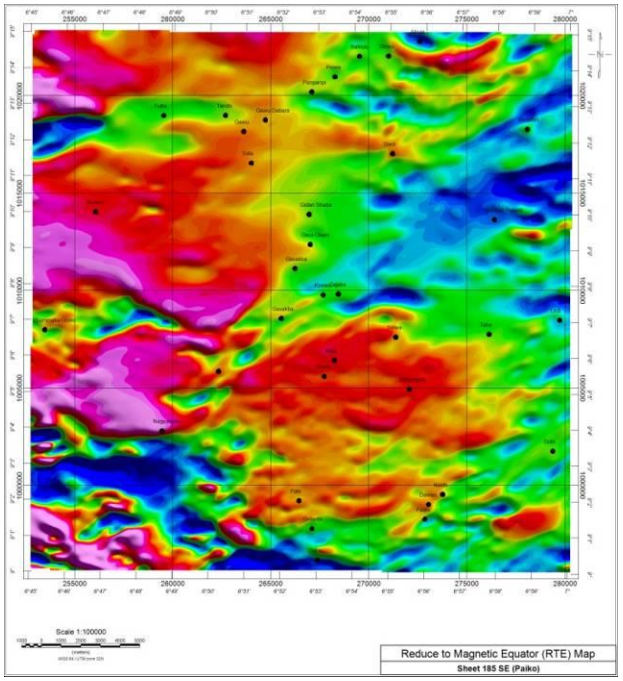

RTE

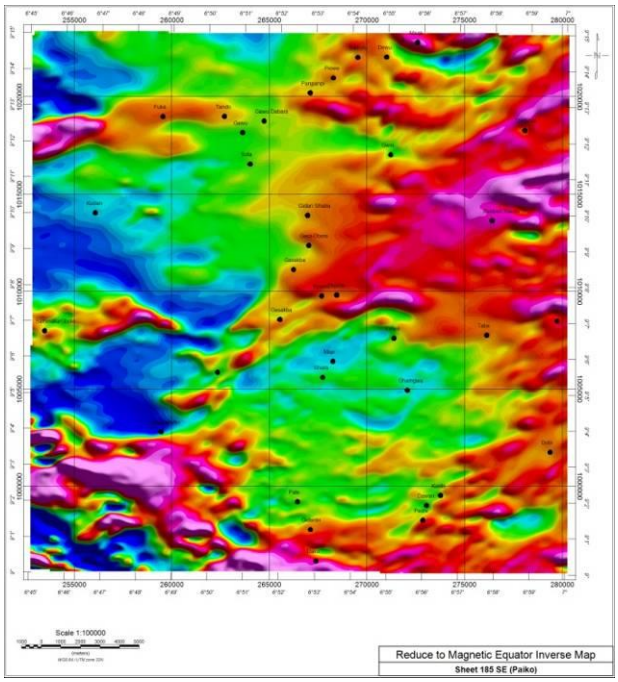

RTE (Inverted)

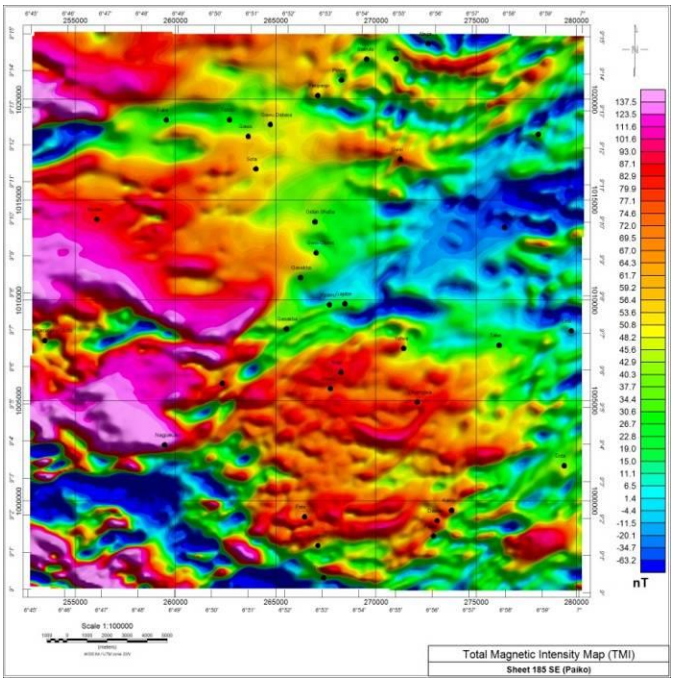

Original TMI

Figure 4.2: Comparison of the RTP, RTE and an inverted RTE with the TMI map covering Sheet 185 (Paiko SE)

The Total Magnetic Intensity map shows large oval magnetic anomaly around the north-western and adjacent south-eastern portion of the study area giving rise to magnetic closures. These closures are referred to as 'MC1 and MC2' (Fig. 4.1a), which are circular shaped bodies suspected to be intrusives. MC1 has a corresponding surface expression on the digital terrain model (SRTM) as a ridge, but the MC2 was interpreted as fairly deep seated as the area coincides with drainage channel which was about the lowest elevation within the study area. There are other closures and disseminated contrasting high and low magnetic signatures depicting a tectonized region where deformation episodes are virtually more than one. This is also a characteristic of the basement complex with very eractic magnetic signature in terms of amplitude and frequency. High Total Magnetic Intensity (TMI) field values ranging in residual values from around 80 nT to 130 nT after removing magnetic gradient were observed within the study area, from the western section of the study area trending from the north to the south, from Kudan village to below Nagpakuku village in the southwest. Thus, base on the magnetic intensity and textural classification, the study area was further classified into magnetic zones refered to as MZ1 to MZ6 (Fig. 4.1b).

The magnetic zonations are closely associated with lithological contrast and hence were delineated as lithological zonations. Prominent observable lineament trending northeast-southwest from Nagpakuku in the southwest, through Gasaka up to Babban Tsauni in the northeast was also observed and delineated.

4.1.1 Image Enhancement for Local Structural Delineation

The magnetic data shows both regional structures with long wavelengths and much younger structures with shorter wavelengths. These structures originated from tectonism leading to structural deformation. These structures have been established to be a controlling factor to the emplacement of the associated sulphide mineralisation within the study area. The magnetic anomalies are due to the changes and variation in the physical properties including susceptibility and thickness of the various rock types. The acquired magnetic data is a combination of causative sources with regional effect and subtle causative sources that can easily me masked off. In most cases, the subtle anomalies are

well related to mineralisation, especially where the mineralisation is within a geological setting with multiple deformation episodes. For effective and qualitative interpretation, the relief and texture of the grids are always manipulated, using various algorithm based on Fast Fourier Transform (FFT) to attenuate subtle anomalies by removing or suppressing the effect of the regional effect.

Analytic Signal (Total Gradient)

The analytic signal, although often more discontinuous than the simple horizontal gradient, has the property that it generates a maximum directly over discrete bodies as well as their edges (Fig. 4.3). The width of a maximum, or ridge, is an indicator of depth of the contact, as long as the signal arising from a single contact can be resolved. This transformation is often useful at low magnetic latitudes because of the inherent problems with RTP, (at such low latitudes). It is calculated using both the horizontal and vertical gradients of the magnetic anomalies. The enhancement allows shallow causative sources and broad anomalies, removing magnetization direction to a very reduced level. Thus, it is noisier with lesser textural information

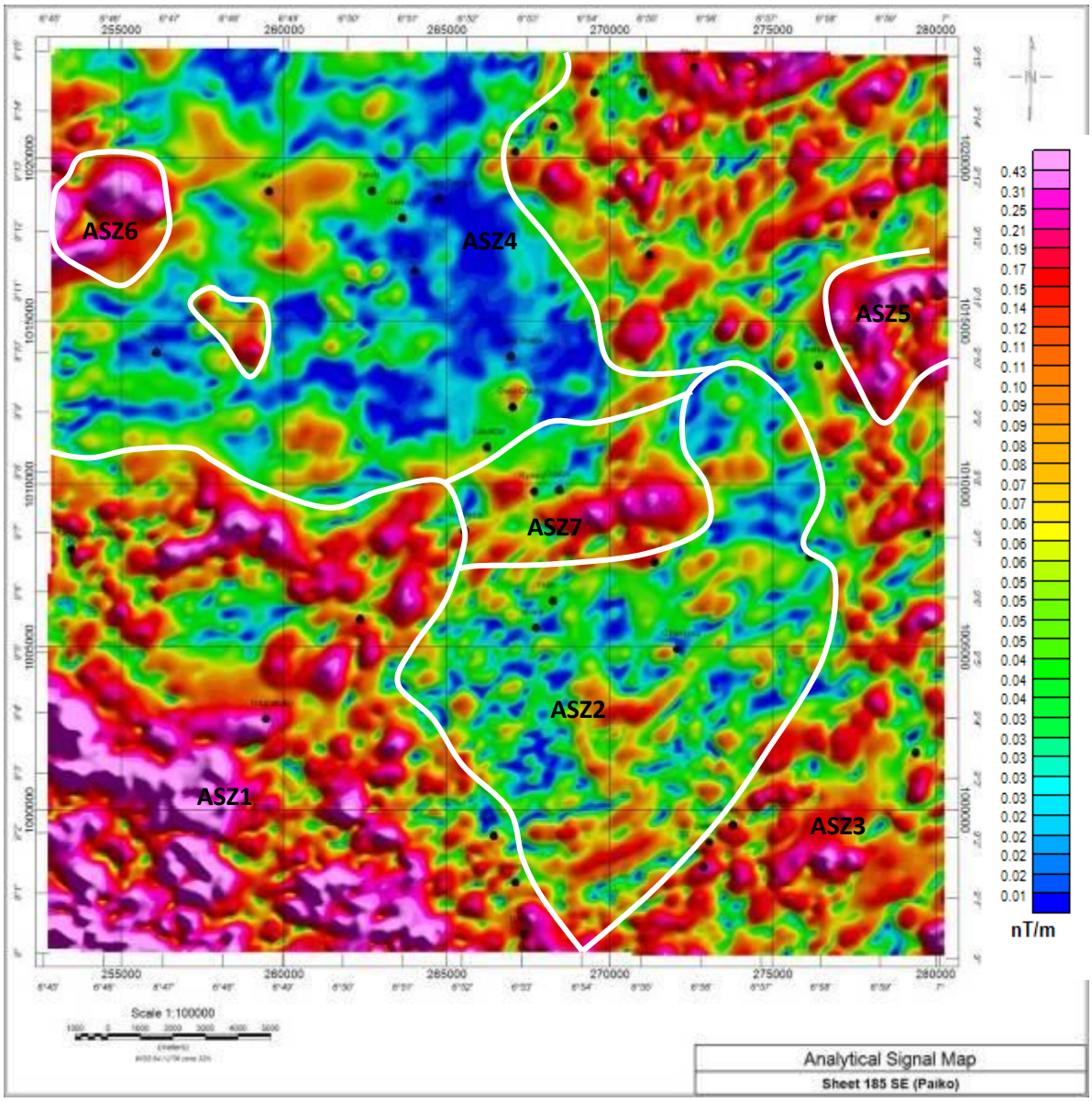

Figure 4.3: Analytic signal map showing magnetization amplitude zonation over the Sheet 185 (Paiko SE)

The analytic signal map was used for magnetic zonation referred to as ASZ1 to ASZ7 (Fig. 4.3), which relates to lithological variation within the study area as different rock type shows different amplitude of magnetization due to their magnetic susceptibility. The isolated peaks can be well correlated to intrusive with high magnetic susceptibility as observed around Babban Tsauni, Yelwa, Gwoi and around Dobi among others. South of Fuka is a large circular body with low magnetic susceptibility as correlated from the digital terrain model. While more discontinuous than a normal horizontal gradient, the analytic signal produces a peak directly over distinct bodies and their boundaries. As long as the signal from a single contact can be resolve, the width of the peak, or ridge, is a measure of contact depth. This transformation removes the inherent problems with RTP.

Vertical Derivatives

The derivatives of the Total Magnetic Intensity field data were computed to enhance the data set for both source and edge detection. Thus, the first and second vertical derivatives (1VD and 2VD) were computed and gridded (Figs. 4.4a and 4.4b). These derivatives were computed to separate anomalies on the basis of their wave-length (that is regional and local effect) so as to be able to bring out geological and structural features, by removing the effect of the deep seated regional structure and attenuate the effect of the more near surface structures. Computation of vertical derivatives helps to attenuates source edge of an anomaly and enhances shorter wavelengths anomalies which are of shallow sources.. Thus, the vertical derivatives is use to delineate high frequency causative bodies readily that would have been masked off by large amplitude bodies with low frequencies.

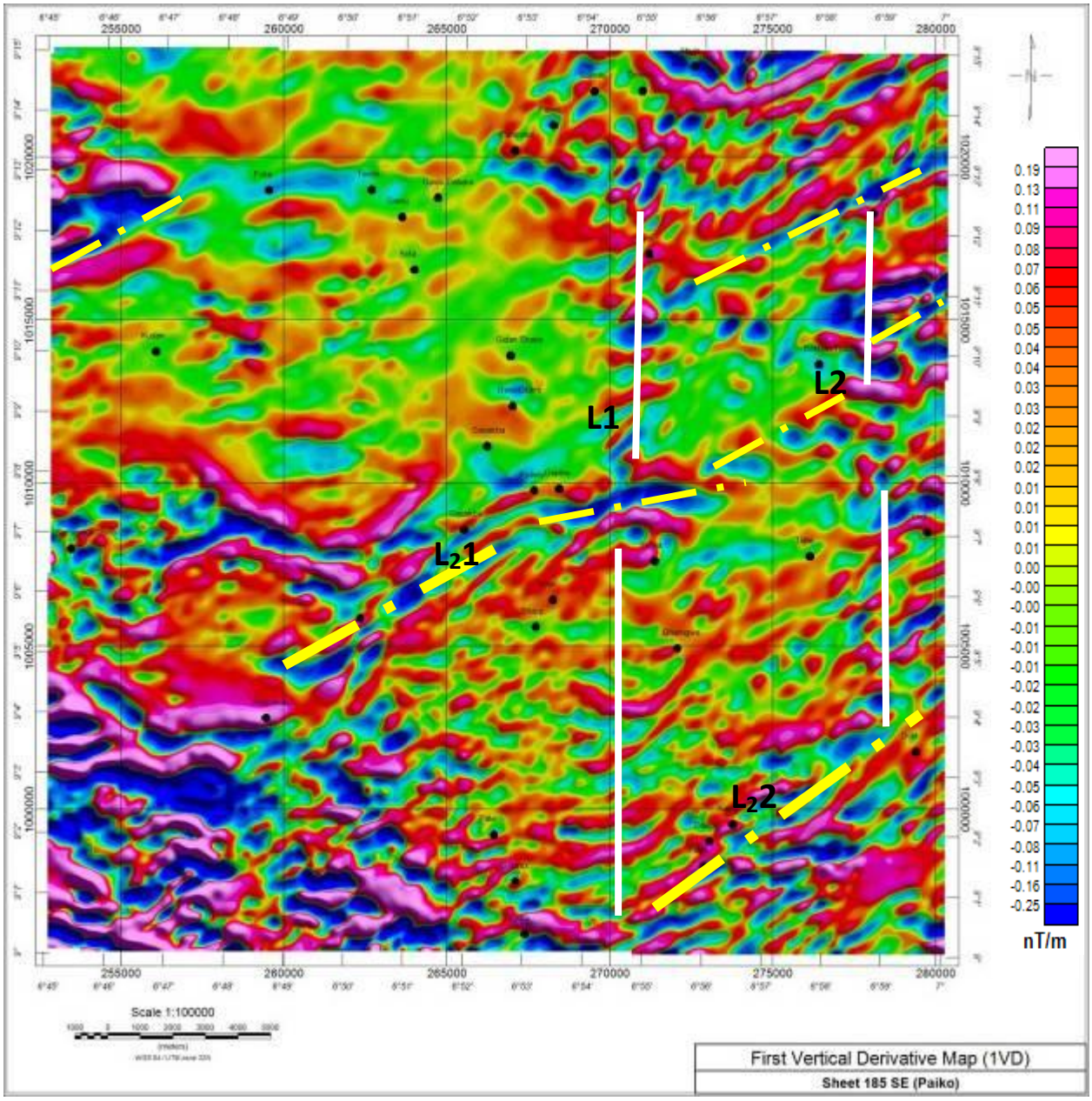

Figure 4.4a: First vertical derivative map covering the Sheet 185 (Paiko SE) showing more nearer surface structures than the Total Magnetic Intensity (TMI) Map

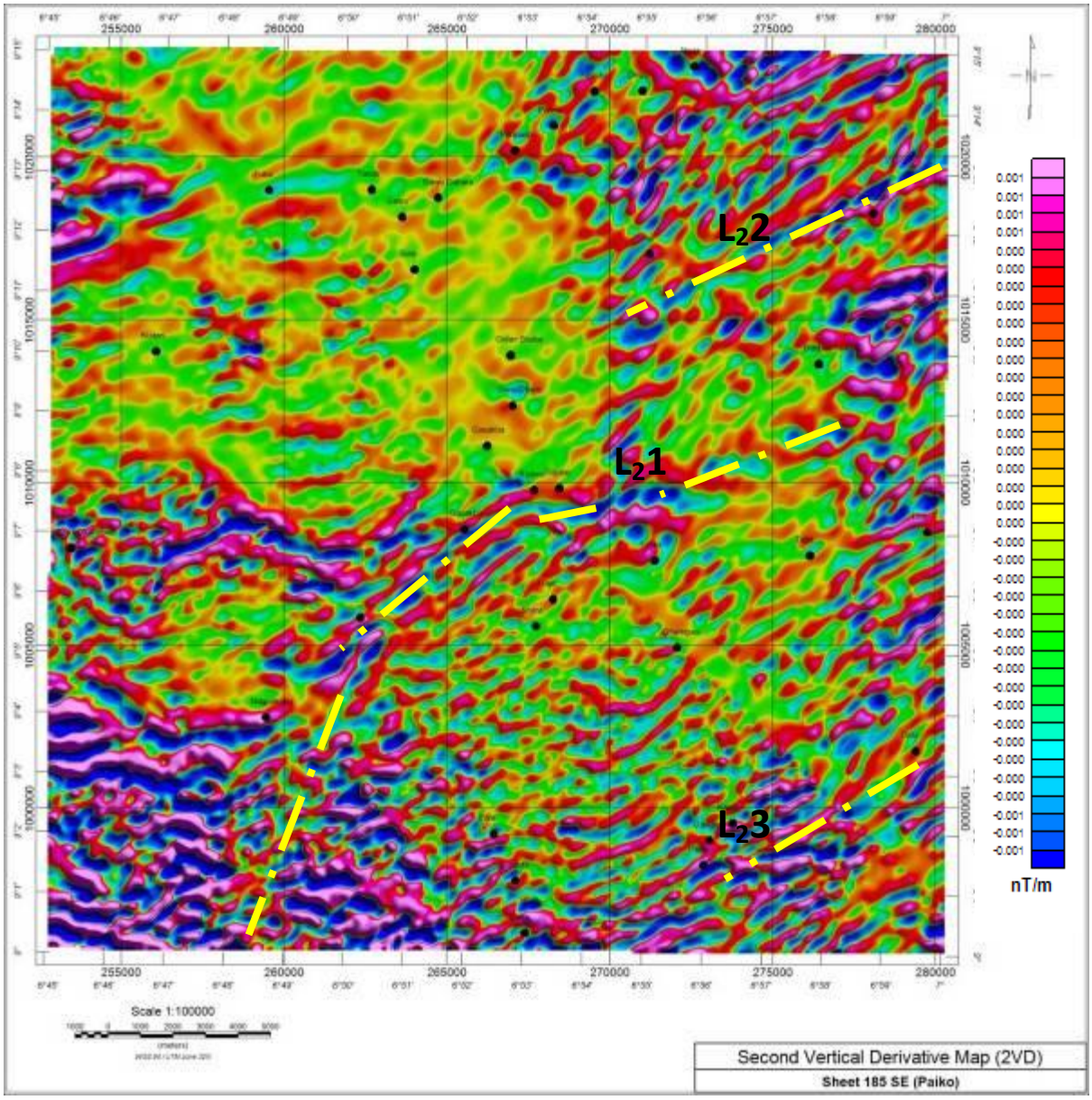

Figure 4.4b: Second verical derivative map covering the Sheet 185 (Paiko SE) showing much more near surface structures and anomalies

Horizontal Gradient

The horizontal gradient derivative was able to enhance the edge/contact while the vertical derivatives help to narrow the width of the observed anomalies thereby locating the source. Horizontal gradient (HGRAD) derivative enhances discontinuities such as fault and contact features within the study area. It complements the first vertical derivative enhancements above and produces a more exact location for faults than the vertical derivative. Discontinuities in processed magnetic data could be due to faults, lithological contacts among others. Also, the horizontal gradient of the Magnetic field was equally computed and gridded (Fig. 4.5).

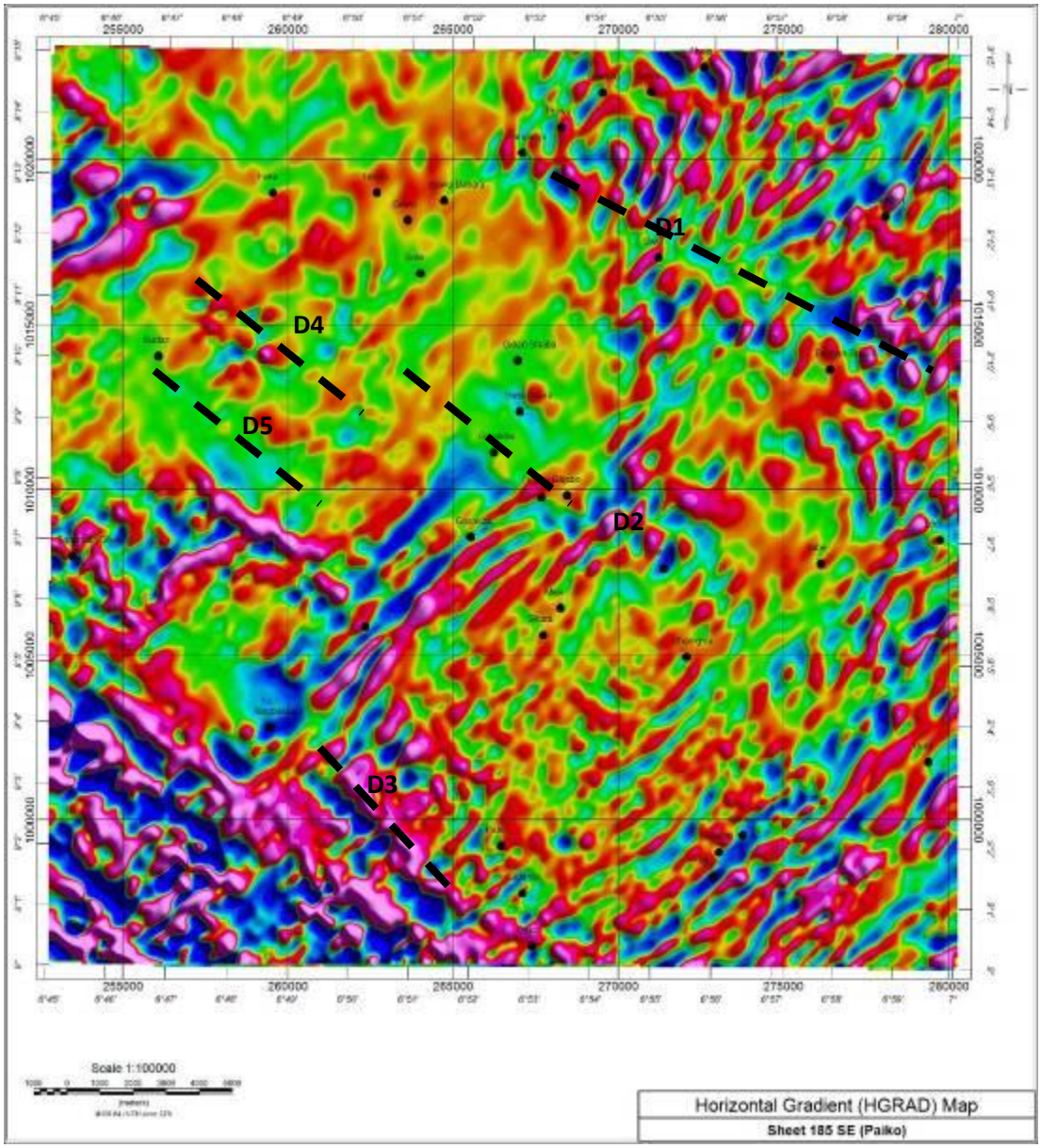

Figure 4.5: Horizontal Gradient map covering the Sheet 185 (Paiko SE) showing edge enhancement of the causative structures or bodies

The vertical derivative maps (first and second vertical derivatives) attenuated structures in the NE-SW directions which are been interpreted as regional structures. The structures attenuated are more of shorter wavelengths. These structures were truncated by the oval intrusives delineated from the textural classification of the gridded total magnetic intensity map and analytical signal. Prominent are the lineaments labelled L1, L2 and L3 (fig. 4.4a and b). The horizontal gradient map on the other hand attenuated more of discontinuities in the regional trends which are been interpreted as faulting. These discontinuities are marked D1, D2, D3, D4 and D5 (fig. 4.5).

4.1.2 Delineated Geological Structures

Sequel to compilation and processing of the aeromagnetic data over the study area, the structures observed were delineated in Geographic Information System (GIS) environment and vectorized as shapefiles. These structures ranges from been deep seated to near surface, textural classification and source-edge detection. The structures were correlated from one derivative to the other to be sure that they are not artificially imposed or noise due to higher order degree of polynomial in the vertical derivatives (Fig. 4.6).

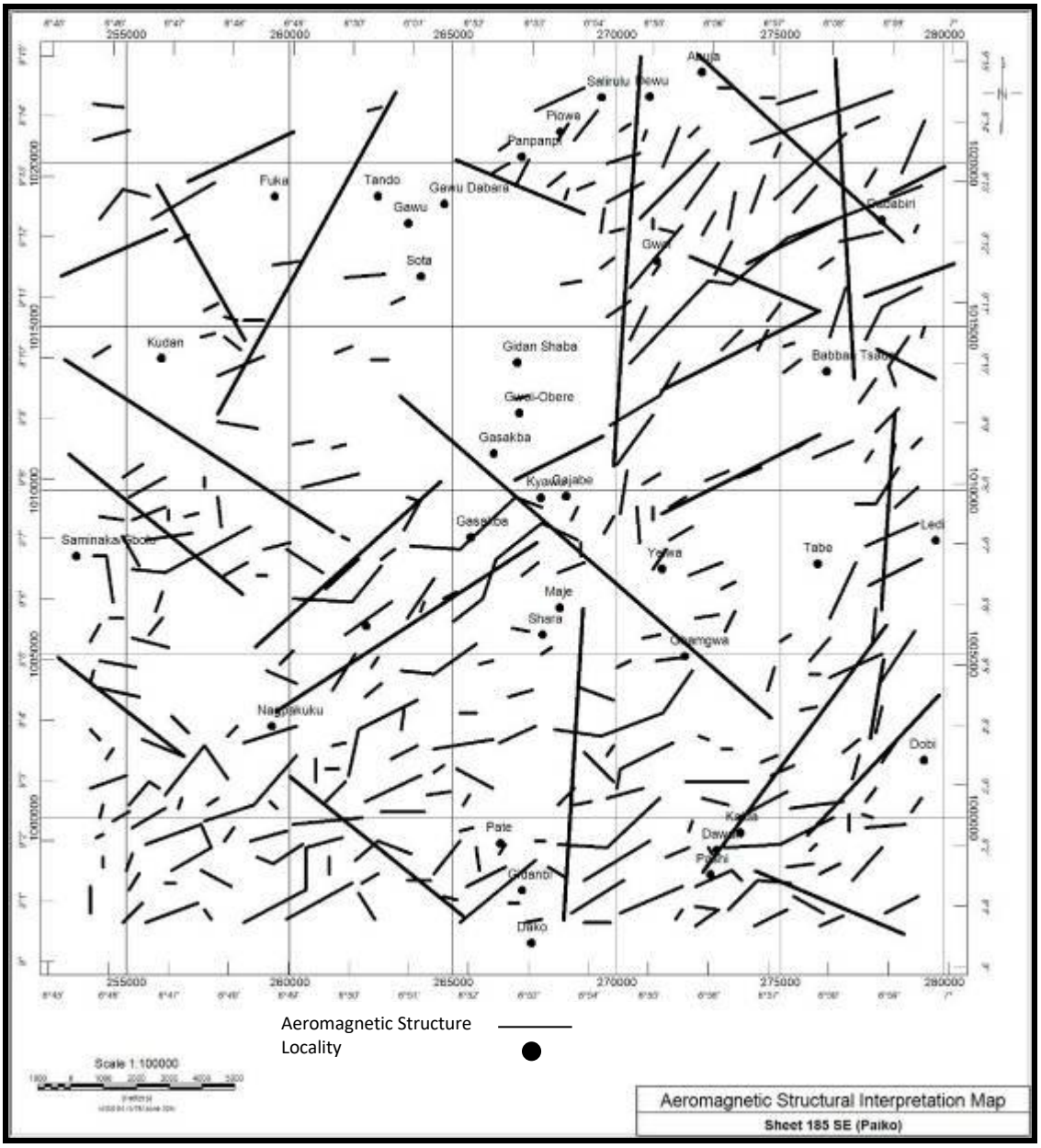

Figure 4.6: Delineated Aeromagnetic Structural Interpretation map covering the Sheet 185 (Paiko SE) showing both Regional and Local Structures

The ‘relief’ of the grids are relatively objective and made up majorly of amplitude’s effect of the anomaly, while ‘texture’ deals with the causative source geometry and continuity, and its more subjective. There were three prominent structural trends delineated from the grids within the study area as processed and interpreted. From the cross cutting relationship and field evidences, the nearly north-south structure which are interpreted as Pan-African are the youngest. These structures, though occurring randomly over the study area are more prominent towards the eastern section. This trend was also observed to be controlling the flow direction of the major drainage within the study area. From the published geological map of the Paiko sheet 185, by the Nigerian Geological Survey Agency, this structural trend had also been delineated and interpreted as Pan-African.

There are other prominent discontinuities delineated from the processed magnetic derivative maps, and although older than the north-south trend, they trend in a northwest-southeast and north northwest-south southeast direction discontinuing the much older structures that are dominantly in the northeast-southwest direction. In chronological succession from cross cutting relationship, the NE-SW structural trends are the oldest. These were discontinued in several locations by the NW-SE to NNW-SSE and the youngest been the nearly N-S structures.

Folding was observed around Baban Tsauni area where a prominent ridge was observed on the digital terrain model (SRTM) to have been folded. This had also been accounted for by Okunlola *et al*. (2007), having axial plane trending NW-SE. From the structural interpretational map, the rose diagram of both the major/regional structures and the local structures were computed as a function of frequency on a bi-directional rose plot (Figs. 4.7a and 4.7b).

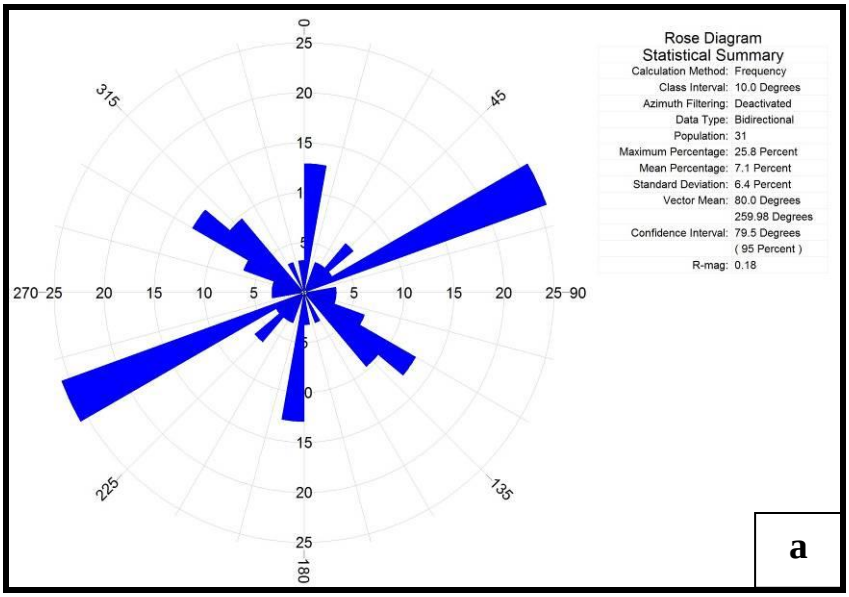

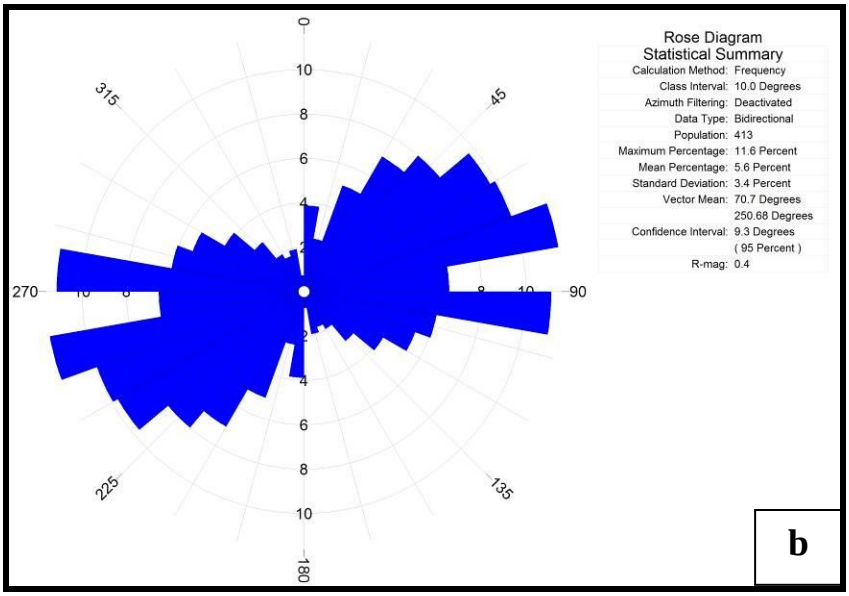

Figure 4.7: a-Rose diagram for the major/primary structures within the study area. b- Rose diagram for the Local/Secondary structures within the study area

As observed, there are varying structural directions with the dominant structural trend being the northeast-southwest trend agreeing with the deductions of Oluyide (2004) that the N-S and NE-SW trending foliation are the main structural trends within the study area. The major/regional structures shows dominant trend in a NE-SW direction with N-S and NW-SE structures suspected to be arising from fractures, joints and faults (Fig. 4.7a). The local structure from the rose diagram (Fig. 4.7b) shows great similarity with the major structure as the dominant trend occurs along the NE-SW direction and the other trends showing up with greater density and slight variation in angles due to varying deformation phases. Interesting to note is the nearly east-west trend, precisely WNW-ESE trend which could be due to re-alignment of mineral fabrics in the host rocks.

Okunlola *et al*. (2007) postulated that the quartz vein play host to the sulphide mineralisation within the study area and that these veins trend in a NNW-SSE direction as observed around Baban-Tsauni from the southern end around Ledi village and also around the central portion passing through Yelwa. Thus, it is being postulated from this research study that the local structures in the NW-SE to NNW-SSE direction are the major structures controlling the mineralisation within the study area.

4.2. Lithological/Geological Boundaries Delineation

The radiometric maps generated show the spatial variations of radio-elements that are controlled among other things by the complex surface processes and the inherent statistical fluctuations of radioactive decays. For classification which could be related to geological events and hence lithology, the radiometric data were gridded individually and then ratios were calculated to evaluate variations and spatial-restriction with distinctive signature, which provides local baselines of the surface concentrations of the natural radio-elements.

4.2.1 Radio-Elements Concentrations

The gamma-ray spectrometry shows the potassium concentration in percentage, equivalent thorium (eTh) and uranium (eU) from shallow near surface between depths of about 0 - 50 cm. Due to the disequilibrium potentials, the concentration of thorium and

uranium are given as equivalent values. The concentration values showing the spatial distribution of the radioelement are presented as a grid image for interpretational ease (Figs. 4.8a, b and c)

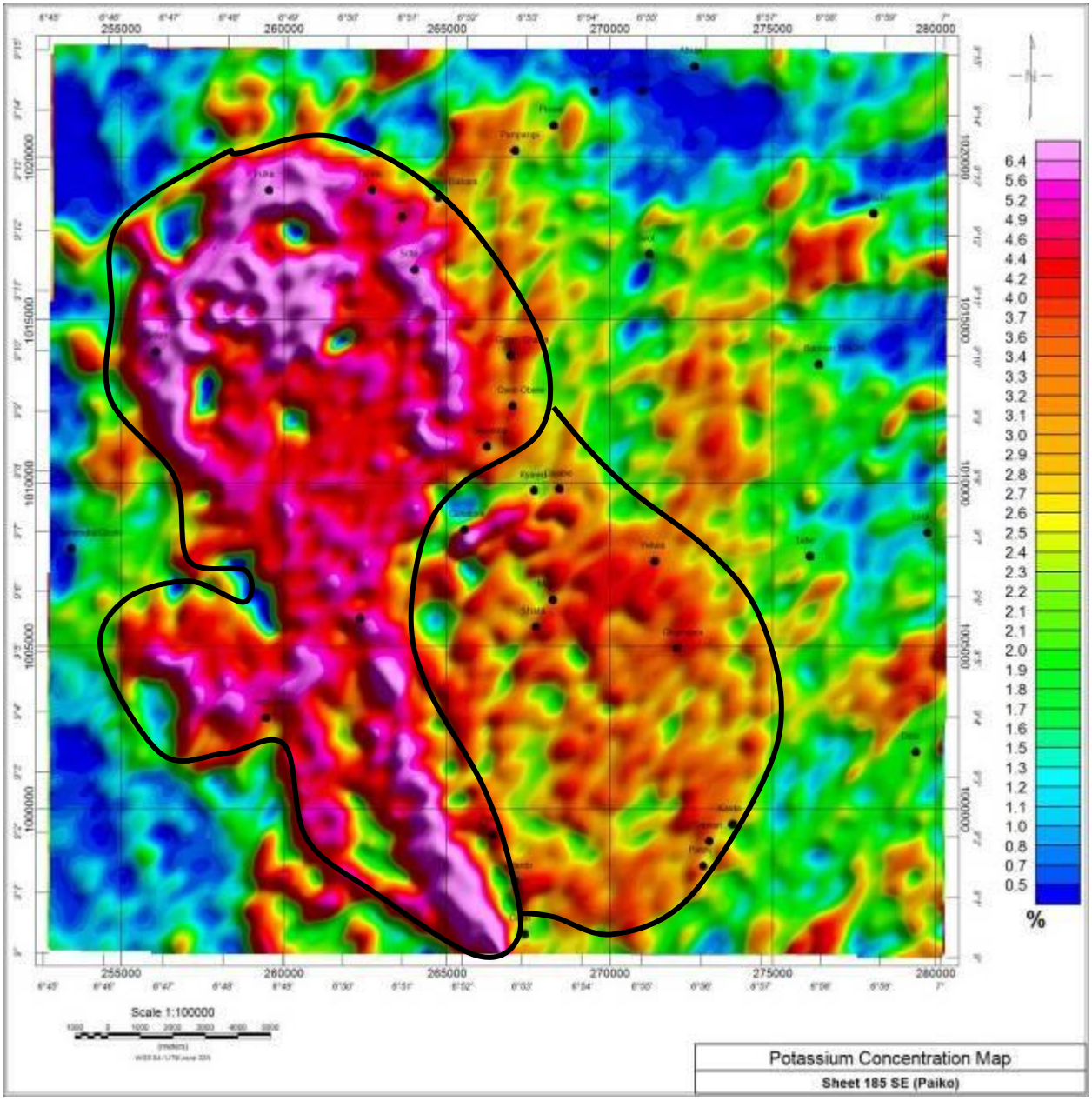

Figure 4.8a: Potassium concentration map covering the Sheet 185 (Paiko SE) showing enrichment spatial variation

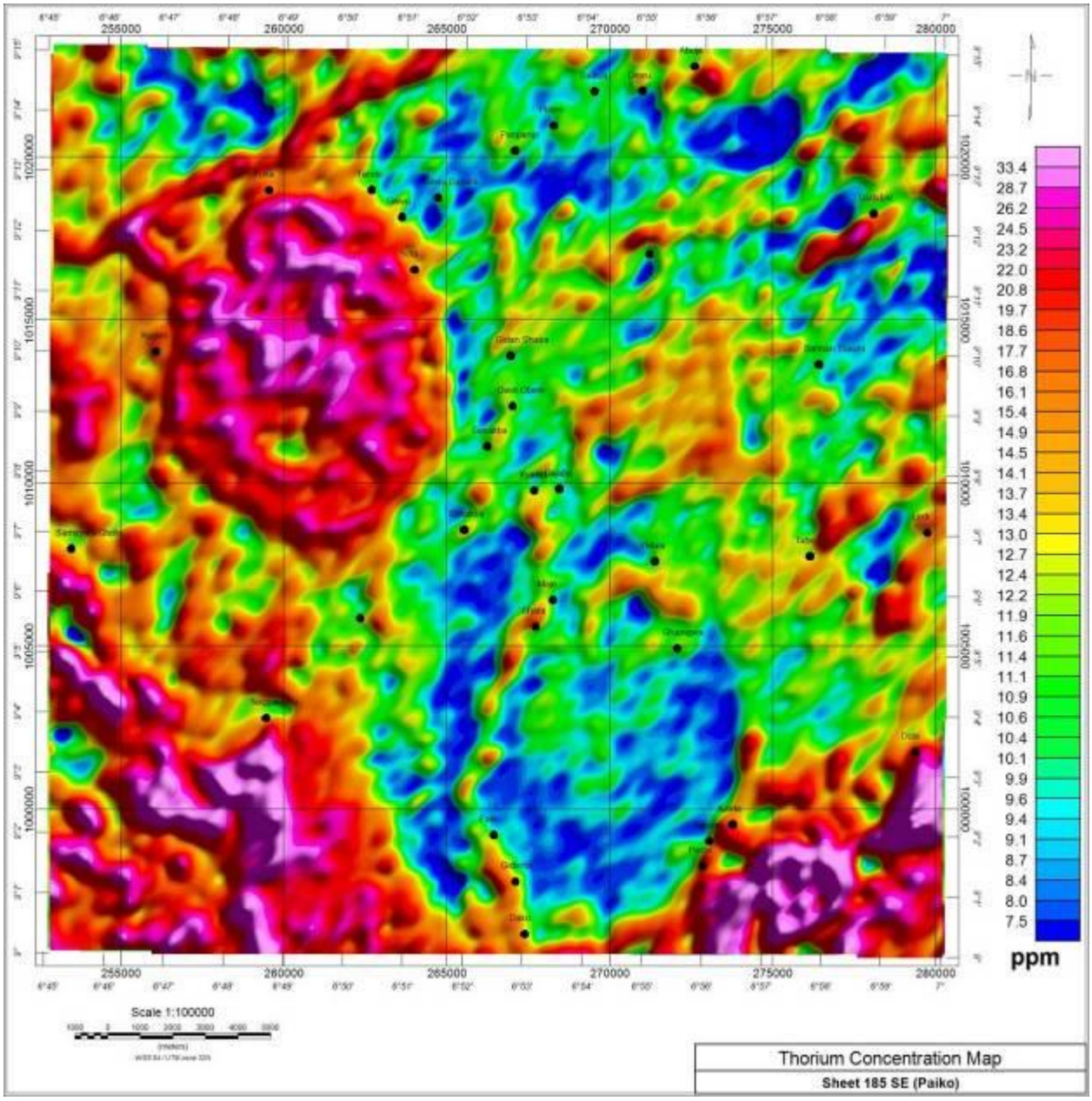

Figure 4.8b: Thorium concentration (eTh) map covering the Sheet 185 (Paiko SE) showing enrichment spatial variation

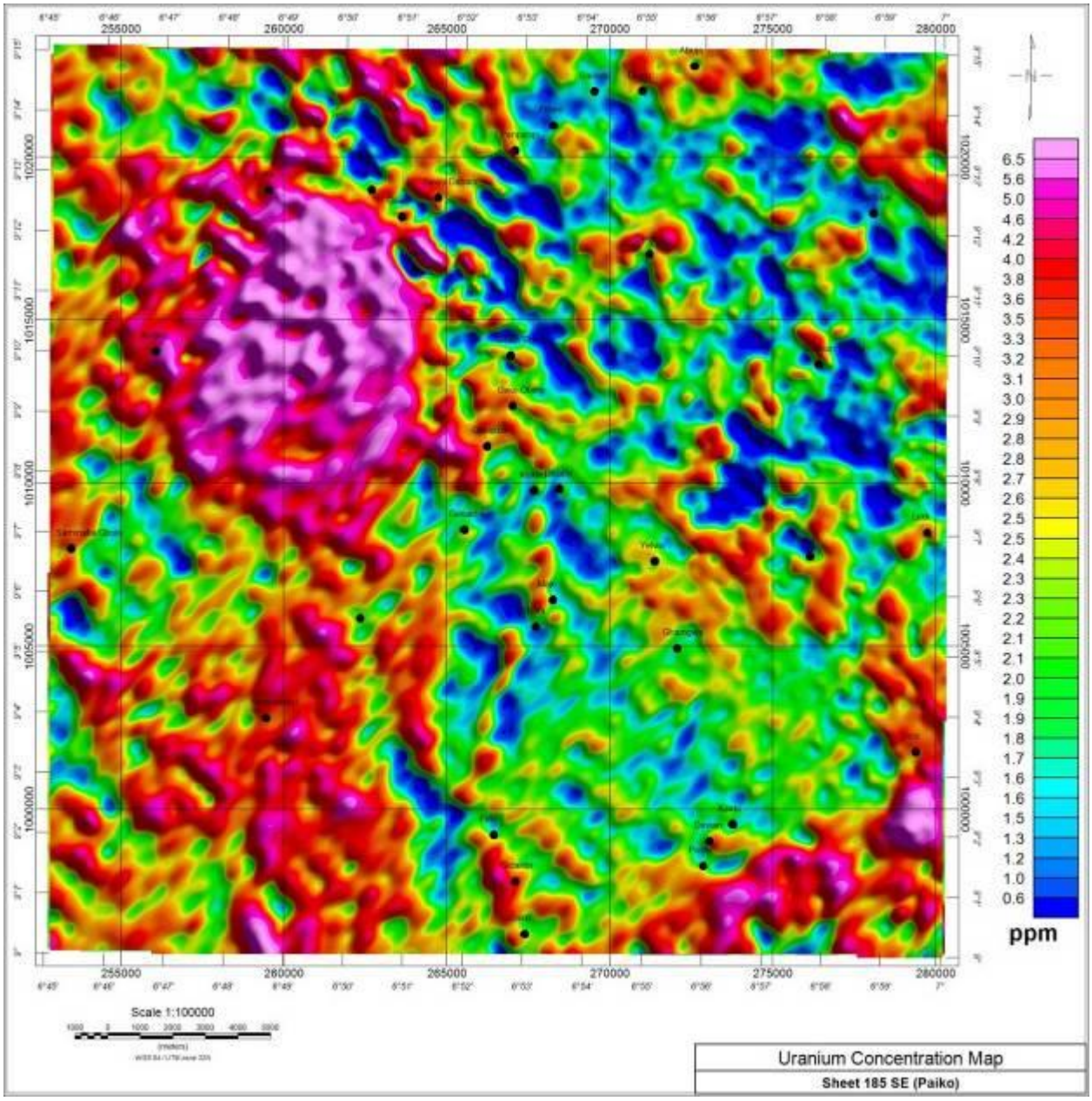

Figure 4.8c: Uranium concentration (eU) map covering the Sheet 185 (Paiko SE) showing enrichment spatial variation

Discussion

The gridded maps (fig. 4.8a-c) shows distribution of areas with distinctive signature relating to various lithology, geologic history and on-going events. The classification shows the spatial distribution in the overall percentage as related to various classifications within the study area.

Thus, the potassium concentration map (fig. 4.8a) clearly shows a relatively very high potassium-rich unit than the surrounding around the north-western part of the study area. Adjacent to this large oval lenses is another body equally rich in potassium but interpreted as deep seated as interpreted from the aeromagnetic and the digital terrain model. These two anomalous units were equally mapped by the thorium and uranium map. Though the thorium concentration of the interpreted deep seated body was contrastingly lower than the surrounding, but its signature was mapped out effectively by the thorium concentration map (fig. 4.8b).

Uranium which is highly mobile was observed to be having a peak in the uranium map about the observed ridge delineated up by the aeromagnetic, digital terrain model as well as other radiometric maps. This shows that it is truly richer in uranium than the surrounding.

4.2.2 Ratio of Th/K, U/K and U/Th

Ratio maps of the three radioelements (Figs. 4.9a to 4.9c) were computed and processed as a way of delineating the signatures associated with the lithology which could serve as a guide for mineralisation characterization. These ratios help to identify areas with high concentrations of both potassium and thorium which are generally immobile unlike the uranium which is highly mobile.

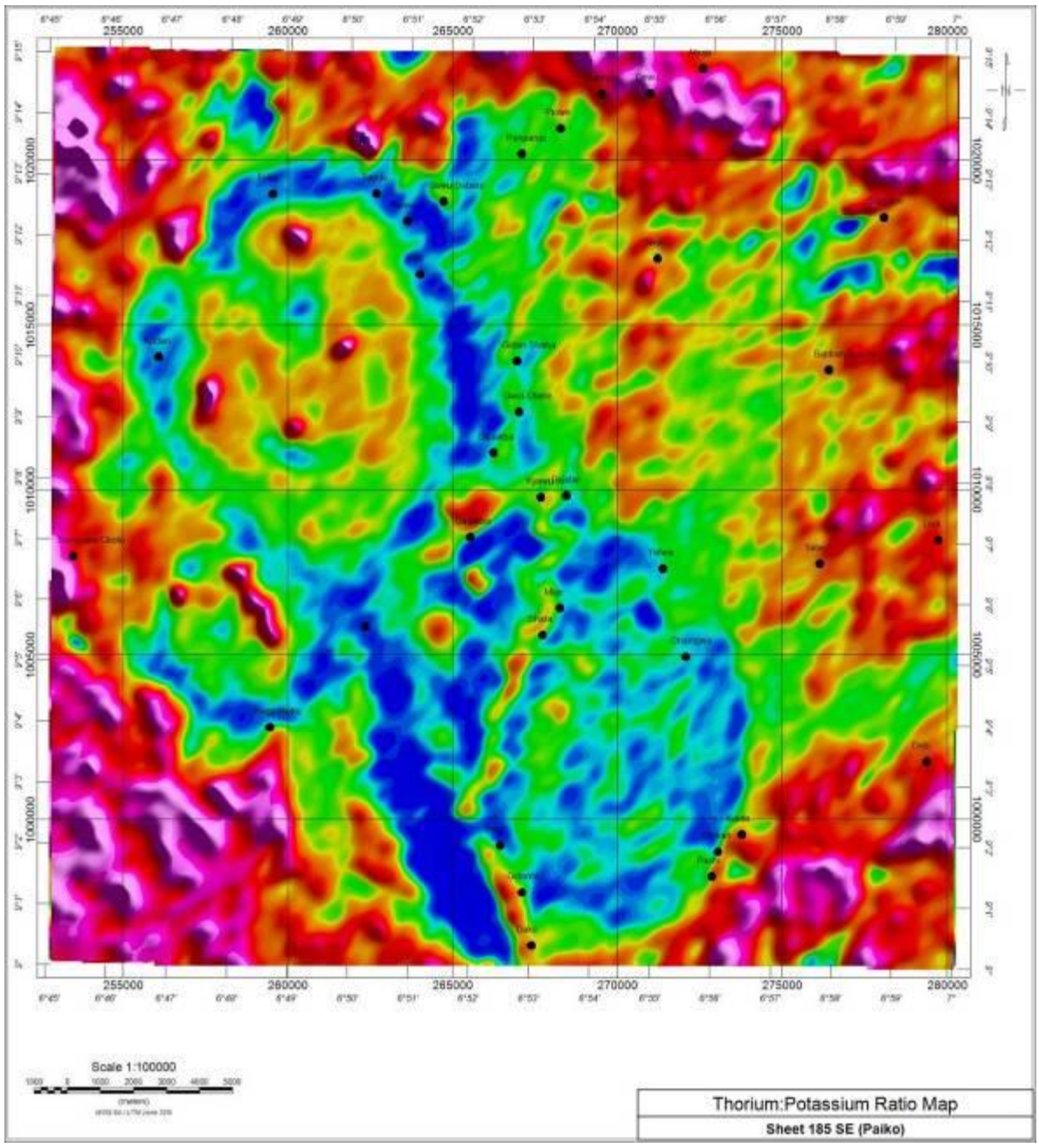

Figure 4.9a: Thorium-Potassium Ratio Map covering the Sheet 185 (Paiko SE) showing enrichment of thorium to potassium

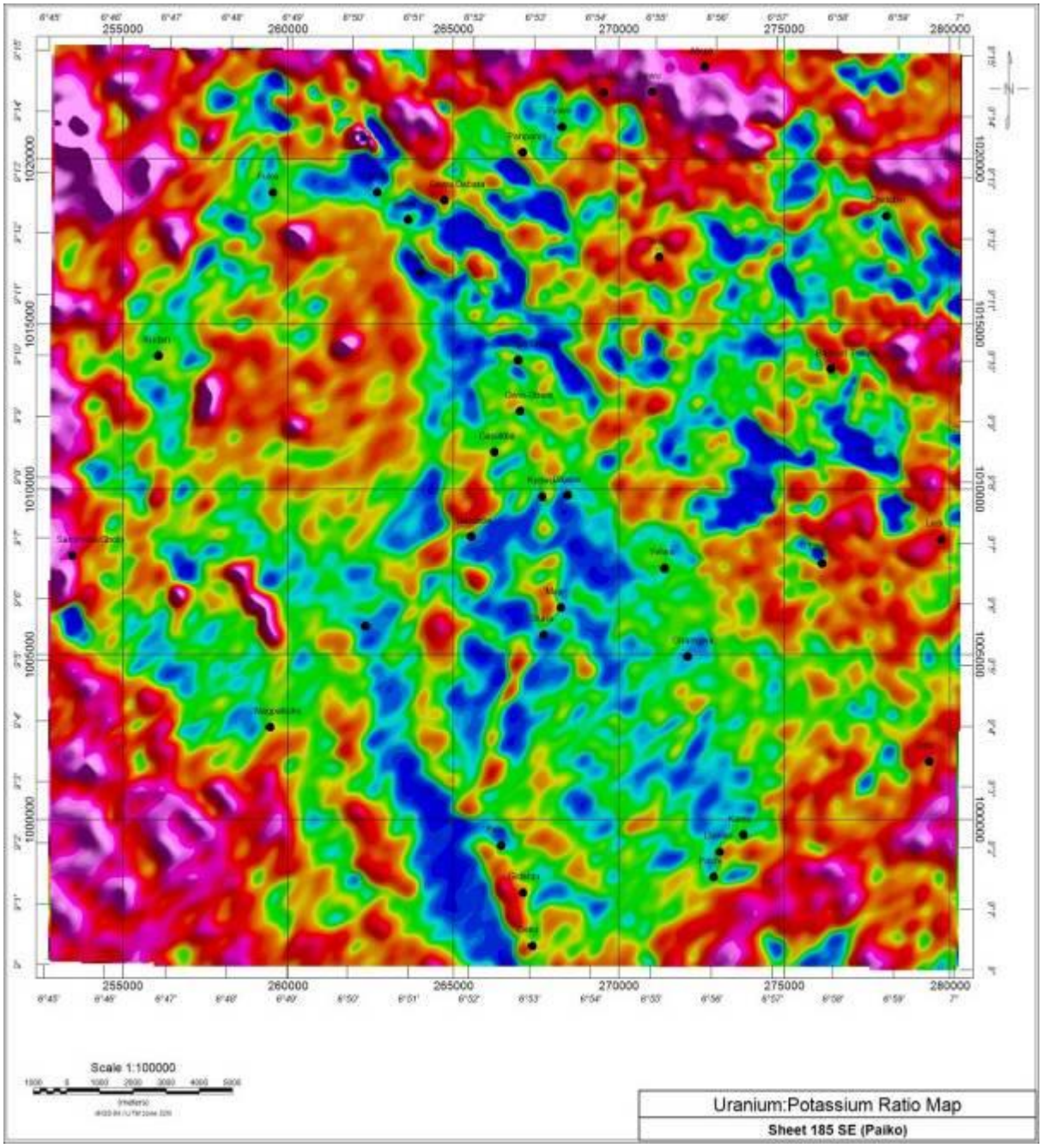

Figure 4.9b: Uranium-Potassium Ratio Map covering the Sheet 185 (Paiko SE) showing enrichment of Uranium to potassium

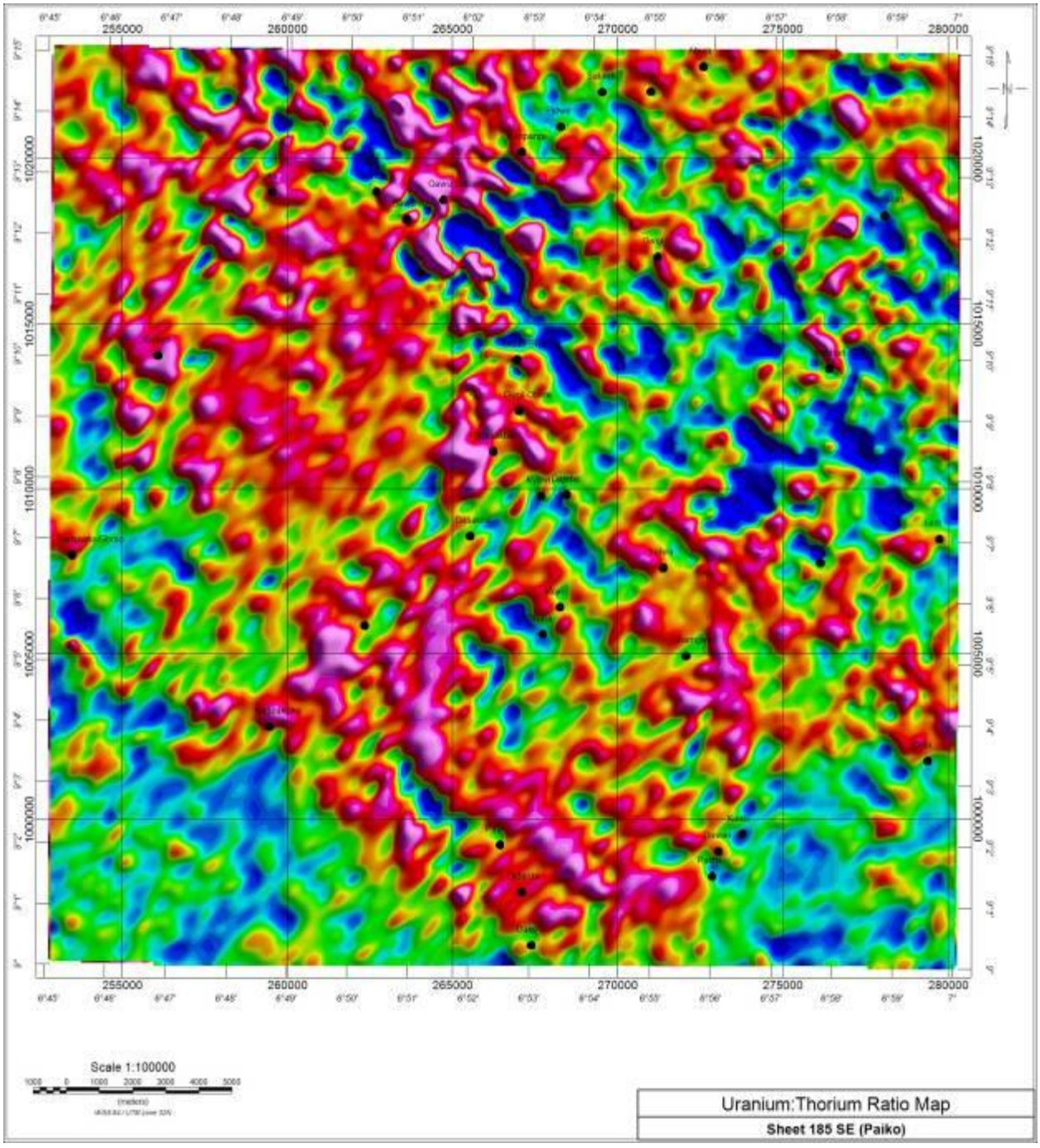

Figure 4.9c: Uranium-Thorium Ratio Map covering the Sheet 185 (Paiko SE) showing enrichment of Uranium to potassium

Rationing of the radioelements helps to maximize contrast and highlight subtle features in the data. Since the K response is associated with readily weathered rocks, while Th and U are usually associated with residual clay, oxides, and accessory minerals, the thorium channel and ratio map of Th/K (Fig. 4.9a) helps to determine the magnitude of leaching and weathering of the source body (Wilford *et al*.,1997).

It was also observed that the intrusive delineated on the magnetic occurring at the northwest and also adjacent southeast are both rich in potassium content, but the one at the southeast is more deep seated than the one in the northwest. In contrast, uranium which is highly mobile was observed to have a relatively higher concentration than the surrounding low land as compared with the digital elevation model. This shows that the enrichment is in-situ and not transported materials.

4.2.3 Composite Images (Ternary map)

The composite grid (Fig. 4.10) was generated from ratios of the three radioelements of K (%), eTh and eU. These ratios were assigned red, green and blue respectively (RGB). The ternary map represents spatial variation in intensity of the enrichment of each. Potassium was assigned to red, uranium to blue and thorium to green.

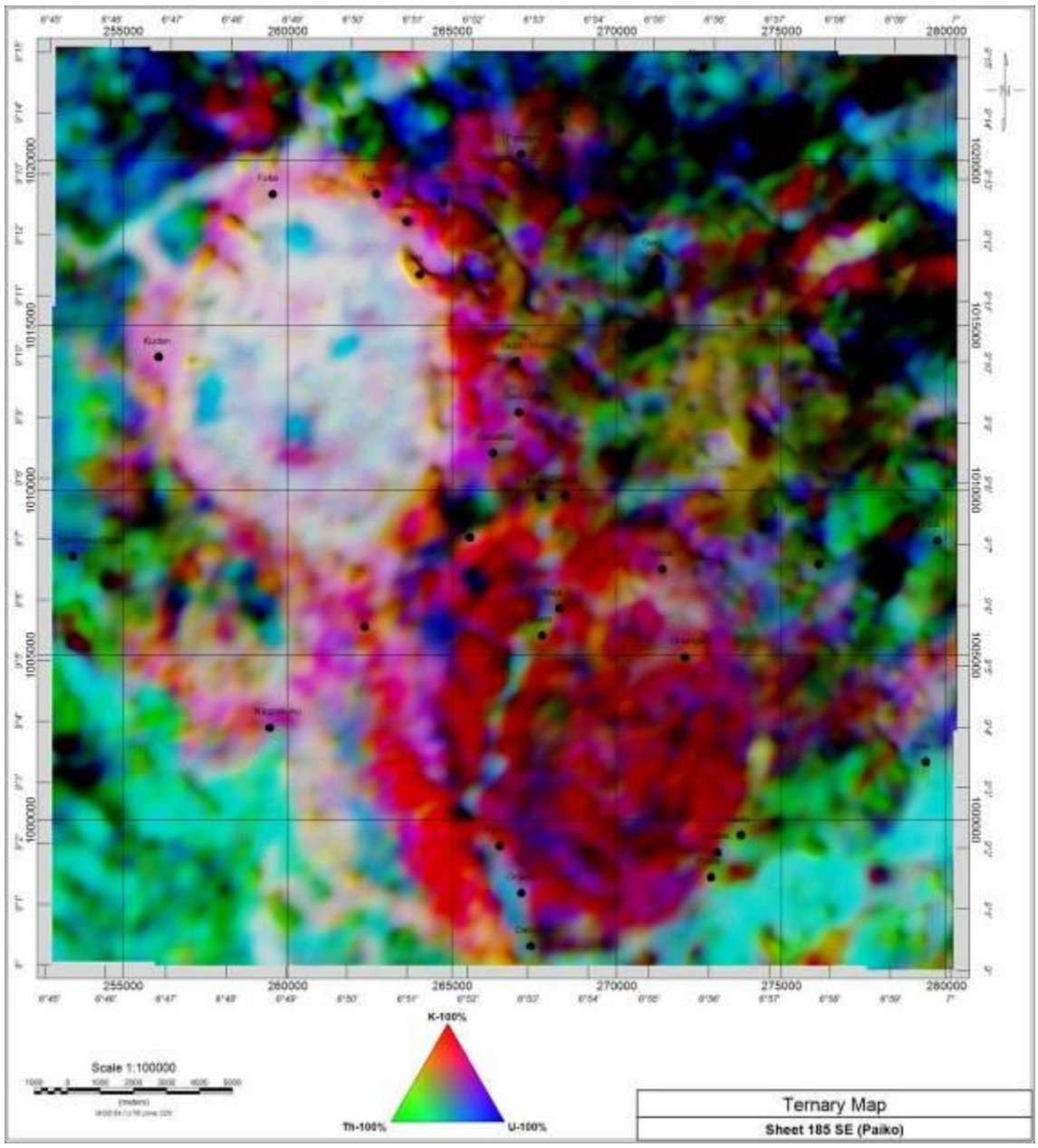

Figure 4.10: Composite Ratio Map of potassium, thorium and uranium covering the Sheet 185 (Paiko SE) showing spatial variation in radioelement concentration

The darker regions represent areas with very low values of all the three radio-elements while the white regions represents areas with higher values of the three radio-elements of potassium, thorium and uranium. Areas with low thorium concentration but with relatively high potassium and uranium concentration are expressed with magenta color, while yellow coloration denotes regions with high potassium and thorium values and a corresponding relatively low uranium value. The white region is conspicuously observed on the ridge mapped by the magnetic on the north-western section south of Fuka, while the more deep seated circular body to the southeast around Yelwa is richer in potassium concentration with in-fillings of thorium rich lenses due to debris within the drainage channel.

4.2.4 Interpretation of Geological and Structural Setting

Data integration was done in ArcGIS environment where the radiometric grid files were characterized/delineated based on the spatial distribution of the radio-elements. This classification was equally supported by textural classification of the aeromagnetic dataset from the Total Magnetic Intensity map and the Analytic signal map.

Aeromagnetic structures (Fig. 4.6) extracted from the different derivative of the aeromagnetic data were equally compared and were overlaid on the interpreted lithology and the boundary adjusted for geological unit with structural boundary delineations. This integration of the aeromagnetic dataset, radiometric and the digital terrain model from the Shuttle Radar Thematic Mapper (SRTM) gives a baseline overview of the geological and structural map for the study area as interpreted (Fig. 4.11).

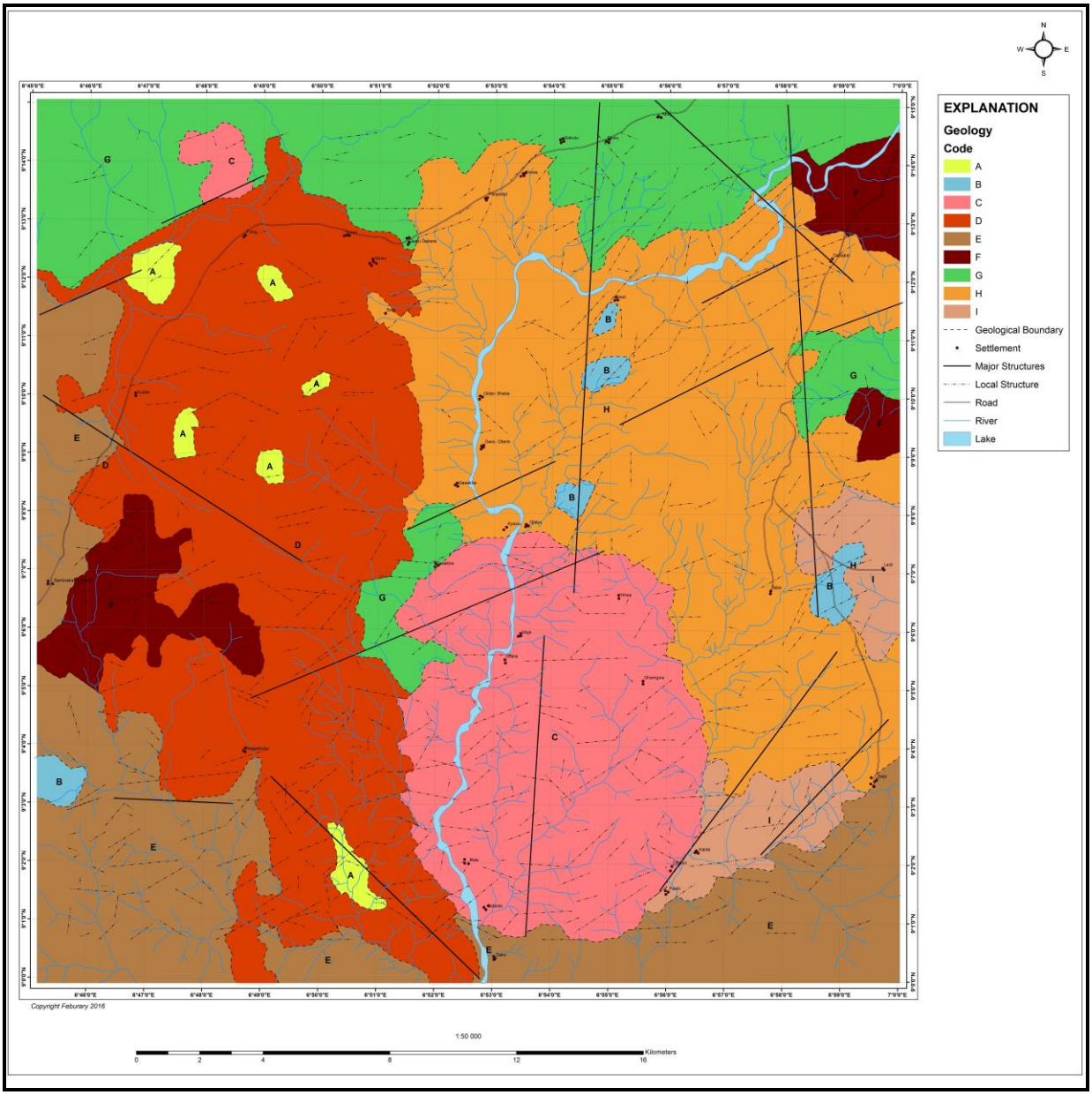

Figure 4.11a: Interpreted geological and structural map from airborne magnetic and radiometric, covering the Sheet 185 (Paiko SE)

As observed from the rose diagram plotted for both the primary and secondary structures, the structural trend in the N-S direction agrees with previous work within the study area and also typify the pan-African orogenic structural imprint having an approximately N-S structure and had been established over the years as been the youngest orogenic event recorded thus far within the craton. There are both major and minor magnetic discontinuities and lineament that traverse the study area in a NE-SW, NW-SE and approximately N-S trending patterns. Some of these lineaments are being interpreted as minor since they are not deep seated and extensive to correlate with the Orogeny. Notwithstanding, they show a trend that align with the fracture trend of the Chain and Romanche that cut through on a regional scale. According to Ajakaiye *et al.* (1991), there are magnetic lineaments with definite characteristics that exist within the Nigerian continental landmass. Thus, these lineaments can be in association with the St. Paul, Romanche, Chain and Charcot fracture zones, since they are believed to be part of the major zones of weakness in the crust and predate the opening of the Atlantic Ocean and they were reactivated in early stages of continental rifting (Ajakaiye *et al*., 1991).

When compared with the existing geological map of the study area extracted from the 1:100,000 scale (Fig. 4.11b) for the southeastern quadrant, the lithology C and D agrees with what was described as coarse grained granitic intrusive. These two bodies were equally delineated by the aeromagnetic data. The variation in the concentration of the percentage of potassium could be attributed to the fact that radiometric survey's depth of penetration is shallow and there are superficial covers over lithology C as compared with D where the surface expression forms a ridge observable from the digital terrain model. The lithology H agrees with the Migmatite gneiss which was equally mapped by Okunlola *et al*. (2007) and described as pegmatised gneiss. The lithology G which mark the northern fringe was also shown and mapped as migmatite schist with the intrusive (lithology C) outcropping towards the western portion. All these interpretation are subject to ground truthing. In essence, the radiometric data had been used to produce an updated geological map of the study area with the structural features overlaid (Fig. 4.11a) and it's subject to ground truthing for the actual lithological description and subsequent name.

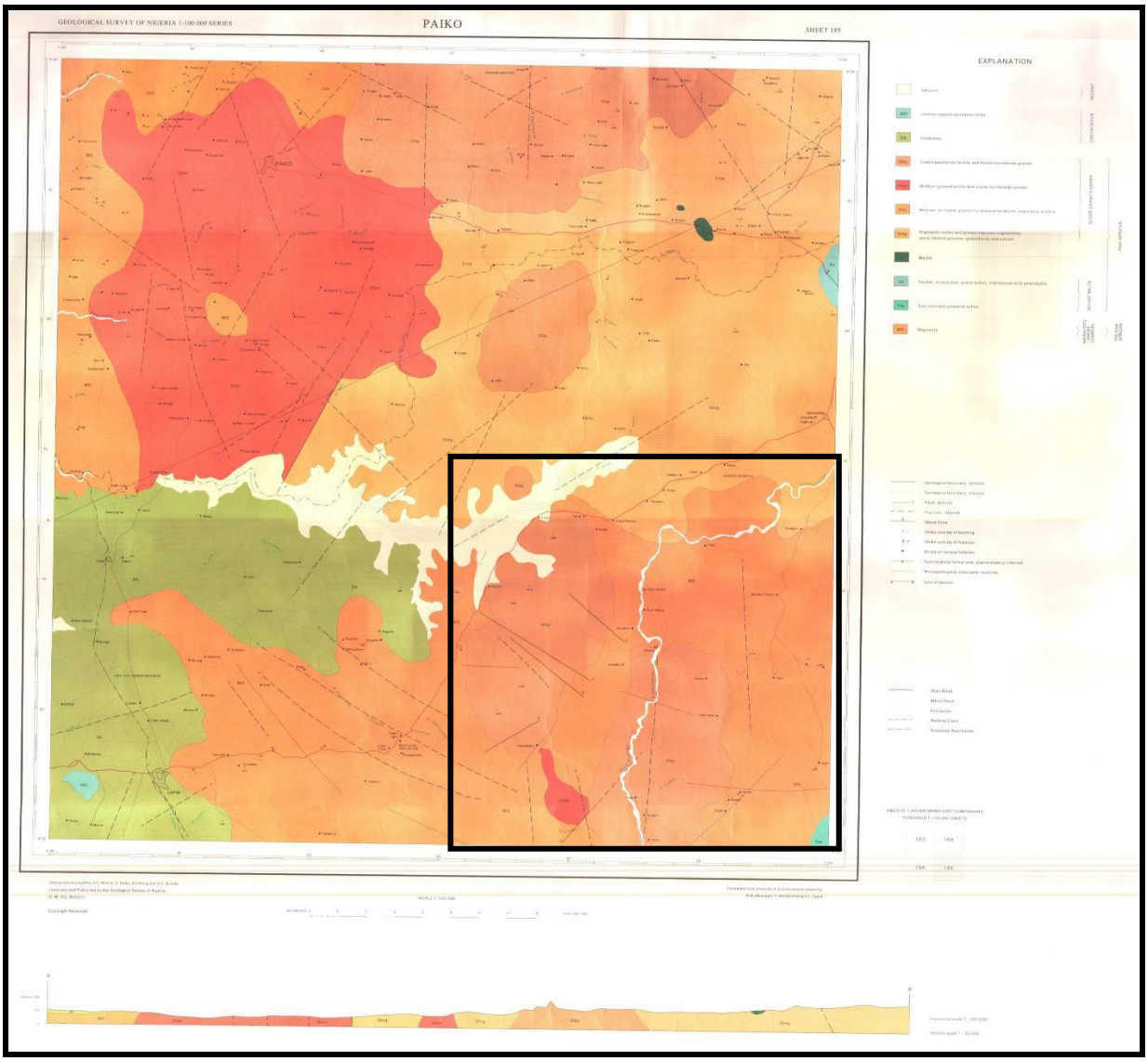

Figure 4.11b: Geological Map of Sheet 185 Paiko showing the south-eastern quadrant in black box. (Source: Geological Survey of Nigeria, 2000)

4.3 Geological and Structural Ground Truthing

The ground truthing started with reconnaissance survey which was followed by a more detail mapping over a target area (Figs. 4.12). The target area was carved out after careful interpretation of the airborne magnetic structural interaction from cross-cutting relationship and lithological characterisation with the radio-elements from the airborne radiometric data, Geological ground truthing (reconnaissance), literature review and artisanal workings within the area.

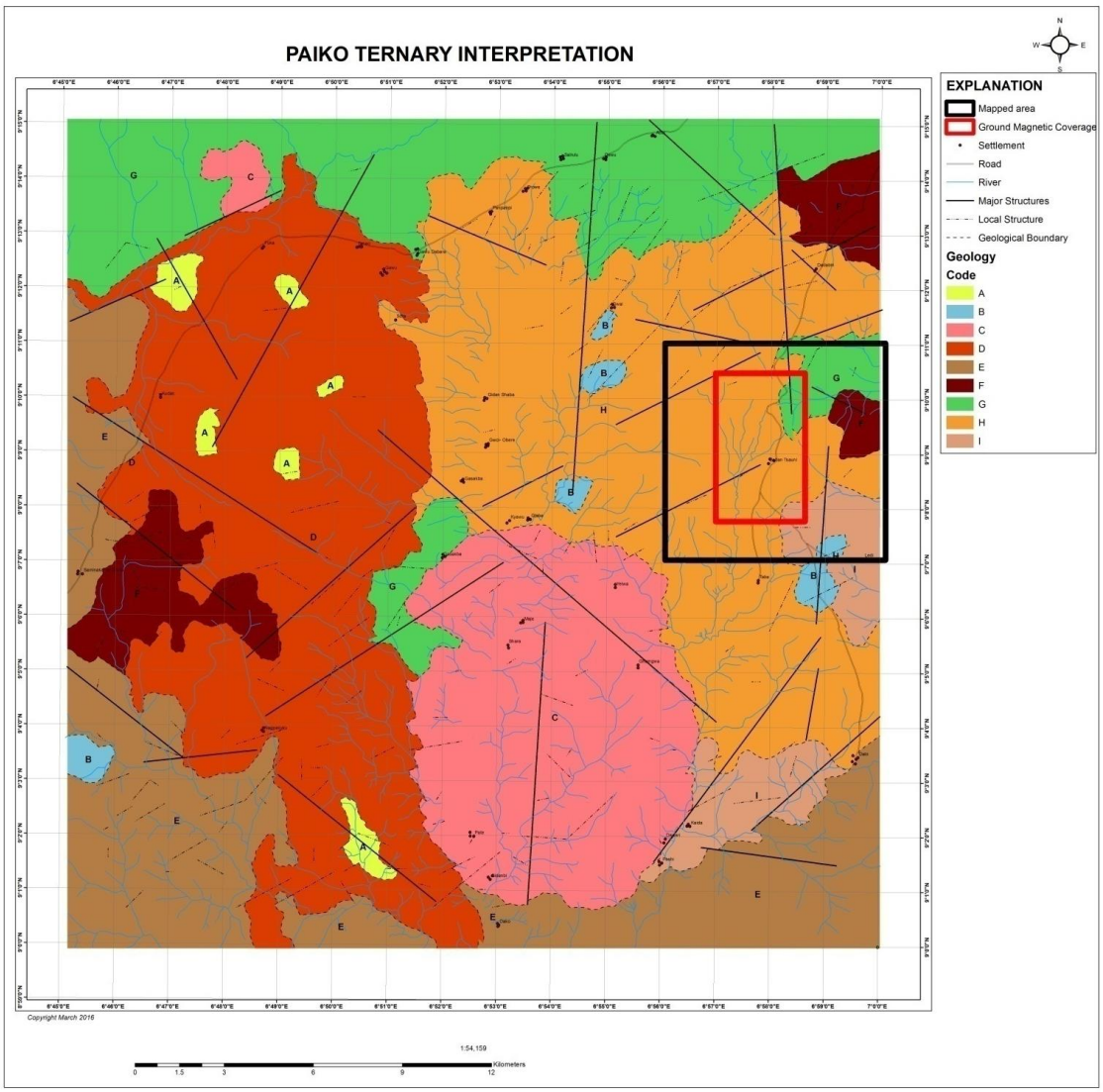

Figure 4.12: Interpreted geological and structural map of the area showing the mapped area in black box and the ground magnetic coverage in red box

4.3.1 Rock Types Mapped

Gneissose Rock

The banded gneiss, granite gneiss and biotite-gneiss are the most abundant rock units in the project area. The rock forms a few hills within the area. One of these hills is the most prominent topographical feature in the area, it is a N-S trending ridge, about 1.7 km long and about 400 m wide, it rises to a height of about 250 m above sea level. However, the rock units are generally poorly exposed (Fig.4.13a-d). The hills especially are covered by a fairly thick layer of soil which supports equally thick savannah vegetation. Only boulders of varying sizes, most of which are not in place occur along the slopes and tops of the hills (Fig. 4.14a-b).

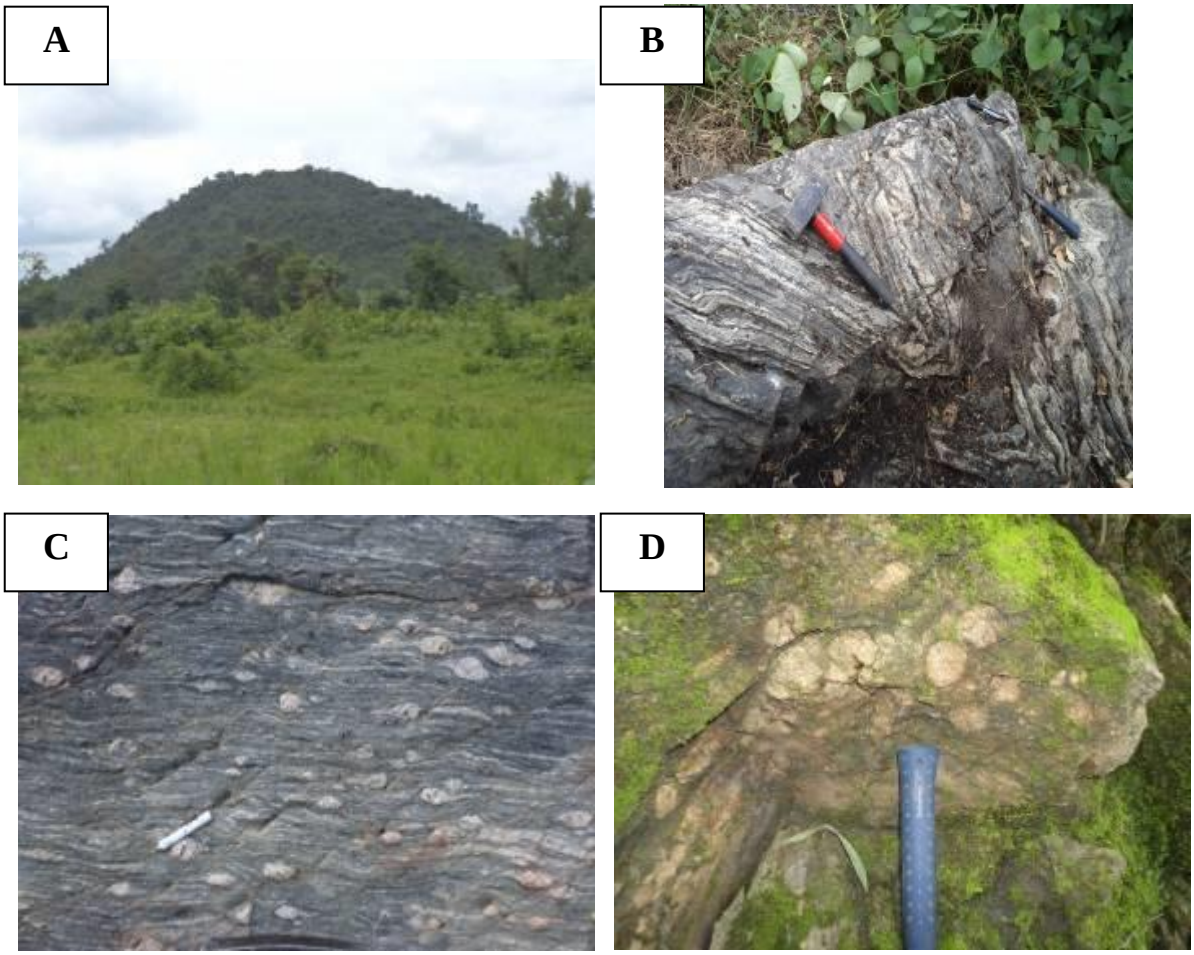

Figure 4.13: A-Vegetation covered biotite-gneiss ridge. B - Folding observed on the biotite-gneiss showing mineral segregation (banding) and the incipient development of a later shear related planar surface, marked by closely spaced cleavages C - Augen texture displayed by the biotite-gneiss. D - The biotite-gneiss with large sub-rounded pebbles of feldspar

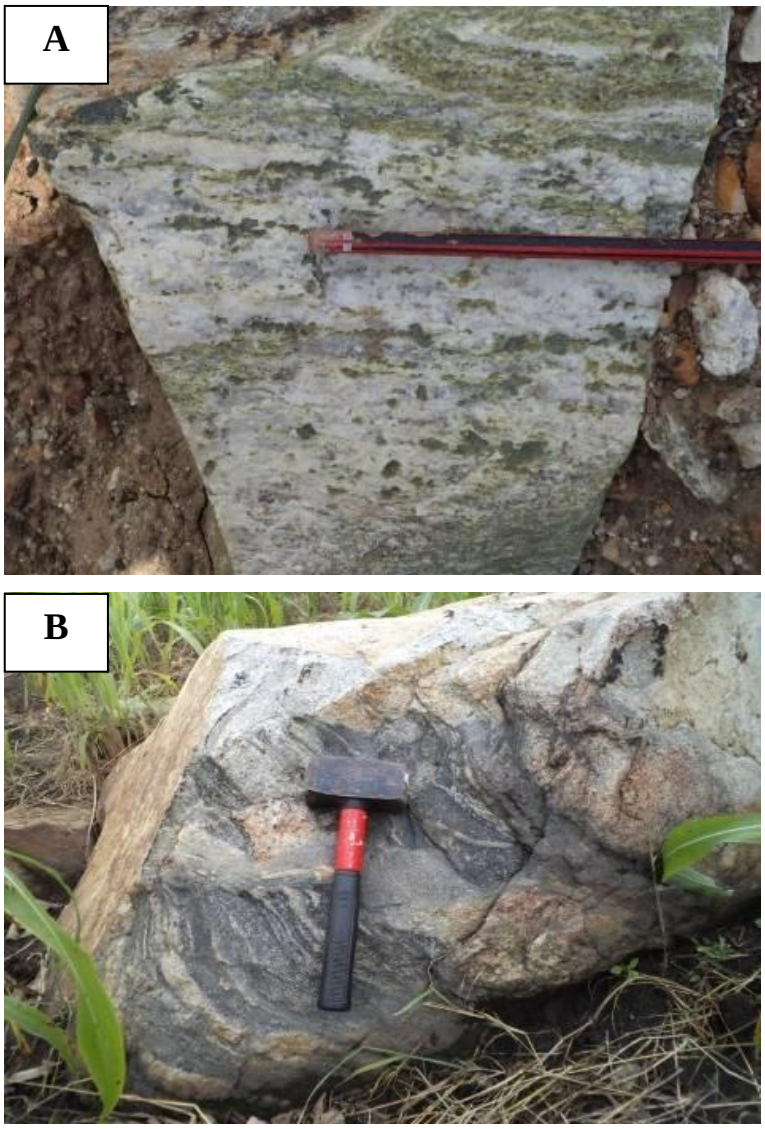

Figure 4.14: A - The biotite-chlorite gneiss with thick bands of felsic and mafic minerals. Note the alteration of the mafic minerals into greenish chlorite. B - The biotite-chlorite gneiss in an advanced stage of migmatization. Note the schollen migmatitic structure with fragments of the gneiss floating within rocks of quartzo-feldspathic composition.

The biotite-gneiss is grayish to dark-grey in colour; it is medium to coarse-grained and composed of feldspar, quartz, biotite and chlorite. The biotite-gneiss is thinly to fairly thickly band in some locations, making a textural classification for banded gneiss. The granite gneiss, biotite gneiss and banded gneiss grades imperceptibly into each other. The gneiss becomes migmatitic in places, with the lit-per-lit injection of quartzo–feldspathic materials.

The rock displays porphyroblastic texture in some localities. In some places, the porphyroblastic gneiss displays typical augen texture. In other localities, especially towards the western part of the area, the feldspar porphyroblasts occur as larger sub-rounded pebbles in the gneiss. Some of the pebbles measures up to 6 cm by 10 cm. In some other localities towards the south east, the feldspar grains have been deformed and stretched to form lenses which are aligned parallel to the bands in the gneiss (Figs. 4.13a-d)

The banded gneiss to the south-east assumes colours which vary from grey, greenish-grey to pinkish-brown. This is due to different degree of weathering and alterations of the feldspar, biotite and suspected amphibole minerals. The rock is medium to coarse-grained and consists of feldspar, quartz and biotite as the major constituents.
The dark bands are mostly constituted by biotite and suspected hornblende and amphibole minerals, which have been altered in several places into greenish chlorite minerals. The light bands are made up of feldspar and quartz (Figs. 4.14a-b). The gneiss becomes highly migmatitic in several localities. Migmatitic structures such as schollen, dicktyonitic and agmatitic structures are common.

The Medium-Coarse Grained Granite

The medium-coarse grained granite is of minor occurrence in the project area. The rock does not form any topographic height. Exposures are generally small, low lying elongated ridges or mounds. They have been partly weathered in most places into large boulders. The rock is pinkish to pinkish-brown in colour. The constituent minerals include feldspar, quartz and biotite. The granite appears to be intrusive into the gneisses, and the contact is commonly a sharp one (Figs. 4.15a-b).

Figure 4.15: A - Medium grained granite occurring as scattered boulders. B - Exposures of Disseminated boulders of the medium grain granite

Aplite and Pegmatite

Aplite and in some places quartzofeldsparthic rocks occurs mostly as veins in the gneisses. It occurs in almost all part of the project area. The veins which are either concordant or discordant to the strike of foliation in the host rock vary in widths from about 0.5m to 2m. Due to poor exposure, their extent along strike lengths has been difficult to establish.

Being more resistant to weathering than the gneisses, aplite veins commonly stand out as low-lying tabular ridges. This is particularly so in several places where the host rock (gneiss) is not exposed. The aplite is generally pinkish in colour; it is fine to medium-grained and consists of feldspar with subordinate amount of quartz (Fig. 4.16a). Pegmatite also occurs as veins and veinlets (Fig. 4.16b). They are not as abundant as the aplite veins.

Figure 4.16: A - An aplite vein displayed by a minor fault. Note the thin vein quartz emplaced along the fault plane. B - Pegmatite intruded Gneissic Rock.

Vein Quartz

Like the aplite, quartz veins are common features in the area. They occur as concordant and discordant veins and veinlets in all other lithologies. From field observations, there appears to be at least two generations of quartz veins. The earlier veins associate concordantly mostly with the gneisses. They have been deformed and folded with the host rocks. The late quartz veins appear to be the youngest lithological unit in the project area. It cuts and associates in a NNE-SSW and NNW-SSE with all other rock types.

The veins are mostly steeply dipping parallel sided tabular masses, which could be concordant or discordant with strike of foliation in the host rocks (Figs. 4.17). The earlier veins are more mineralized with lead, while the late quartz veins are suspected to be mineralized with smaller grains of sulphide minerals and gold.

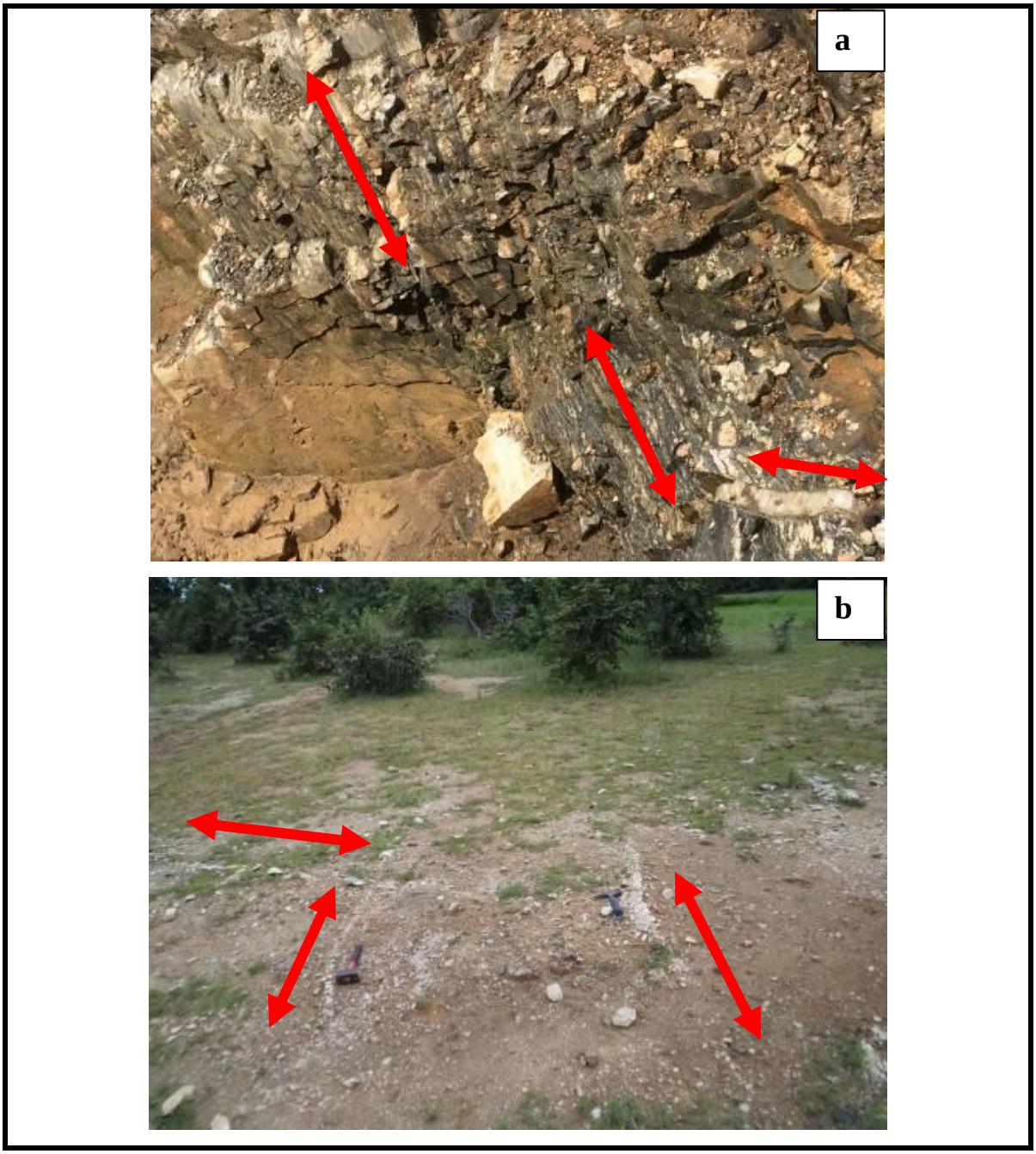

Figure 4.17: a-Gneissic Rock concordantly and discordantly intruded by Quartz veins. b-Some closely related quartz veins showing the cross-cutting relationship between them

The study area is underlain by the crystalline rocks of the Nigerian Basement Complex. The major rock units in the area belong to the Migmatite-gneiss-quartzite group. The gneisses constitute the country rocks with which other rock units of minor occurrences associate with. The gneisses form a number of low to moderately high hills in the area. However, the rocks are generally poorly exposed. Most of the exposures are in form of boulders, most of which have been dislodged.

As observed from the rose diagram plotted for both the primary and secondary structures, the structural trend in the N-S direction agrees with previous work within the study area and also typify the pan-African orogenic structural imprint having an approximately N-S structure and had been established over the years as been the youngest orogenic event recorded thus far within the craton. There are both major and minor magnetic discontinuities and lineament that traverse the study area in a NE-SW, NW-SE and approximately N-S trending patterns. Some of these lineaments are being interpreted as minor since they are not deep seated and extensive to correlate with the Orogeny. Notwithstanding, they show a trend that align with the fracture trend of the Chain and Romanche that cut through on a regional scale. According to Ajakaiye *et al.* (1991), there are magnetic lineaments with definite characteristics that exist within the Nigerian continental landmass. Thus, these lineaments can be in association with the St. Paul, Romanche, Chain and Charcot fracture zones, since they are believed to be part of the major zones of weakness in the crust and predate the opening of the Atlantic Ocean and they were reactivated in early stages of continental rifting (Ajakaiye *et al*., 1991). When compared with the existing geological map of the study area extracted from the 1:100,000 scale (Fig. 4.11b) for the southeastern quadrant, the lithology C and D agrees with what was described as coarse grained granitic intrusive.

4.3.2 Petrographic Studies and Modal Analysis

From a hand specimen of a rock grap, it might be impossible to identify all the mineral assemblages in the hand specimen. Thus, a petrographic thin section of some selected rock grab was prepared for use under the electron microscope. A thin chip from the rock is cut with a diamond saw and mounted on a glass slide. This was then grinded to a thickness of about 30µm. The petrographic thin section slides were observed under the petrological electron microscope.

Petrography of Granite

The rock slides were subjected to petrographic studies both under *crossed nicols* and *plane polarized light* (Fig. 4.18a and b). Based on the relative mineralogical abundance ratio from the thin sections, a modal analysis was computed (Fig. 4.18b).

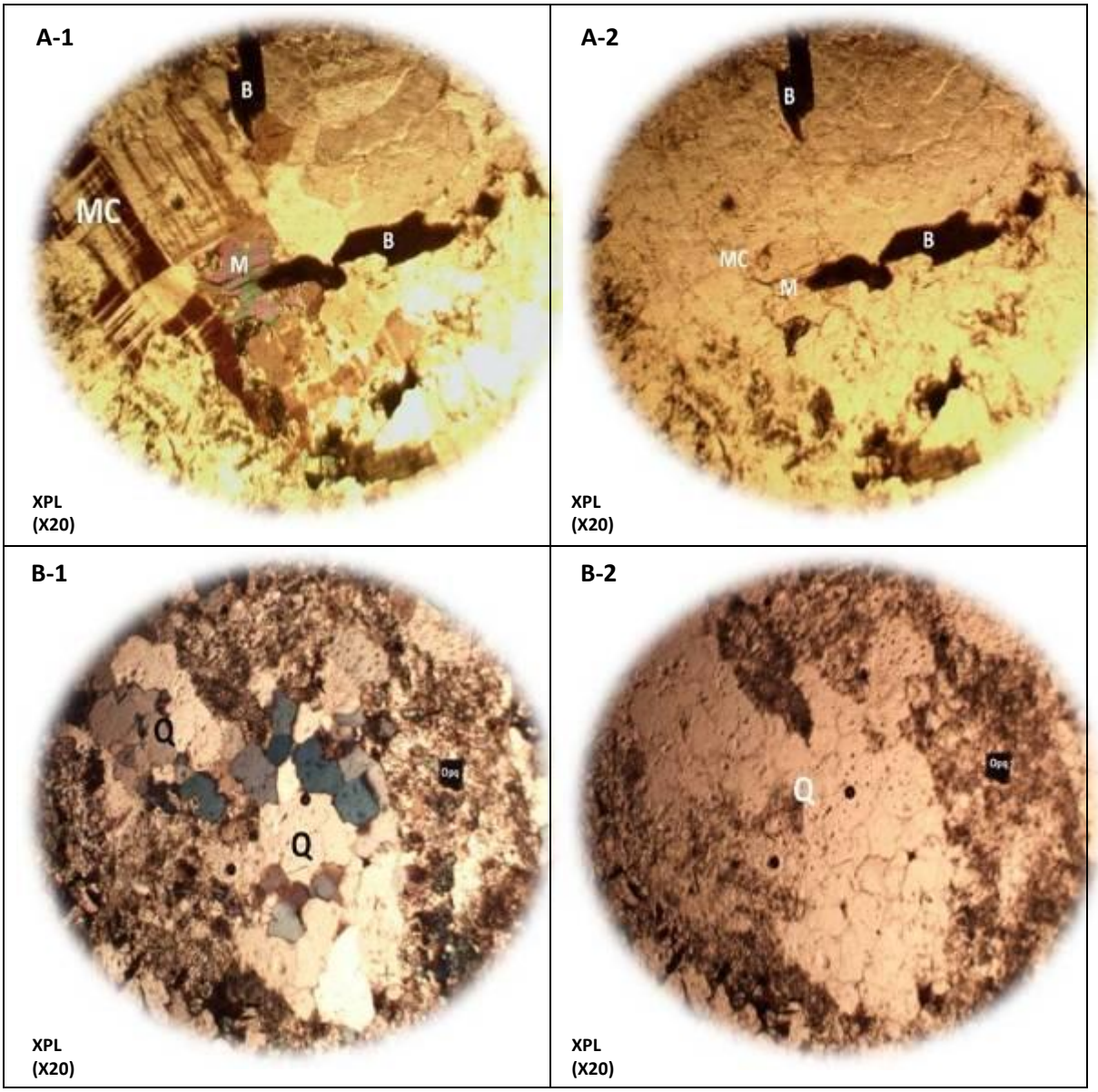

Fig. 4.18a: Photomicrographs of minerals within the granite both under crossed nicols and plane polarized light.

(KEY: Q-quartz, B-biotite, MC-microcline, M-muscovite, OA-opaque/Accessory, PL-plagioclase)

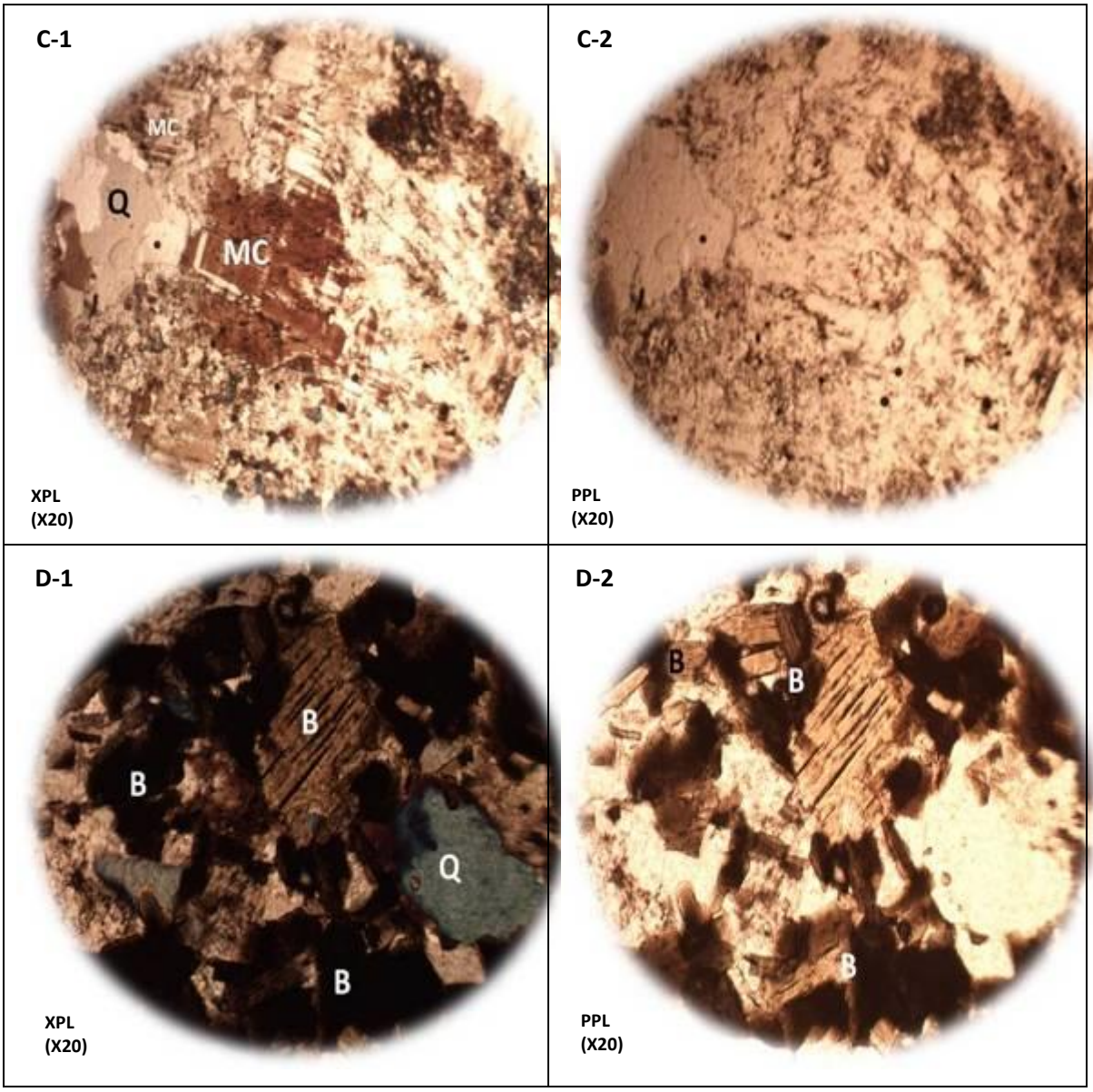

Fig. 4.18b: Photomicrographs of minerals within the granite both under crossed nicols and plane polarized light.

(KEY: Q-quartz, B-biotite, MC-microcline, M-muscovite, OA-opaque/Accessory, PL-plagioclase)

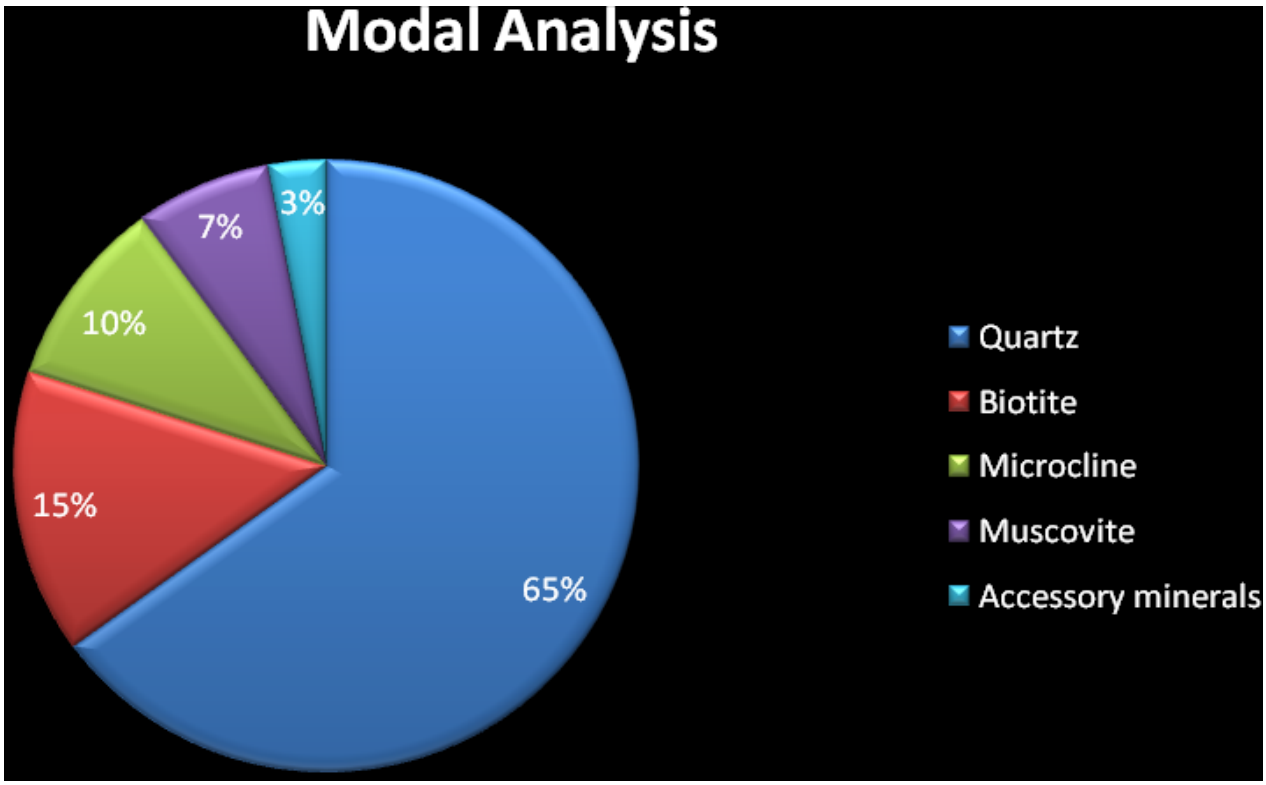

Figure 4.18c: Pie Chart showing the modal distribution of constituent mineralogy for the granite

Generally, the rocks appear to be fine to medium grained in texture and the following minerals were observed: Quartz, Biotite, Microcline feldspar, Muscovite, Opaque and Accessory minerals.

Quartz – Quartz is one of the most common rock forming minerals. It was recognized by its clarity and lacks of cleavage. It disappears under plane polarized light but shows white to bluish grey interference color under crossed nicols. It goes into wavy extinction and the shape is euhedral to subhedral. The nature of the grain boundary is fairly polygonal and shows a moderately low relief.

Biotite - The biotite present in this granite is partly elongated and platy and partly tabular. It is light brown under plane polarized light and dark brown under crossed nicol. It is strongly pleiochroic changing colour from light brown to dark brown. Also, it shows speckled surface, a distinct feature of biotite when close to extinction position. It has perfect and continuous cleavage.

Microcline feldspar – This was observed under crossed nicol with its unique cross hatched or ‘’tartan’’ twinning with a greyish brown colour. It has a low relief and is less visible probably due to alteration.

Muscovite – the muscovite mineral appears colorless under plane polarized light but exhibits interference colors under crossed nicol as it changes from pink to shades of green. It has a perfect cleavage and shows a low relief. Its colorlessness is as result of absence of iron and magnesium which differentiates it from biotite even though they belong to the same mica family.

Accessory and Opaque minerals – In addition to these minerals above, the thin section studies revealed that there are accessory and opaque minerals that are mostly ores (magnetite, ilmenite and pyrite) that came out black under polarizing microscope.

Petrography of Gneiss

The slides were subjected to thin section study, viewed both under crossed nicol and plane polarized light (Fig. 4.19a and b). Based on the relative mineralogical abundance ratio from the thin sections, a modal analysis equally was computed (Fig. 4.19c).

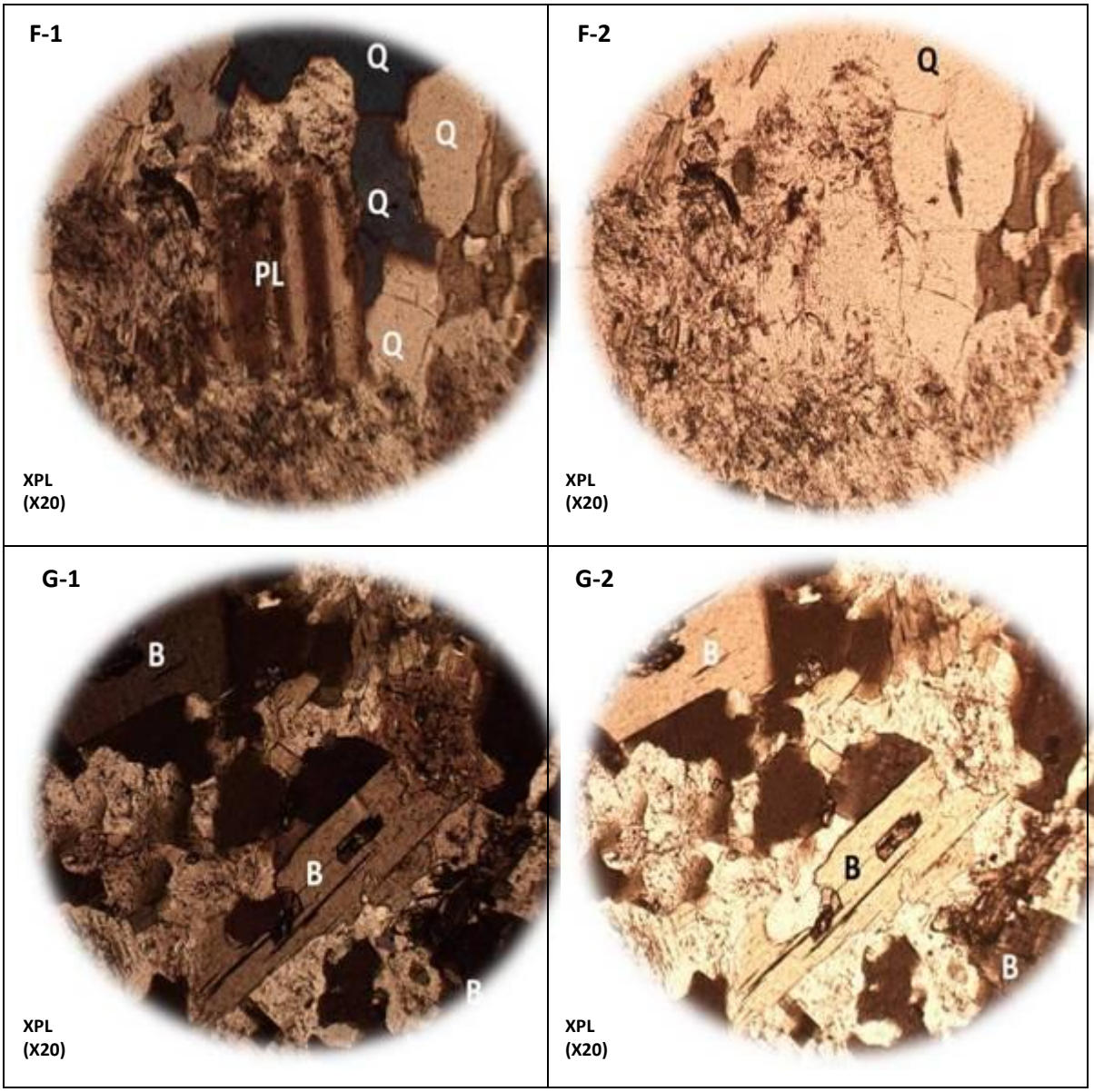

Fig. 4.19a: Photomicrographs of minerals within the gneisses both under crossed nicols and plane polarized light.

(KEY: Q-quartz, B-biotite, MC-microcline, CHL- chlorite, PL-plagioclase)

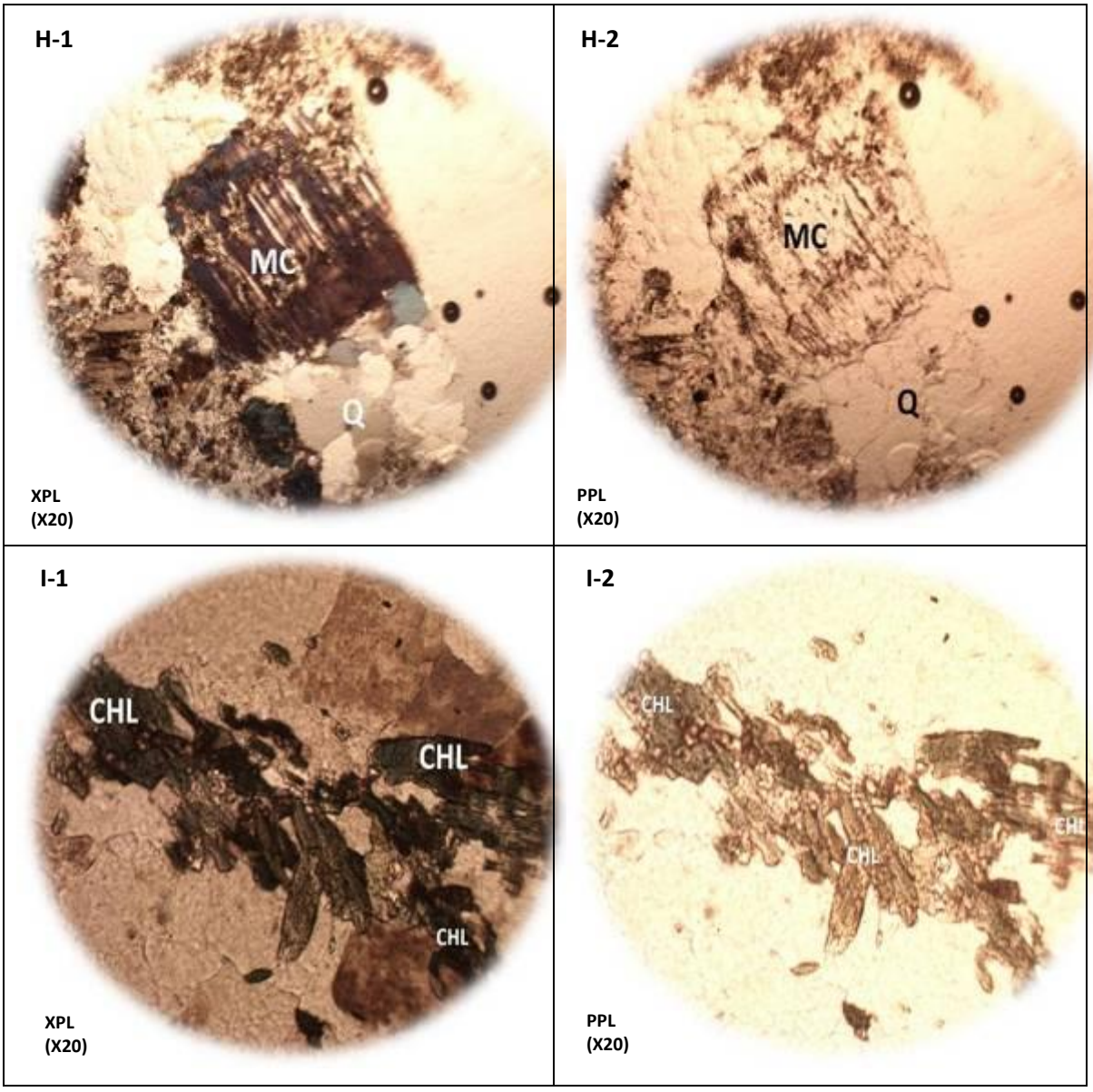

Fig. 4.19b: Photomicrographs of minerals within the gneisses both under crossed nicols and plane polarized light.

(KEY: Q-quartz, B-biotite, MC-microcline, CHL- chlorite, PL-plagioclase)

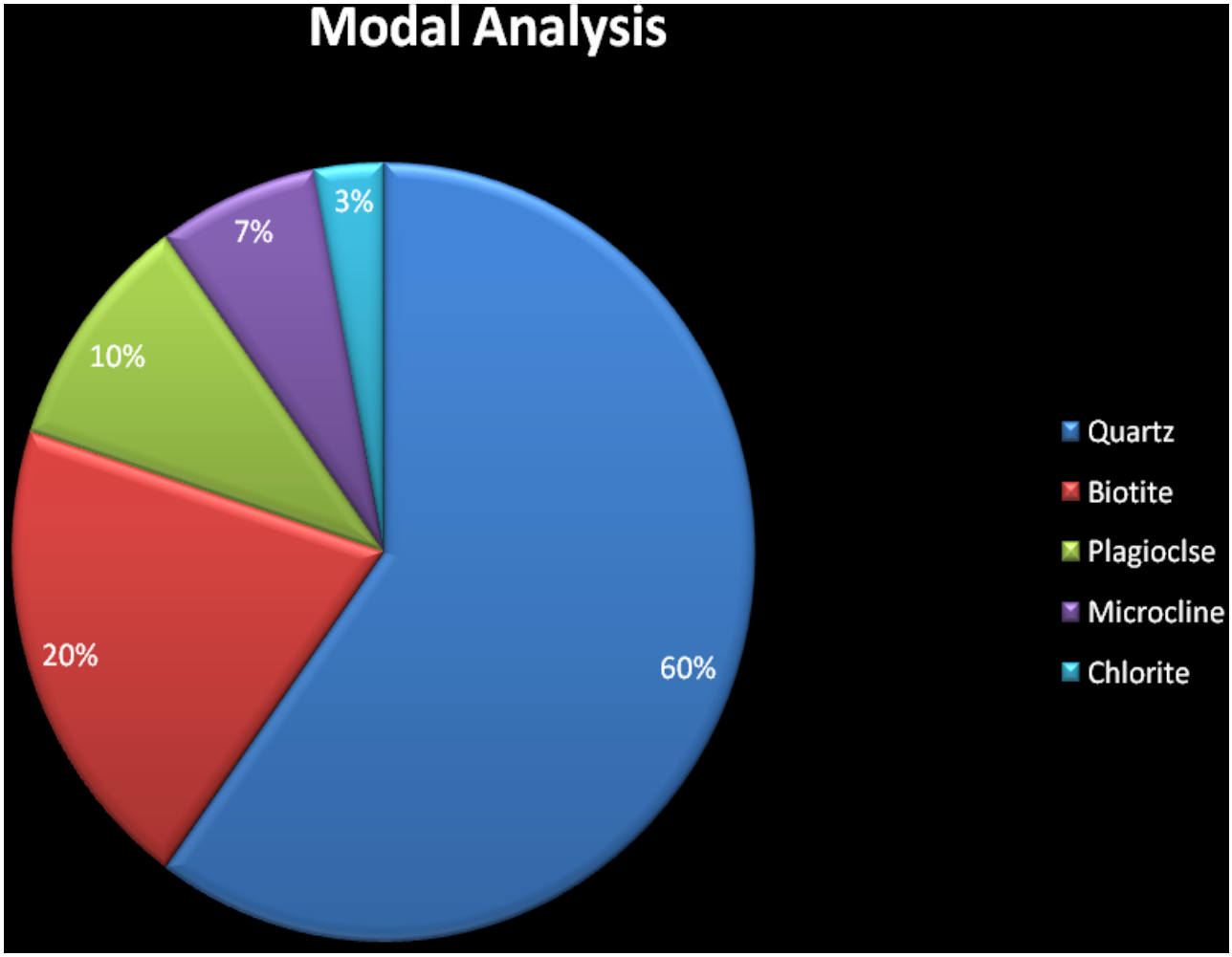

Figure 4.19c: Pie Chart showing the modal distribution of constituent mineralogy for the gneisses

The rock samples are mainly medium to coarse grained with the following minerals observed, Quartz, Biotite, Plagioclase feldspar, Chlorite and microcline,.

Brief descriptions

Quartz – It was recognized in thin section by the fact that it is invariably clear and unaltered. Viewing quartz under crossed nicol, it displayed interference colors as it goes from white to light grey color. It has no cleavage and the shape is euhedral to subhedral. The nature of the grain boundary is fairly polygonal to the preferred orientation of biotite. It exhibits a low to medium relief.

Biotite – Under plane light it displayed light to dark brown and dark brown under crossed nicol. It is strongly pleiochroic changing colour from light brown to dark brown. The biotite present is elongated and platy. Also, it shows speckled surface, a distinct feature of biotite when close to extinction position. It has perfect and continuous cleavage.

Plagioclase feldspar – This was observed under crossed nicol with its unique multiple (polysynthetic) twinning which appears as dark and light bands in the crystal. The most common type of this twinning is the **'*albite twinning'*** showing its twin lamellae lie parallel to a very good cleavage.

Chlorite – The chlorite is a product of alteration of biotite with a low 'relief' when observed under plane light. It appears to be greenish in color and also exhibits pleichroism as the color changes to pale straw yellow color when rotating the stage. It also shows a good cleavage like the micas.

Microcline feldspar – The microcline was observed under crossed nicol and it appears to be highly altered. It display its unique cross hatched or ''tartan'' twinning with a greyish brown colour. It has a low relief and is less visible probably due to alteration.

Structures

Rocks of the project area like those in other parts of the Nigeria basement complex are multiply deformed, but due to poor exposure, structural data collected from the field are very scanty. This has made the identification of the various phases of deformation difficult. However, going by the varying trends of foliation across the area, there are at least two or more generations of planer fabrics. The gneissic rocks are strongly foliated. The foliations are marked by alternating bands of felsic and mafic minerals. A number of minor folds of varying styles and forms have also been mapped. At least also, two fold phases F1 and F2 were identified in the field (Fig. 20).

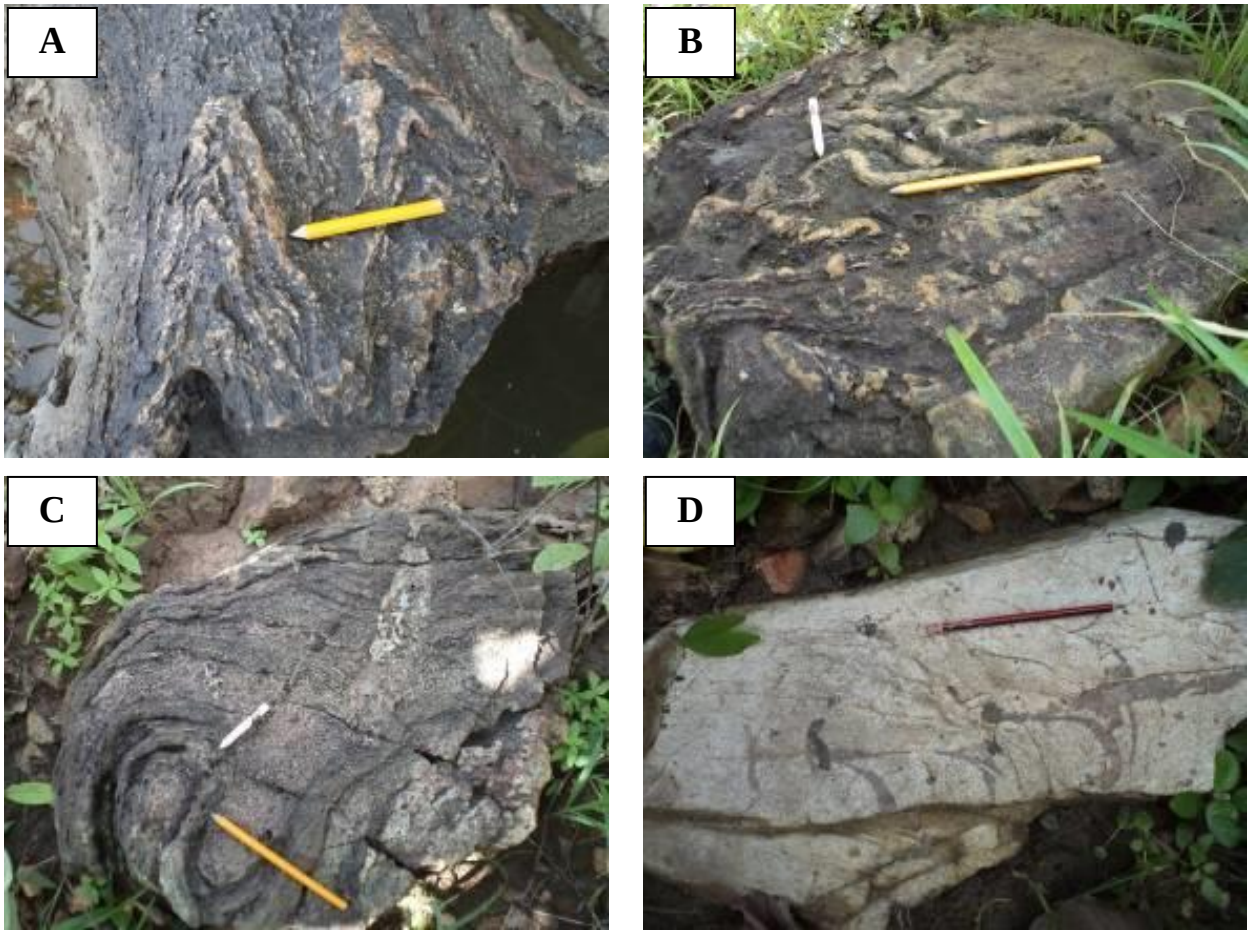

Figure 4.20: A- Some tight folds in the biotite-gneiss. The folds plunge gently in the direction of NE. B - Folds of different generations displayed by the biotite-gneiss. C - A refolded fold, hooke interference fold structures in the hornblende gneiss. D - An exposure of a mylonite of probably an aplite or pegmatite

Mineralisation

Mineralisation within the study area was observed from artisanal mining pits and trenches (Figs. 4.21). These pits and trenches were scattered all over the study area where miners were washing for both gold, lead-zince and other associated minerals including silver.

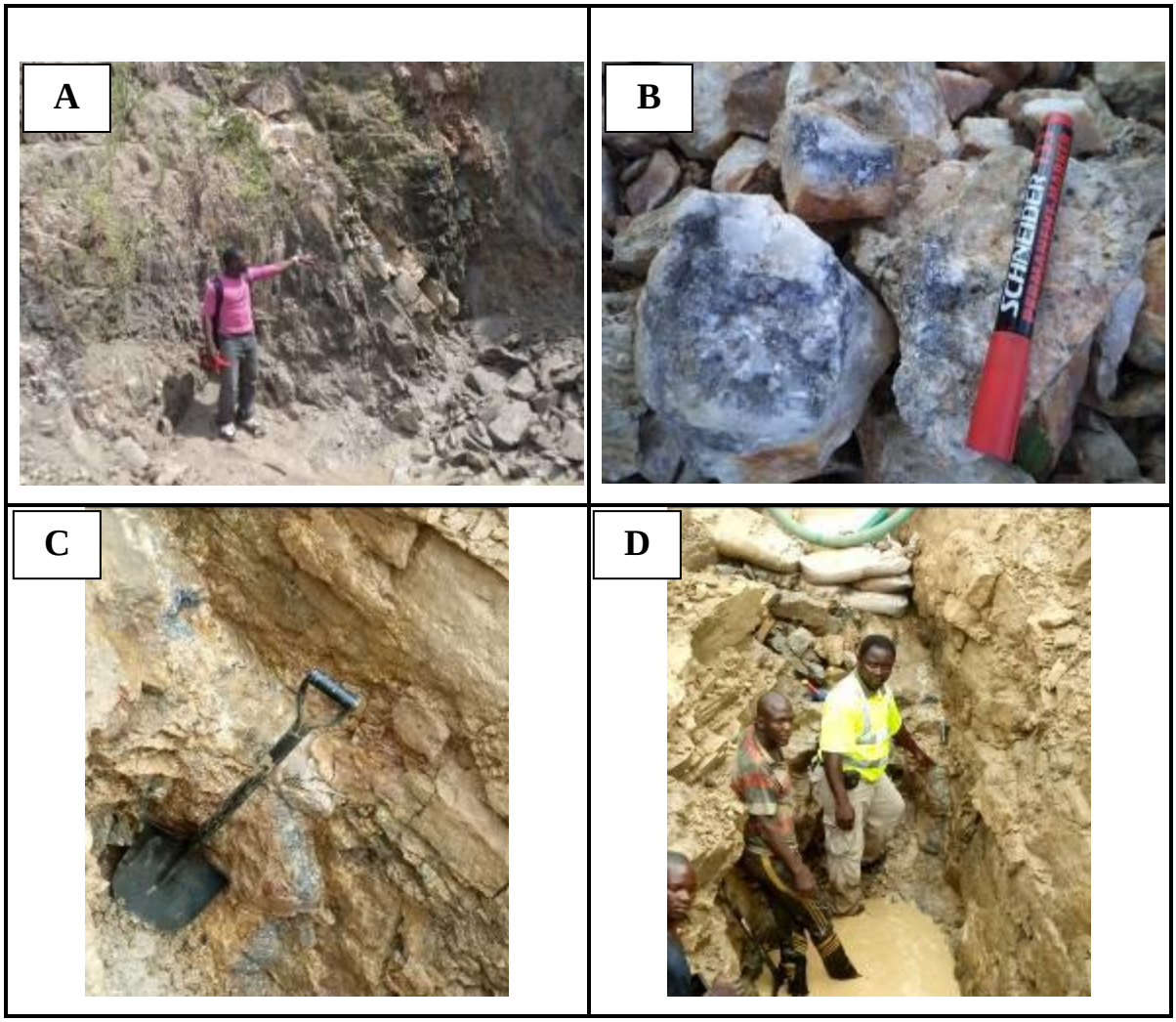

Figure 4.21: A - Two sub-parallel quartz veins. B - Lead sulphide borne by boulders from the vein quartz. C - A close-in view of the quartz-sulphide vein measuring about 12cm in width and discordant to the host rock foliation trend. D - Artisanal work pit with quartz-sulphide vein trending about 310° (NW-SE).

The quartz-sulphide veins occur as both concordant and discordant bodies mostly in the gneisses. The late vein quartz appears to be the youngest lithological unit in the area. The rock cuts all other rocks types. The quartz vein occur mostly as steeply dipping, parallel sided tabular masses, the vein quartz is milky to white, massive and lacks any form of foliation. Quartz is the major mineral. Sulphide mineral have been observed in some of the veins. Lead sulphide is the most common. It occurs as large masses in association with the quartz. It also occurs as thin veins and disseminated grains in the quartz and in the alteration zones of the wall rock.

The late vein quartz is suspected to be the main host of primary gold in the area. Apart from the specs of alluvial gold observed from winnings made by the artisans, no visible primary gold mineralisation has been mapped. However, pathfinder minerals mostly lead sulphide with some pyrite minerals are borne by the vein quartz. In fact some of the vein could be described as quartz- sulphide vein.

4.3.3 Geological Interpretations

The field results were integrated in a geographic information system with structures delineated from the magnetic and radiometric interpretation (Fig. 4.22a) to produced the final updated geological map for the study area (Fig. 4.22b).

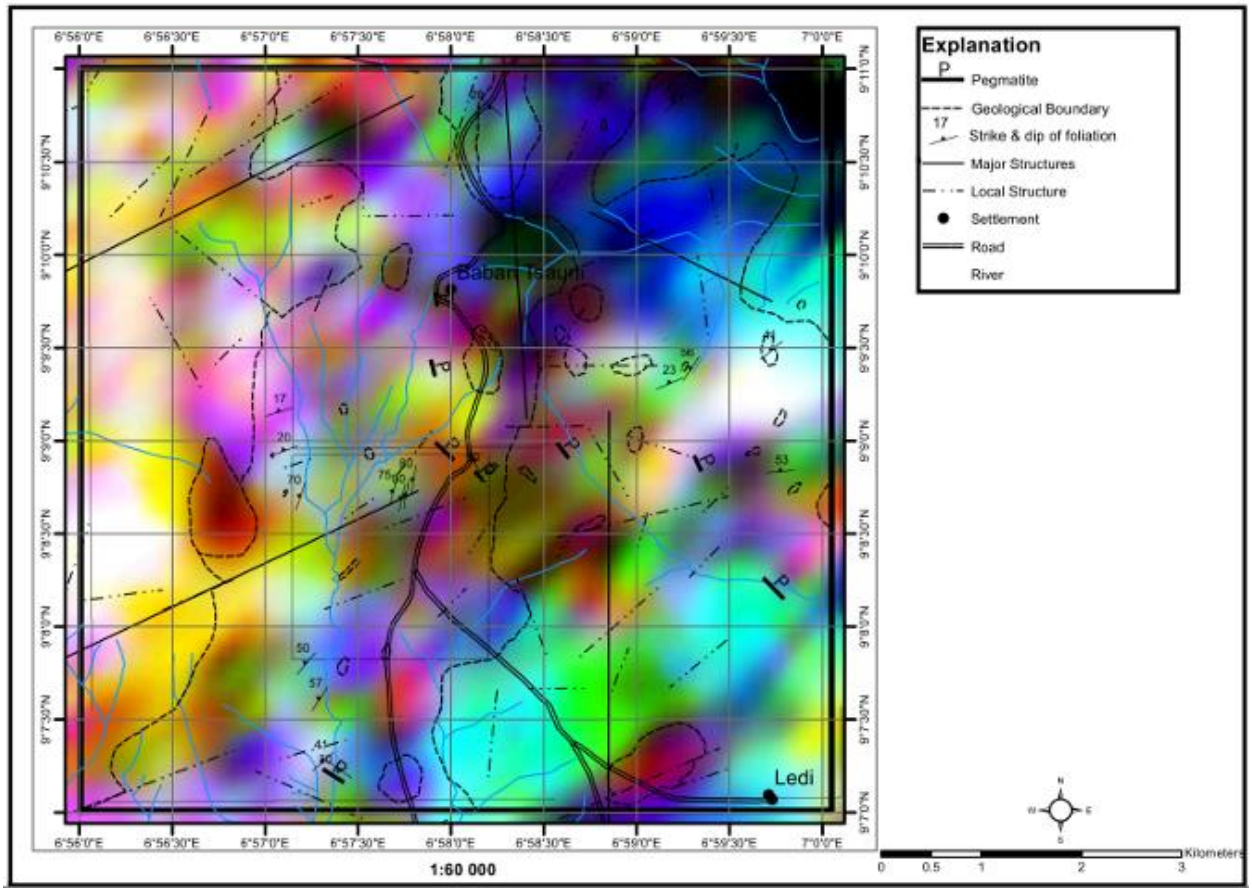

Figure 4.22a: Geology ground truthing and Radiometric Data (Ternary Image) Integration

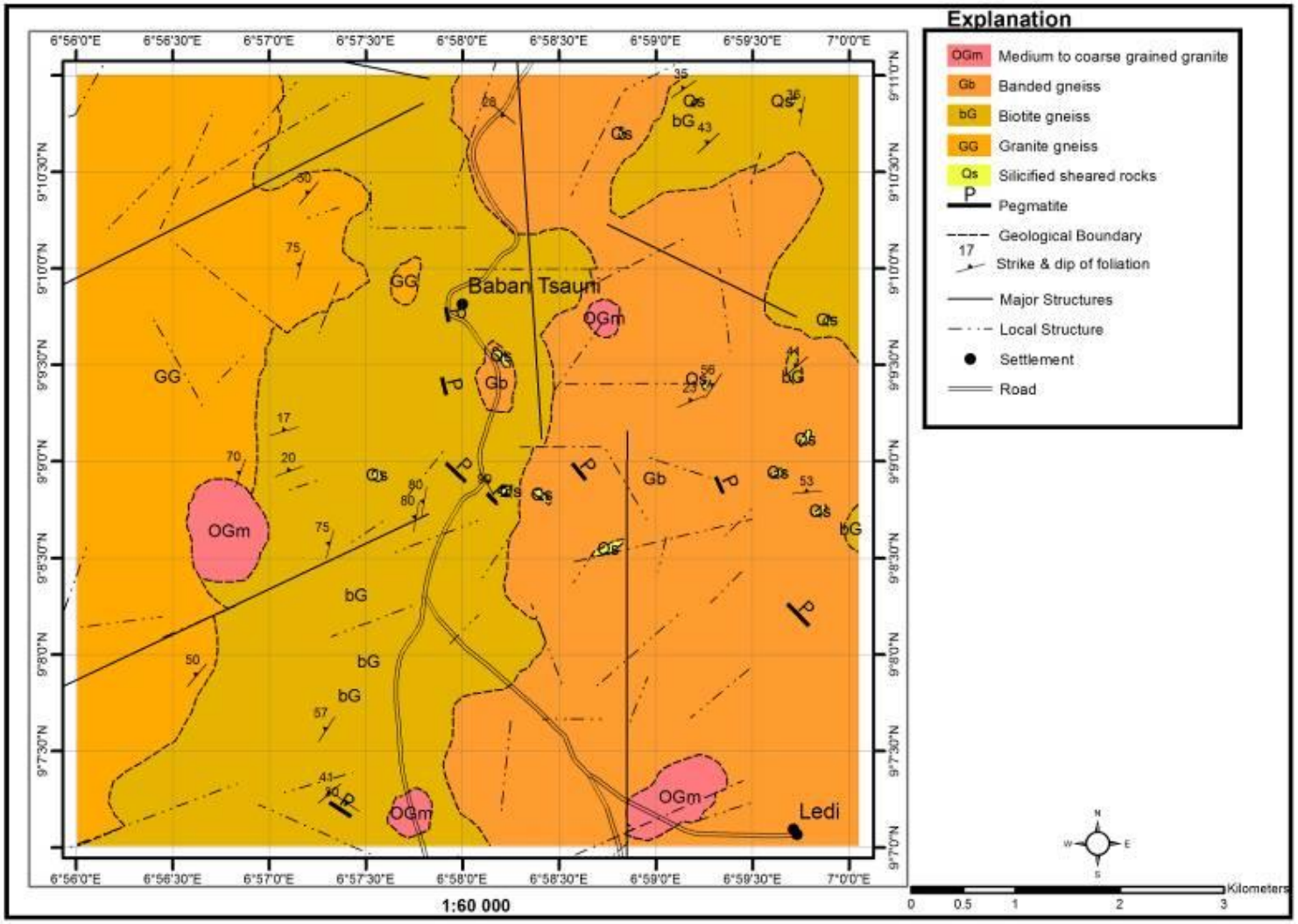

Figure 4.22b: Geology and structural map of the study area obtained from the integration of the aeromagnetic, airborne radiometric and geological ground truthing

The research locality is sitting on the basement complex rocks, mainly the biotitic – gneiss and the hornblende – gneiss, with minor occurrence of medium – grained granite, aplites/pegmatites and quartz veins of varying widths associated with the gneisses in almost all parts of the area. At least two generation of quartz veins were established in the field. The emplacement of these veins, which might have exploited the channel ways provided by some pre – existing fractures, are probably the latest geological events in the area. It was suspected that the quartz vein was emplaced by metal bearing hydrothermal solutions which could have originated from a consolidating intrusive igneous mass. Tectonically, the area falls within the impact zones of two major structural lineaments and shear zones towards the western half of Nigeria. These two fractures are believed to serve as conduits that fed several other subsidiary fractures within the zone of impact with metal bearing solutions.

The geological mapping field data which was deployed in a database system was integrated with the interpreted radiometric map of the target area for ease in comparison and delineating contact, which due to poor exposures were not always definite. The structural information from the processed aeromagnetic data was equally integrated. This integration was then use to produce the geological map of the target area. The integration of the structural delineation from the aeromagnetic data interpretation, lithological boundary delineation using radio-elements from the airborne radiometric data interpretation and the ground-truthed geological and petrographical studies were used as a base map to present and discuss the results of objective four (delineation of high resolution structure from ground magnetic data).

4.4 Evaluation of Higher Resolution Mineralizing Structures

As a ground follow-up to the airborne structural delineation, a ground magnetic survey at close exploration profile interval was conducted over the delineated area that are showing higher tendencies for associated sulphide mineralisation. The magnetic data acquired was compiled, corrected, filtered and levelled using Minty's approach. The levelled data was gridded using the minimum curvature method for data gridding to generate the Total Magnetic Intensity map over the delineated area (Fig. 4.23a).

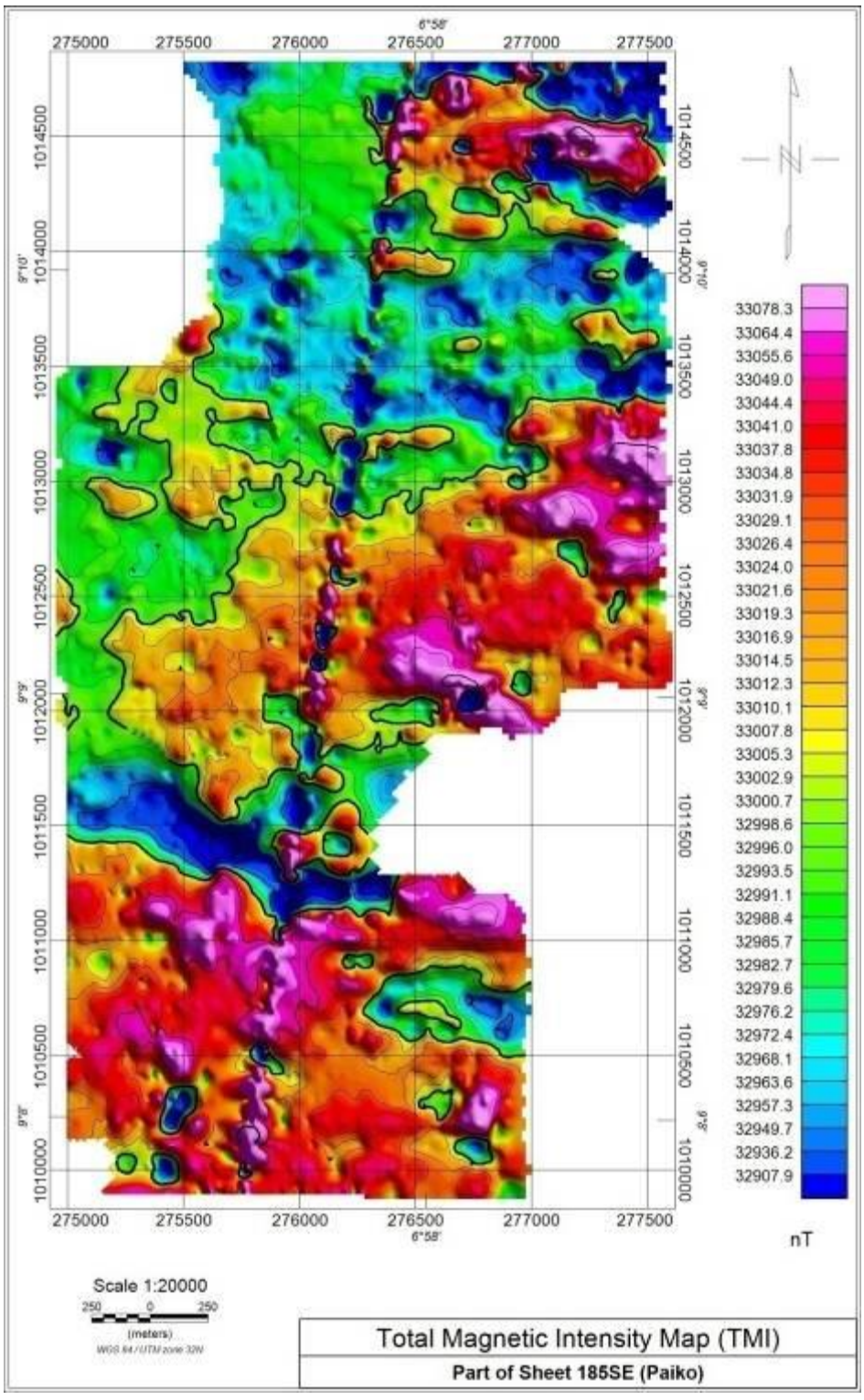

Figure 4.23a: Total Magnetic Intensity Map showing the variation in magnetic susceptibility and remanent magnetization within the target area (Note the NNPC Pipeline running NNE-SSW at the central portion of the map).

The Total Magnetic Intensity (TMI) Map (Fig. 4.23a) has magnetic intensity signatures ranging from about 32,907 nT to about 33,078 nT with a total maximum variation of about 171 nT. The regions with higher magnetic intensity values were being interpreted as a shallow magnetic basement. The southern portion was dominated with the high magnetic intensity and also at the middle-eastern part. Apart from some low signatures intermittently forming lenses, the low magnetic signatures are mostly confined to the northern part of the study area.

A prominent magnetic closure with a NW-SE trend was observed around the southern part of the study area. The observed magnetic closure is a low magnetic closure. Other inferred low magnetic closures are towards the northern margin of the map with high magnetic values at the basal southern portion and the mid-eastern section. The nature of the closures is an indication of depth of burial and size of intrusive bodies that are within the basement complex.

There are magnetic discontinuities and lineament that traverse the study area in a NW-SE and an almost N-S trend, cross-cutting the interpreted NE-SW older structures. These discontinuities are being interpreted as local structures since they are not extensive to correlate with the Pan-African Orogeny. Notwithstanding the older NE-SW structures shows trends that align with the fracture trend of the Chain and Romanche that cut through on a regional scale. According to Ajakaiye, *et al.* (1991), there are magnetic lineaments with definite characteristics that exist within the Nigerian continental landmass. Thus, these lineaments can be in association with the St. Paul, Romanche, Chain and Charcot fracture zones, since they are believed to be part of the major zones of weakness in the crust and predate the opening of the Atlantic Ocean and they were reactivated in early stages of continental rifting. Due to the noise level suspected, the Total Magnetic grid was upward continued to 50m, 100m and 150m (Fig. 4.23b).

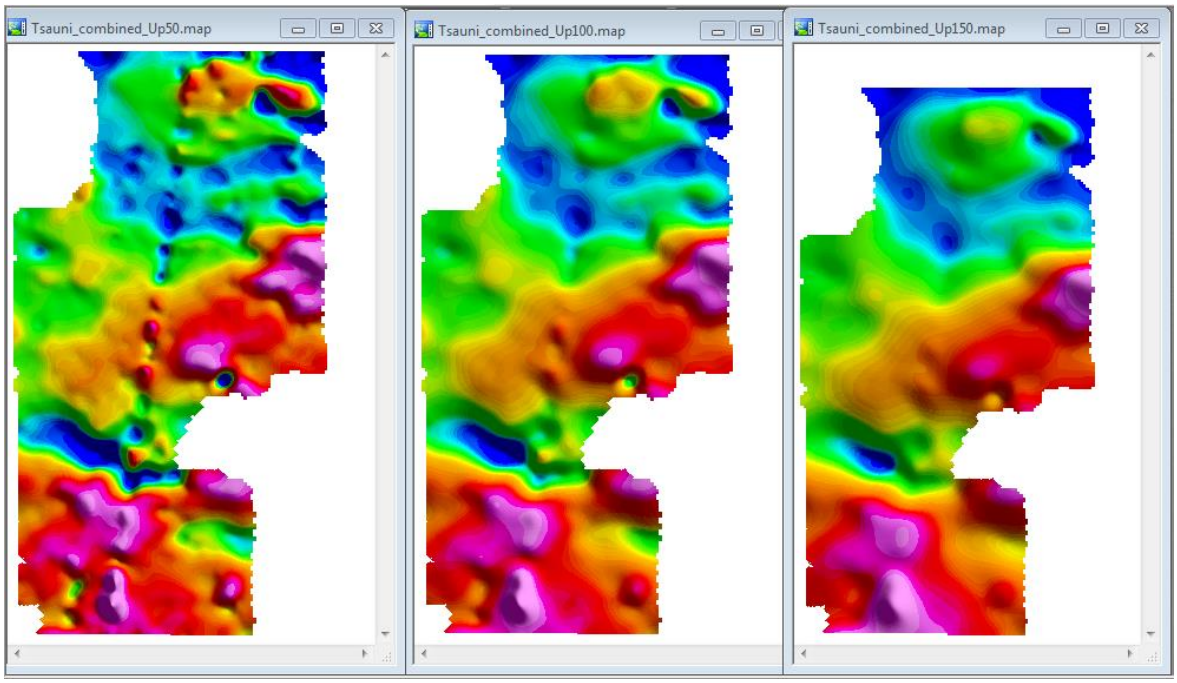

Figure 4.23b: Upward continuations to mask-off artificially induce signatures (noise). Noticeable is the pipe line which trends NNE-SSW about the central portion. The continuation was taken to 50m, 100m and 150m.

The micro-leveled Total Magnetic Intensity grid though not so contrasting to the diurnal corrected grid still had some of the very much near surface man-made anomaly (example is the NNPC Pipe-line) which its depth of emplacement might be within ranges of some geological structure. To remove this, the data was upward continued to 50 m, 100 m and 150 m (Fig. 4.21b). Though, the effect was removed at about 150 m, the micro-levelled grid was still used for computing the other derivatives and enhancement so as not to miss out subtle information.

4.4.1 Structural Enhancement of Ground Magnetic data

The first vertical derivative filter (Fig. 4.24) sharpens irregularities over bodies and helps to minimize anomaly uncertainty, making imaging of the causative structures smoother. Since it amplifies shorter wavelength, the transformation can be noisy. In the magnetic grid, it simply delineates regions of varying data resolution.

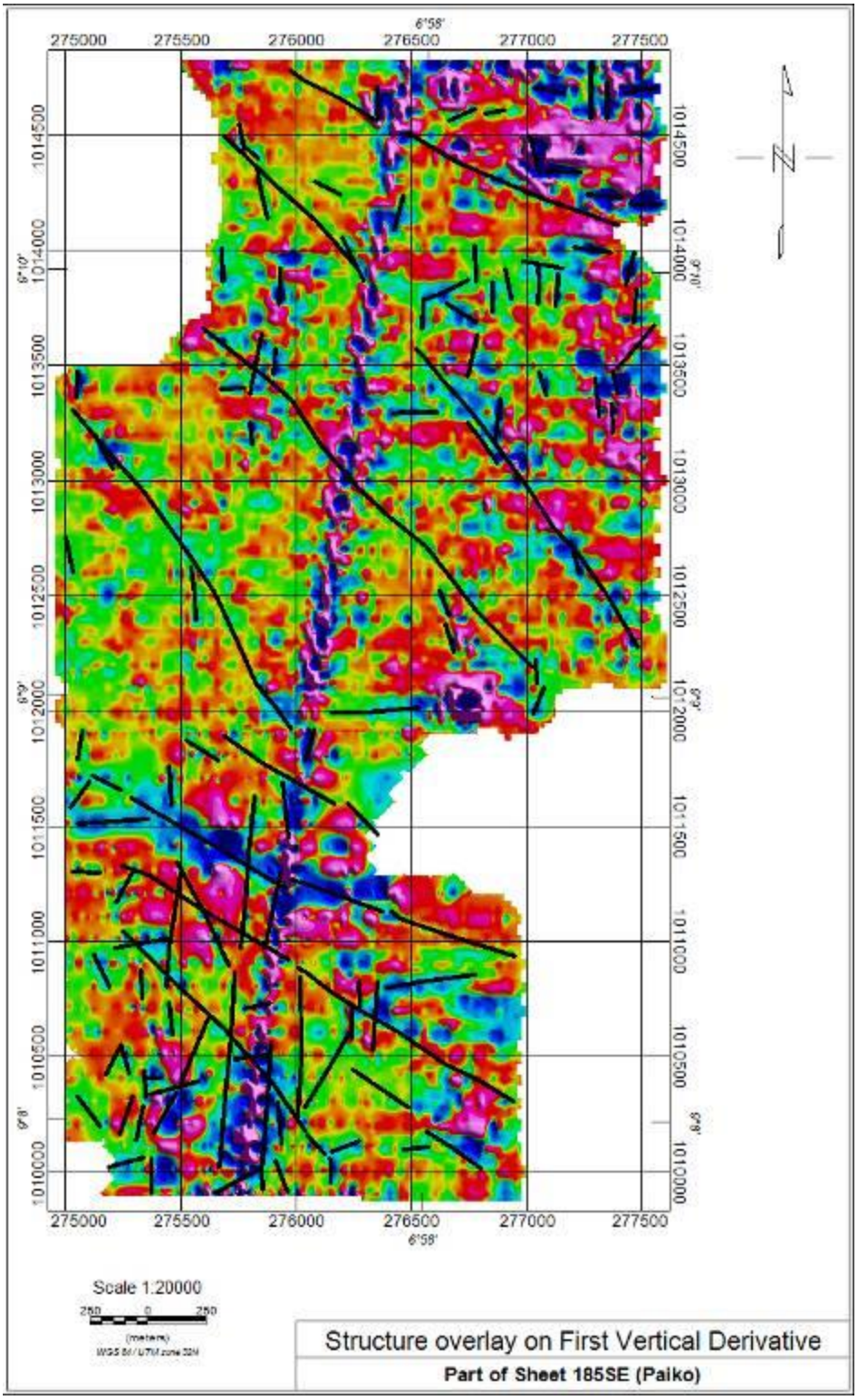

Figure 4.24: First Vertical Derivative Map

The second vertical derivative has a similar effect with ‘residual' filtering in that it highlights local features while excluding the effects of large anomalies or regional effects. It's especially useful in the processing stage, where it can be used to show line noise or misleveling, as with other derivative indicators.

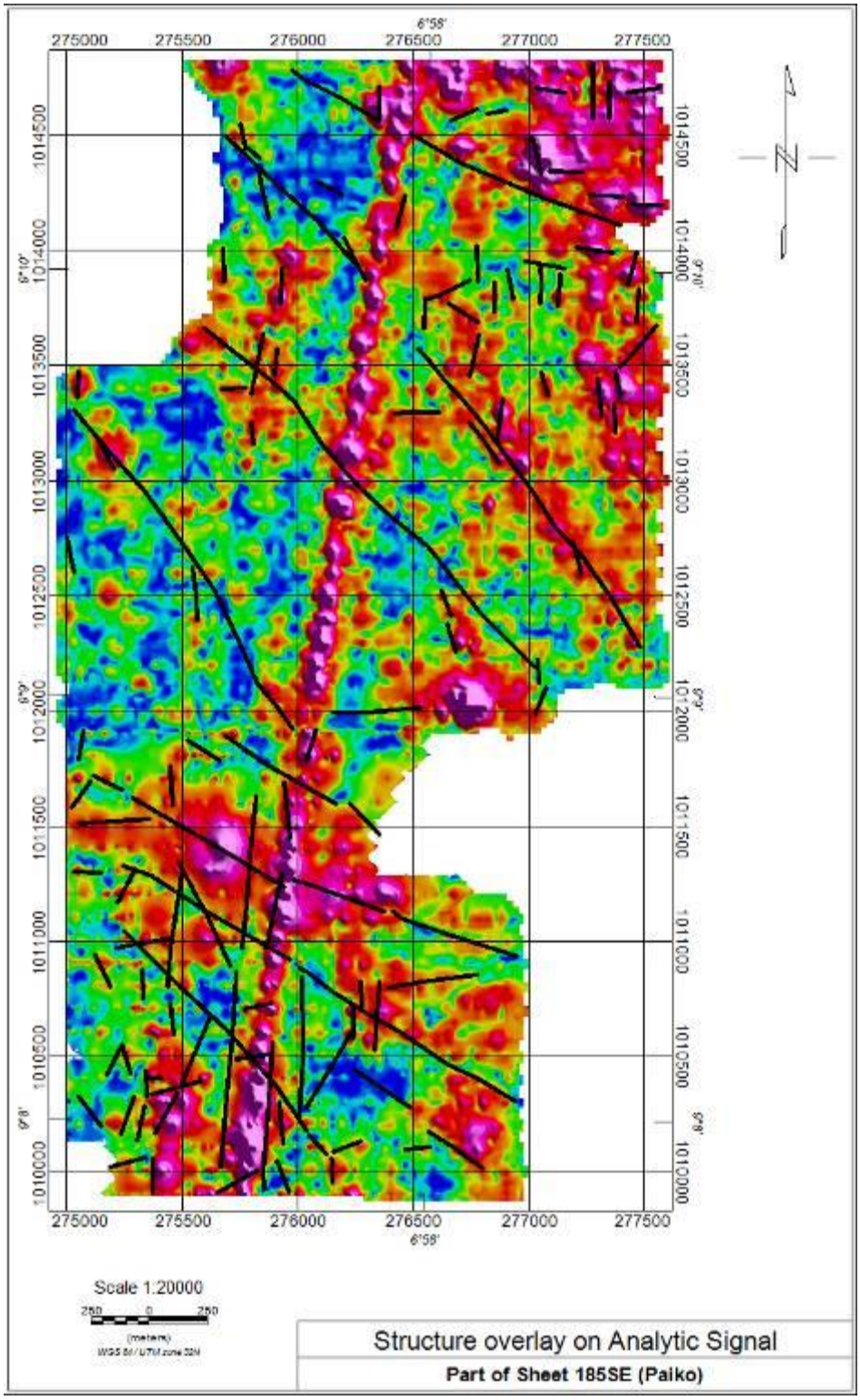

Figure 4.25: Analytic Signal Map

The analytic signal (Fig. 4.25) which is often more discontinuous than the basic horizontal gradient (Fig. 4.26), has the property of producing a maximum directly over the source bodies as well as their edges. As long as the signal from a single contact can be delineated, the distance of a maximum or ridge, is a measure of contact depth. Because of the intrinsic issues with RTP, this transition is often used at low magnetic latitudes (at such low latitudes).

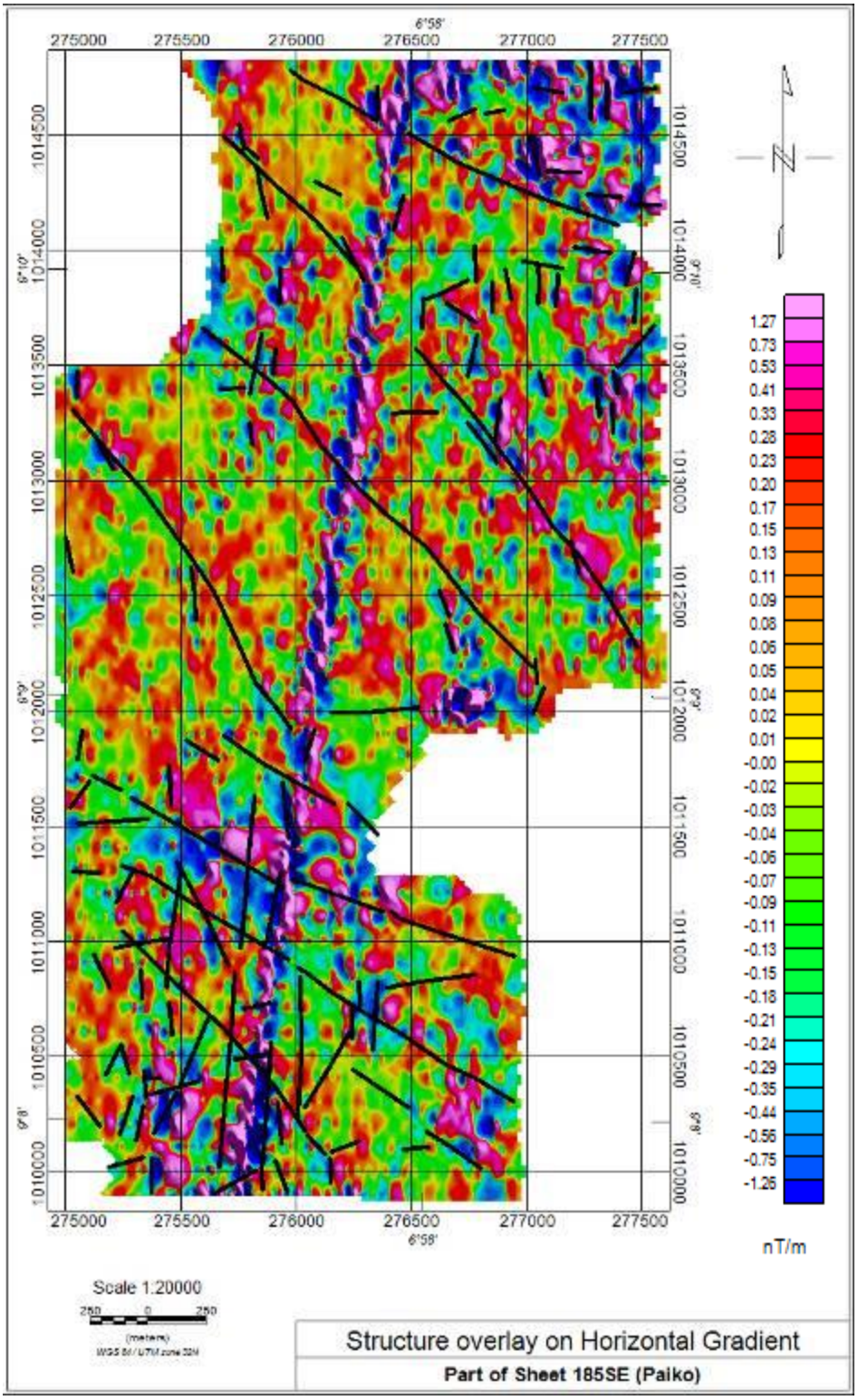

Figure 4.26: Horizontal Gradient Map

Horizontal Gradient (HGRAD) derivative enhances discontinuities such as fault and contact features in the data. It works hand in hand with the filtered and first vertical derivative improvements. It normally yields a more precise fault position than the first vertical derivative. Tilt derivative (TDR) is an edge detection method and is used for mapping shallow basement structures and mineral exploration targets. It also helps for enhancing features and causative body edge detection in potential field images. The tilt derivative (Fig. 4.27) produces a zero value over or close to the source edges and, therefore, is used to trace the outline of the edges. Positive values are located directly above the sources while negative values are located away from them.

The Total Horizontal Derivative and the tilt derivative are both useful in mapping out shallow near surface structures. These enhancements are also designed to look at fault and contact features. They are complementary to the filtered and first vertical derivative enhancements above. They usually produce a more exact location for faults than the first vertical derivative.

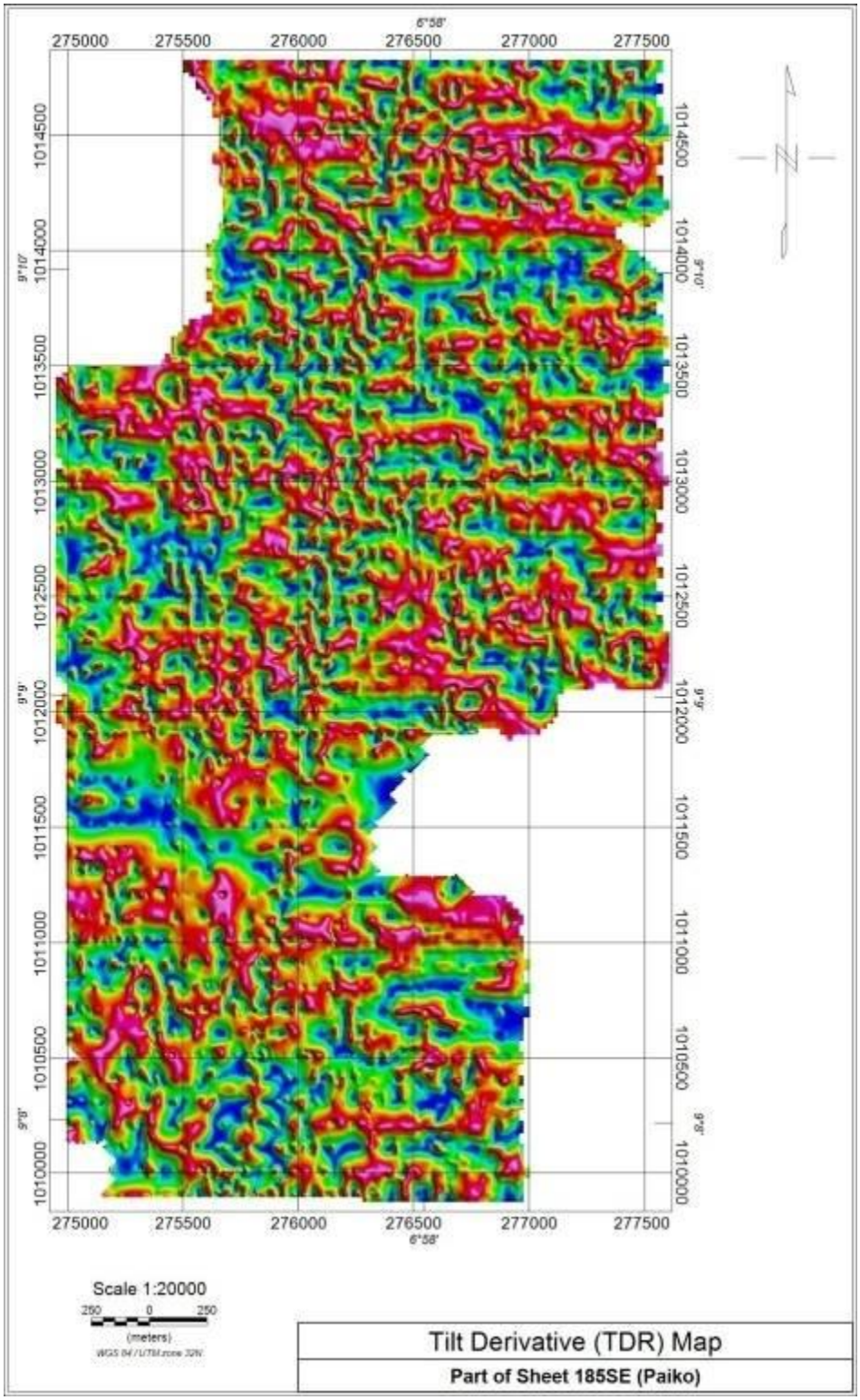

Figure 4.27: Tilt Derivative Map

Information extraction was done in a Geographic Information System (GIS) using ArcMap software. Structural information such as lineament, contacts, faults or discontinuities were digitised from processed magnetic data (Fig. 4.28). The derivative grids in Geotiff file format was imported into the GIS environment where layers were created and trends/lineaments were digitized into the shapefile layers.

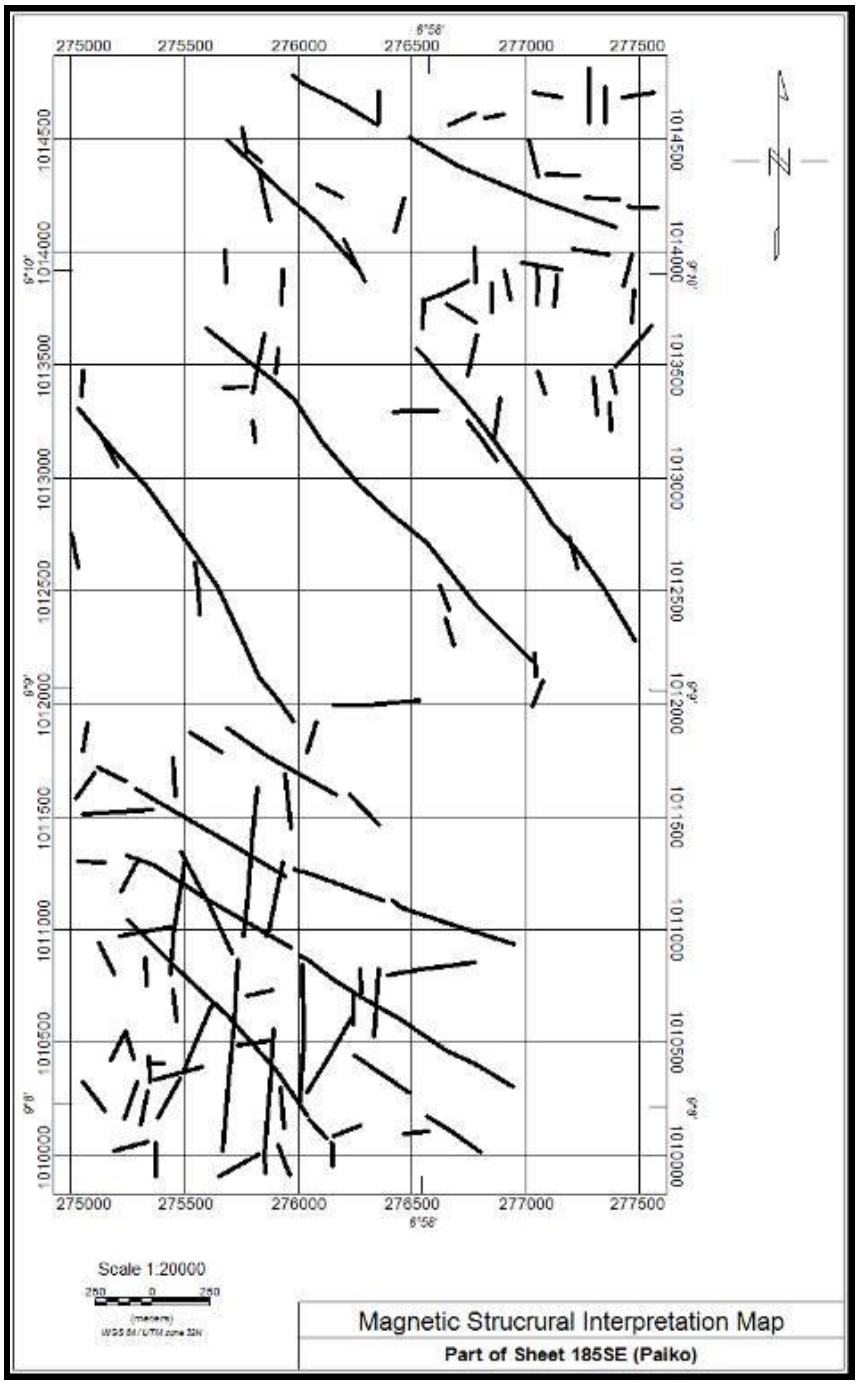

Figure 4.28: Structural Interpretation Map with structures dominantly NW-SE and few in the NNE-SSW direction

The total magnetic intensity (TMI) map of the area varies gentle with interwoven long and short wavelength disseminated over the survey area. There are varying high and low magnetic closures prominent within the study area. There are high magnetic values around the northeast and southern section of the study area, with a peak of about33078 nT. These suggest regions where the magnetic sources are near surface or outcropping to the surface. This was also evident from the analytic signal map. There are minor magnetic discontinuities and lineament that traverse the study area in a NE-SW and NW-SE trending patterns. The regional NE-SW trend can be attributed to the fracture trend of the Chain and Romanche that cut through on a regional scale. According to Ajakaiye *et al.* (1991), there are magnetic lineaments with definite characteristics that exist within the Nigerian continental landmass. Thus, these lineaments can be in association with the St. Paul, Romanche, Chain and Charcot fracture zones, since they are believed to be part of the major zones of weakness in the crust and predate the opening of the Atlantic Ocean and they were reactivated in early stages of continental rifting (Ajakaiye *et al..*, 1991).

Linear structures are observable mostly trending in NW-SE and NNE-SSW directions. The interpreted magnetic structures showed prominent magnetic anomalies some of which have steep horizontal gradients. Most of the major magnetic anomalies trends in the NW–SE direction with few in the NNE-SSW and an almost N-S which are in some cases associated with faulting.

Various tectonic movements and tensional stresses in the project area have given rise to fracture zones aligned in the three main directions, an E-W system, a N – S system and a NW – SE system

In conclusion, at least two distinct tectonic phases have been responsible for the evolution of the structures in the project area and the associated mineralization. The structures are in two main directions (NW-SE and NNE-SSW). The NW-SE is older than the NNE-SSW from the cross-cutting relationship and field evidences. The NW-SE trend are suspected to be mineralized with the sulphides, while the NNE-SSW which are Pan-African are associated with gold mineralisation with fewer disseminated sulphide mineralization.

4.5 Ore Body Geometry Configuration

The lead and associated sulphide mineralisation within the study area are observed to be epigenetic structurally controlled and occur in disseminated form within the vein quartz and quartzitic material. The quartz veins are typified with very high resistivity values as they are crystalline and not conductive. Thus, with the impregnation of the sulphide/metallic minerals (e.g. lead) which are chargeable, the induce polarization response was thus characterize with high values. The acquired induced polarization data were processed and plotted to generate 2-D pseudo sections showing the variation of the chargeability and apparent resistivity along each traverses. The two sections are plotted over each other for enhanced comparison and interpretational ease. The uppermost section is the induced polarization chargeability plot, while the lower section is the apparent resistivity over the same traverse. For the two sections, the highest value was assigned purple while the lower values were assigned blue. The induced polarization and apparent resistivity data were collected simultaneously using the time domain induced polarization system (GDD) transmitter and multi-electrode receiver.

The acquisition profile layout follows anomaly picked from the integration of the geology and ground magnetic survey where secondary structures which are localized and suspected to controlled the sulphide mineralisation trends mainly in the northwest-southeast and north-northeast-south-southwest directions.

The post processed data were compiled into a database system in Geosoft Oasis Montaj software environment using the IP extension menu. With the compiled database, the pseudo-section for both the induced polarization and apparent resistivity (Figs. 4.27a-n) were computed and plotted for each of the 14 profiles. The plot shows the pseudo-section from the northern-most profile to the south. A sample plot of the Electrical Resistivity Tomography and corresponding Chargeability responses if the Induced Polarization is shown in figure 4.29, while the complete plots of the 14 profiles are shown in appendix.

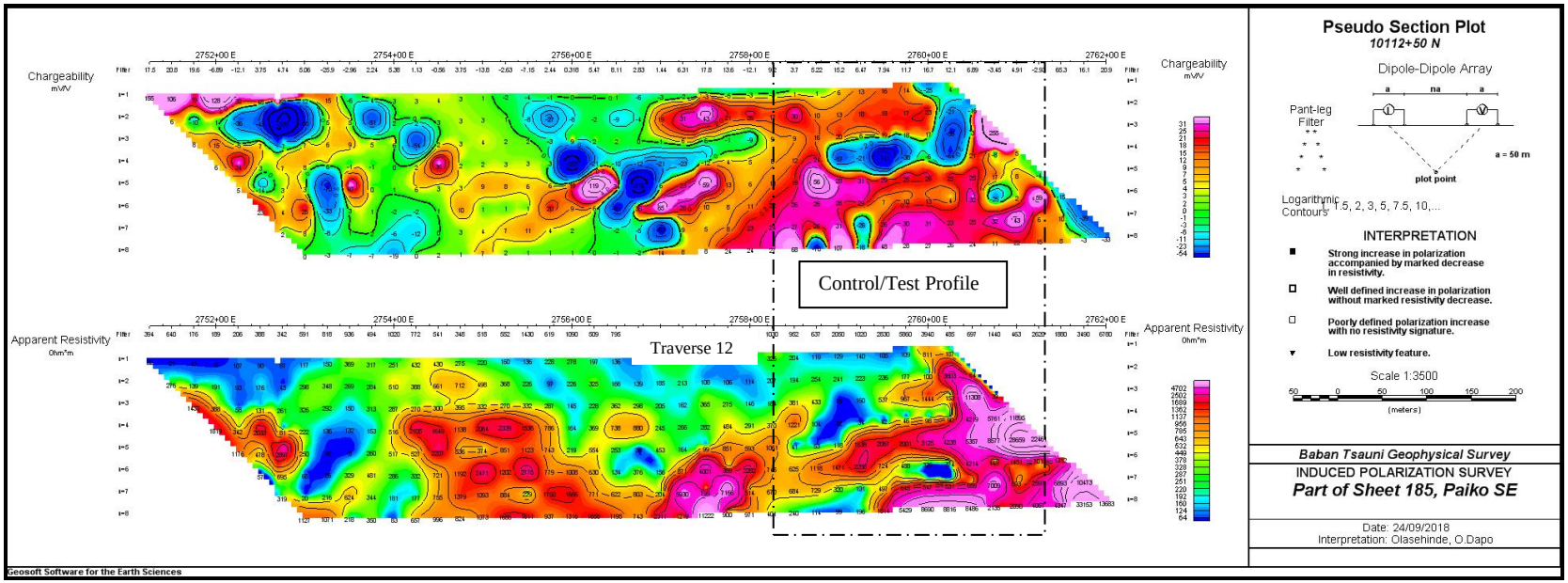

Figure 4.29: 2-Dimension Pseudo-Section plot of both the chargeability (top) with its corresponding apparent resistivity (bottom) for the control/test profile. The purple colouration marks the highest chargeability values and corresponding resistivity while the blue marks the low chargeability and low resistivity. Note the dip of the resistivity structures

The stack plots (Figs. 4.30a and b) for each of the two sub-methods were equally generated to compare the trend in line with the structural direction as obtained from the geological ground truthing, ground magnetic and the airborne data set. The stack plot shows the results for each profile starting from the north down to the south.

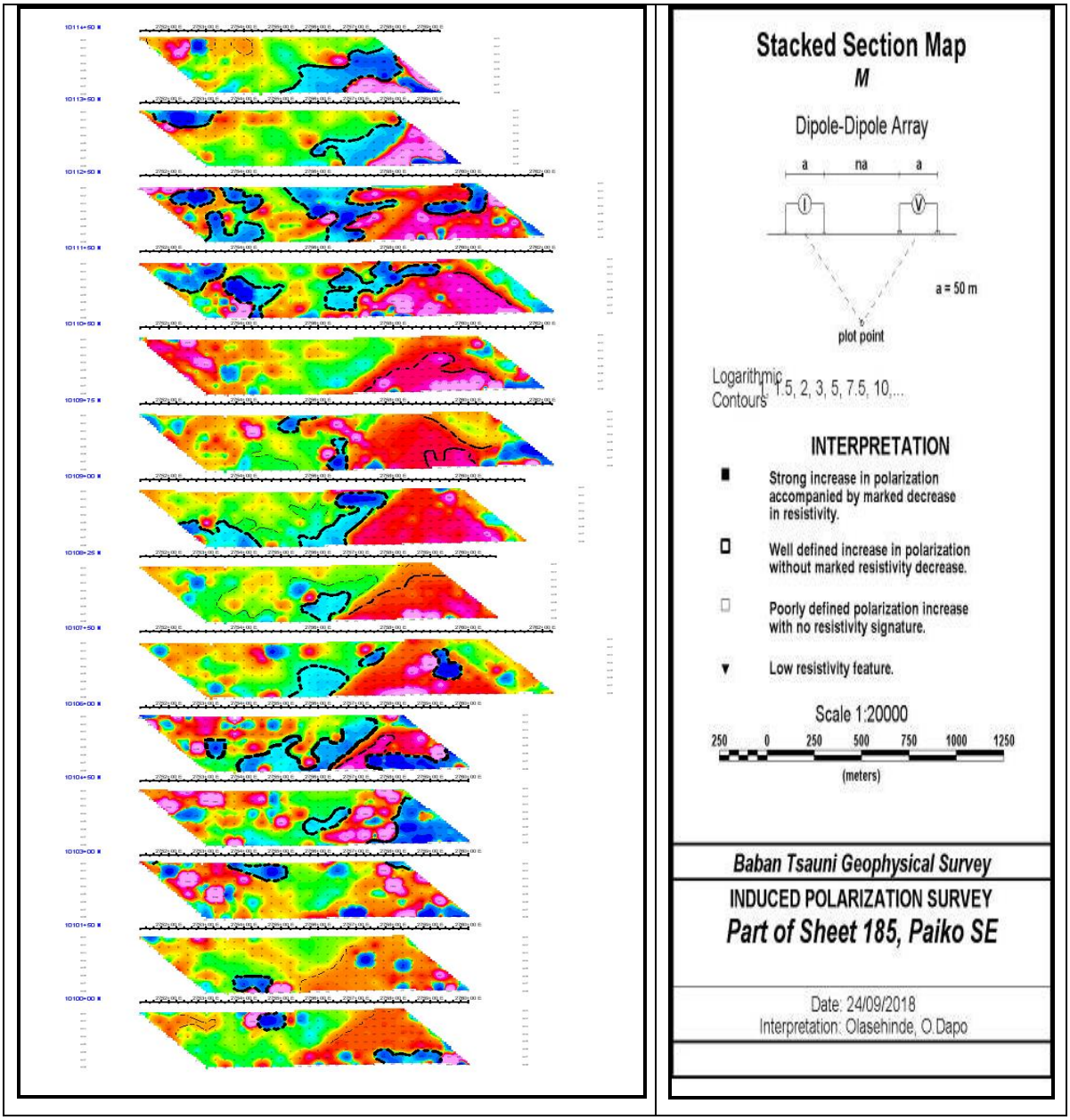

Figure 4.30a: Stacked pseudo-section plot for the chargeability 2-demension grid of each of the 14 traverses. The stack plot shows the correlation over mapped structures

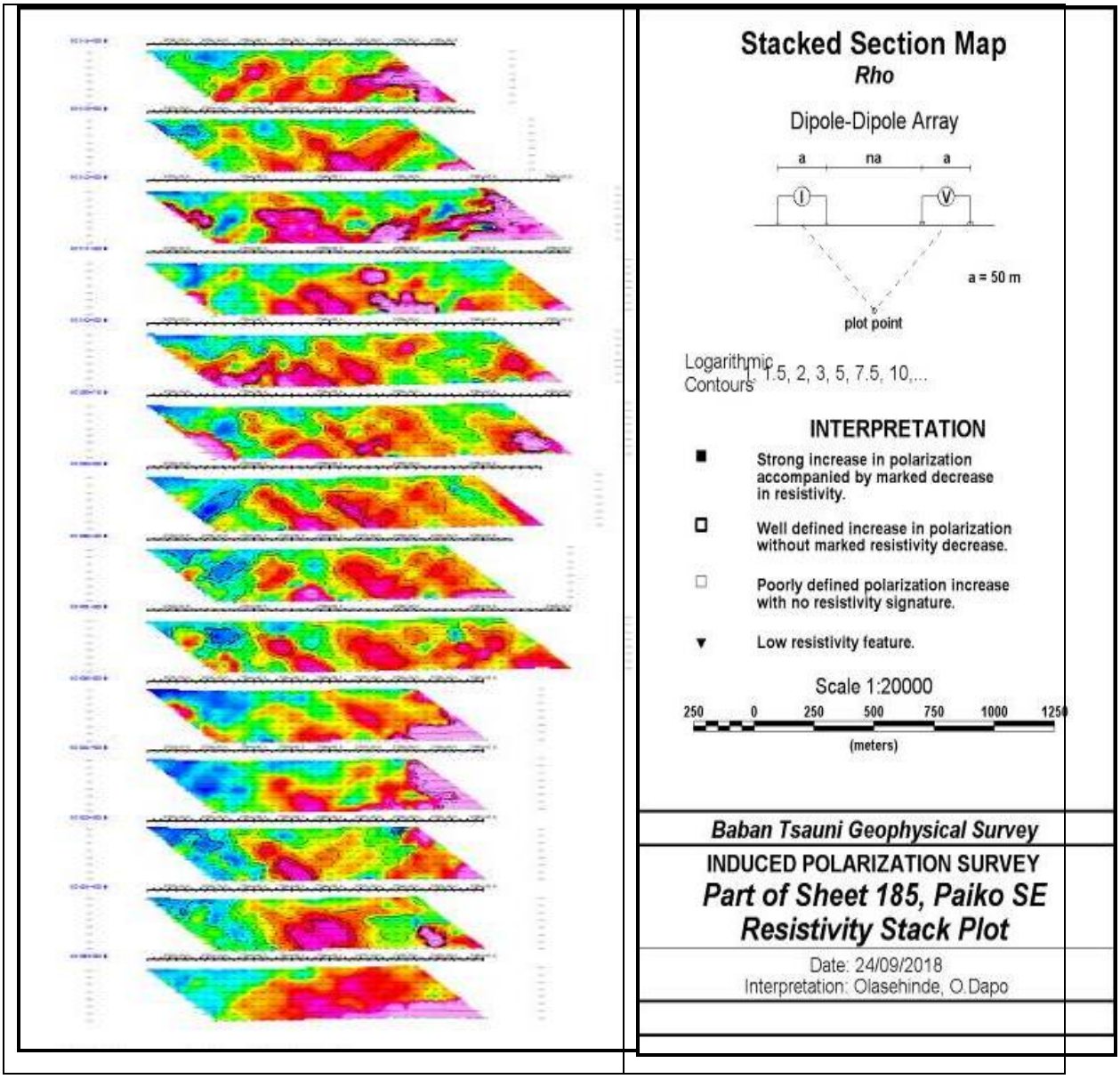

Figure 4.30b: Stacked pseudo-section plot of the resistivity 2-dimension grid for each of the 14 traverses showing the correlation in the resistivity structure as related to the mapped structures

4.5.1 Interpretation of the Induced Polarization and Apparent Resistivity Data

The time domain induced polarization coupled with apparent resistivity ($_a$Rho) shows that the area under investigation had the presences of disseminated sulphide mineralisation which are believed to be near surface, i.e. less than 20 m as shown from the pseudo-section plot of both the chargeability and apparent resistivity. The plots shows relatively high chargeability from n=1, which theoretically is estimated at about 75 m but in actual sense it is approximately 20m (Loke, 2001). The estimated depths of penetration for each of the 'n' values of the survey specification are as computed by Loke (2001) and it's as listed in the Table 4.2.

The high chargeability which relates also to the relatively high resistivity are distributed over the study area but more confined to the west of the target area as shown from the stack plot of both the chargeability and apparent resistivity (Figs. 4.28a & b). From ground truthing evidences, the expected geophysical signature is a region with high resistivity value arising from the host rock, with a corresponding high chargeability due to the effect of the disseminated sulphide and gold within the host rock.

The resistivity structure shows an area with highly varied lithology contrast owing to emplacement of different rock types of different geological episodes or ages as observed from the geological field mapping and interpreted structural map from the magnetic data processing. There are also evidences of intrusive cross-cutting each other depicting fracturing and faulting.

Table 4.2: Dipole-dipole arrays estimated investigation depth (after Edwards 1977).
L = lateral length for the 'n' stations.

n values	L	z e/a	z e/L	Geometric Factor	Inverse Geometric Factor (Ratio)	Estimated Depth of Penetration (m)
n = 1	150	0.416	0.139	18.85	0.05305 (0.3333)	21
n = 2	200	0.697	0.174	75.398	0.01326 (0.0833)	35
n = 3	250	0.962	0.192	188.5	0.00531 (0.0333)	48
n = 4	300	1.22	0.203	376.99	0.00265 (0.0166)	61
n = 5	350	1.476	0.211	659.73	0.00152 (0.0096)	74
n = 6	400	1.73	0.216	1055.6	0.00095 (0.0060)	86
n = 7	450	1.983	0.22	1583.4	0.00063 (0.0040)	99
n = 8	500	2.236	0.224	2261.9	0.00044 (0.0028)	112

As observed from the ground magnetic structural interpretation map (Fig. 4.26) there is a prominent structure trending NNE-SSW which was interpreted and confirmed to be the NNPC pipeline after ground truthing. Equally, there are structures which are closed to the NNPC pipeline as delineated from the upward continued magnetic grid. Some of these structures orient almost parallel to the pipeline and shows significant evidences of sulphide mineralisation from the chargeability and resistivity pseudo-sections and stack plots. Thus, the NNPC pipeline was researched into and discovered to be made from carbon steel (API 5L) material with concrete coating around it to prevent rusting. As at the time of this write-up, confirmation could not be made if there are cathodic protections on the pipeline. Some of these localized structured parallel to the pipeline equally shows significant high chargeability with corresponding relatively high apparent resistivity and there could be possibilities of effect of the pipeline on the signature if there are cathodic protection interferences. Though the carbon steel would be expected to give a very low chargeability signature due to the fact that steel are not chargeable. Coupled with the concrete coating, rusting is highly prevented from dispersing into the surrounding when it does occur. Thus, the induced polarization response and resistivity signature are believed to be attributed to disseminated sulphide mineralisation and precious metals (gold and associated silver).

There are prominent anomalies delineated from the integration of the induced polarization data with the apparent resistivity (Fig. 4.31 and Fig. 4.32). There is a mapped body trending NW-SE in pockets. Its signature can be seen at the southeastern end and trends in a disseminated cluster to the northwest and cross-cut through the pipeline. Another distinctive anomaly was isolated at the south-central portion, which correlated from field evidence of an artisanal gold working pit. The anomaly was seen trending NNE-SSW. All these mapped structures/body correlates with high resistivity except for the mapped anomaly at the western section. This body shows significant high chargeability but with a contracting low resistivity. This was interpreted to be clay-rich zones.

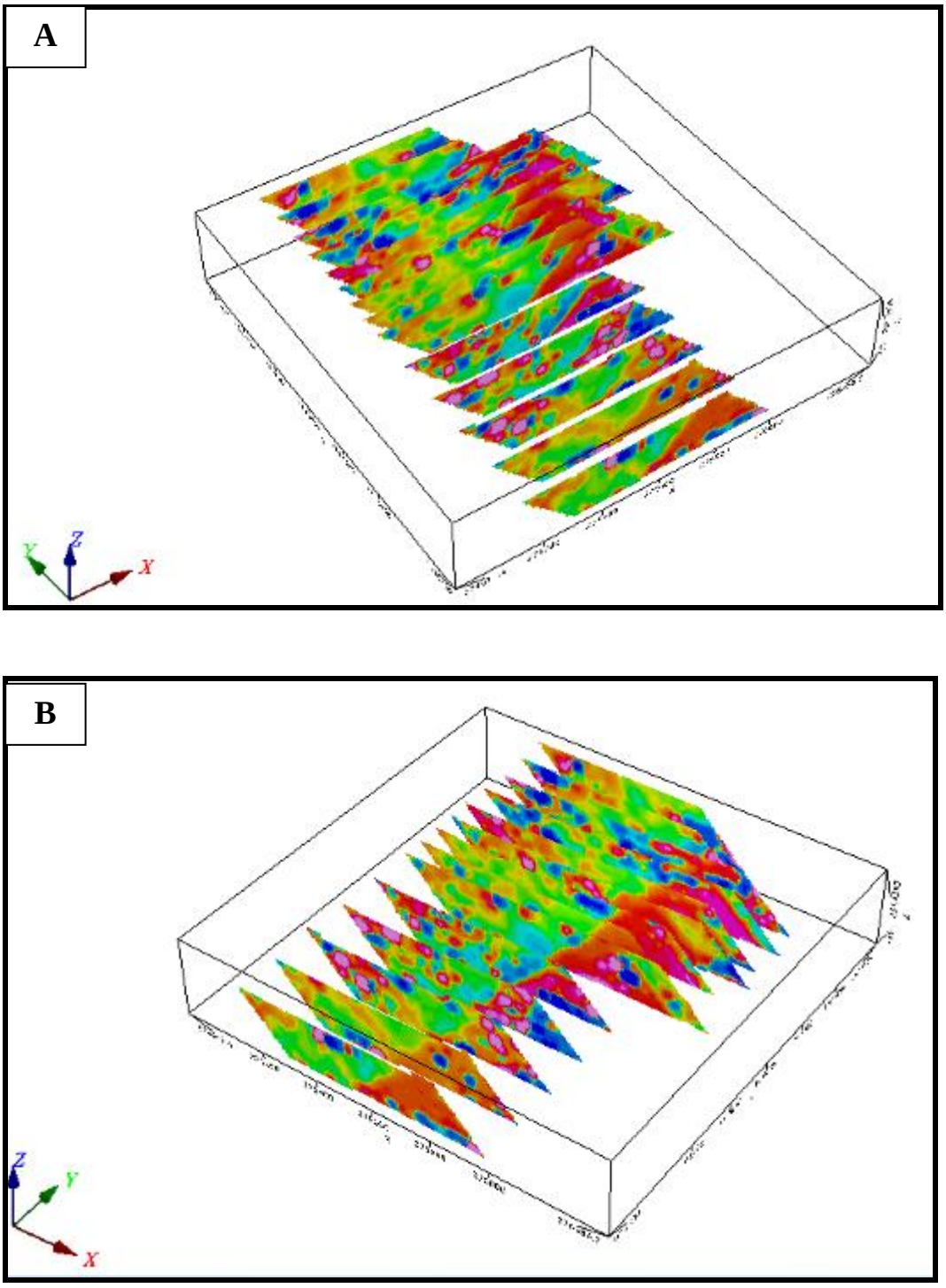

Figure 4.31: A - Chargeability Stack Pseudo-section plot in a 3-dimensional view from the southwestern end. B - Chargeability Stack Pseudo-section plot in a 3-dimensional view from the southeastern end

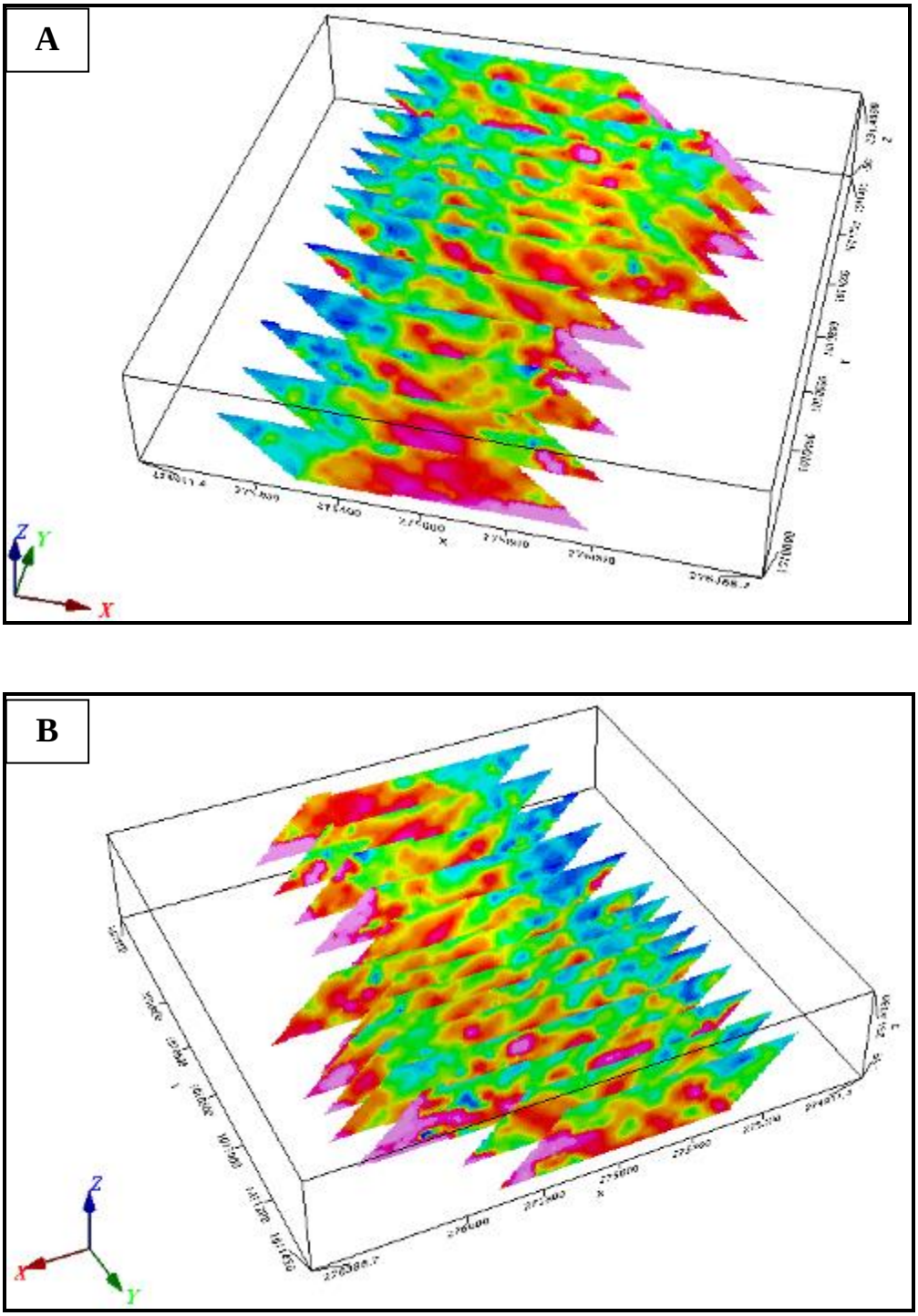

Figure 4.32: A - Apparent Resistivity Stack Pseudo-section plot in a 3-dimensional view from the north-eastern end. B - Apparent Resistivity Stack Pseudo-section plot in a 3-dimensional view from the south-western end

A sample grid plot (Fig. 4.33) for the N-values from the dipole-dipole spacing was computed and generated to visualize the spatial distribution of the chargeability in relation to the apparent resistivity across a given depth. This was done to evaluate the continuity or discontinuity of the anomaly on the z-axis which is the depth information or thickness of the anomaly. From the plot, it was clearly observed that most of the anomalous chargeability values recorded are deep seated, though the distribution varies from one N-value layer to the other showing the in-situ inhomogeneity distribution of sulphide and associated sulphide mineralisation.

Also, the depth slicing shows that the NNPC pipeline might be having little or no influence on the high chargeability with the apparent resistivity values observed around the pipeline. This was interpreted from signatures observed at depth having the same trend as observed near surface.

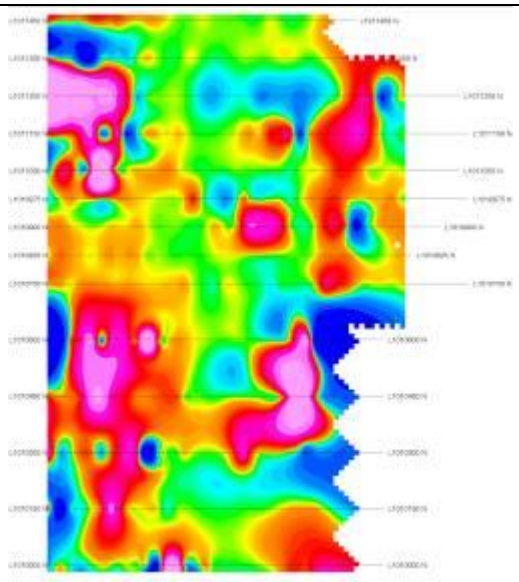

N=1 (Chargeability)

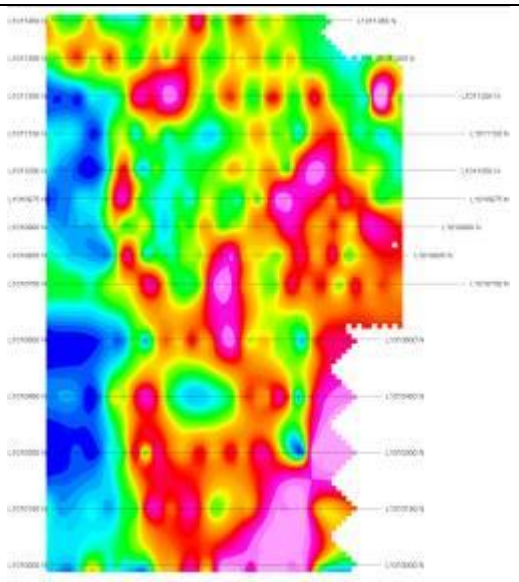

N=1 (Apparent Resistivity)

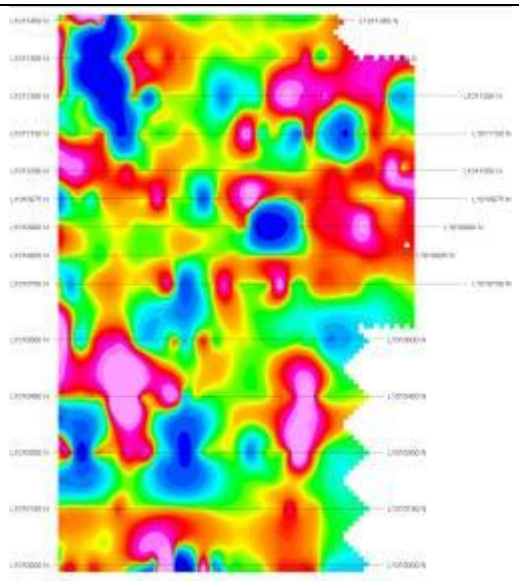

N=2 (Chargeability)

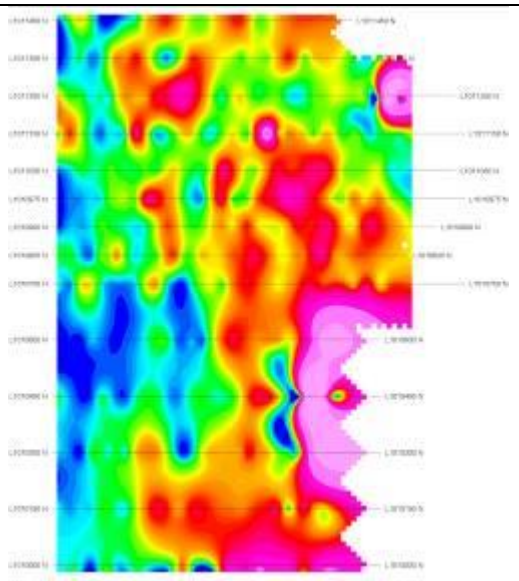

N= 2 (Apparent Resistivity)

Figure 4.33: Sample Plot of the iso-layers of the chargeability and Apparent Resistivity using the N-values from the dipole-dipole depth of investigation. It shows the spatial distribution with continuity/discontinuity of the zones across depth from N=1 and 2.

4.5.2 A 3-Dimensional View and Ore Body geometry configuration

From the integration of the acquired data sets, which are the aeromagnetics, airborne radiometric, geological ground truthing, ground magnetic and electrical data of both induced polarization and electrical resistivity, a 3-dimension ore body geometry model was developed for both the chargeability (Fig. 4.34a) responses as well as the apparent resistivity signature (Fig. 4.34b) to give an insight into the geometry configuration of the subsurface.

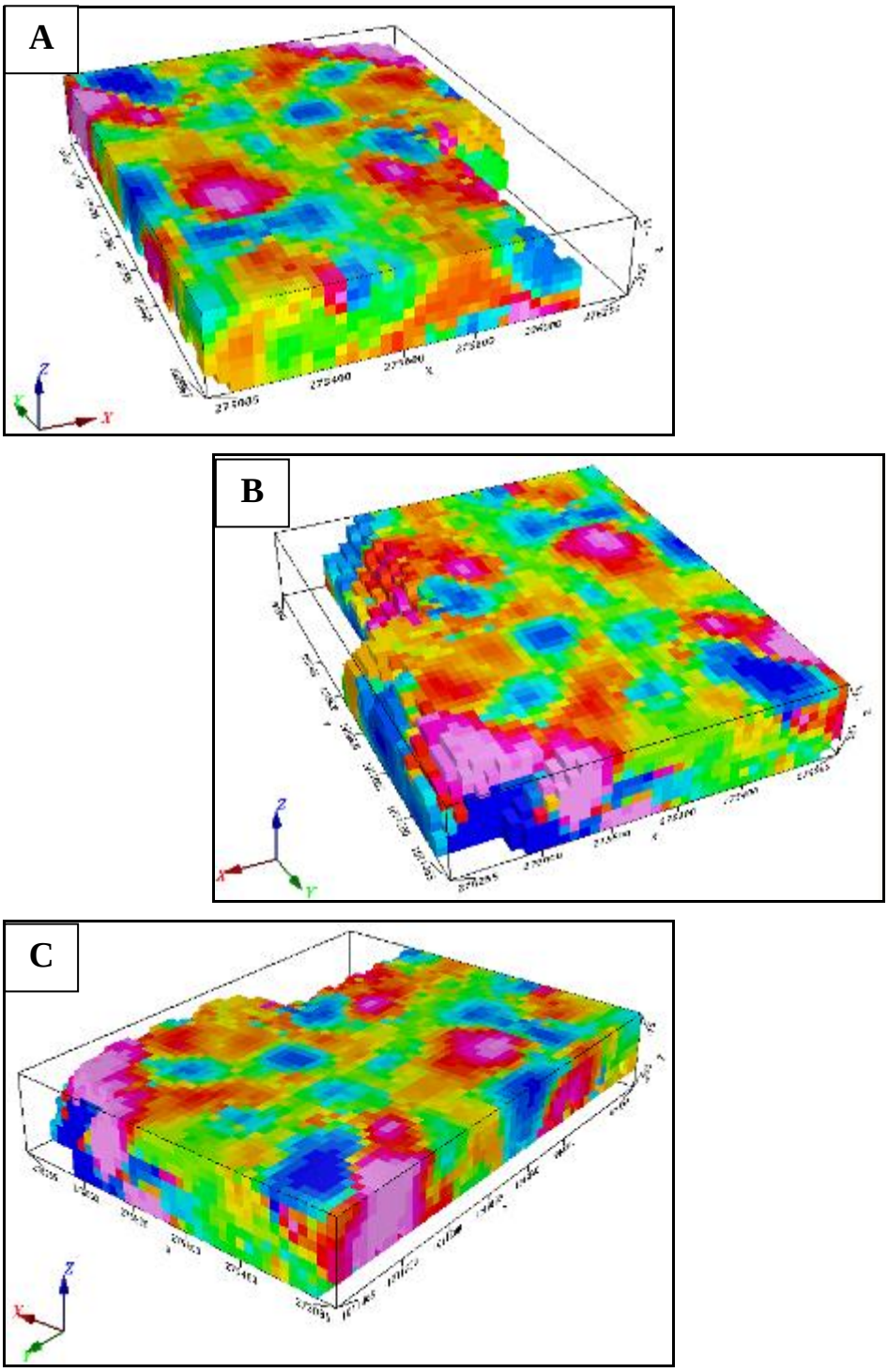

Figure 4.34a: A 3-dimensional view of the induced polarization response over the delineated target area from different views (A, B and C) as shown by the x, y and z-axis

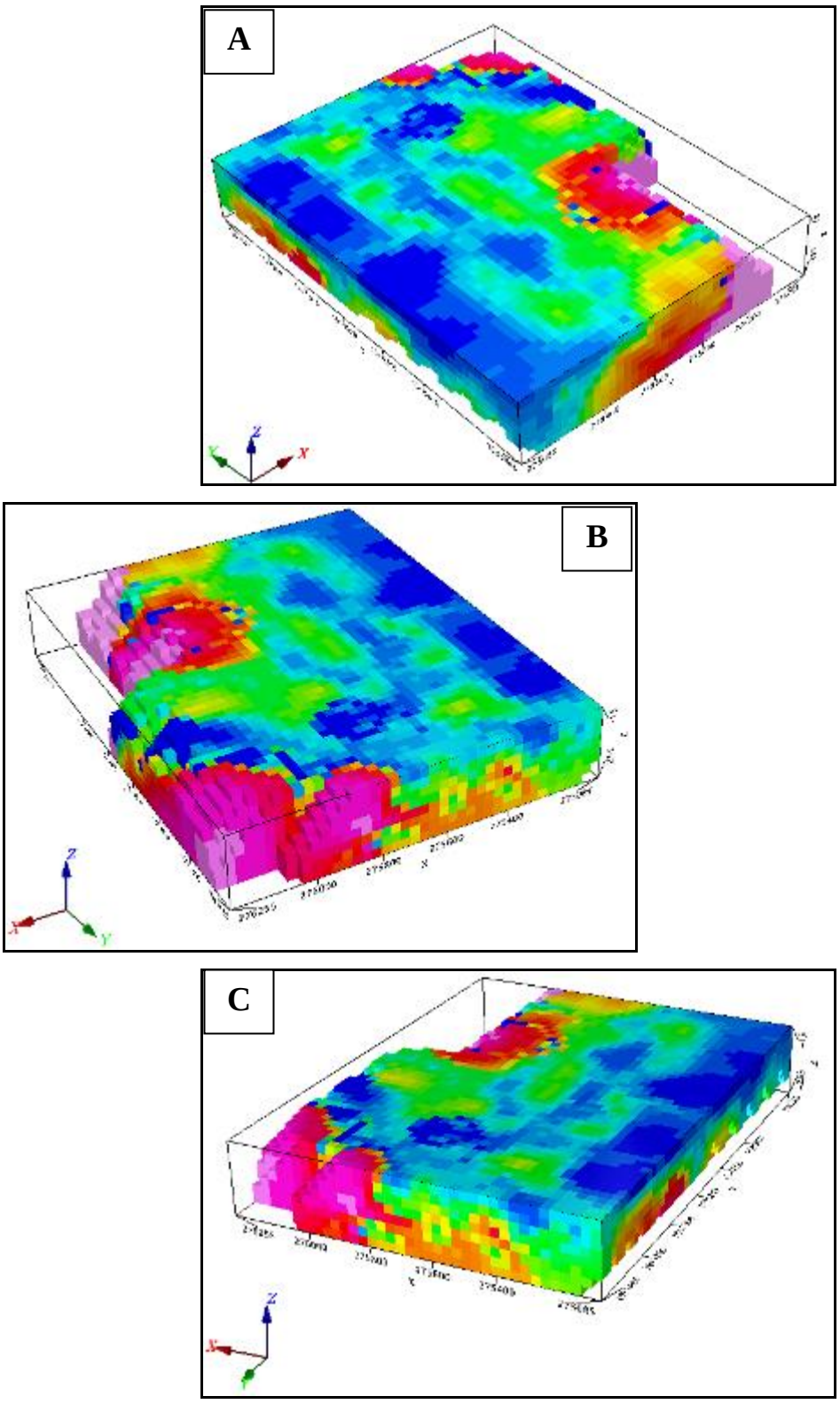

Figure 4.34b: A 3-dimensional view of the apparent resistivity signature over the delineated target area from different (A, B and C) as shown by the x, y and z-axis

A control profile over an artisanal pit where the vein is expose at a depth of about 6.4m trending 310° (NW-SE) at a latitude of 1011250N, covering a total of 250m (traverse 12 west) was evaluated for anomaly characterization. The chargeability response that correspond to the vein is about 30mV/V and an apparent resistivity of 1000Ωm and above over the pit. Thus these values were use to be narrow in on the target anomalies. An iso-surface was computed for chargeability values greater than 30 millivolt/volt (mV/V) as obtained over the test site and used as a threshold value for separating anomaly from the background values. An iso-resistivity model was also computed for the apparent resistivity for values greater than 1000 Ωm. These two models integrated together clearly define the regions with suspected mineralisation of the disseminated sulphide (Fig. 4.35a and b).

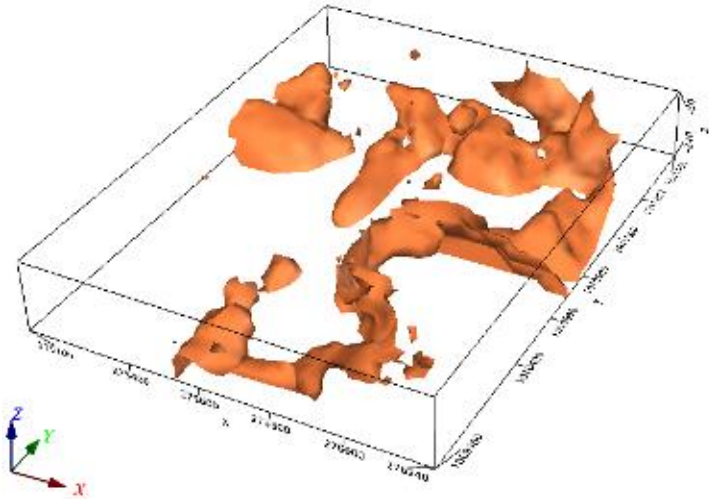

Iso-Surface of Apparent Resistivity greater than 1000 Ωm

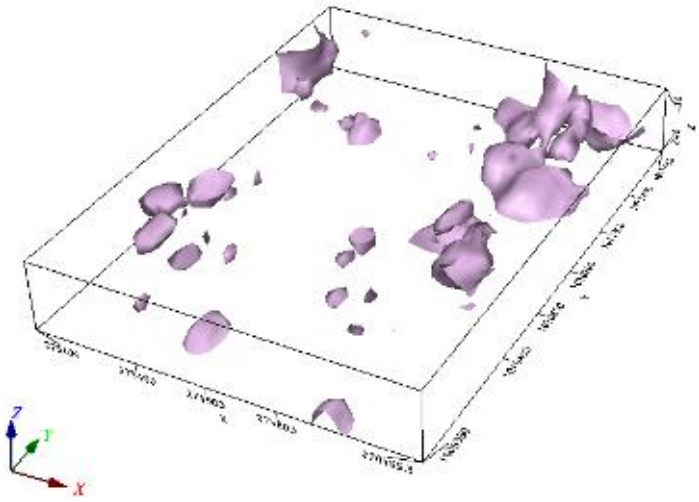

Iso-Surface for Chargeability greater than 30 mV/V

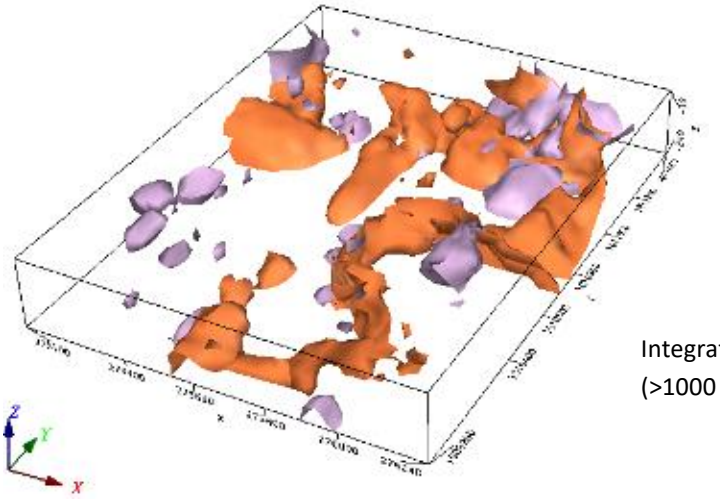

Integrated Iso-Surfaces of both Apparent Resistivity (>1000 Ωm) and Chargeability (>30 mV/V)

Figure 4.35a: A 3-dimensional model of integrated iso-surfaces of both apparent resistivity and chargeability (southeast view)

Iso-Surface of Apparent Resistivity greater than 1000 Ωm

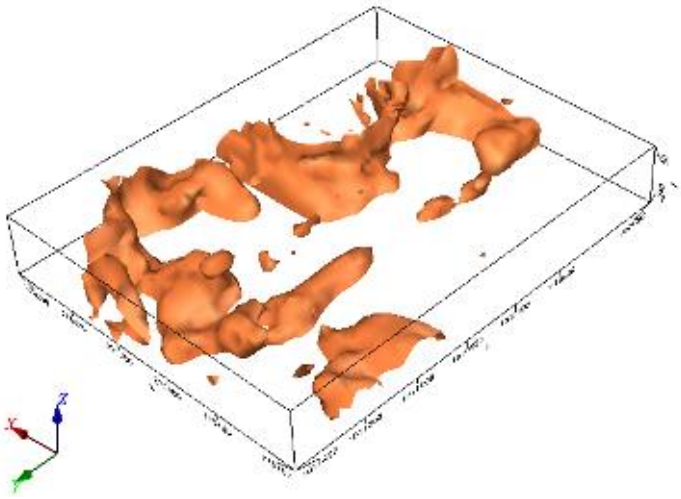

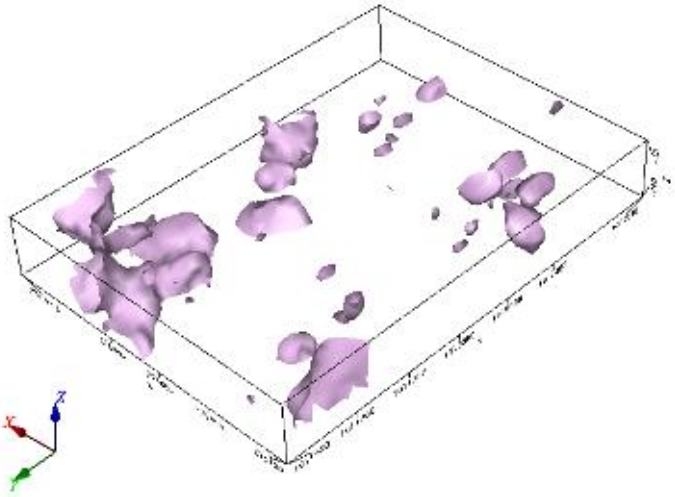

Iso-Surface for Chargeability greater than 30 mV/V

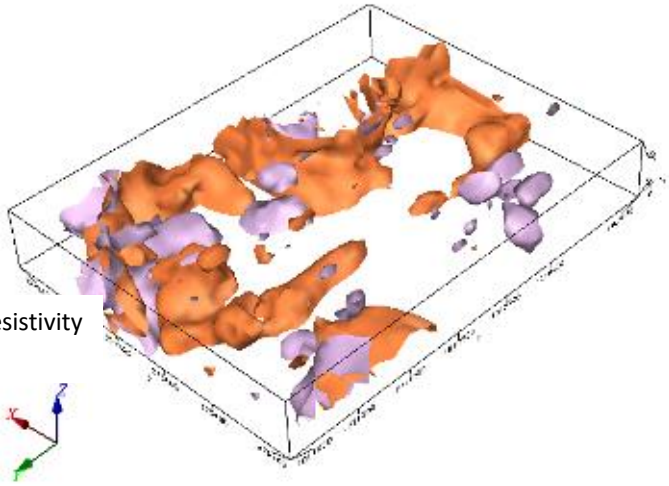

Integrated Iso-Surfaces of both Apparent Resistivity (>1000Ωm) and Chargeability (>30 mV/V)

Figure 4.35b: A 3-dimensional model of integrated iso-surfaces of both apparent resistivity and chargeability (northwest view)

With the control profile constraints, the interpreted structural trends from the magnetic data was overlaid on the iso-surface (Fig. 4.36).

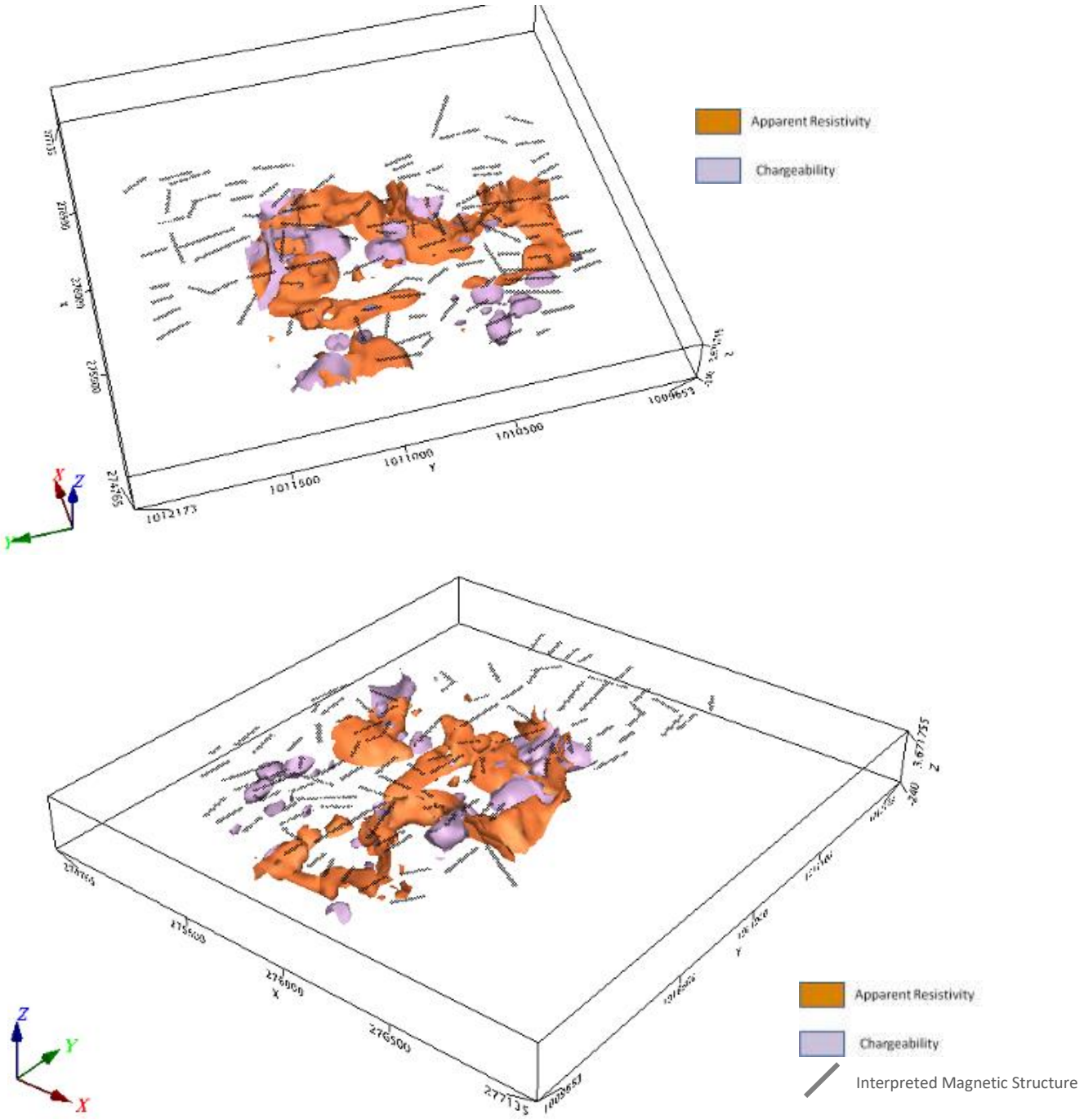

Figure 4.36: An integrated 3-dimensional model of ore body geometry using apparent resistivity and chargeability with integrated interpreted structure from ground magnetic survey from northwest (A) and southeast (B) views

Though the chargeability response can be directly delineated, the resistivity signature was interpreted to vary widely over the area. The following reasons were attributed to this:

- The degree of weathering varies from one lithological unit to another and thus, the resistivity signature varies accordingly due to the degree of porosity and permeability created by the effect of weathering.
- The sulphide and associated mineralisation within this area was interpreted to be structurally controlled. This makes it possible for the structure to cut through various host lithological unit with varying resistivity signature even before weathering takes place.
- From the generated digital terrain model using the global positioning system receiver data acquired concurrently with the ground magnetic data in continuous mode over the area, the topography of the area has been greatly affected by weathering and tectonic events that possibly could have caused uplift.
- The resistivity signature from the 2-dimensional pseudo-section and planner view of the N-value iso-resistivity layer shows that there are in-homogeneity in the lithological units as well as possible intrusive at the subsurface.

4.5.3 Volumetric Estimation of the Interpreted Suspected Ore Body

Volumetric estimation is an important part in mineral exploration for resource size estimation. A routine method of assigning points to each voxel blocks and counting the numbers of voxels that are filled was used. In order to reduce the exaggeration in the computation, the Oasis Montaj software introduces an improved algorithm to estimate the volume of a 3D model using a voxel-based method which will correct for the overestimation. After voxel space transformation, each voxel which contains points was reduced to the volume of its surrounding bounding box. Voxels are identified by a neighbourhood analysis in the X and Y direction of each filled voxel. Finally, the approximate volume of the 3D geometry was composed by the sum of the bounding box volumes of the filled voxels (Figs. 4.37 and 4.38).

Several attempts had been made with the use of voxel-model (block-model) by various researchers. Li *et al*. (2005) proposed an algorithm for 3D model based on iso-surfaces, noting two (2) major problems with the algorithm. These problems are; lack of precision with the cubes of the voxel and redundancy when matching model with voxel space. The volume calculated is therefore an estimated volume for the ore body. Conventionally, model-based mineral prospectivity mapping have been done in 2-dimensions, but this is limited because mineralisation occurs in 3-dimensions.

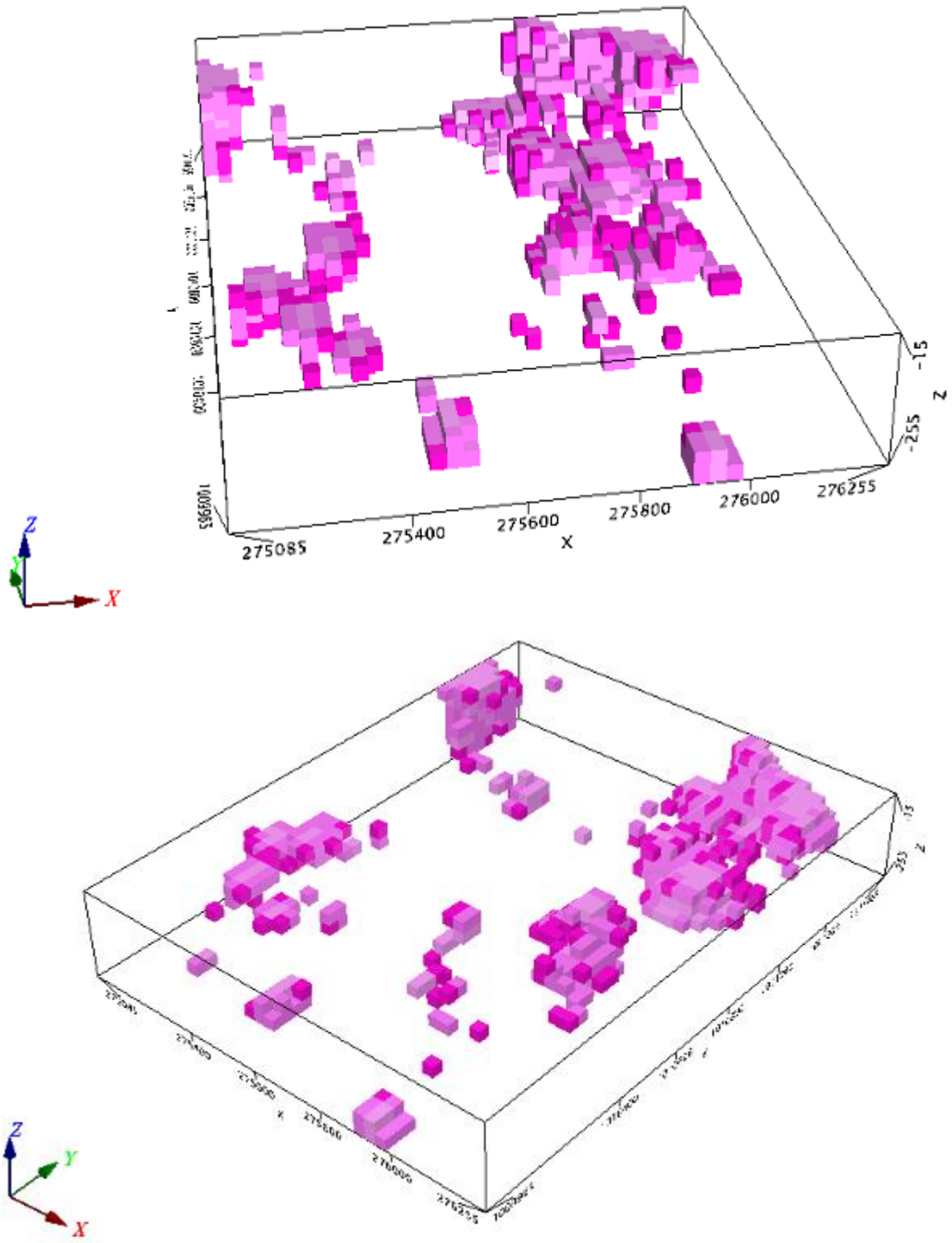

Figure 4.37: A 3-dimensional model of the chargeability response from different views as illustrated by the x, y and z-axis showing a cut-off value of 30 mV/V

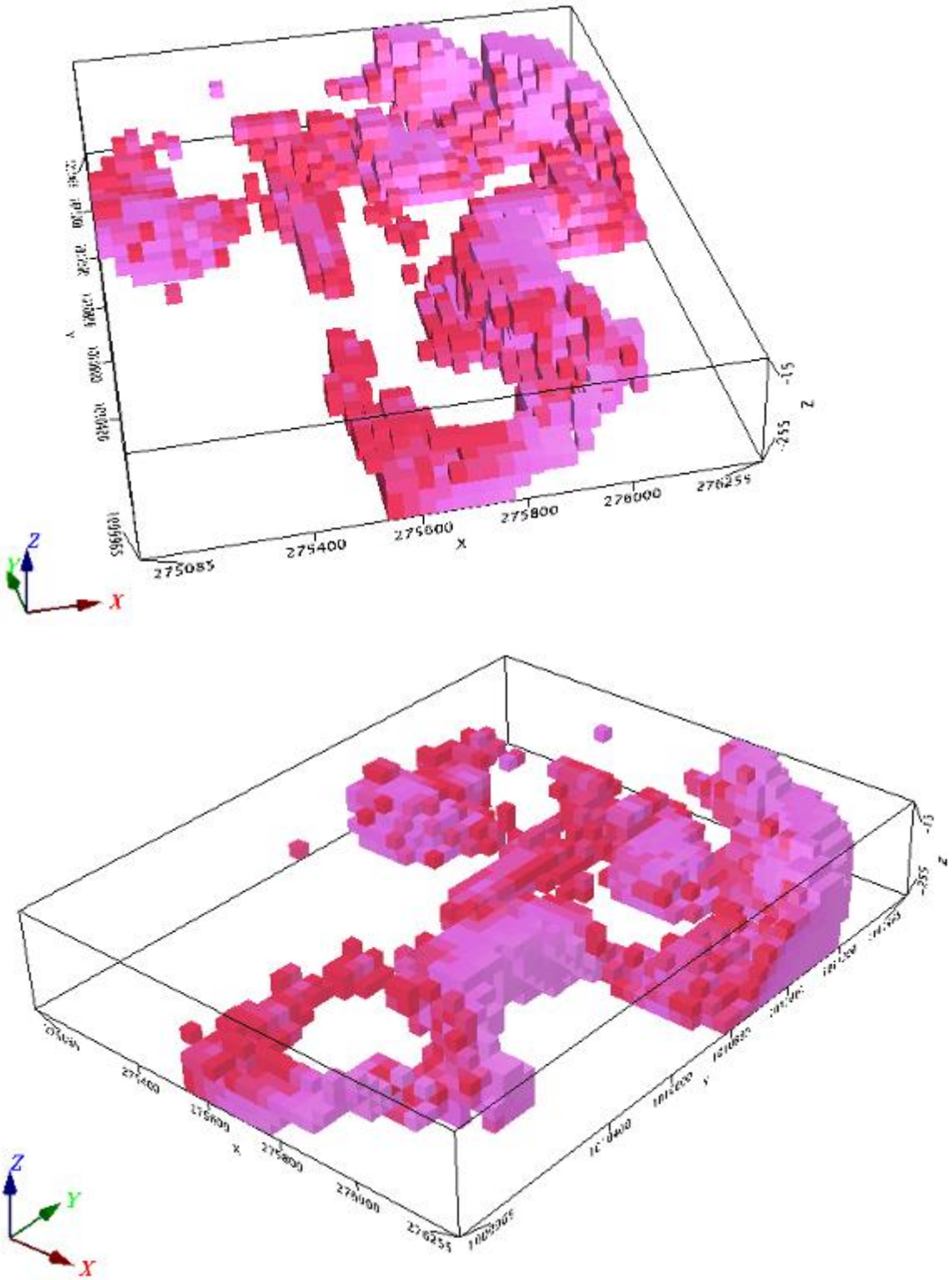

Figure 4.38: A 3-dimensional model of the apparent resistivity signature from different views as illustrated by the x, y and z-axis showing a cut-off value of 1000 Ωm

Assessment of the 3-dimensional model and ore body geometry gives to a great accuracy an estimated volume of the ore body based on the threshold value of 30 mV/V used for the chargeability value. Thus it was being assumed that chargeability values less than 30 mV/V typifies less chargeable zones and its response as a mineralized zone is therefore masked off the model. The volumetric value of the suspected ore body based on its geometry configuration was computed using voxel statistics for visible cell, an algorithm embedded in the Oasis Montaj software. The estimated volume was computed as ***23,328,000 m^3*** with a mean chargeability value of 54.98 mV/V.

CHAPTER FIVE

SUMMARY, CONCLUSIONS AND RECOMMENDATIONS

5.1 Summary

Aeromagnetic and airborne radiometric dataset covering sheet 185 (Paiko SE) of the 1:50,000 Nigerian Standard Topographic sheet division were compiled, processed and interpreted for lithological characterization and understanding the structural setting in line with suspected associated sulphide mineralisation within the study area.

Enhancement and filtering technique applied to the aeromagnetic data started with reduction-to-pole, analytic signal, first and second vertical derivative, horizontal gradient and tilt derivative. All these enhancement and filtering techniques were applied for source and edge detection of signatures arising from anomalies. Structures identified include lithological boundary in magnetic textural analysis of the Total Magnetic Intensity (TMI) and the analytic signal. Lineaments, joints, folds, dikes and foliation trends were enhanced and attenuated for either regional/major or local structures. Faults within the study area were effectively mapped using the horizontal gradient derivative of the Total Magnetic Intensity.

As a way of understanding the lithological differentiation, the spatial distribution of the radio-elements' abundances from the airborne radiometric data were compiled, processed and gridded. These gridded images provides information on the potassium (K), thorium (Th) and uranium (U) concentrations, which were use to characterize the signatures into lithology units. The ratios Th/K, U/K and Th/U were calculated and gridded with the aim of eliminating ambiguity in lithology similarities, which could be from effects of varying moisture contents in soil, source geometry that are non-planar and ambiguity from elevation adjustment or corrections. Areas with elevated uranium concentrations were delineated using ratios of U/K and U/Th, whereas thorium abundance was associated with ore bodies.

The interpreted airborne data was subsequently ground-truth with more detail geological mapping over delineated area carved out from integration of the airborne interpretation, literature review, reconnaissance survey as well as information gathered from artisanal miners around the area.

The geological ground truthing confirms that the area is underlined by the following basement rocks; biotite – gneiss, hornblende – gneiss, medium – grained granite, aplites/ pegmatite, quartz veins of varying width which are associated with the gneisses in almost all parts of the area.

At least two generation of quartz veins were established in the field – the undeformed late quartz veins which are suspected to be the main host of mineralisation. The emplacement of these veins, which might have exploited the channel ways provided by some pre – existing fractures, are probably the latest geological events in the area. It was suspected that the quartz veins were emplaced by metal bearing hydrothermal solutions which could have originated from a consolidating intrusive igneous mass.

The ground magnetic which covers portion of the mapped area revealed the local structures controlling the structurally controlled mineralisation within the area to be majorly trending in the northwest-southeast and north northeast-south southwest directions. From the cross-cutting relationship and displacement as attenuated from the horizontal gradient, the NW-SE structures area older than the NNE-SSW. The sulphide mineralisation, though present in the NNE-SSW direction also are mainly confined to the NW-SE trends as observed from the artisanal pits. The NNE-SSW structures which are Pan-African are associated with gold mineralisation with disseminated sulphide.

The electrical resistivity coupled with induced polarization had been used as a follow-up geophysical method over the interpreted structures. The mineralisation as evidenced from ground truthing occurs as disseminated deposit in association with quartzitic rock. Thus a high resistivity was proposed as resistivity signature over the host rock. Though the resistivity varies greatly as the study area falls within the basement complex which has undergone series of deformation and tectonic events. Thus, the chargeability response was used to correlate the resistivity signature. A threshold resistivity value of greater the 1000 Ωm and chargeability of greater than 30 mV/V was

used to delineated the anomalous value from the background value as obtained from the control profile.

The result shows agreement with the interpreted magnetic structure with trends in the NW-SE and NNE-SSW. The mineralisation is near surface with estimated depth of less than 20 m in some locations. The 3-dimensional model was generated and filtered using the threshold values of the changeability and a volumetric value of ***23,328,000 m^3*** was estimated for the associated sulphide mineralisation which from field evidences comprises of lead, zinc, silver and gold.

5.2 Conclusions

The integrated geophysical approach methodology adopted was able to give a better insight into the structurally controlled epigenetic mineralisation in terms of structural trend and the ore body geometry.

Delineated structural trend from the geophysical signatures of the anomalies corresponds to structural trend earlier postulated by previous works such as Okunlola *et al*. (2007), Oluyide (2004) and the Nigerian Geological Survey Agency (2006).

Three structural deformation episodes i.e. NE-SW, NW-SE and an almost N-S trend were observed from the aeromagnetic data. The NE-SW structures were interpreted as the oldest from the cross-cutting relationship. These structures were seen and observed to have been discontinued and relatively displaced by the NW-SE structures, while the NNW-SSE and the NNE-SSW structures were observed to be the youngest within the study area. This is in agreement with the Pan-African system which is the youngest tectonic episode trending N-S and covering most parts of the country.

The mapped lithological units from the airborne radiometric survey were able to delineate lithological units which might possibly not have surface expression in term of exposures. The mapped intrusives shows great similarities, but the differences in the intensity of the signature colour designation might possibly be due to the depth of occurrence as the sensor of the radiometric survey penetrates only to a shallow depth. The relative increase and decrease in K and Th/K ratio respectively as showed from radiometric data interpretation, are indications of hydrothermal alterations. The ground

magnetic reveals more of the local structure which correlates with inferences from the aeromagnetic interpretation.

The geological ground truthing was able to effectively classify the observed interpretation from the radiometry data.

Follow up geophysical method using an combination of electrical resistivity tomography and induced polarization has helped to characterized signatures arising from causative bodies and structures for the presence or absent of chargeable bodies suspected to be disseminated sulphide association.

The application of integrated airborne magnetic and radiometric, geological ground truthing, ground magnetic studies coupled with interpretation from the induced polarization and electrical resistivity within the study area has helped to evaluate the structural setting and mode of mineralisation of the associated sulphide within the study area. The integrated approach equally assisted in estimating the geometric configuration as well as volume of the suspected ore bodies.

The radiometric together with the ground truthing has been used to map the lithology while the aeromagnetic and ground magnetic data has been used to identify structures which play host to the sulphide mineralisation. The induced polarization and electrical resistivity has help in characterization of the structures for sulphide mineralisation.

This technique is potent and could be applied in deeply weathered terrains or regolith regions to pick exploration targets for blind ore deposits. Thus, the following have been achieved:

1. Evaluation of the structural setting within the study area.
2. Updating of the geological map over the study area.
3. Production of a geological and structural map of the study area
4. Identification of target area that could play host to the associated sulphide mineralisation
5. Ground truthing of the target area
6. Production of a 2D pseudo-section showing the suspected ore bodies dip directions.
7. Generation of a 3-dimension geometry of the ore body

5.3 Recommendation

The study area falls within the basement complex as opposed to the associated sulphide mineralisation found within the Benue trough. Thus, a more detail geological mapping covering a wider area than the study area and extending southward to the sedimentary basin is necessary to ascertain the relationship of the mineralisation in term of the controlling structures as found in both the sedimentary and basement and compare their age relationship. It is recommended that geochemical data be integrated to compare the geochemical anomalies (enrichments) of the geochemical composition in terms of their elemental composition and oxides. This can be use to constraints their origin for both the sedimentary and basement.

This research work is basically an integration of basic geology and geophysical methods of exploration. It is recommended that geochemical studies be carried out to correlate the geochemical dispersion pattern with the delineated and interpreted structures. This would further delineate the chargeable bodies that are structurally controlled, as the area is mineralized with other chargeable materials such as gold, zinc and silver as found from the artisanal workings and ground truthing.

The geometry configuration and volume calculated are subject to drilling as the volume calculated is that of chargeable bodies. Thus, there is a need for drilling operations to confirm the source bodies causing the high chargeability within the resistive host.

The structures identified from the airborne data extend beyond the study area. It is therefore recommended that more work be carried out outside the present study area especially towards the southern part around Gwagwalada, Federal Capital Territory.

5.4 Contribution to Knowledge

The sedimentary Benue trough has long been synonymous with associated sulphide mineralisation containing lead-zinc ore in Nigeria. However, findings have revealed the occurrence and possible deposit of sulphide mineralisation within the basement complex, with the controlling structural setting and geometry not fully understood. Consequently, this research work evaluates the structural setting associated with the epigenetic

disseminated structurally controlled mineralisation within the basement complex section of central Nigeria (Paiko Sheet 185), its mode of occurrence and ore body geometry.

Thus, improved knowledge about the associated sulphide mineralisation within the basement complex would enhance the solid mineral development within the country and create channel for economy growth and economic diversification. The findings of this research work and further studies will leads into mining activity within and around the study area, thereby aiding better infrastructures and human development for the host communities.

5.5 Suggestion for Further Studies

The associated sulphide mineralisation within the study area are structurally controlled and epigenetic. The mineralising fluid gets emplaced within the host structures. Consequently, other sulphide associated minerals apart from lead and zinc are equally formed. Thus, a detail geochemical study is needed to help characterise the geochemical dispersion pattern and delineate the geochemical hotspots. Processing and interpretation of geochemical datasets, especially geostatistics can help classify the mineral assemblages and mineralisation styles.

Understanding the overburden thickness can also be used to evaluate if the mineralisations are primary or elluvial deposits. A correlation study with similar serological and structural settings beyond the study are can be conducted to determine possibilities of the associated sulphide mineralisation including lead-zinc extending to other provinces within the basement complex. As against the biased postulation of the lead-zinc mineralisation been confined to the sedimentary basin of the Benue trough.

References

Adefolalu, D.O. (1988). Precipitation trends evapotranspiration and the ecological zones of Nigeria. Theoretical & Applied Climatology 39(2): 81-89.

Adekoya, J. A. (1993). Proterozoic Maru and Birnin Gwari Banded Iron Formation, Northwestern Nigeria. *Jour. Mining Geol. (Nigeria). Vol. 29, No. 1*, pp. 63 – 76.

Ajakaiye D.E., Hall, D. H., Ashiekaa, J.A and Udensi, E.E., 1991. Magnetic anomalies in the Nigeria continental mass based on aeromegnetic surveys. Tectonophysics, 192:211-230.

Ajibade, A C and Wright, J B. 1989. The Togo-Benin-Nigeria Shield: evidence of crustal aggregation in the Pan-African belt. *Tectonophysics*, 165 (1-4), 125–129.

Ajibade, A C, Woakes, M and Rahaman, M A. 1987. Proterozoic crustal development in the Pan-African regime of Nigeria In: Proterozoic lithospheric evolution. 259–271 In: Kröner, A. (editor). (American Geophysical Union.)

Auken E, Pellerin L, Christensen NB, Sorensen K (2006). A survey of current trends in near-surface electrical and electromagnetic methods. Geophys., 71(5): 249-260.

Ayoade, J. O. 1974. Statistical Analysis of Rainfall over Nigeria. Journal of Tropical Geography, 39: 11-23.

Beard, L. P. and Goitom, B. (2000). Some problems in interpreting low latitude magnetic surveys. 6thEAGE/EEGS Meeting.

Bleil, D. F., 1953, Induced polarization: a method of geophysical prospecting: Geophysics, **18**, 636-661.

Boadi B, Wemegah D.D and Preko K., 2013. Geological and structural interpretation of the Konongo area of the Ashanti gold belt of Ghana from aeromagnetic and radiometric data. International Research Journal of Geology and Mining (IRJGM) (2276-6618) Vol. 3(3) pp. 124-135, April 2013.

Bruguier, O, Dada, S and Lancelot, J R. 1994. Early Archaean component (>3.5 Ga) within a 3.05 Ga orthogneiss from northern Nigeria: U–Pb zircon evidence. *Earth and Planetary Science Letters*, 125(1–4), 89–103.

Burger, H. R., Sheehan, A. F., & Jones, G. H. (2006). Introduction to applied geophysics: Exploring the shallow subsurface. Published by W. W. Norton, 600 p., New York: W.W Norton.

Burke, K.C. and Dewey, F.J., 1972: Orogeny in Africa. In: African Geology. Ibadan, Eds. Dessauvagie, A and Whiteman, C. Geol. Dept. Univ. Ibadan Nigeria, pp 583-608.

Charbonneau, B. (1991). Geochemical evolution and radioactive mineralogy of the Fort Smith radioactive belt, Northwest Territories, Canada. In Primary Radioactive Minerals (The textural patterns of radioactive mineral paragenetic associations), pages 21–48. Theophrastus Publications.

Chopin,G. R. (1988). Humics and radionuclide migration. Radiochima Acta, 44/45:23–28.

Clark,D.A.(1997). Magnetic properties of rocks and minerals. AGSO Journal of Australian Geology and Geophysics, 17(2).

Clark, D. A. and Emerson, D. W. (1991). Notes on rock magnetic characteristics in applied Geophysical studies. Exploration Geophysics, Vol. 22:547–555.

Cratchley, C.R. and Jones, G.P. (1965). An interpretation of the Geology and gravity nomalies of the Benue Valley, Nigeria. Overs. Geol. Surv. Geophys. Paper, No. 1.

Dada, S S. 1998. Crust-forming ages and Proterozoic crustal evolution in Nigeria: a reappraisal of current interpretations. *Precambrian Research*, 87(1–2), 65–74.

Dada, S S. 2006. Proterozoic evolution of Nigeria. In: The basement complex of Nigeria and its mineral resources (A Tribute to Prof M A Rahaman). 29–44. In. Oshi, O. (editor). (Akin Jinad & Co. Ibadan.)

Dada, S S, Brick, J L, Lancelot, J R and Rahaman, M A. 1993. Archaean migmatite-gneiss complex of northcentral Nigeria: its geochemistry, petrogenesis and evolution. International Coloquium on African Geology. Mbabane, Swaziland 97–102.

Dahlin,T. and Loke, M.H., 1998. Resolution of 2D Wenner resistivity imaging as assessed by numerical modelling, Journal of Applied Geophysics, 38, 237-249.

Darnley, A. G. (1996). Uranium exploration data and global geochemical baselines: The need for coordinated action. In Uranium Exploration Data and Techniques Applied to the Preparation of Radioelement Maps. IAEA-TECDOC-980.

Dickson, B. L. and Scott, K. M. (1997). Interpretation of aerial gamma ray surveys-adding the geochemical factors. AGSO Journal of Australian Geology and Geophysics, 17(2):187–200.

Dobrin, M.B., 1976 Introduction to geophysical prospecting, 3rd edition, McGraw Hill Book Co., inc, New York

Edwards L.S., 1977. A modified pseudo-section for resistivity and induced polarization. Geophysics, 42, 1020-1036.

Ferré, E C, Déléris, J, Bouchez, J-L, Lar, A U and Peucat, J-J. 1996. The Pan-African reactivation of contrasted Eburnean and Archaean provinces in Nigeria: structural and isotopic data. *Journal of the Geological Society of London*, 153, 719–728.

Fertl, W. H. (1983). Gamma-ray spectral logging: a new evaluation frontier. World Oil, pages 79–91.

Fitches, W R, Ajibade, A C, Egbuniwe, I G, Holt, R W and Wright, J B. 1985. Late Proterozoic Schist Belts and plutonisn in NW Nigeria. *Journal of the Geological Society of London*, 142, 319–337.

Garba, I. (2000). Gold prospects of the Nigerian Pan-African terrain of West Africa. *Jour. Mining Geol. (Nigeria). Vol. 36, No. 2*, pp. 123-136.

Geological Survey of Nigeria (1964). Simplified Geological Map of Nigeria

Geological Survey of Nigeria (2000): 1:100,000 Map Series. Geological Map of Sheet 185 Paiko

Grant, N K. 1967. Complete Late Pre-Cambrian to Early Palaeozoic Orogenic Cycle in Ghana, Togo and Dahomey. *Nature*, 215(5101), 609–610.

Grant, N K. 1969. The Late Precambrian to Early Paleozoic Pan-African Orogeny in Ghana, Togo, Dahomey, and Nigeria. *Geological Society of America Bulletin Bulletin*, 80 (1), 45–56.

Grant, N K. 1970. Geochronology of Precambrian basement rocks from Ibadan, southwestern Nigeria. *Earth and Planetary Science Letters*, 10, 26–38.

Grant, N. K. (1978). Structural distinction between metasedimentary cover in an underlying basement in the 600 m.y. old Pan-African domain of northwestern Nigeria. *Geol. Soc. Amer. Bull. 89*, pp. 50-58.

Grant, F.S. and West, G.F. 1965: Interpretation Theory in Applied Geophysics. New York: McGraw-Hill.

Grant, N K M, Hickman, M, Burkholder, F R, and Powell, J L. 1972. Kibaran matamorphic belt in Pan-African domain of West Africa? *Nature (Physical Science)*, 238, 90–91.

Gregory, A. F. and Horwood, J. L. (1961). A laboratory study of gamma-ray spectra at the surface of rocks. Department of Energy, Mines and Resources, Ottowa. Mines Branch Research Report R85.

Gunn, P. J. (1975). Linear transformations of gravity and magnetic fields. Geophysical Prospecting, 23:300–312.

Gunn, P.J., Minty B.R.S. and Milligan P. (1997). The airborne gamma-ray spectrometric response over arid Australian terranes. Exploration, 97:733–740.

Herndon, J. M. (1996). Substructure of the inner core of the Earth. pages 646–648

Holt, R., Egbuniwe, I. G., Fitches, W. R. and Wright, J. B. (1978). The relationship between low grade metasedimentary belts, calc-alkaline volcanism and the Pan-African Orogeny in N.W. Nigeria. *41 Geol. Rundsch. Ed. 67. Heft 2, Seite 631-646.*

Hunting Geology and Geophysics Ltd, 1975: Airborne – magnetometer and Gama-Ray Spectrometer survey over central Northern (Katsina – Jos) area.

Kearey P, Brooks M, Hill I (2002), An introduction to geophysical Exploration third Edition. TJ international. pp. 2-160

Keller, G.V. and Frischknecht, F.C. (1966) Electrical Methods in Geophysical Prospecting. Pergamon Press, Oxford.Slater and Lesmes, 2002

Key, R M and Pitfield, P E J. 2009. The prospectivity of the global network reference (GRN) cells in Nigeria: solid minerals based on a national stream sediment geochemical survey Nigerian Geochemical Mapping Technical Assistance Project. *British Geological Survey. Commissioned Report*, CR/09/086. 44pp.

Killeen,P.G.(1979). Gamma-ray spectrometric methods in uranium exploration–application and interpretation.In Geophysics and Geochemistry in the Search for Metallic Ores,edited by P.J. Hood, pages 163–230.

Kono M. and Schubert G. 2007 Geomagnetism (Treatise on Geophysics) Volume 5.

Krishnaswami, S. (1999). Thorium. Encyclopedia of Geochemistry, page 712. Kluwer Academic Publishers, London.

Kröner, A, Ekwueme, B N and Pidgeon, R T. 2001. The Oldest Rocks in West Africa: SHRIMP Zircon Age for Early Archean Migmatitic Orthogneiss at Kaduna, Northern Nigeria. *Journal of Geology*, 109, 399–406.

Kunetz G (1966). Principles of Direct Current Resistivity Prospecting. Gebruder Borntraeger, Berlin, p. 103.

Langmuir, D. and Hermans, J. S. (1980). The mobility of thorium in natural waters at low temperatures. Geochimica et Cosmochimica Acta, 44:1753–1766.

Li, F., Pan, M., Zhu, L., 2005. Research on the algorithm for 3D raster buffer-generation. J. Comp.-Aided Des. Comp. Graph. 17, 1928–1932.

Loke, M. H. (2001). Electrical Imaging Surveys for Environmental and Engineering Studies. A Practical Guide to 2-D and 3-D Surveys. RES2DINV Manual. IRIS Instruments. www.iris-intruments.com

Marshall, D.J., and Madden, T.R., 1959, Induced polarization, a study of its causes: Geophysics, **24**, 790-816.

McConnel, R. B. (1949). Notes on the lead-zinc deposits of Nigeria and the Cretaceous Stratigraphy of the Benue and Cross River valleys. Unpubl. Geol. Surv. (Nigeria). Report No. 408.

Milligan,P.R.and Gunn,P.J.(1997).Enhancement and presentation of airborne geophysical data. AGSO Journal of Australian Geology and Geophysics, 17(2):64–774.

Milsom, J. (2003). Field Geophysics, the geological field guide series. John Wiley and Sons Ltd, The Atrium, Southern Gate, Chichester, West Sussex PO198SQ, England, third edition.

Minty, B. R. S. (1991).Simple micro-leveling for Aeromagnetic data: Exploration Geophysiscs, 22, 591-592

Minty, B. R. S. (1996). The fundamentals of airborne gamma-ray spectrometry. AGSO Journal of Australian Geology and Geophysics, 17(2):39–50.

Nations Online Project (2021). https://www.nationsonline.org/oneworld/map/nigeria-administrative-map.htm

Nicolet,J.P.and Erdi-Krausz, G. (2003). Guidelines for radioelement mapping using gamma ray spectrometry data. IAEA-TECDOC-1363. IAEA.

Nigerian Geological Survey Agency (2006). Geological map of North-central Nigeria

Nigerian Geological Survey Agency (2014). Simplified Geological and Structural map of Nigeria

Odekunle, T.O. (2006). "Determining rainy season onset and retreat over Nigeria from precipitation amount and number of rainy days" Theoretical and Applied Climatology 83: 193201.

Odeyemi, I B. 1981. A review of the orogenic events in the Precambrian basement of Nigeria, West Africa. *Geologische Rundschau*, 70, 879–909.

Ogezi, A E O. 1977. Geochemistry and Geochronology of basement rocks from north-western Nigeria (Unpublished Ph.D. thesis). University of Leeds, England. 295pp. 14 4

Ogilvy, A.A. and Kuzmina, E.N. (1972). Hydrologic and Engineering Geologic Possibility for Employing the method of Induced Potentials. Geophysics. Vol. 32 (5) pp. 839 – 861.

Okunlola, O.A. and Jimba, S., 2006: Compositional trends in relation to Ta-Nb mineralisation in Precambrian pegmatites of Aramoko-Ara- Ijero area, southwestern Nigeria, Jour. Min. Geol. Vol.42, No 2, pp. 113 – 126.

Okunlola, O.A, Oladunjoye, M.A and Osinowo, O.O, 2007. Geological Setting and Integrated Geophysical Exploration for Pb- Zn Sulphide Mineralisation in Baban Tsauni Area Federal Capital Territory Abuja, Central Nigeria. 369-388 in European Journal of Scientific Research. Vol. 18, No 3.

Olayinka, A.I. and Yaramanci, U., 2000, Use of block inversion in the 2-D interpretation of apparent resistivity data and its comparison with smooth inversion: Journal of Applied Geophysics, 45, 63-82.

Olorunfemi, O. M. (2006). Lecture Notes on Self Potential (SP); Induced Polarization (IP); Electrical Resistivity and Electromagnetic Methods of Geophysical Prospecting for Nigerian Geological Survey Agency, Abuja Capacity Building Programme: Geophysics Division

Oluyide, P.O., Akinyosoye, O.M., Nnolim, A. (2004). Lead Sulphide and gold mineralisation in the Nigerian Basement Complex. An example of Babban-Tsauni, Abuja. Unpublished NGSA Report.

Oversby, V M. 1975. Lead isotopic study of aplites from the Precambrian basement rocks near Ibadan, Southwestern Nigeria. *Earth and Planetary Science Letters*, 27 (2), 177–180.

Parasnis, D. S. (1971) Analysis of some multi-frequency, multi-separation electromagnetic surveys. *Geophysical Prospecting*, 19 (2). 163-179

Pelton, W.H., Ward, S.H., Hallof, P.G., Sill, W.R. and Nelson, P.H., 1978. Mineral discrimination and the removal of inductive coupling with multifrequency IP.

Petersen, N. (1990). Curie temperature. In James, D. E. (ed.), The Encyclopedia of solid Earth Geophysics, pages 166–173. NewYork: Van Nostrand Reinhold.

Rahaman, M A. 1988. Recent advances in the study of the basement complex of Nigeria. 11–43. In: *Precambrian Geology of Nigeria*. Oluyide, P O. (editor). (Kaduna, Nigeria: Esho Printers Ltd.)

Rajagopalan,S. (2003). Exploration Geophysics, Vol. 34(No. 4):257–262.

Reeves, C. V. (1989). Aeromagnetic interpretation and rock magnetism. First Break, Vol. 7:275–286.

Russ, W. 1957. *The geology of parts of Niger, Zaria and Sokoto Provinces with Special Reference to the Occurrence of Gold*. Geological Survey of Nigeria, Bulletin No. 27.

Shives, R.B.K., Charbonneau, B.W., Ford, K.L., 1997, The detection of potassic alteration by gamma-ray spectrometry - recognition of alteration related to mineralisation; in "Geophysics and Geochemistry at the Millennium", Proceedings of the Fourth Decennial International Conference on Mineral Exploration (Exploration 97), September, 1997

Silva, A. M., Pires, A. C. B., McCafferty, A., Moraes, R. A. V., and Xia, H. (2003). Application of airborne geophysical data to mineral exploration in the uneven exposed terrains of the Rio Das Velhas greenstone belt. Revista Brasileira de Geociências, 33(2):17–28.

Slater, L. & Lesmes, D. (2002). IP interpretation in environmental investigations, Geophysics, 67(1), 77–88

Strangway, D. W. (1970). History of the Earth's Magnetic Field. NewYork: McGraw Hill.

Summer, J.S., 1976, Principles of induced polarization for geophysical exploration. Elsevier Scientific Publishing Company.

Stummer P, Maurer HR (2001). Real-time experimental design applied to high-resolution direct-current resistivity surveys. International Symposium on Optical Science and Technology, Expanded Abstracts, 143-150.

Telford, W. M., Geldart, L. P., and Sheriff, R. E. (1990). Applied Geophysics. Cambridge University Press, second edition.

Truswell, J.F. and Cope, R.N., 1963: the geology of parts of Niger and Zaria provinces. Geological Survey of Nigeria Bulletin No. 29, 53p.

Turner, D C. 1983. Upper Proterozoic schist belts in the Nigerian sector of the Pan African province of West Africa. *Precambrian Research*, 21, 55–79.

Ward S.H. and Hohmann, G.W. (1987) Electromagnetic Theory for Geophysical Applications. In: Nabighian, M.N., Ed., Electromagnetic Methods in Applied Geophysics, Vol. 1, Society of Exploration Geophysicists, 131-311.

Ward S. H., Sternberg B. K., LaBrecque D. J., and Poulton M. M., 1995, Recommendations for IP research: The Leading Edge, April 1995, 243-247.

Wemegah, D.D., Menyeh, B. A., and Danuor, S. K. (2009). Magnetic Susceptibility Characterization of mineralized and non mineralized rocks of the Subenso Concession of Newmont Ghana Gold Limited. In Ghana Science Association Biennial Conference.

Whitham, K.(1960). Measurement of the geomagnetic elements. In Methods and techniques in Geophysics, volume Vol. 1, pages 134–48. S. K. Runcorn.

Wilford,J.R., Bierwirth,P.N., and Craig,M.A. (1997). Application of airborne gamma-ray spectrometry in soil/regolith mapping and applied geomorphology. AGSO Journal of Australian Geologyand Geophysics, 17(2):201–216.

Woakes, M. and Bafor, B.E., 1984: Primary Gold Mineralisation in Nigeria. In Foster R.P. (Ed): Geology, Geochemistry and Genesis of Gold Deposits, pp 661 – 671.

Wright, J B. 1985 *Geology and Mineral Resources of West Africa*. (George Allen & Unwin, London), 187pp.

Appendix I

Thin Section (petrography) Study and taking of photo-micrograph at the Nigerian Geological Survey Agency

Appendix II

Setting up of the Magnetometer base station (b) Field data acquisition (operation) in the continuous (walkmag) mode (c) Field data acquisition in continuous mode

Appendix III

Field set up of the GDD 5000 Transmitter and 16C receiver; (b) Current injection electrode; and (c) Copper Sulphate Electrode Porous Pot

Appendix IV

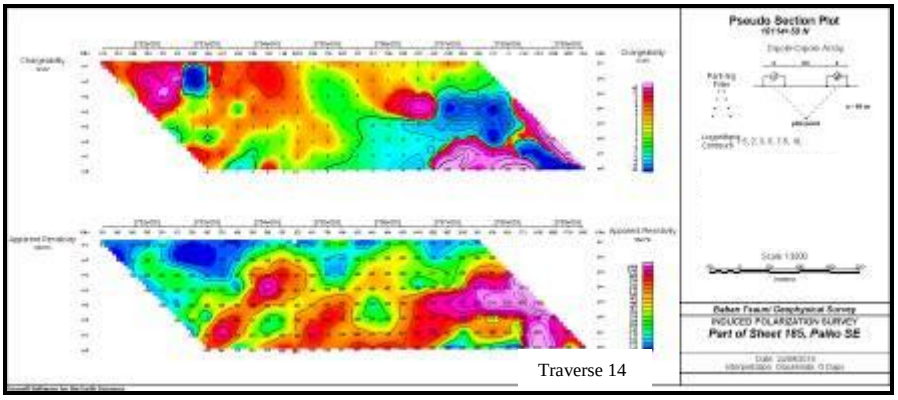

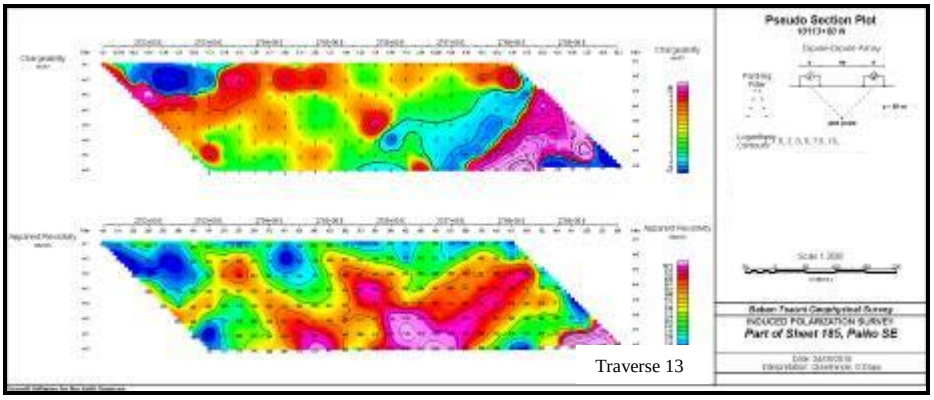

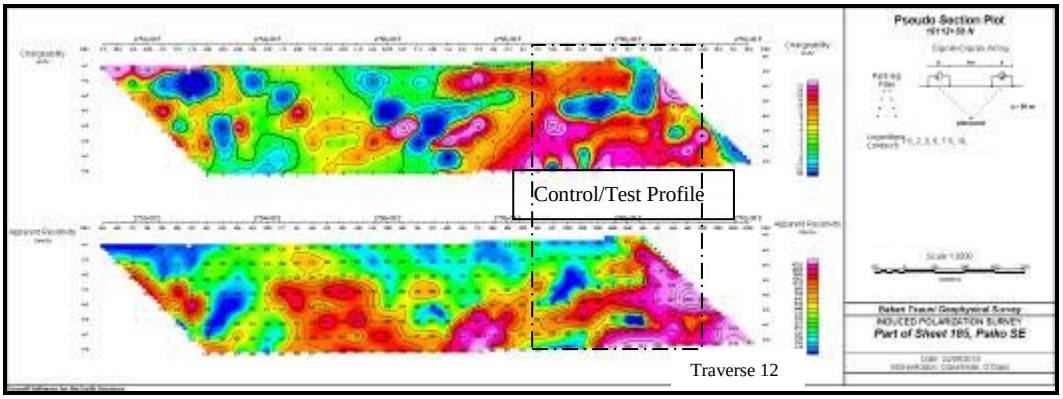

2-Dimension Pseudo-Section plot of both the chargeability (top) with its corresponding apparent resistivity (bottom) for each of the profiles arranged from northern most profile down to the south. The purple colouration marks the highest chargeability values and corresponding resistivity while the blue marks the low chargeability and low resistivity. Note the dip of the resistivity structures

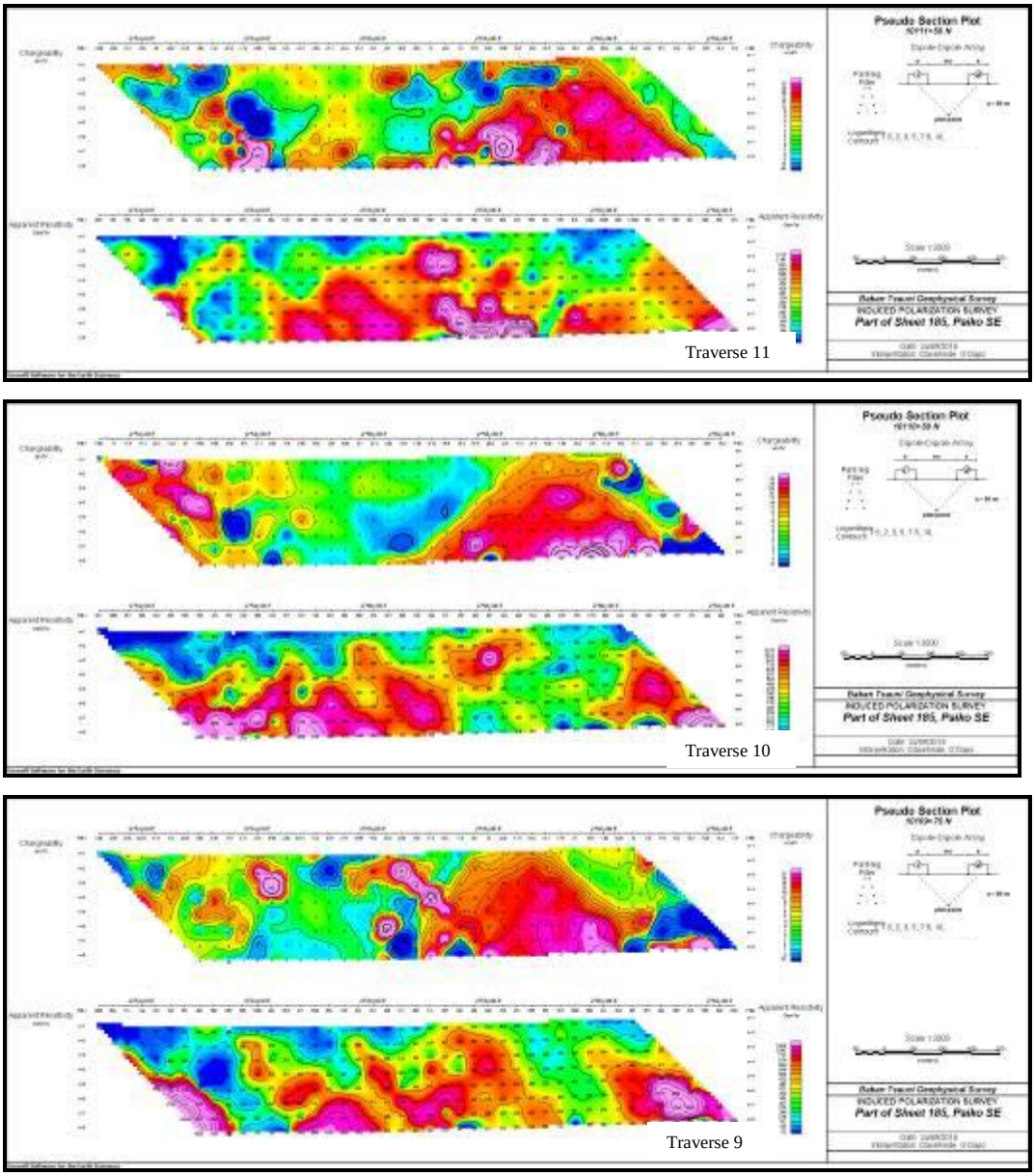

2-Dimension Pseudo-Section plot of both the chargeability (top) with its corresponding apparent resistivity (bottom) for each of the profiles arranged from northern most profile down to the south. The purple colouration marks the highest chargeability values and corresponding resistivity while the blue marks the low chargeability and low resistivity. Note the dip of the resistivity structures

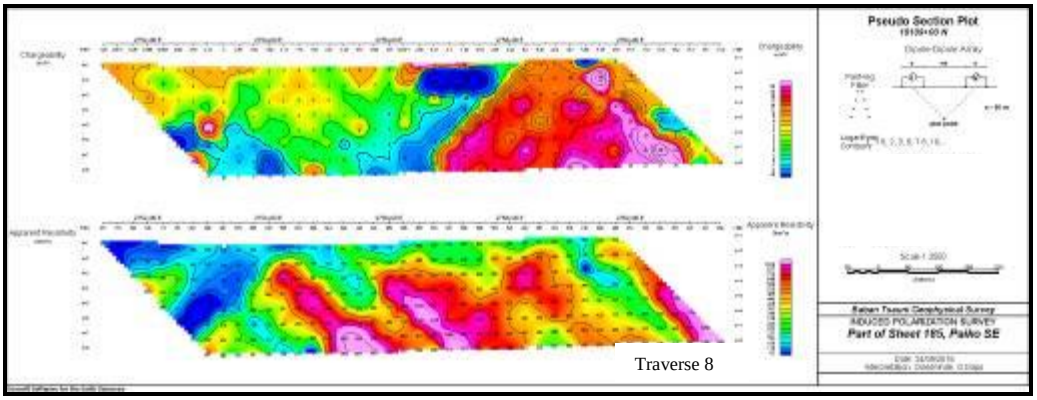

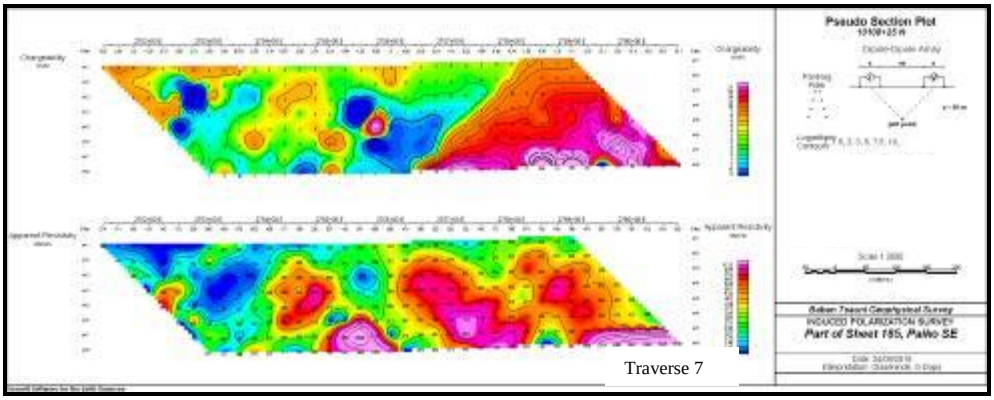

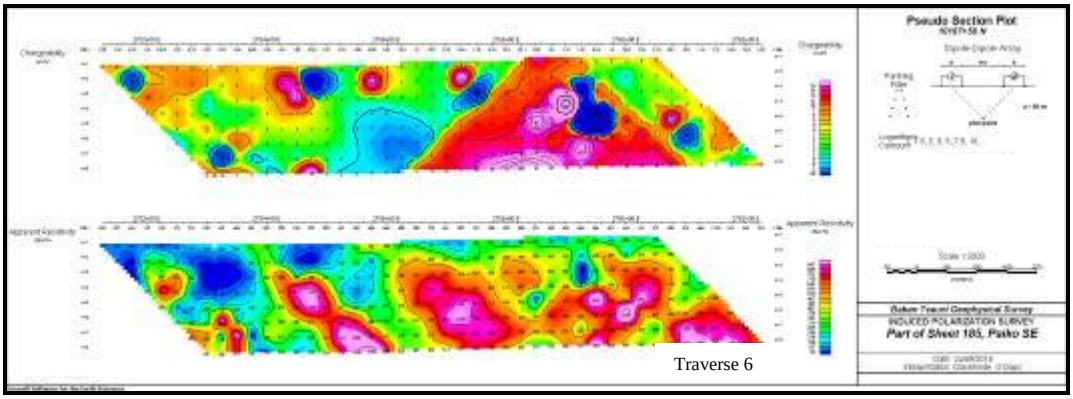

2-Dimension Pseudo-Section plot of both the chargeability (top) with its corresponding apparent resistivity (bottom) for each of the profiles arranged from northern most profile down to the south. The purple colouration marks the highest chargeability values and corresponding resistivity while the blue marks the low chargeability and low resistivity. Note the dip of the resistivity structures

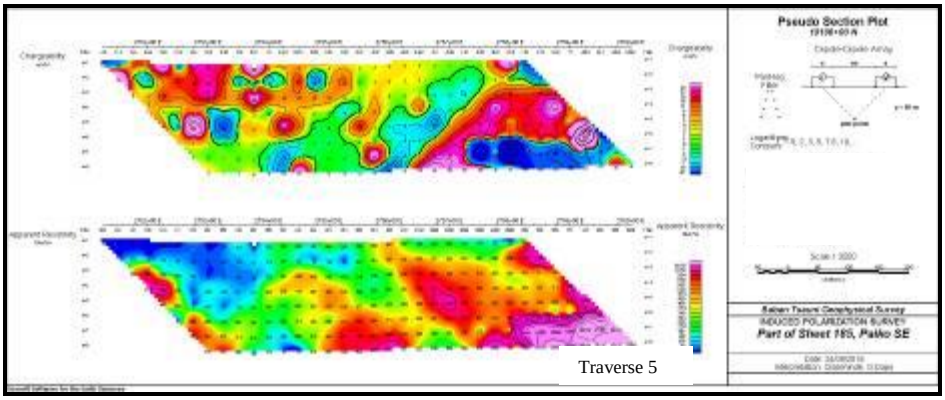

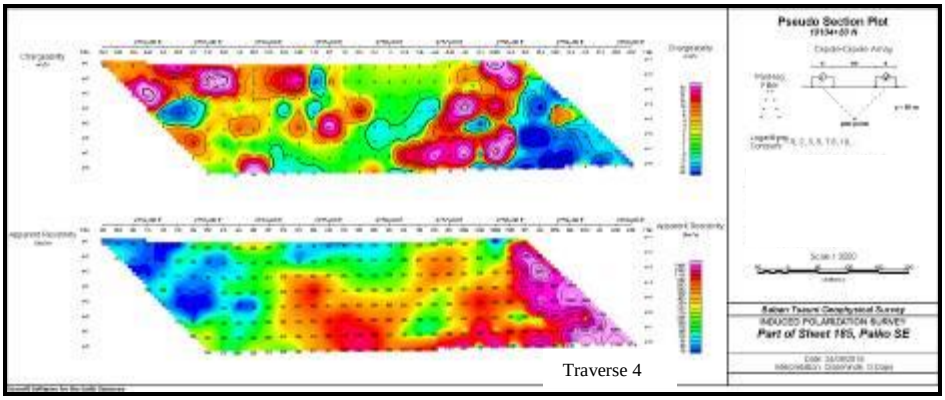

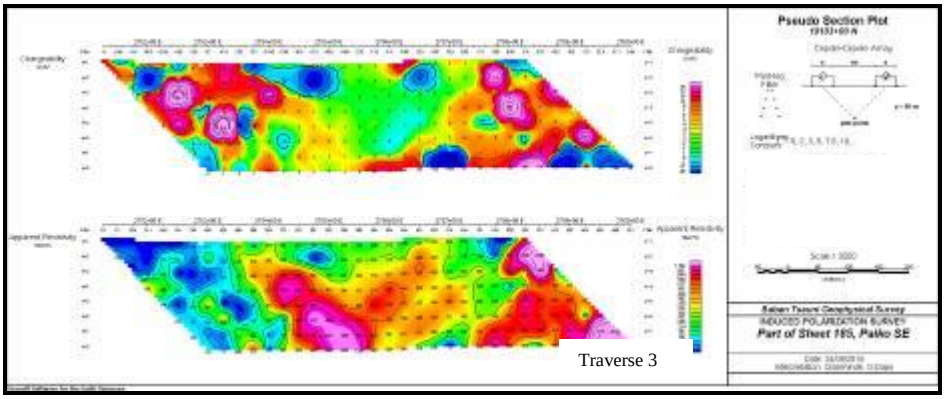

2-Dimension Pseudo-Section plot of both the chargeability (top) with its corresponding apparent resistivity (bottom) for each of the profiles arranged from northern most profile down to the south. The purple colouration marks the highest chargeability values and corresponding resistivity while the blue marks the low chargeability and low resistivity. Note the dip of the resistivity structures

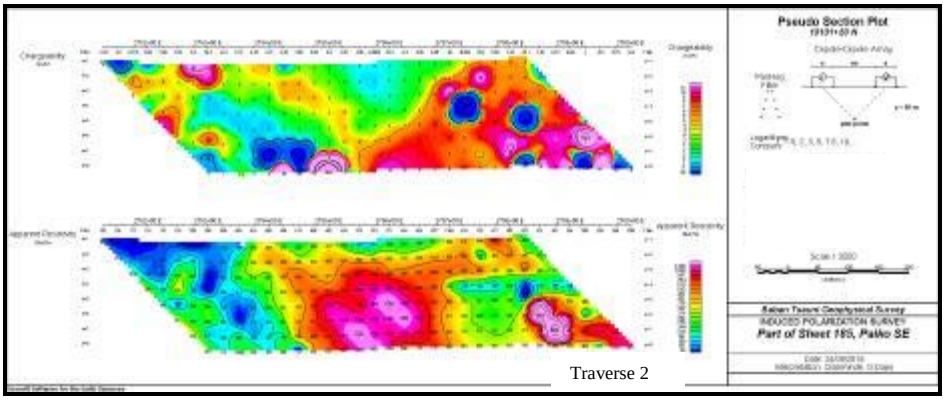

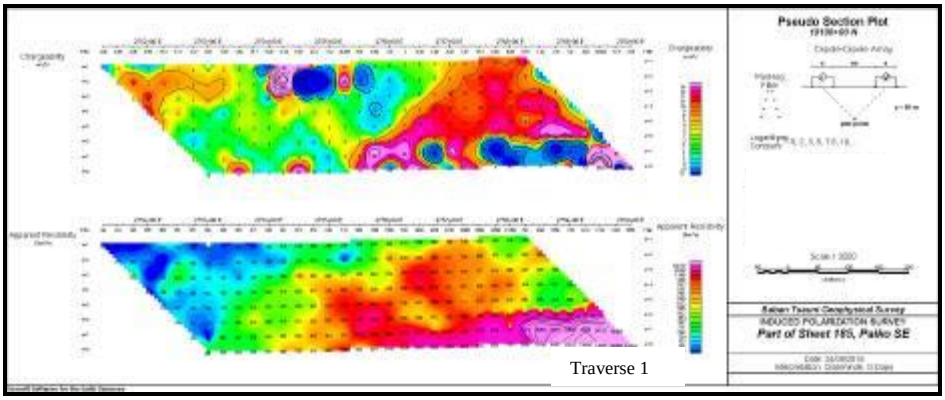

2-Dimension Pseudo-Section plot of both the chargeability (top) with its corresponding apparent resistivity (bottom) for each of the profiles arranged from northern most profile down to the south. The purple colouration marks the highest chargeability values and corresponding resistivity while the blue marks the low chargeability and low resistivity. Note the dip of the resistivity structures

Appendix V

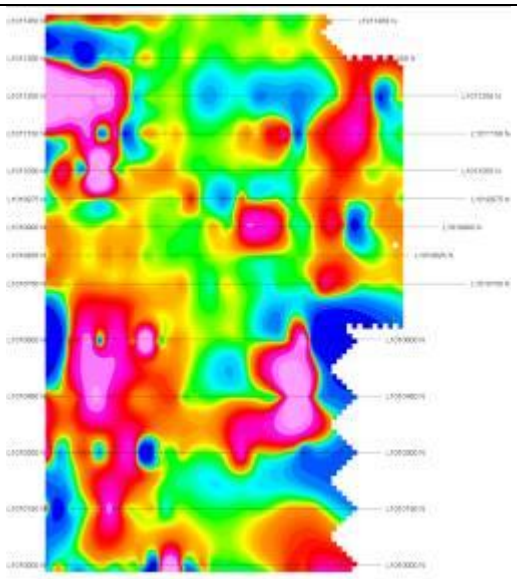

N=1 (Chargeability)

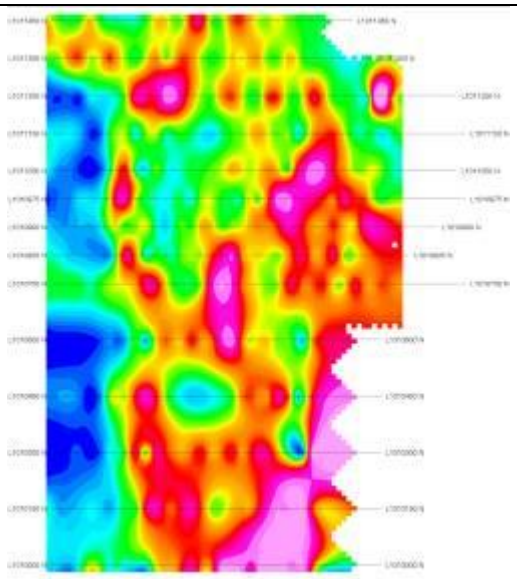

N=1 (Apparent Resistivity)

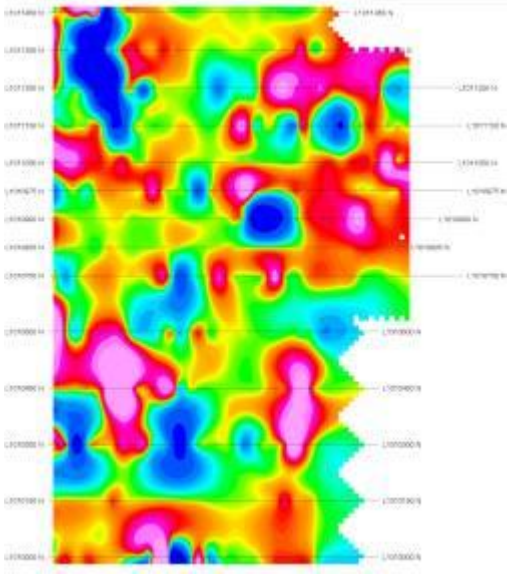

N=2 (Chargeability)

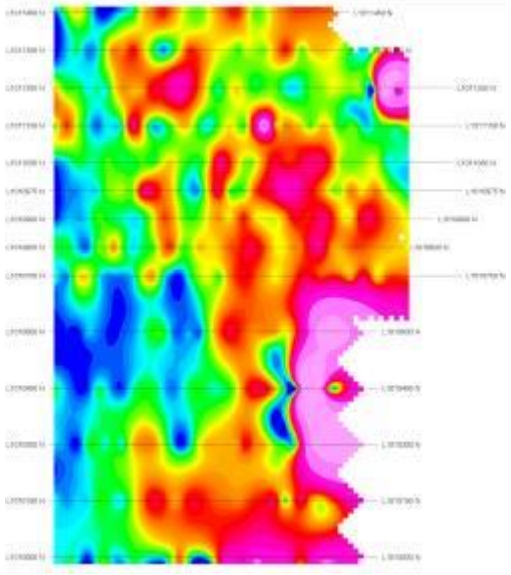

N= 2 (Apparent Resistivity)

Plot of the iso-layers of the chargeability and Apparent Resistivity using the N-values from the dipole-dipole depth of investigation. It shows the spatial distribution with continuity/discontinuity of the zones across depth from N=1 and 2.

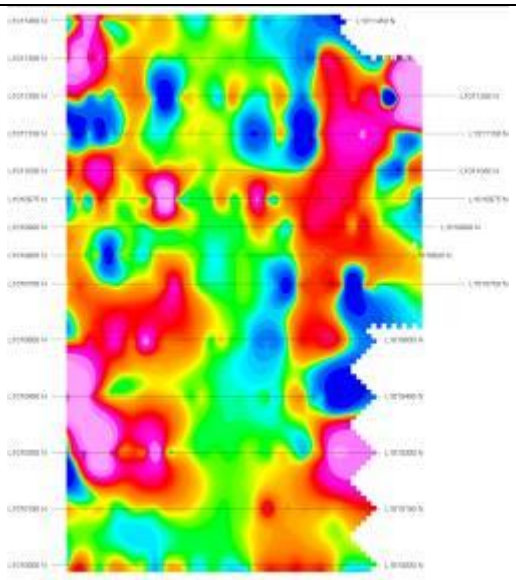	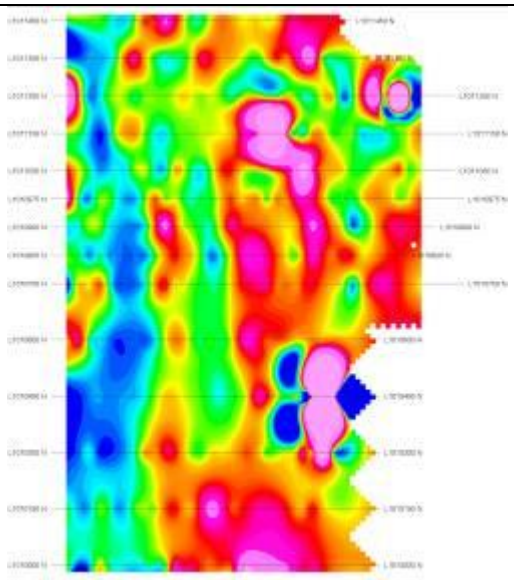
N = 3 (Chargeability)	N = 3 (Apparent Resistivity)
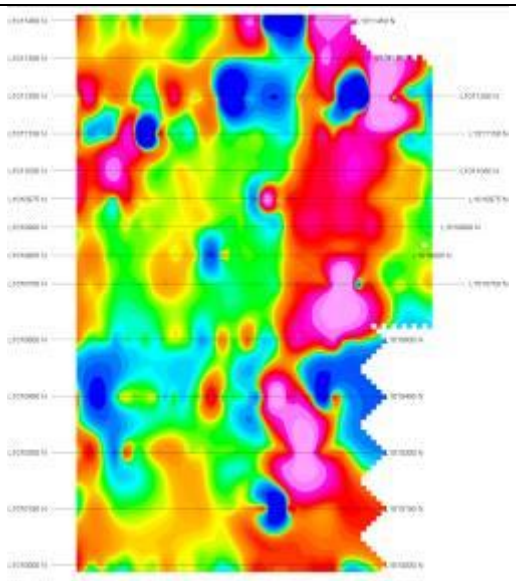	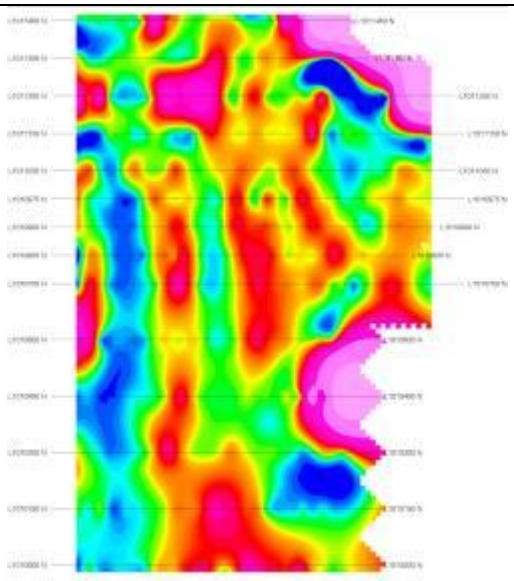
N = 4 (Chargeability)	**N = 4 (Apparent Resistivity)**

Plot of the iso-layers of the chargeability and Apparent Resistivity using the N-values from the dipole-dipole depth of investigation. It shows the spatial distribution with continuity/discontinuity of the zones across depth from N=3 and 4.

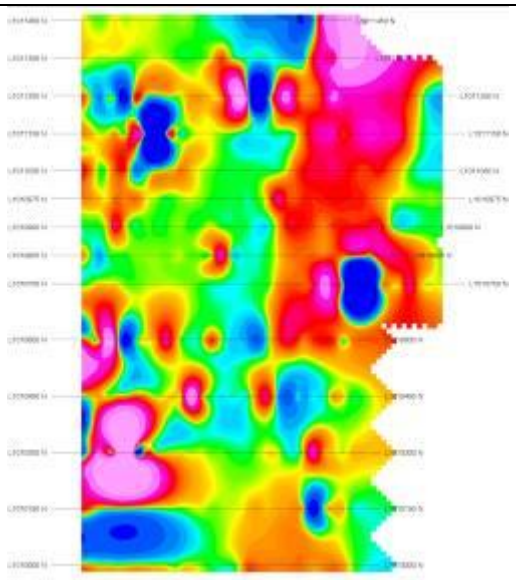

N=5 (Chargeability)

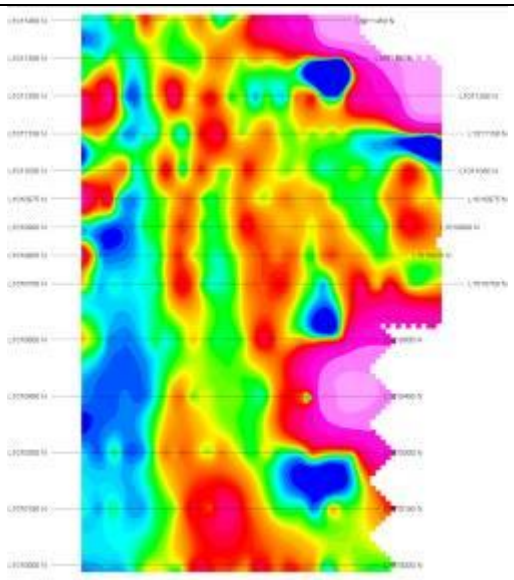

N=5 (Apparent Resistivity)

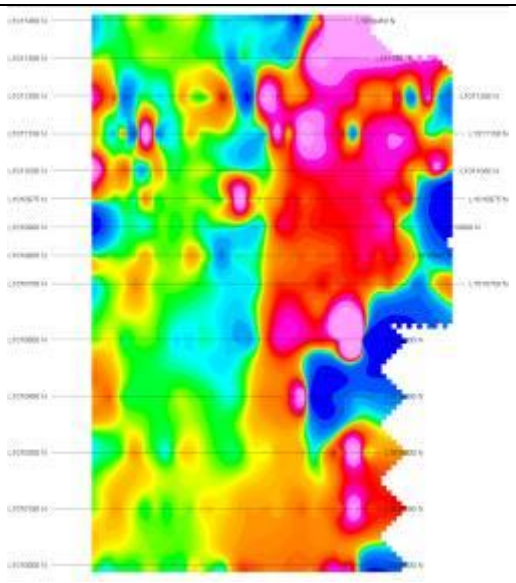

N=6 (chargeability)

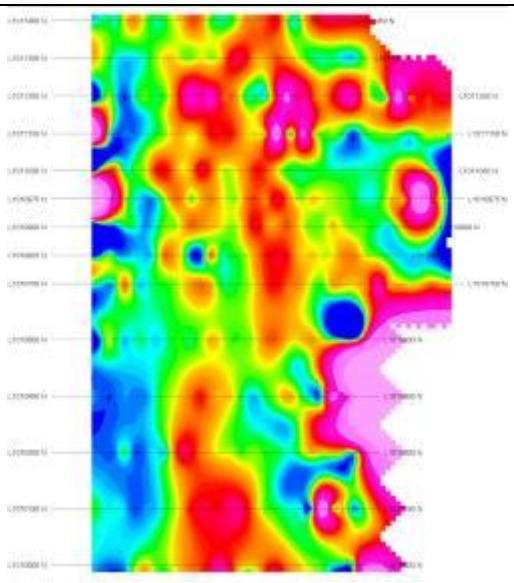

N=6 (Apparent Resistivity)

Plot of the iso-layers of the chargeability and Apparent Resistivity using the N-values from the dipole-dipole depth of investigation. It shows the spatial distribution with continuity/discontinuity of the zones across depth from N=5 and 6.

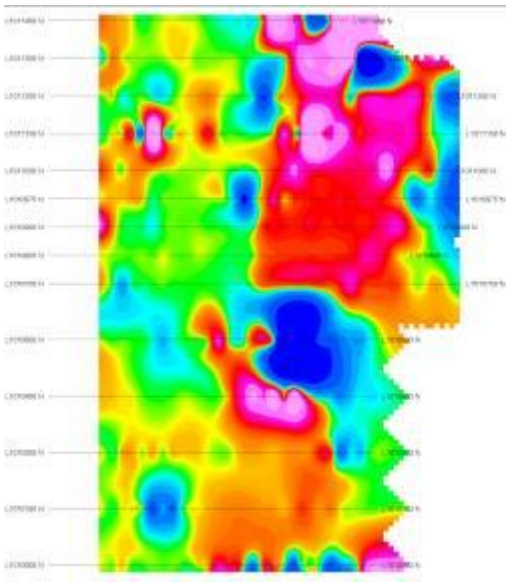

N=7 (Chargeability)

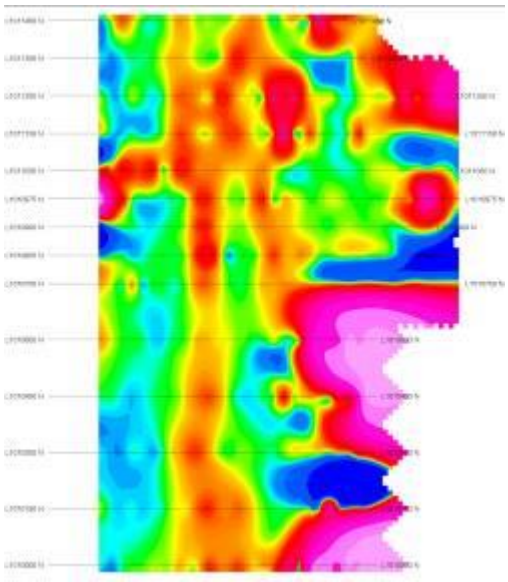

N=7 (Apparent Resistivity)

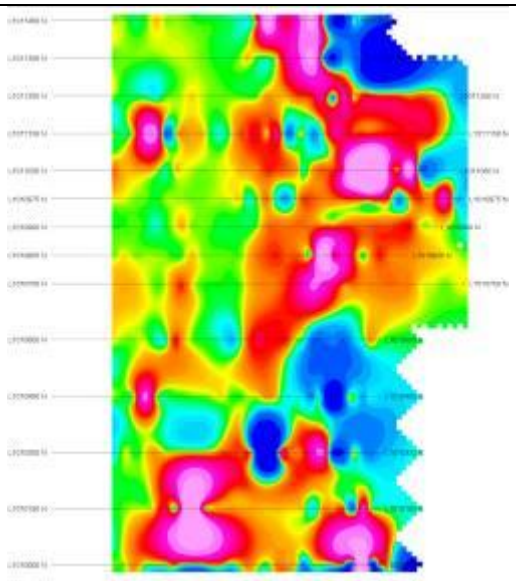

N=8 (chargeability)

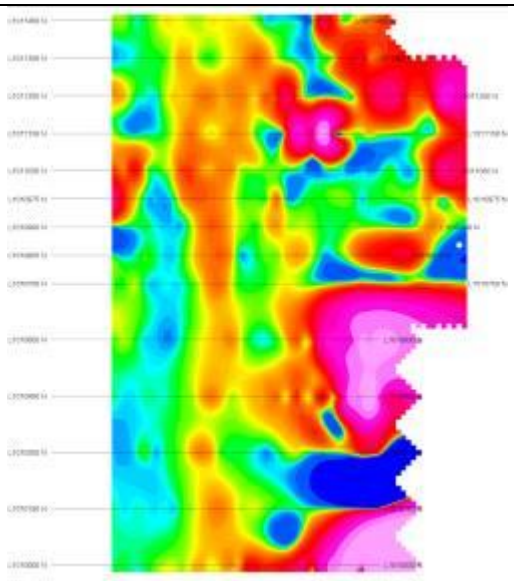

N=8 (Apparent Resistivity)

Plot of the iso-layers of the chargeability and Apparent Resistivity using the N-values from the dipole-dipole depth of investigation. It shows the spatial distribution with continuity/discontinuity of the zones across depth from N=7 and 8.